

# **Glacial and periglacial history of the Bale Mountains, southern Ethiopian Highlands**

Inauguraldissertation  
der Philosophisch-naturwissenschaftlichen Fakultät  
der Universität Bern

vorgelegt von  
**Alexander Raphael Groos**  
aus Deutschland

Leiter der Arbeit:  
Prof. Dr. Heinz Veit  
Geographisches Institut, Universität Bern  
PD Dr. Naki Akçar  
Institut für Geologie, Universität Bern



# **Glacial and periglacial history of the Bale Mountains, southern Ethiopian Highlands**

Inauguraldissertation  
der Philosophisch-naturwissenschaftlichen Fakultät  
der Universität Bern

vorgelegt von  
**Alexander Raphael Groos**  
aus Deutschland

Leiter der Arbeit:  
Prof. Dr. Heinz Veit  
Geographisches Institut, Universität Bern  
PD Dr. Naki Akçar  
Institut für Geologie, Universität Bern

Von der Philosophisch-naturwissenschaftlichen Fakultät angenommen

Bern, 11<sup>th</sup> August 2020

Der Dekan  
Prof. Dr. Z. Balogh



*Dedicated to the memory of Kemal Mohammed, our beloved guide and friend, who introduced me to the people and nature of the Bale Mountains; to Georg Miehe, one of my mentors, who has encouraged my enthusiasm for high mountain research and inspired me for the study of the afro-alpine environment; and to Inge Groos and Dieter Stähler, my parents, who have always given me the freedom to deal with the subjects that fascinate me.*



*“In considering the study of physical phenomena, not merely in its bearings on the material wants of life, but in its general influence on the intellectual advancement of mankind, we find its noblest and most important result to be a knowledge of the chain of connection, by which all natural forces are linked together, and made mutually dependent upon each other; and it is the perception of these relations that exalts our views and ennobles our enjoyments.”*

Alexander von Humboldt (Cosmos, 1845-58)



## List of Papers

This cumulative thesis is based on the following scientific articles:

1. **Groos, A. R.**, N. Akçar, S. Yesilyurt, G. Miehe, C. Vockenhuber, and H. Veit (in revision). "Asynchronous Late Pleistocene glacier fluctuations in tropical Eastern Africa". In: *Science Advances*.
2. **Groos, A. R.**, J. Niederhauser, L. Wraase, F. Hänsel, T. Nauss, N. Akçar, and H. Veit (in review). "Implications of present ground temperatures and relict stone stripes in the Ethiopian Highlands for the palaeoclimate of the tropics". In: *Earth Surf. Dynam. Discuss.* DOI: 10.5194/esurf-2020-53.
3. Ossendorf, G., **A. R. Groos**, T. Bromm, M. G. Tekelemariam, B. Glaser, J. Lesur, J. Schmidt, N. Akçar, T. Bekele, A. Beldados, S. Demissew, T. H. Kahsay, B. P. Nash, T. Nauss, A. Negash, S. Nemomissa, H. Veit, R. Vogelsang, Z. Woldu, W. Zech, L. Opgenoorth, and G. Miehe (2019). "Middle Stone Age foragers resided in high elevations of the glaciated Bale Mountains, Ethiopia". In: *Science* 365, pp. 583-587. DOI: 10.1126/science.aaw8942.

In addition, the following communication, report, short lay-summary, interactive comment, and book chapter, complementing the scientific articles above, arose out of the doctorate:

- **Groos, A. R.**, N. Akçar, and H. Veit (2017). "Projektvorstellung: Rekonstruktion der Glazialgeschichte im südlichen Hochland von Äthiopien". In: *Geowissenschaftliche Mitteilungen* 68, pp. 80–82.
- **Groos, A. R.**, N. Akçar, G. Miehe, S. Yesilyurt, C. Vockenhuber, and H. Veit (2018). "Glacial history of the Bale Mountains in Ethiopia – <sup>36</sup>Cl surface exposure dating of moraines in tropical Africa". In: *Annual Report, Ion Beam Physics, ETH Zurich* 57.
- **Groos, A. R.** (2020). "Living the high life: the early arrival of hunter-gatherers in the glaciated Ethiopian Highlands". In: *The Science Breaker*. DOI: 10.25250/thescbr.brk344.
- **Groos, A. R.** (2020). "Interactive comment on "Holocene glaciation in the Rwenzori Mountains, Uganda" by Margaret S. Jackson et al.". In: *Clim. Past Discuss.* 61, pp. C1-8. DOI: 10.5194/cp-2020-61-SC1.
- Veit, H., and **A. R. Groos** (2020). "Kapitel 2.1 Globale Klima- und Gletscherveränderungen im Pleistozän und Holozän". In: *Warnsignal Klima: Hochgebirge im Wandel*.



## *Abstract*

The magnitude of cooling in the equatorial East African mountains and Ethiopian Highlands during the last glacial period and its impact on the afro-alpine environment and human expansion into higher elevations is still poorly understood. Quasi-continuous archives like ice or sediment cores that provide insights into palaeoclimatic and -environmental changes at high elevations in the region are extremely rare and cover mainly the Holocene. Glacial deposits and periglacial landforms are often the only remaining evidence of Pleistocene climatic and environmental changes in the tropical mountains of Eastern Africa. One of the least studied alpine areas in the region with respect to the glacial and periglacial history are the Bale Mountains in the southern Ethiopian Highlands, although they comprise the continent's largest area above 4000 masl and provide geomorphological evidence for past glaciations. Glacial and periglacial landforms have been reported from the Bale Mountains, but they have never been systematically mapped, dated, and investigated. To close this gap and explore the potential of this afro-alpine archive for the reconstruction of past glacier fluctuations and regional high-altitude climate and -environmental changes, is therefore the overarching goal of this dissertation.

More specifically, this implies the reconstruction of the former ice extent(s) by means of geomorphological mapping, the development of a glacial chronology through  $^{36}\text{Cl}$  surface exposure dating of erratic boulders, and the investigation of recent and past periglacial landforms and processes in the Bale Mountains. Knowing the extent and timing of past glaciations and periglacial processes is a prerequisite for (i) drawing conclusions about the magnitude of high-altitude tropical cooling during the last glacial period, (ii) elaborating the impact of Quaternary climate and environmental changes on the afro-alpine ecosystem, and (iii) understanding the context of a hypothesised early dispersal of humans into the high mountains.

The geomorphological mapping in the valleys and on the central plateau shows that glacial and periglacial landforms are well preserved in the Bale Mountains and enable the reconstruction of the former ice extent and periglacial area. Characteristic for the Bale Mountains was the formation of an extensive plateau glaciation covering up to 265 km<sup>2</sup> and extending down into the northern valleys during the Pleistocene. Beyond the limits of the former ice cap, relict large sorted stone polygons and stripes (up 1000 m long, 15 m wide, and 2 m deep) occur. Geomorphological patterns of similar size are extremely rare and have before only been known from the mid and high latitudes, but not from the tropics. They are interpreted as the result of frost heave and sorting and are thus an indicator of several decimetre deep seasonal or permanent frost on the plateau during the last glacial period.

By developing a first glacial chronology for the region, this thesis demonstrates that the stabilisation age of moraines in the volcanic Ethiopian Highlands can be successfully determined using  $^{36}\text{Cl}$  surface exposure dating. The dating of moraines in the valleys and of erratic boulders on the plateau testifies to an initial glaciation in the Bale Mountains during the Mid Pleistocene (presumably Marine Isotope Stage 6), an early local Last Glacial Maximum (local LGM) lasting from 50 to 30 ka, a glacier extent at 19-17 ka similar to the local LGM, and the disintegration of the valley glaciers after 16-14 ka.

In cross-comparison with available glacial chronologies and reconstructions from other tropical mountains in the region, the new data from the Bale Mountains contribute to a better understanding of past glacier fluctuations and climate variations across Eastern Africa. The comparison of glacial chronologies from the Bale Mountains, Rwenzori Mountains, Mount Kenya, and Kilimanjaro indicates differences in the timing of the local LGM and subsequent readvances that have not been pointed out before. This asynchronicity suggests that regional hydroclimatic variations as well as topographic differences were important drivers of the palaeoglacier dynamics across Eastern Africa and should therefore be given greater attention.

Glacial and periglacial landforms in the Bale Mountains provide by their presence alone clear evidence for a strong cooling and pronounced climate and environmental changes, but they also support the quantitative estimate of the temperature depression during the last glacial period. The difference between the present-day climate and reconstructed past climatic conditions suggests a temperature decrease of 4-8 °C during Marine Isotope Stages 3/2. In comparison with temperature reconstructions from lower areas in the region, these findings emphasise an amplified cooling with increasing elevation in tropical Eastern Africa during the Late Pleistocene. A strong cooling in tandem with the formation of glaciers and ground frost must have had a considerable, yet unknown, impact on the afro-alpine ecosystem and endemic species in the Bale Mountains.

By combining the glacial chronological with archaeological, soil biogeochemical, and zoogeographical data, the thesis contributes essentially to the corroboration of the hypothesised advance of humans into the high mountains already during the last glacial period. The combined findings reveal that the early colonisation of the Bale Mountains (47-31 ka cal BP) coincided with the local LGM (50-30 ka) and therefore with a relatively cold period. Beside obsidian as raw material and an abundant rodent as key food source, perennial melt water from the glaciers was presumably one of the afro-alpine key resources, which might have attracted hunter-gatherers. The interdisciplinary findings therefore not only prove that the resources of the world's high mountains have already been accessed during the Late Pleistocene, but also that the prehistoric foragers in the Bale Mountains were familiar with cold and glaciated environments.

The main results of the dissertation summarised above highlight the value of glacial and periglacial landforms in the Bale Mountains as geomorphological archive for the reconstruction of past glacier fluctuations and regional high-altitude climate and -environmental changes, especially in a palaeoecological and archaeological context. Therefore, this contribution lays the foundation for future glacial chronological research in other parts of the Ethiopian Highlands and fosters our understanding of the natural and anthropogenic history of the highlands and mountains in tropical Eastern Africa.

## *Acknowledgements*

This dissertation is the result of an intensive and fruitful cooperation with many different people. I regret that I can only mention a few here personally. First of all, I would like to express my deepest appreciation to my supervisors Heinz Veit and Naki Akçar for the excellent guidance, the continuous support, the enlightening discussions, and the memorable time in the field. You have given me all the freedom one could wish for as a young scientist and at the same time were always available when I needed advice or feedback. I would also like to extend my deepest gratitude to Georg Miehe who, as he likes to say, made me an offer (a first field trip to the Bale Mountains in 2012) I could not refuse. You have encouraged my enthusiasm for high mountain research and inspired me for the study of the afro-alpine environment. Furthermore, I'm extremely grateful to my co-authors and colleagues from the research unit "The Mountain Exile Hypothesis" for their contribution and support as well as the many exciting debates. I hope there are more to come...

An integral part of the dissertation was the extensive field work in the Bale and Arsi Mountains. I'm deeply indebted to many people in Ethiopia for their unparalleled support and long-term friendship. Without their commitment, care, knowledge, and talent for improvisation, exploring the remote areas of the highlands just on food and horseback would not have been possible. I hereby apologise again for the long marches and cold nights in the tent. Representative for many others, I would like to say "ameseginalahu"/"galatoma" to Mekbib Fekadu, Beriso Kemal, Edris Abduku, Wege Abebe, Terefe Endale, Awol Asseffa, Geremew Mebratu, and Fiseha Getachew. Many thanks at this point also to our project coordinators Katinka Thielsen and Tiziana Koch for their unwavering assistance with the accounting and field work preparation. I would also like to mention here the unforgettable time I had in the field with Lukas Munz, Julian Struck, Sabrina Erlwein, and Serdar Yesilyurt. Thanks for joining me on this adventure!

Special thanks go to my colleagues from the Institute of Geography in general and my peers Leonor Rodrigues, Lukas Munz, Tobias Sprafke, Armin Rist, Mareike Trauerstein, and Umberto Lombardo from the Palaeo-Geoecology Group in particular. During the last years, you supported me wherever possible. I am grateful for the fruitful discussions, your helpful advice, and your constructive feedback, but most of all I will remember the climbing "competitions" in our underground boulder room, the joint field work and excursions, swimming in the Aare, and last but not least our social evenings. I also wish to thank Roland Zech for introducing me to the surface exposure dating of rocks and sharing his knowledge. The months together with Julian in your lab were a good preparation before starting with the processing of my own samples in Naki's lab. Serdar, it was a pleasure to work with you in the lab. I have benefited greatly from your experience and efficiency. I cannot complete without mentioning Mark Malgwi, my friend, flat mate, and colleague. Thank you for all the insightful political and scientific conversations, the enjoyable table tennis matches, and the exhaustive proofreading.

Above all, however, I would like to express my deepest gratitude to Sabrina and my family for their everlasting support and great patience. Sabrina, without your company in the field, your meticulous proofreading of my manuscripts and thesis, and your care and love, the completion of the dissertation would not have been possible. Thank you!



# Contents

<b>List of Papers</b>	<b>v</b>
<b>Abstract</b>	<b>vii</b>
<b>Acknowledgements</b>	<b>ix</b>
<b>1 Introduction</b>	<b>1</b>
1.1 Motivation . . . . .	2
1.2 Background – The Ethiopian Highlands . . . . .	6
1.2.1 Geography and climate . . . . .	6
1.2.2 Glacial and periglacial context . . . . .	7
1.3 Objectives of the thesis . . . . .	11
1.4 Structure of the thesis . . . . .	12
References . . . . .	13
<b>2 Asynchronous Late Pleistocene glacier fluctuations in tropical Eastern Africa</b>	<b>17</b>
Abstract . . . . .	18
2.1 Introduction . . . . .	18
2.2 Results . . . . .	20
2.2.1 Hypsography of Africa’s glaciated mountains . . . . .	20
2.2.2 Glacial history of the Bale Mountains . . . . .	21
2.2.3 Glacial history of the Arsi Mountains . . . . .	25
2.2.4 Reconstructed ELAs and temperature depression . . . . .	26
2.2.5 Late Pleistocene glacial fluctuations in Eastern Africa . . . . .	27
2.3 Discussion . . . . .	28
2.4 Conclusion . . . . .	33
2.5 Materials and Methods . . . . .	34
2.5.1 Terrain analysis . . . . .	34
2.5.2 Glacial geomorphological mapping . . . . .	34
2.5.3 Surface exposure dating . . . . .	35
2.5.4 Glacial chronology . . . . .	36
2.5.5 Glacial extent . . . . .	37
2.5.6 Equilibrium line altitude and temperature reconstruction . . . . .	38
Acknowledgements . . . . .	39
References . . . . .	39

<b>3 Implications of present ground temperatures and relict stone stripes in the Ethiopian Highlands for the palaeoclimate of the tropics</b>	<b>45</b>
Abstract . . . . .	46
3.1 Introduction . . . . .	46
3.2 Study Area . . . . .	48
3.3 Data and Methods . . . . .	50
3.3.1 Mapping of periglacial landforms . . . . .	50
3.3.2 Ground-penetrating radar measurements . . . . .	52
3.3.3 <sup>36</sup> Cl surface exposure dating of periglacial landforms . . . . .	52
3.3.4 Ground temperature measurements . . . . .	53
3.3.5 Meteorological measurements . . . . .	55
3.3.6 Statistical data interpolation and analysis . . . . .	56
3.3.7 Ground temperature modelling and palaeoclimate reconstruction . . . . .	57
3.4 Results . . . . .	59
3.4.1 Distribution and characteristics of periglacial landforms . . . . .	59
3.4.2 Present frost occurrence and ground temperature variations . . . . .	63
3.4.3 Modelled palaeo ground temperatures . . . . .	66
3.5 Discussion . . . . .	68
3.6 Conclusion . . . . .	73
Data Availability . . . . .	74
Acknowledgements . . . . .	74
References . . . . .	74
<b>4 Middle Stone Age foragers resided in high elevations of the glaciated Bale Mountains, Ethiopia</b>	<b>79</b>
Abstract . . . . .	80
4.1 Main Text . . . . .	80
4.2 Materials and Methods . . . . .	87
4.2.1 Archaeological survey and excavation . . . . .	87
4.2.2 Anthrosol analyses . . . . .	88
Background . . . . .	88
Fecal biomarker analysis . . . . .	88
4.2.3 Total element analysis . . . . .	89
4.2.4 Black carbon analysis . . . . .	89
4.2.5 Electron microprobe analysis of obsidian . . . . .	90
4.2.6 Radiocarbon dating and calibration . . . . .	90
4.2.7 Lithic analysis . . . . .	91
4.2.8 Faunal analysis . . . . .	92
4.2.9 Glacial chronology of the Harcha and Wasama Valleys . . . . .	93
Background . . . . .	93
Mapping . . . . .	93
Glacial extent . . . . .	93

Sampling strategy . . . . .	94
Laboratory procedure . . . . .	94
Surface exposure age calculation . . . . .	95
Glacial chronology . . . . .	95
4.2.10 Derivation of palaeoenvironmental conditions from ground beetle data .	96
Background . . . . .	96
Data collection . . . . .	97
Reconstruction of palaeoenvironmental conditions . . . . .	97
Acknowledgements . . . . .	97
References . . . . .	98
<b>5 Synthesis</b>	<b>105</b>
<b>6 Conclusions</b>	<b>123</b>
<b>7 Outlook</b>	<b>127</b>
<b>A Supplements to Chapter 2</b>	<b>131</b>
<b>B Supplements to Chapter 3</b>	<b>171</b>
<b>C Supplements to Chapter 4</b>	<b>175</b>
<b>Declaration of Consent</b>	<b>193</b>
<b>Curriculum Vitae</b>	<b>195</b>



# List of Figures

1.1	Topographic overview maps of Africa, the Ethiopian Highlands, and Bale Mountains, showing the highest peaks and most important locations of the study area.	5
1.2	Schematic mean low-level (925 hPa) wind directions for the African continent . . .	7
2.1	Overview map of Quaternary glaciations in Africa . . . . .	19
2.2	Hypsography of high African mountains . . . . .	21
2.3	Glacial geomorphology of the northern valleys in the Bale Mountains . . . . .	22
2.4	Glaciation map and $^{36}\text{Cl}$ glacial chronology of the Bale Mountains . . . . .	24
2.5	Glaciation map and $^{36}\text{Cl}$ glacial chronology of the Arsi Mountains . . . . .	26
2.6	Comparison of different climate proxies and glacial chronologies from Eastern Africa for the last 71 ka . . . . .	29
3.1	Overview map of the experimental setup and observation network in the Bale Mountains . . . . .	49
3.2	Field work in the Bale Mountains . . . . .	51
3.3	Measurement period(s) of each ground temperature data logger between January 2017 and January 2020 . . . . .	55
3.4	Periglacial environment of the Bale Mountains . . . . .	60
3.5	Overview map of periglacial landforms and other characteristic geomorphological features in the Bale Mountains . . . . .	61
3.6	3D aerial view and radargram of the sorted stones stripes . . . . .	62
3.7	Hourly ground temperatures and seasonal ground temperature variations on the Sanetti Plateau . . . . .	63
3.8	Mean multiannual and multiseasonal diurnal ground temperature cycle, frost depth, and ground temperature gradients on the Sanetti Plateau . . . . .	64
3.9	Mean multiannual and multiseasonal lapse rate in the Bale Mountains . . . . .	66
3.10	Comparison of the seasonal ground temperature variations between a northern and southern slope as well as between vegetated and unvegetated areas . . . . .	66
3.11	Relationship between hourly ground temperatures in 2 cm depth and different meteorological variables . . . . .	67
3.12	Simulated daily mean ground temperatures . . . . .	68
4.1	Geographic location and setting of the study area . . . . .	81
4.2	Stratigraphic sequence of the archaeological deposits . . . . .	82
4.3	Soil profile and depth functions of biogeochemical proxies representing soil organic matter quantity and human influence . . . . .	83

4.4	Selected findings from the MSA deposits . . . . .	84
A.1	Photographs of all 81 sampled and dated glacial and periglacial features from the Bale and Arsi Montains . . . . .	132
A.2	Glacial and periglacial geomorphology of the Sanetti Plateau . . . . .	146
A.3	<sup>36</sup> Cl surface exposure age and location of the large sorted stone stripes . . . . .	147
A.4	TAS (total alkali versus silica) classification of all sampled boulders from the Bale and Arsi Mountains . . . . .	148
A.5	Mean annual air temperature for three different locations and elevations in the Bale Mountains . . . . .	149
A.6	Equilibrium line altitudes calculated for the palaeoglaciers in the Arsi Mountains	150
C.1	Photographs of obsidian outcrops at Wasama Ridge . . . . .	176
C.2	Photograph of lithic surface scatters at Wasama Ridge . . . . .	177
C.3	Schematic plan view of Fincha Habera rock shelter . . . . .	178
C.4	Schematic representation of excavation spits at Fincha Habera rock shelter . . . . .	179
C.5	Relative frequency of faunal remains at Fincha Habera . . . . .	180
C.6	Images of sampled boulders from the Harcha and Wasama valleys . . . . .	181
C.7	Overview map of the <sup>36</sup> Cl surface exposure ages obtained from 21 boulders sampled in the Harcha and Wasama Valleys of the Bale Mountains . . . . .	182
C.8	Frequency distribution of 19 <sup>36</sup> Cl surface exposure ages used for the determination of the glacial stages in the Harcha and Wasama Valleys of the Bale Mountains	183
C.9	Occurrences of micro-areal endemic species of the genus <i>Trechus</i> Clairville in the Bale Mountains . . . . .	184

# List of Tables

3.1	Description of periglacial features on the Sanetti Plateau sampled for $^{36}\text{Cl}$ surface exposure dating . . . . .	53
3.2	Overview of the installed ground temperature data loggers . . . . .	54
3.3	Overview of the installed automatic weather stations in the Bale Mountains . . . . .	56
3.4	Coefficients and goodness of fit of the three established multiple linear regression models . . . . .	59
A.1	Quaternary glaciations in Africa and estimated LGM extent. . . . .	151
A.2	Geographic location and description of the sampled glacial and periglacial features from the Bale and Arsi Mountains. . . . .	152
A.3	Major and trace element data of the rock samples from the Bale and Arsi Mountains. . . . .	156
A.4	Cosmogenic $^{36}\text{Cl}$ data and surface exposure ages of the rock samples from the Bale and Arsi Mountains . . . . .	160
A.5	Input data table for easy reproducibility of the $^{36}\text{Cl}$ surface exposure ages using the latest version of the CRONUS web calculator . . . . .	164
A.6	$^{36}\text{Cl}$ surface exposure ages of the rock samples from the Bale and Arsi Mountains using different $^{36}\text{Cl}$ production rate scalings . . . . .	165
A.7	Age and uncertainty of the different LPG Stages in the Bale Mountains . . . . .	167
A.8	Input data for the TAS diagram . . . . .	168
B.1	Overview of periglacial landforms and other characteristic geomorphological features in the Bale Mountains . . . . .	172
B.2	System settings of the used Pulse EKKO PRO GPR . . . . .	173
B.3	Major and trace element data of the six rock samples from the Sanetti Plateau . . . . .	174
B.4	Cosmogenic $^{36}\text{Cl}$ data and surface exposure ages of the rock samples from the Sanetti Plateau . . . . .	174
C.1	Total organic carbon, black carbon, total N, total P, total Ca and total K contents, as well as content of $5\beta$ -stanols of the sampled Fincha Habera rock shelter sediments and coprolite samples (C1/C2) . . . . .	185
C.2	$^{14}\text{C}$ AMS ages from Fincha Habera rock shelter. . . . .	186
C.3	Lithic assemblage composition of Fincha Habera rock shelter . . . . .	187
C.4	Fauna from unit H11 at Fincha Habera according to the NISP (Number of Identified Specimens). . . . .	188

C.5 Geographic location and description of the sampled boulders from the Harcha and Wasama Valleys in the Bale Mountains . . . . . 189

C.6 Major and trace element data of the rock samples from the Harcha and Wasama Valleys in the Bale Mountains . . . . . 189

C.7 Cosmogenic <sup>36</sup>Cl data and surface exposure ages of the samples from the Harcha and Wasama Valleys in the Bale Mountains . . . . . 189

C.8 Micro-areal endemic species of the genus *Trechus Clairville* strictly adapted to humid and humus-rich soil known to occur on different slopes of the Bale Mountains . . . . . 190

# List of Abbreviations

<b>AMS</b>	<b>Accelerator Mass Spectrometry</b>
<b>CAB</b>	<b>Congo Air Boundary</b>
<b>cal BP</b>	<b>calibrated Before Present</b>
<b>DFG</b>	<b>Deutsche ForschungsGemeinschaft</b>
<b>DSM</b>	<b>Digital Surface Model</b>
<b>ELA</b>	<b>Equilibrium Line Altitude</b>
<b>global LGM</b>	<b>global Last Glacial Maximum</b>
<b>ITCZ</b>	<b>InterTropical Convergence Zone</b>
<b>ka</b>	<b>kilo annum</b>
<b>LPG</b>	<b>Late Pleistocene Glaciation</b>
<b>local LGM</b>	<b>local Last Glacial Maximum</b>
<b>masl</b>	<b>meter above sea level</b>
<b>MELM</b>	<b>Maximum Elevation of Lateral Moraines</b>
<b>MIS</b>	<b>Marine Isotope Stage</b>
<b>MPG</b>	<b>Mid Pleistocene Glaciation</b>
<b>MSA</b>	<b>Middle Stone Age</b>
<b>NASA</b>	<b>National Aeronautics Space Administration</b>
<b>SNSF</b>	<b>Swiss National Science Foundation</b>
<b>SRTM</b>	<b>Shuttle Radar Topography Mission</b>
<b>THAR</b>	<b>Terminus-to-Headwall-Altitude-Ratio</b>



## **Chapter 1**

# **Introduction**

## 1.1 Motivation

Today's ice caps and glaciers on the African continent are restricted to the highest tropical mountains (>5000 masl). Beside slope and plateau glaciers on Kilimanjaro, afro-alpine glaciers persist in the equatorial Rwenzori Mountains and on Mount Kenya (Kaser, 1999; Veetil and Kamp, 2019). However, well preserved moraine sequences and other glacial deposits from lower elevations show that a much larger area of these mountains was covered by ice in the past. Moreover, glacial and periglacial landforms on lower equatorial mountains (e.g. Aberdare Range and Mount Elgon) and in the Ethiopian Highlands (e.g. Arsi, Bale, and Simien Mountains) testify to more extensive and numerous mountain glaciations in tropical Eastern Africa during the Quaternary (e.g. Osmaston, 2004; Osmaston and Harrison, 2005). Provided that moraines are well preserved and accurately mapped and dated, they allow to reconstruct the glacial history of individual valleys or entire mountains (e.g. Mark and Osmaston, 2008). Since afro-alpine glaciers respond sensitively to changes in insolation, temperature, cloudiness, and precipitation (Mölg, Georges, and Kaser, 2003; Mölg and Hardy, 2004; Mölg et al., 2008; Mölg, Cullen, and Kaser, 2009; Nicholson et al., 2013), past glacier fluctuations provide direct insights into palaeoclimatic and -environmental changes at high elevations in the tropics (e.g. Mark et al., 2005; Barrows et al., 2011).

Information on past glaciations and high-altitude palaeoclimatic and -environmental changes in tropical Eastern Africa are of great relevance because little is known about the magnitude and manifestation of cooling at high elevations in the region during the last glacial period and the impacts on the afro-alpine ecosystem (e.g. Farrera et al., 1999). According to the outputs of global climate models, the tropics experienced a moderate cooling of 0-4 °C (relative to the pre-industrial climate) during the global Last Glacial Maximum (LGM,  $22 \pm 4$  ka after Shakun and Carlson, 2010), compared to maximum temperature decrease of 13-28 °C over the northern hemisphere ice sheets (Schneider von Deimling et al., 2006). Such a moderate low-latitude cooling during the global LGM is in line with a reconstructed tropical sea surface temperature decrease of  $\sim 2$  °C (MARGO Project Members, 2009). However, the distinct depression of altitudinal vegetation belts and equilibrium line altitudes on tropical mountains inferred from terrestrial palaeoclimate records argues for a much stronger and more heterogeneous LGM cooling in the order of 2-14 °C (e.g. Farrera et al., 1999; Mark et al., 2005). Furthermore, the comparison of terrestrial palaeoclimate proxy data from different elevations indicates an amplified LGM cooling in the tropics with increasing elevation (Farrera et al., 1999; Tripathi et al., 2014). Whether the amplified cooling of tropical mountains is the consequence of a drier atmosphere and steeper lapse rate during the global LGM, is subject of ongoing scientific debate (e.g. Kageyama, Harrison, and Abe-Ouchi, 2005; Tripathi et al., 2014).

Since many endemic plant and mammal species in tropical Eastern Africa are restricted to the equatorial mountains and Ethiopian Highlands (e.g. Yalden and Largen, 1992; Miede and Miede, 1994; Dimitrov, Nogués-Bravo, and Scharff, 2012), severe climatic changes along with the formation of ice caps and valley glaciers during the cold phases of the Quaternary (e.g. Mark and Osmaston, 2008) must have had a considerable, yet unknown, impact on the habitat, distribution, and migration of afro-alpine species. To assess these impacts and elucidate

the role of abiotic and biotic factors and processes leading to the high biodiversity and endemism in the equatorial mountains and Ethiopian Highlands, a profound understanding of Quaternary high-altitude climate fluctuations and landscape evolution is crucial (e.g. Yalden and Lagen, 1992; Miehe and Miehe, 1994; Dimitrov, Nogués-Bravo, and Scharff, 2012). Furthermore, knowing the climatic and environmental context is a prerequisite for understanding the early human dispersal (e.g. Foerster et al., 2015) and potential colonisation of tropical mountains during the last glacial cycle. Tropical mountains are widely perceived as natural ecosystems that have experienced relatively little and late anthropogenic disturbance (e.g. Ellis et al., 2010). However, latest archaeological findings from the Peruvian Andes between 4300-4500 masl show that hunter-gatherers already started to colonise high-altitude environments about 12 ka years ago at the Pleistocene-Holocene transition (Rademaker et al., 2014). In light of these findings, a similar or even older occupation of the Ethiopian Highlands and equatorial East African mountains, which are located not far from the oldest hominid sites in the Great Rift Valley (e.g. Asfaw et al., 2002), seems likely.

Despite the potential and relevance of glacial and periglacial landforms for the reconstruction of past glaciations as well as palaeoclimatic and -environmental changes in Eastern Africa, they have received little attention over the last two decades (see Section 1.2.2). Thanks to the pioneering expeditions and evaluation of the first aerial images from the mid-20<sup>th</sup> century, rough overview maps of distinct moraines exists for most of the tropical mountains in Eastern Africa (Osmaston and Harrison, 2005; Mark and Osmaston, 2008), although glacial field evidence for some regions like the Bale Mountains in the southern Ethiopian Highlands is still very poor (Osmaston, Mitchell, and Osmaston, 2005). For insights into the glacial history of a mountain and the palaeoclimatic interpretation and comparison of past moraine stages and associated glacier extents from different locations, the development of robust glacial chronologies is inevitable.

With the emergence of novel dating techniques that use cosmogenic nuclides like <sup>36</sup>Cl in rocks for determining the exposure age of moraines and other landforms, it has become possible to establish glacial chronologies for individual valleys or mountains. One of the pioneering studies using in-situ <sup>36</sup>Cl for the direct dating of moraine boulders was carried out on Mount Kenya and Kilimanjaro (Shanahan and Zreda, 2000). The only other location on the African continent, where moraines have been directly dated, is one valley in the Rwenzori Mountains on the border between Uganda and the Democratic Republic of Congo (Kelly et al., 2014). Due to the absence of surface exposure ages of moraines from the Aberdare Range, Mount Elgon, and the Ethiopian Highlands as well as from additional locations in the Rwenzori Mountains, on Mount Kenya, and on Kilimanjaro, regional similarities and differences regarding the timing of local glacier advances and the onset of deglaciation remain little explored (Osmaston and Harrison, 2005; Mark and Osmaston, 2008). However, especially the knowledge about regional similarities and differences is important to reconstruct potential changes in Quaternary atmospheric circulation patterns and elucidate the role of the regional climate and topography on palaeo glacier dynamics (e.g. Zech et al., 2005; Ivy-Ochs, Kerschner, and Schlüchter, 2007; Ivy-Ochs et al., 2008; Zech et al., 2011; Akçar et al., 2014; Wirsig et al., 2016). Considering that, the

(peri)glacial landforms in the equatorial mountains and Ethiopian Highlands constitute a valuable and comprehensive archive for high-altitude palaeoglacial, -climatic and -environmental reconstructions in Eastern Africa that has not yet received the respective attention in the scientific community.

A suitable test site for studying in depth the glacial, climatic, ecological, and anthropogenic history of the tropical afro-alpine environment are the plateau-like Bale Mountains in the southern Ethiopian Highlands (Miehe and Miehe, 1994). The Bale Mountains comprise Africa's largest afro-alpine area above 4000 masl and have faced relatively little anthropogenic disturbance (Kidane, Stahlmann, and Beierkuhnlein, 2012) – an important precondition for the conservation of climatic, environmental, and archaeological archives. Erratic boulders and enigmatic large sorted patterned grounds have been reported from the central plateau and moraines and other glacial landforms like roche moutonnées from the northern valleys (Miehe and Miehe, 1994; Umer, Kebede, and Osmaston, 2004; Osmaston, Mitchell, and Osmaston, 2005). These glacial and periglacial features have so far not been mapped systematically, dated, and investigated, but constitute a valuable archive for reconstructing the local glacial and periglacial history (see Section 1.2.2). Furthermore, the Bale Mountains are home to a high number of endemic species from different taxonomic groups (Miehe and Miehe, 1994) and provide first evidence for pre-historic human activity dating to 2.5 ka (Kuzmicheva et al., 2013).

To unravel the natural and anthropogenic history of the Bale Mountains, a new interdisciplinary research unit (no. 2358) entitled “The Mountain Exile Hypothesis” has been established in 2016 with funding from the German Research Foundation (DFG) and additional financial support of the Swiss National Science Foundation (SNSF). The joint Ethio-European research unit combines expertise from the fields of archaeology, (palaeo)geoecology, (palaeo)climatology, soil sciences, and Quaternary geology. The main objectives of the research unit are to reconstruct the natural and anthropogenic history of an afro-alpine model environment, to determine the processes and drivers of palaeoclimatic and -environmental changes at high elevations, and to assess the long-term anthropogenic impact on the afro-alpine ecology and landscape evolution. Based on the hypothesis that the mountain archipelagos in Eastern Africa were a potential glacial refuge, the research unit postulates that humans started to occupy the afro-alpine environment already during the Pleistocene. The underlying assumption of this hypothesis is that tropical mountains were much wetter than the surrounding lowlands during the dry phases of the last glacial period and provided sufficient fresh water and the necessary basic food resources for humans – both criteria have yet to be proven.

This thesis is embedded as subproject “P6 – Glacial Chronology” in the research unit and aims to reconstruct the glacial and periglacial history of the Bale Mountains. More specifically, this implies the reconstruction of the former ice extent(s) by means of geomorphological mapping, the development of a glacial chronology through  $^{36}\text{Cl}$  surface exposure dating, and the investigation of recent and past periglacial landforms and processes. Knowing the extent and timing of past glaciations and periglacial processes is a prerequisite for (i) drawing conclusions about the magnitude of high-altitude tropical cooling during the last glacial period, (ii) elaborating the impact of Quaternary climate and environmental changes on the afro-alpine ecosystem, and (iii) understanding the probable early dispersal of humans into the mountains.

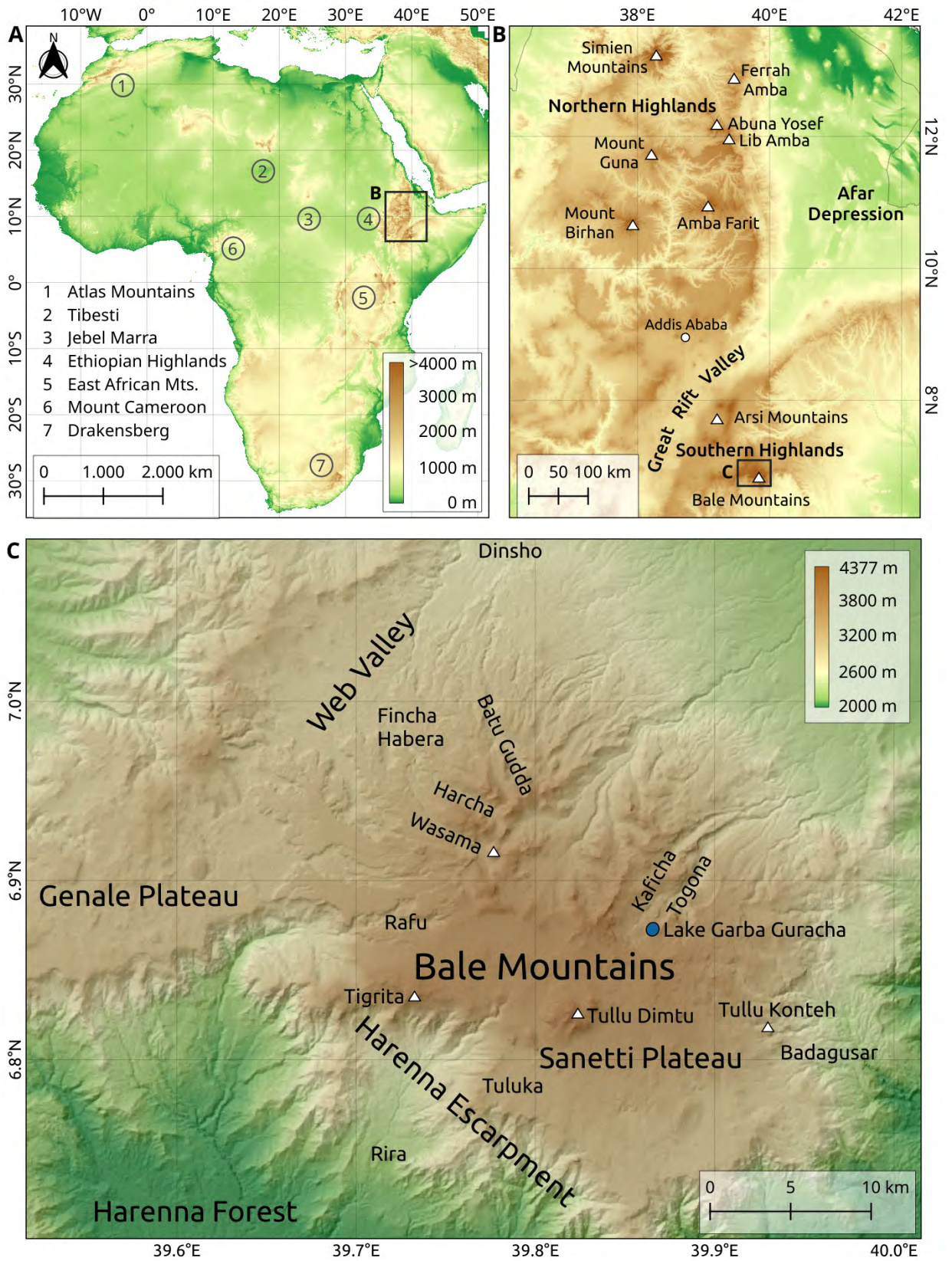


FIGURE 1.1: Topographic overview maps of Africa (A), the Ethiopian Highlands (B), and the Bale Mountains (C), showing the highest peaks and most important locations of the study area.

## 1.2 Background – The Ethiopian Highlands

### 1.2.1 Geography and climate

The Ethiopian Highlands (5–15 °N, 35–41 °E) are located in tropical Eastern Africa (see Fig. 1.1) and constitute the largest continuous elevated area above ~1500 masl on the continent. Precambrian rocks superimposed by Mesozoic marine sediments form the base of the highlands (e.g. Hurni, 1989). These rocks are covered by several hundred to thousand metre thick Cenozoic basaltic and trachytic lava flows which are associated with fissure eruptions along fractures in the Earth's crust and the formation of the Great Rift Valley (Mohr, 1983). The Great Rift Valley runs from southwest to northeast and divides the Ethiopian Highlands into a northern and southern part (see Fig. 1.1). While the northern part comprises the rugged Simien Mountains, the highest peak Ras Dejen (4543 masl) (e.g. Hurni, 1989), and numerous isolated mountains that exceed 4000 masl (e.g. Hendrickx et al., 2015), the southern part is made up of the Arsi and adjacent Bale Mountains (e.g. Mieke and Mieke, 1994; Umer, Kebede, and Osmaston, 2004; Osmaston, Mitchell, and Osmaston, 2005). Characteristic for the Bale Mountains, the main study area of this thesis, is the central afro-alpine Sanetti Plateau (see Fig. 1.1). It has a mean elevation of ~4000 masl and covers an area of more than 300 km<sup>2</sup>. The highest peak Tullu Dimtu (4377 masl) and other cinder cones and volcanic plugs rise several tens or hundreds of meters above the base level of the plateau (Osmaston, Mitchell, and Osmaston, 2005). Distinct topographic differences exist between the northern declivity and southern escarpment. The northern part of the plateau merges into broad, U-shaped valleys, whereas the southern margin is bounded by the Harennna Escarpment (Mieke and Mieke, 1994).

The climate of the Ethiopian Highlands is mainly controlled by topography and the seasonal movement of the Intertropical Convergence Zone (ITCZ) and Congo Air Boundary (CAB). Both the ITCZ and CAB define important divides in Eastern Africa between air masses of different origin (see Fig. 1.2). While the ITCZ separates the rather dry northeasterly trade winds from the moisture-laden southeasterly trade winds, the CAB describes the confluence of air masses from the Atlantic and Indian Ocean (e.g. Levin, Zipser, and Cerling, 2009; Tierney et al., 2011; Costa et al., 2014). The large-scale circulation patterns are modulated by the rugged and cool highlands. Orographic effects lead to much higher and spatially more variable precipitation in the mountains than in the Great Rift Valley and surrounding lowlands (Gebrechorkos, Hülsmann, and Bernhofer, 2019). The Ethiopian Highlands are the source of many larger rivers and thus a crucial fresh water source for the downstream population. The Blue Nile originates from Lake Tana in the northern highlands and the main tributaries of the only two perennial rivers in the Somali lowlands, Shebelle and Jubba, stem from the Bale Mountains. The current climate of the highlands is characterised by a dry season (traditionally called “Bega”) and two subsequent rainy seasons (“Belg” and “Kiremt”) which differ regionally in intensity (Mieke and Mieke, 1994). The dry season lasts roughly from November to February and the two rainy seasons prevail from March to June (“Belg”) and July to October (“Kiremt”), respectively. “Kiremt” is generally more pronounced northeast of the Great Rift Valley, including the northern highlands and catchment of the Blue Nile (Conway, 2000), whereas “Belg” plays a major role in the southern highlands, including the study area (e.g. Seleshi and Zanke, 2004).

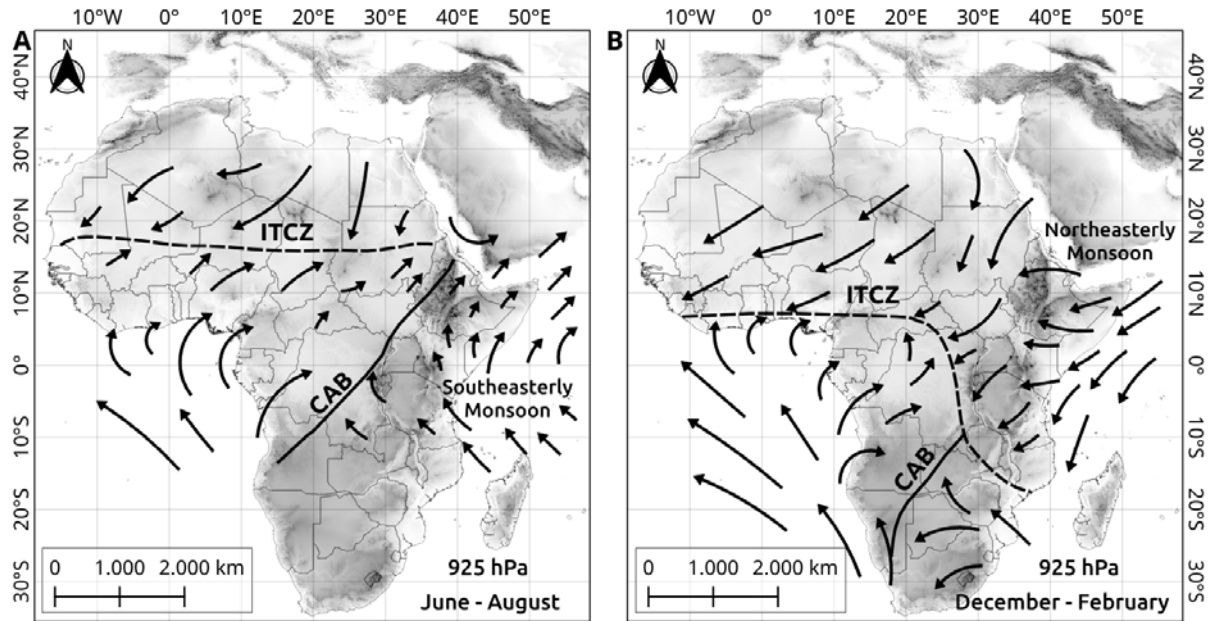


FIGURE 1.2: Schematic mean low-level (925 hPa) wind directions for the African continent as well as approximate location of the Intertropical Convergence Zone (ITCZ) and the Congo Air Boundary (CAB) during the boreal summer (A) and austral summer (B). After Levin, Zipser, and Cerling (2009).

Dry northeasterly trade winds from the Arabian Peninsula and Sea dominate in the Bale Mountains during the dry season. They are the result of the location of the ITCZ south of the equator and the formation of high-pressure cells over the Sahara and Western Asia. The northward movement of the ITCZ from its southernmost position towards the Tropic of Cancer causes a change in the prevailing wind direction from northeast to southeast (Fig. 1.2). The southeasterly monsoon transports moisture from the Indian Ocean to the southern Ethiopian Highlands and heralds the start of the rainy season “Belg” (e.g. Levin, Zipser, and Cerling, 2009). Intrusions of moist air from the Gulf of Guinea and the Congo Basin are a relevant source of precipitation in the northern highlands during the rainy season “Kiremt” (Costa et al., 2014), but their contribution to the rainfall in the Bale Mountains has yet neither been verified nor quantified. Due to the lack of long-term meteorological records from different elevations and locations in the Bale Mountains, altitudinal precipitation gradients and spatial precipitation variations are not well understood. The mean annual rainfall varies spatially between 600-1500 mm. Snow can fall on the plateau and highest peaks during the rainy season, but usually does not persist longer than a few hours or maximum some days (Miehe and Miehe, 1994).

### 1.2.2 Glacial and periglacial context

Increasing evidence of past glaciations on several of the highest mountains (>4000 masl) in the Ethiopian Highlands has been gathered over the last decades (see overview in Umer, Kebede, and Osmaston, 2004; Osmaston and Harrison, 2005). Our understanding of the glacial and periglacial history of the Ethiopian Highlands is based almost entirely on pioneering field studies and evaluation of the first aerial images from the mid and late 20<sup>th</sup> century (Nilsson, 1935;

Nilsson, 1940; Hövermann, 1954a; Hövermann, 1954b; Hastenrath, 1974; Potter, 1976; Hastenrath, 1977; Messerli et al., 1977; Hurni, 1982; Hurni, 1989; Miehe and Miehe, 1994); quasi the golden age of Quaternary high mountain research in this region. Apart from the Simien Mountains in the northernmost part of the highlands, moraines have been interpreted rather on aerial photographs than directly verified, documented, and mapped in the field (e.g. Potter, 1976; Hastenrath, 1977). During the last thirty years, the interest in the glacial and periglacial landforms has decreased. Additional geomorphological studies with a focus on the glacial and periglacial environment have only been performed in the Bale Mountains (Umer, Kebede, and Osmaston, 2004; Osmaston, Mitchell, and Osmaston, 2005) and on three mountains (Ferrah Amba, Lib Amba, and Abuna Yosef) in the northern highlands (Hendrickx et al., 2015). Despite the emergence of novel dating methods, which allow the direct dating of moraines using cosmogenic nuclides (e.g. Shanahan and Zreda, 2000), a glacial chronology has not yet been established for any of the formerly glaciated mountains in the Ethiopian Highlands.

#### *Northern Ethiopian Highlands*

The by far best studied area in terms of geomorphological mapping and photographic documentation are the Simien Mountains (Fig. 1.1) which comprise several peaks above 4400 masl, including the highest peak Ras Dejen (4543 masl) (e.g. Hastenrath, 1977; Hurni, 1982). Most of the mapped moraines are located between 4000 and 4200 masl in northwest- to northeast-facing cirques below the highest peaks, but some reach further down to 3750 masl (Hastenrath, 1974; Hurni, 1982). Based on the detailed moraine mapping, Hurni (1982) inferred that about 13 km<sup>2</sup> of the Simien Mountains were glaciated during the local LGM. This finding contradicts the first estimation of Nilsson (1940), who postulated a maximum Pleistocene ice extent of 60-440 km<sup>2</sup>. It remains unclear when glaciers reached their last glacial maximum extent in the Simien Mountains and when deglaciation set in. <sup>14</sup>C dating of organic material deposited on ground moraines in different catchments yielded a minimum age for deglaciation of 4.1 ka (Hurni, 1982). However, the author admits that the Holocene was most likely too warm for the persistence of glaciers and proposes that the Simien Mountains were already ice-free by 14-10 ka. Historical reports from the 1620s suggest that perennial snow fields still existed on top of Ras Dejen during the Holocene, at least temporarily. The last snow patches disappeared by the early 1900s (Miehe and Miehe, 1994). Today, the 0 °C isotherm is located at ~4800 masl, about 250 m above the highest peak, as the extrapolation of recent air temperature gradients shows (Hurni, 1989). Modern periglacial processes associated with nocturnal frost like the formation of needle ice or small-scale patterned grounds are restricted to the highest peaks. Altitudinal vegetation belts and the lower limit of periglacial deposits were reduced by 800 m during the last glacial cycle, corresponding to an air temperature depression of  $7.0 \pm 1.5$  °C (Hurni, 1982).

The isolated, slightly lower mountains in the northern highlands south of the Simien Mountains have yet received little attention. Evidence for glacial and periglacial activity during the last glacial period was completely lacking until recently (Osmaston, Mitchell, and Osmaston, 2005). However, geomorphological field investigations by Hendrickx et al. (2015) on Mount Ferrah Amba, Lib Amba, and Abuna Yosef (Fig. 1.1) demonstrate that glacial and periglacial processes also shaped the afro-alpine environment of the lower mountains (3500-4200 masl).

On Abuna Yosef (~4250 masl), moraine riches are preserved below the highest cliffs and are interpreted as the remains of small avalanche-fed glaciers. Furthermore, the authors report on inactive solifluction lobes, scree slopes, and frost cracks on the three investigated mountains. Based on an estimated depression of the lower limits of the periglacial belt in the order of 600 m, the authors propose a regional last glacial cooling of ~6 °C (Hendrickx et al., 2015).

### *Southern Ethiopian Highlands*

Compared to the northern Ethiopian Highlands, the Arsi and Bale Mountains south of the Great Rift Valley (see Fig. 1.1) were glaciated more extensively. The Arsi Mountains consist of the 55 km long, up to 4200 masl high, north-south running Galama Ridge and several isolated volcanoes like Mount Chilalo (4000 masl), Mount Kaka (4200 masl), and Mount Enguolo (3800 masl) (Hastenrath, 1977). Numerous valleys descend to the west, north, and east from the central Galama Ridge. Most of them contain well preserved moraine ridges which have first been mapped by Potter (1976). The mapping clearly shows that the palaeoglaciers reached further down in the eastern (3200 masl) than in the western valleys (3700 masl). Potter (1976) stated that in total more than 140 km<sup>2</sup> of ice covered the Galama Ridge during the last glacial cycle. However, it later turned out that the glaciated area was overestimated due to a scale error. Osmaston and Harrison (2005) provided a corrected estimate for the glaciated area in the order of 85 km<sup>2</sup>. The radiocarbon age of the base of a 3 m long core taken from a bog at 4040 masl suggests that the Galama Ridge became ice-free latest by 11.5 ka (Hamilton, 1982).

Although the Bale Mountains comprise with the Sanetti Plateau the largest afro-alpine area above 4000 masl (Miehe and Miehe, 1994), they have received considerably less attention than the slightly higher Simien Mountains in the northern highlands. Helmer Smeds, a Finish geographer, wrote in 1959 “[...] that the Bale plateau is in every respect terra incognita” (Smeds, 1959). He was the first to report evidence for glacial erosion and overdeepening in the Togona valley, a broad and deep U-shaped valley draining north from the plateau. Based on very little field evidence, Messerli et al. (1977) claimed in a short conference abstract that 600 km<sup>2</sup> of the Bale Mountains, including the entire Sanetti Plateau, was covered by ice during the last glacial period. Such a palaeo glaciation would have been the largest on the continent (Osmaston and Harrison, 2005). The accumulation of large erratic boulders encircling the highest peak Tullu Dimtu indicate indeed the presence of a palaeo ice cap (Miehe and Miehe, 1994), but Osmaston, Mitchell, and Osmaston (2005) concluded on the basis of apparently unglaciated features that the plateau glaciation was less extensive. They proposed that the ice cap on the plateau together with up to 10 km long glaciers in the north-draining valleys covered about 180 km<sup>2</sup> of the Bale Mountains. A range of 3750–4230 masl was estimated for the ELA of the valley glaciers and ice cap. However, a thorough geomorphological mapping of glacial landforms on the plateau, in the valleys, and along the southern escarpment is still pending. Most of the remote valleys have not yet been investigated – neither in the field nor on aerial or satellite images. Thus, the reconstructed ice extent is fraught with uncertainty. Osmaston, Mitchell, and Osmaston (2005) collected rock samples from moraines in the Togona valley and from erratic boulders on the Sanetti Plateau for surface exposure dating, but never reported or published any results. A sediment core from lake Garba Guracha, which is located at 4050 masl in a cirque

in the upper part of the formerly glaciated Togona valley, provides insights in the deglaciation history of that valley. The base of the 16 m long core was dated to 16.7 ka cal BP and implies that the cirque became ice-free latest at that time (Tiercelin et al., 2008).

The periglacial environment of the Bale Mountains has never been studied systematically. Messerli et al. (1977) reported a periglacial landscape above 4300 masl and Messerli and Winiger (1992) located the lower limits of periglacial activity during the last glacial cycle at ~3000 masl, but did not back their remarks with any concrete observations. Direct evidence for past periglacial processes on the Sanetti Plateau has been provided by Mieke and Mieke (1994). They documented large sorted stone circles (4-8 m wide) near Mount Tigrita at ~4100 masl in the southwestern part of the plateau and large sorted stone stripes (2-4 m wide and 50-80 m long) below volcanic outcrops in the southern part between 3800 and 3850 masl. Structures of similar size have neither been reported from any other mountain in Eastern Africa nor the tropics in general. The discovered stone circles and stripes on the plateau are similar to distinct patterned grounds in the permafrost regions of the high latitudes. The only known processes that can theoretically explain the formation of such large forms and patterns are the frost heave and sorting of clasts due to cyclic freezing and thawing of the ground (e.g. Kessler and Werner, 2003; Hallet, 2013). Grab (2002) interpreted the large dimension of the features on the Sanetti Plateau therefore as an indicator for past sporadic permafrost in the Bale Mountains. If the large sorted patterned grounds are interpreted as the result of frost-induced processes associated with a mean annual ground temperature  $<0^{\circ}\text{C}$ , these features could serve as palaeothermometer. However, that would require a better understanding of the genesis of these structures and information on the present-day ground temperature variations as modern reference for the temperature reconstruction. Field observations of needle ice along saturated stream banks and active small-scale patterned grounds on the plateau prove that superficial frost still occurs in the Bale Mountains. Nocturnal frost is also verified through short-term ground temperature measurements between December 1989 and March 1990, but frost depth, seasonal ground temperature variations, and elevational temperature gradients have not yet been constrained (Mieke and Mieke, 1994).

As previous studies have already pointed out, the plateau-like topography of the Bale Mountains was favourable for the formation of one of the largest glaciations and periglacial environments on the African continent during the last glacial period (Mieke and Mieke, 1994; Osmaston, Mitchell, and Osmaston, 2005). The comprehensive and diverse repertoire of glacial and periglacial landforms provides great potential for insights into past cryogenic processes and the reconstruction of the palaeolandscape and -climate. Considering the large unexplored areas in the valleys and on the plateau, the discovery of additional (peri)glacial landforms is likely and would help to better constrain the extent and characteristics of the former ice extent and periglacial environment. Furthermore, the erratic boulders on the plateau and in the valleys seem appropriate for cosmogenic nuclide dating and the development of a glacial chronology (Osmaston, Mitchell, and Osmaston, 2005). A glacial chronology from the Bale Mountains would be the first one for the entire Ethiopian Highlands and enable the comparison with the timing of glacial stages in the equatorial mountains in Eastern Africa. Thus, this thesis aims for a detailed mapping, dating, and interpretation of glacial and periglacial features on the Sanetti Plateau, along the southern escarpment, and in the western, northern, and eastern valleys.

### 1.3 Objectives of the thesis

This thesis addresses the following specific research questions which relate to the glacial and periglacial history of the Bale Mountains and are closely linked to the main objectives and hypotheses of the joint Ethio-European DFG Research Unit 2358 “The Mountain Exile Hypothesis” (see Section 1.1):

1. What was the extent of the ice cover in the Bale Mountains during the last glacial period?
2. When were the Bale Mountains glaciated? When did the glaciers reach their maximum expansion? When did deglaciation set in?
3. When, how, and under which climatic and environmental conditions did the relict large sorted stone stripes and polygons on the Sanetti Plateau form?
4. Which cooling can be inferred from the presence of glacial and periglacial landforms and what does it imply for the palaeoclimate and -ecology of tropical mountains?
5. How did the palaeoclimate and -environment look like at the time when humans started to colonise the Bale Mountains?

To tackle these questions, the following objectives (O) and work packages (WP) were defined:

- O1: Reconstruction of the extent of past glaciations in the Bale Mountains.
- WP1: Geomorphological mapping of moraines, erratic boulders, and other glacial landforms like *roche moutonnées* both in the field and on high-resolution satellite images.
- O2: Development of a glacial chronology for the Bale Mountains.
- WP2:  $^{36}\text{Cl}$  surface exposure dating of moraine boulders in the valleys and on the plateau.
- O3: Investigation of relict and modern periglacial landforms and processes in the Bale Mountains.
- WP3: Geomorphological mapping of modern and relict periglacial landforms both in the field and on high-resolution satellite images.
- WP4: Experimental  $^{36}\text{Cl}$  surface exposure dating of the relict large sorted stone stripes to determine the stabilisation age of these features.
- WP5: Excavation of a cross-section profile in tandem with ground-penetrating radar measurements to study the interior structure and genesis of the stone stripes.
- WP6: Installation of a ground temperature measurement network to analyse present frost occurrence and seasonal ground temperature variations.
- O4: Reconstruction of palaeotemperatures in the Bale Mountains.
- WP7: Estimation of the air temperature depression during the local last glacial maximum through the comparison of the reconstructed equilibrium line altitude and recent meteorological observations.
- WP8: Estimation of the minimum air and ground temperature depression required as precondition for the formation of the relict large sorted patterned grounds.

## 1.4 Structure of the thesis

Three scientific articles that are either published in or under review for internationally renowned peer-reviewed journals constitute the core of this cumulative thesis. Each article corresponds to a separate chapter (2, 3, 4) and is embedded in the broader scientific context through the introduction (1), synthesis (5), conclusion (6), and outlook (7), which form the frame of the thesis.

**Chapter 1** gives an overview of the state of knowledge at the beginning of the project, emphasises the most important scientific challenges, introduces the study area, and defines the objectives of the thesis.

**Chapter 2** is a manuscript currently in revision (after a first review round) for publication in the open-access journal *Science Advances*. The manuscript is entitled “Asynchronous Late Pleistocene glacier fluctuations in tropical Eastern Africa” and presents a first comprehensive glacial reconstruction and chronology for the southern Ethiopian Highlands (comprising the Bale Mountains and adjacent Arsi Mountains) based on geomorphological mapping and  $^{36}\text{Cl}$  surface exposure dating of moraines.

**Chapter 3** is a manuscript entitled “Implications of present ground temperatures and relict stone stripes in the Ethiopian Highlands for the palaeoclimate of the tropics”. It is currently under review for publication in the open-access journal *Earth Surface Dynamics* and elaborates ground temperature variations as well as the origin and implications of enigmatic large sorted stone stripes and polygons on the Sanetti Plateau in the Bale Mountains.

**Chapter 4** is a research article entitled “Middle Stone Age foragers resided in high elevations of the glaciated Bale Mountains, Ethiopia” (Ossendorf et al., 2019) that evolved out of an interdisciplinary collaboration within the joint Ethio-European DFG Research Unit 2358 “The Mountain Exile Hypothesis” and was published in *Science*. The article reports on the earliest evidence of a prehistoric high-elevation residential site worldwide and highlights that Middle Stone Age foragers in the Bale Mountains resided in close proximity to the palaeo glaciers and made use of the available alpine resources.

**Chapter 5** provides a synthesis of the main findings, discusses their implications for the glacial, climatic, environmental, and human history of tropical mountains and highlands in Eastern Africa, and introduces new research questions arising from the thesis and collaborations within the joint Ethio-European DFG Research Unit 2358 “The Mountain Exile Hypothesis”.

**Chapter 6** briefly summarises the key findings, implications, and conclusions of the thesis.

**Chapter 7** outlines ideas for future research.

## References

- Akçar, N. et al. (2014). "Glacier Response to the Change in Atmospheric Circulation in the Eastern Mediterranean during the Last Glacial Maximum". In: *Quat. Geochronol.* 19, pp. 27–41. DOI: 10.1016/j.quageo.2013.09.004.
- Asfaw, B. et al. (2002). "Remains of Homo Erectus from Bouri, Middle Awash, Ethiopia". In: *Nature* 416.6878, pp. 317–320. DOI: 10.1038/416317a.
- Barrows, T. T. et al. (2011). "Late Pleistocene Glaciation of the Mt Giluwe Volcano, Papua New Guinea". In: *Quat. Sci. Rev.* 30.19-20, pp. 2676–2689. DOI: 10.1016/j.quascirev.2011.05.022.
- Conway, D. (2000). "The Climate and Hydrology of the Upper Blue Nile River". In: *Geogr. J.* 166.1, pp. 49–62. DOI: 10.1111/j.1475-4959.2000.tb00006.x.
- Costa, K. et al. (2014). "Isotopic Reconstruction of the African Humid Period and Congo Air Boundary Migration at Lake Tana, Ethiopia". In: *Quat. Sci. Rev.* 83, pp. 58–67. DOI: 10.1016/j.quascirev.2013.10.031.
- Dimitrov, D., D. Nogués-Bravo, and N. Scharff (2012). "Why Do Tropical Mountains Support Exceptionally High Biodiversity? The Eastern Arc Mountains and the Drivers of Saintpaulia Diversity". In: *PLoS ONE* 7.11, pp. 1–15. DOI: 10.1371/journal.pone.0048908.
- Ellis, E. C. et al. (2010). "Anthropogenic Transformation of the Biomes, 1700 to 2000: Anthropogenic Transformation of the Biomes". In: *Glob. Ecol. Biogeogr.* Pp. 589–606. DOI: 10.1111/j.1466-8238.2010.00540.x.
- Farrera, I. et al. (1999). "Tropical Climates at the Last Glacial Maximum: A New Synthesis of Terrestrial Palaeoclimate Data. I. Vegetation, Lake-Levels and Geochemistry". In: *Clim. Dyn.* 15.11, pp. 823–856. DOI: 10.1007/s003820050317.
- Foerster, V. et al. (2015). "Environmental Change and Human Occupation of Southern Ethiopia and Northern Kenya during the Last 20,000 Years". In: *Quat. Sci. Rev.* 129, pp. 333–340. DOI: 10.1016/j.quascirev.2015.10.026.
- Gebrechorkos, S. H., S. Hülsmann, and C. Bernhofer (2019). "Long-Term Trends in Rainfall and Temperature Using High-Resolution Climate Datasets in East Africa". In: *Sci. Rep.* 9.1, pp. 1–9. DOI: 10.1038/s41598-019-47933-8.
- Grab, S. (2002). "Glacial and Periglacial Phenomena in Ethiopia: A Review". In: *Permafrost Periglacial Process.* 13.1, pp. 71–76. DOI: 10.1002/ppp.405.
- Hallet, B. (2013). "Stone Circles: Form and Soil Kinematics". In: *Proc. R. Soc. A* 371.2004, p. 20120357. DOI: 10.1098/rsta.2012.0357.
- Hamilton, A.C. (1982). *Environmental History of East Africa: a Study of the Quaternary*. London. DOI: 10.2307/2259986.
- Hastenrath, S. (1974). "Glaziale Und Periglaziale Formbildung in Hoch-Semyen, Nord-Äthiopien". In: *Erdkunde* 28, pp. 176–186.
- Hastenrath, S. (1977). "Pleistocene Mountain Glaciation in Ethiopia". In: *J. Glaciol.* 18.79, pp. 309–313.

- Hendrickx, H. et al. (2015). "Glacial and Periglacial Geomorphology and Its Paleoclimatological Significance in Three North Ethiopian Mountains, Including a Detailed Geomorphological Map". In: *Geomorphology* 246, pp. 156–167. DOI: 10.1016/j.geomorph.2015.05.005.
- Hövermann, J. (1954a). "Über die Höhenlage der Schneegrenze in Äthiopien und ihre Schwankungen in historischer Zeit". In: *Nachrichten der Akademie der Wissenschaften in Göttingen* 6, pp. 111–137.
- Hövermann, J. (1954b). "Über glaziale und periglaziale Erscheinungen in Erithrea und Nordabessinien". In: *Veröff. der Akad. für Raumforschung und Landesplanung Abh.* 28, pp. 87–111.
- Hurni, H. (1982). "Simen Mountains - Ethiopia, Vol II (in German): Climate and Dynamics of Altitudinal Belts from the Last Cold Period to the Present Day (Part II in Co-Authorship with Peter Staehli)". In: *Geographica Bernensia* G 13, pp. 4–196.
- Hurni, H. (1989). "Late Quaternary of Simien and Other Mountains in Ethiopia". In: *Quaternary and Environmental Research on East African Mountains*. Rotterdam / Brookfield: Balkema, pp. 105–120.
- Ivy-Ochs, S., H. Kerschner, and C. Schlüchter (2007). "Cosmogenic Nuclides and the Dating of Lateglacial and Early Holocene Glacier Variations: The Alpine Perspective". In: *Quat. Int.* 164-165, pp. 53–63. DOI: 10.1016/j.quaint.2006.12.008.
- Ivy-Ochs, S. et al. (2008). "Chronology of the Last Glacial Cycle in the European Alps". In: *J. Quaternary Sci.* 23.6-7, pp. 559–573. DOI: 10.1002/jqs.1202.
- Kageyama, M., S. P. Harrison, and A. Abe-Ouchi (2005). "The Depression of Tropical Snowlines at the Last Glacial Maximum: What Can We Learn from Climate Model Experiments?" In: *Quat. Int.* 138-139, pp. 202–219. DOI: 10.1016/j.quaint.2005.02.013.
- Kaser, G. (1999). "A Review of the Modern Fluctuations of Tropical Glaciers". In: *Glob. Planet. Chang.* 22.1-4, pp. 93–103. DOI: 10.1016/S0921-8181(99)00028-4.
- Kelly, M. A. et al. (2014). "Expanded Glaciers during a Dry and Cold Last Glacial Maximum in Equatorial East Africa". In: *Geology* 42.6, pp. 519–522. DOI: 10.1130/G35421.1.
- Kessler, M. A. and B. T. Werner (2003). "Self-Organization of Sorted Patterned Ground". In: *Science* 299.5605, pp. 380–383. DOI: 10.1126/science.1077309.
- Kidane, Y., R. Stahlmann, and C. Beierkuhnlein (2012). "Vegetation Dynamics, and Land Use and Land Cover Change in the Bale Mountains, Ethiopia". In: *Environ. Monit. Assess.* 184.12, pp. 7473–7489. DOI: 10.1007/s10661-011-2514-8.
- Kuzmicheva, E. A. et al. (2013). "Holocene Hyrax Dung Deposits in the Afroalpine Belt of the Bale Mountains (Ethiopia) and Their Palaeoclimatic Implication". In: *Environ. Archaeol.* 18.1, pp. 72–81. DOI: 10.1179/1461410313Z.00000000018.
- Levin, N. E., E. J. Zipser, and T. E. Cerling (2009). "Isotopic Composition of Waters from Ethiopia and Kenya: Insights into Moisture Sources for Eastern Africa". In: *J. Geophys. Res.* 114, pp. 1–13. DOI: 10.1029/2009JD012166.
- MARGO Project Members (2009). "Constraints on the Magnitude and Patterns of Ocean Cooling at the Last Glacial Maximum". In: *Nat. Geosci.* 2.2, pp. 127–132. DOI: 10.1038/ngeo411.
- Mark, B. G. and H. A. Osmaston (2008). "Quaternary Glaciation in Africa: Key Chronologies and Climatic Implications". In: *J. Quat. Sci.* 23.6-7, pp. 589–608. DOI: 10.1002/jqs.1222.

- Mark, B. G. et al. (2005). "Tropical Snowline Changes at the Last Glacial Maximum: A Global Assessment". In: *Quat. Int.* 138-139, pp. 168–201. DOI: 10.1016/j.quaint.2005.02.012.
- Messerli, B. and M. Winiger (1992). "Climate, Environmental Change, and Resources of the African Mountains from the Mediterranean to the Equator". In: *Mt. Res. Dev.* 12.4, pp. 315–336. DOI: 10.2307/3673683.
- Messerli, B. et al. (1977). "Bale Mountains, the Largest Pleistocene Mountain Glacier System of Ethiopia". In: *INQUA abstracts*.
- Miehe, S. and G. Miehe (1994). *Ericaceous Forests and Heathlands in the Bale Mountains of South Ethiopia - Ecology and Man's Impact*. Hamburg: Stiftung Walderhaltung in Afrika.
- Mohr, P. (1983). "Ethiopian Flood Basalt Province". In: *Nature* 303, pp. 577–584. DOI: 10.1038/303577a0.
- Mölg, T., N. J. Cullen, and G. Kaser (2009). "Solar Radiation, Cloudiness and Longwave Radiation over Low-Latitude Glaciers: Implications for Mass-Balance Modelling". In: *J. Glaciol.* 55.190, pp. 292–302. DOI: 10.3189/002214309788608822.
- Mölg, T., C. Georges, and G. Kaser (2003). "The Contribution of Increased Incoming Shortwave Radiation to the Retreat of the Rwenzori Glaciers, East Africa, during the 20th Century". In: *Int. J. Climatol.* 23.3, pp. 291–303. DOI: 10.1002/joc.877.
- Mölg, T. and D. R. Hardy (2004). "Ablation and Associated Energy Balance of a Horizontal Glacier Surface on Kilimanjaro". In: *J. Geophys. Res.* 109.D16. DOI: 10.1029/2003JD004338.
- Mölg, T. et al. (2008). "Mass Balance of a Slope Glacier on Kilimanjaro and Its Sensitivity to Climate". In: *Int. J. Climatol.* 28.7, pp. 881–892. DOI: 10.1002/joc.1589.
- Nicholson, L. I. et al. (2013). "Micrometeorological Conditions and Surface Mass and Energy Fluxes on Lewis Glacier, Mt Kenya, in Relation to Other Tropical Glaciers". In: *The Cryosphere* 7.4, pp. 1205–1225. DOI: 10.5194/tc-7-1205-2013.
- Nilsson, E. (1935). "Traces of Ancient Changes of Climate in East Africa. Preliminary Report". In: *Geogr. Ann.* 17, p. 1. DOI: 10.2307/519950.
- Nilsson, E. (1940). "Ancient Changes of Climate in British East Africa and Abyssinia. A Study of Ancient Lakes and Glaciers". In: *Geogr. Ann.* 22, p. 1. DOI: 10.2307/519977.
- Osmaston, H. (2004). "Quaternary Glaciations in the East African Mountains". In: *Developments in Quaternary Sciences*. Vol. 2. Elsevier, pp. 139–150.
- Osmaston, H. A. and S. P. Harrison (2005). "The Late Quaternary Glaciation of Africa: A Regional Synthesis". In: *Quat. Int.* 138-139, pp. 32–54. DOI: 10.1016/j.quaint.2005.02.005.
- Osmaston, H. A., W. A. Mitchell, and J. A. N. Osmaston (2005). "Quaternary Glaciation of the Bale Mountains, Ethiopia". In: *J. Quat. Sci.* 20.6, pp. 593–606. DOI: 10.1002/jqs.931.
- Potter, E. C. (1976). "Pleistocene Glaciation in Ethiopia: New Evidence". In: *J. Glaciol.* 17.75, pp. 147–150.
- Rademaker, K. et al. (2014). "Paleoindian Settlement of the High-Altitude Peruvian Andes". In: *Science* 346.6208, pp. 466–469. DOI: doi:10.1126/science.1258260.
- Schneider von Deimling, T. et al. (2006). "How Cold Was the Last Glacial Maximum?" In: *Geophys. Res. Lett.* 33.14, pp. 1–5. DOI: 10.1029/2006GL026484.
- Seleshi, Y. and U. Zanke (June 2004). "Recent Changes in Rainfall and Rainy Days in Ethiopia". In: *Int. J. Climatol.* 24.8, pp. 973–983. DOI: 10.1002/joc.1052.

- Shakun, J. D. and A. E. Carlson (2010). "A Global Perspective on Last Glacial Maximum to Holocene Climate Change". In: *Quat. Sci. Rev.* 29, pp. 1801–1816. DOI: 10.1016/j.quascirev.2010.03.016.
- Shanahan, D. F. and M. Zreda (2000). "Chronology of Quaternary Glaciations in East Africa". In: *Earth Planet. Sci. Lett.* 177, pp. 23–42.
- Smeds, Helmer (1959). "The Batu Mountains of the Bale Plateau, Ethiopia". In: *Alpine Journal*, pp. 218–227.
- Tiercelin, J.-J. et al. (2008). "High-Resolution Sedimentary Record of the Last Deglaciation from a High-Altitude Lake in Ethiopia". In: *Quaternary Science Reviews* 27.5, pp. 449–467.
- Tierney, J. E. et al. (2011). "Late Quaternary Behavior of the East African Monsoon and the Importance of the Congo Air Boundary". In: *Quat. Sci. Rev.* 30.7-8, pp. 798–807. DOI: 10.1016/j.quascirev.2011.01.017.
- Tripathi, A. K. et al. (2014). "Modern and Glacial Tropical Snowlines Controlled by Sea Surface Temperature and Atmospheric Mixing". In: *Nat. Geosci.* 7.3, pp. 205–209. DOI: 10.1038/ngeo2082.
- Umer, M., S. Kebede, and H. Ostmaston (2004). "Quaternary Glacial Activity on the Ethiopian Mountains". In: *Quaternary Glaciations*, pp. 171–174.
- Veettil, B. K. and U. Kamp (2019). "Global Disappearance of Tropical Mountain Glaciers: Observations, Causes, and Challenges". In: *Geosciences* 9.5, pp. 1–25. DOI: 10.3390/geosciences9050196.
- Wirsig, C. et al. (2016). "Dating the Onset of LGM Ice Surface Lowering in the High Alps". In: *Quat. Sci. Rev.* 143, pp. 37–50. DOI: 10.1016/j.quascirev.2016.05.001.
- Yalden, D. W. and M. J. Lagen (1992). "The Endemic Mammals of Ethiopia". In: *Mammal Rev.* 22.3-4, pp. 115–150. DOI: 10.1111/j.1365-2907.1992.tb00128.x.
- Zech, R. et al. (2005). "Late Quaternary Glacial and Climate History of the Pamir Mountains Derived from Cosmogenic  $^{10}\text{Be}$  Exposure Ages". In: *Quat. Res.* 64.02, pp. 212–220. DOI: 10.1016/j.yqres.2005.06.002.
- Zech, R. et al. (2011). "Early Last Glacial Maximum in the Southern Central Andes Reveals Northward Shift of the Westerlies at ~39 Ka". In: *Clim. Past* 7.1, pp. 41–46. DOI: 10.5194/cp-7-41-2011.

## Chapter 2

# Asynchronous Late Pleistocene glacier fluctuations in tropical Eastern Africa

Alexander R. Groos<sup>1</sup>, Naki Akçar<sup>2</sup>, Serdar Yesilyurt<sup>2,3</sup>, Georg Miehe<sup>4</sup>, Christof Vockenhuber<sup>5</sup>, Heinz Veit<sup>1</sup>

<sup>1</sup>Institute of Geography, University of Bern, Switzerland

<sup>2</sup>Institute of Geological Sciences, University of Bern, Switzerland

<sup>3</sup>Department of Geography, Ankara University, Turkey

<sup>4</sup>Department of Geography, Philipps University of Marburg, Germany

<sup>5</sup>Laboratory of Ion Beam Physics, ETH Zurich, Switzerland

*Author contributions: A.R.G., N.A., H.V., and G.M. designed the research concept and were involved in the glacial geomorphological mapping. A.R.G., N.A., and H.V. conducted field work and sampled moraine boulders in the Bale and Arsi Mountains. A.R.G., S.Y., and N.A. processed the rock samples in the laboratory. C.V. and his team performed the <sup>36</sup>Cl measurements at the AMS in Zurich. A.R.G. analysed the data and prepared the manuscript and figures with contributions from all authors.*

In revision for publication in *Science Advances*

Submitted: 16<sup>th</sup> March 2020

## Abstract

Today's ice caps and glaciers in Africa are restricted to the highest tropical peaks, but during the Late Pleistocene, several mountain ranges on the continent were extensively glaciated. However, little is known about regional differences in the timing and extent of past glaciations and the impact of palaeoclimatic changes on the afro-alpine environment and early dispersal of hunter-gatherers into the high mountains (47-31 ka). Here, we present a comprehensive glacial chronology for the Ethiopian Highlands in comparison with other East African Mountains. In the Ethiopian Highlands, the local Last Glacial Maximum (LGM) occurred at  $39.6 \pm 9.9$  ka, well before the global LGM, and was accompanied by a temperature depression of  $5.1 \pm 0.7$  °C and 700 m downward shift of the alpine vegetation belt, reshaping the human and natural habitats. The glacial chronological comparison reveals that glaciers in Eastern Africa responded asynchronously to Late Pleistocene climate changes and suggests hydroclimatic variations as crucial driver for past tropical glacier fluctuations.

## 2.1 Introduction

The remaining glaciers in Africa are restricted to the summit areas of Mount Kenya, Kilimanjaro and Rwenzori Mountains (Kaser, 1999; Kaser and Osmaston, 2002), but during the cold periods of the Pleistocene, several mountain ranges on the continent were extensively glaciated (Osmaston and Harrison, 2005; Mark and Osmaston, 2008; Hastenrath, 2009). Well-preserved moraine sequences and other glacial landforms testify multiple glacier advances in the High Atlas, East African Mountains and Ethiopian Highlands (Fig. 2.1). Since past glacial fluctuations mainly reflect long-term changes in temperature, precipitation, cloudiness and insolation, glacial landforms are an ideal proxy for reconstructing palaeoclimatic variations and palaeoecological changes in alpine environments (Mark and Osmaston, 2008). Studying the climate and glacial history of the mountains in Eastern Africa is of particular interest since the topography at both sides of the East African Rift favored the formation of numerous ice caps and valley glaciers accompanied by an amplified regional cooling at high elevations (Osmaston and Harrison, 2005; Mark and Osmaston, 2008; Hastenrath, 2009; Loomis et al., 2017). Furthermore, assessing the impacts of past glaciations on the afro-alpine environment plays a key role in understanding the causes for the early migration of Middle Stone Age foragers into the high elevations of the glaciated Ethiopian Highlands 47-31 ka ago (Ossendorf et al., 2019). Information on severe palaeoecological changes in the afro-alpine environment during the Pleistocene are also of high relevance for elucidating why tropical mountains are biodiversity hotspots. The high number of endemic species in the tropical mountains is associated with pre-Quaternary speciation processes and assumed environmental stability over the Pleistocene (Dimitrov, Nogués-Bravo, and Scharff, 2012). However, latest glacial chronological and palaeoclimatological studies from the East African Mountains and Ethiopian Highlands challenge the concept of climatically stable mountaintops as they provide evidence for multiple glacier advances, a pronounced cooling, and depression of altitudinal vegetation belts during the Late

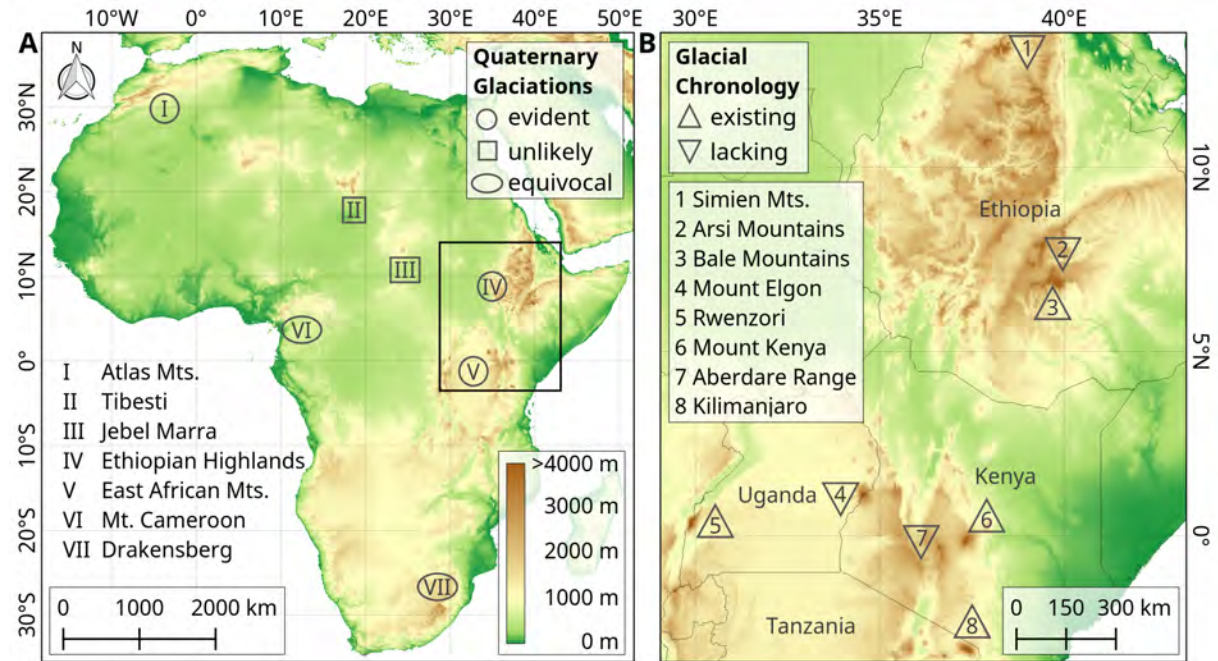


FIGURE 2.1: Quaternary glaciations in Africa. (A) Topographic map showing mountain localities with clear and controversial geomorphological evidence of past glaciations (Osmaston and Harrison, 2005; Mark and Osmaston, 2008). (B) Overview of glacial chronologies from the East African Mountains and Ethiopian Highlands based on  $^{36}\text{Cl}$  and  $^{10}\text{Be}$  cosmogenic nuclide dating (Shanahan and Zreda, 2000; Kelly et al., 2014; Jackson et al., 2019; Ossendorf et al., 2019).

Pleistocene (Shanahan and Zreda, 2000; Kelly et al., 2014; Jackson et al., 2019; Ossendorf et al., 2019).

A recent comparative study focusing on palaeo glacier fluctuations in the Rwenzori Mountains and Andes suggests that tropical glaciers reached their last glacial maxima at  $\sim 29\text{-}20$  ka and hypothesises that high-latitude warming initiated the onset of deglaciation in the tropics at  $\sim 20\text{-}19$  ka (Jackson et al., 2019). However, first  $^{36}\text{Cl}$  surface exposure ages of erratic boulders from two moraine sequences in the Bale Mountains (Ethiopian Highlands) indicate a more complex and non-uniform response of tropical glaciers to Late Pleistocene climate changes (Ossendorf et al., 2019). The glaciers in the northwestern valleys of the Bale Mountains reached their local Last Glacial Maximum (LGM) already at  $\sim 50\text{-}40$  ka during Marine Isotope Stage (MIS) 3. Any evidence for major glacier advances during the global LGM ( $22.1 \pm 4.3$  ka) (Shakun and Carlson, 2010) is missing (Ossendorf et al., 2019). Considering the thermal homogeneity of the tropical atmosphere (Kaser and Osmaston, 2002), the looming discrepancy between the timing of the local LGM in the East African Mountains ( $1^\circ\text{N}\text{-}3^\circ\text{S}$ ) and more northern Ethiopian Highlands ( $7\text{-}13^\circ\text{N}$ ) points towards hydroclimatic variations as a crucial driver for past tropical glacial fluctuations. Hydroclimatic variations in the region are controlled by the seasonal movement of the Intertropical Convergence Zone (ITCZ) and zonal shift of the Congo Air Boundary, which defines the convergence zone of air masses from the Indian Ocean and Atlantic (Levin, Zipser, and Cerling, 2009; Tierney et al., 2011; Costa et al., 2014). Nevertheless, to approve regional differences in the timing and extent of past glaciations in Eastern

Africa and detect changes in large-scale tropical atmospheric circulation patterns, a representative glacial chronology of the Ethiopian Highlands including absolute moraine ages from valleys and mountains over a wide area is necessary.

Here, we present a novel glacial chronology for the Ethiopian Highlands based on 21 previously published (Ossendorf et al., 2019) and 60 new  $^{36}\text{Cl}$  surface exposure ages of moraine boulders and periglacial features from the Bale and adjacent Arsi Mountains. By combining the new  $^{36}\text{Cl}$  ages from the Ethiopian Highlands with available  $^{36}\text{Cl}$  and  $^{10}\text{Be}$  glacial chronologies from Mount Kenya, Kilimanjaro and the Rwenzori Mountains (Shanahan and Zreda, 2000; Kelly et al., 2014; Jackson et al., 2019), this study aims to investigate the response of tropical glaciers in Eastern Africa to Late Pleistocene climate changes and elaborate the palaeoclimatic, palaeoecological and archaeological implications of past glacial fluctuations. Since the extent of past glaciations is not only determined by the prevailing climatic conditions, but also by topography and the potential surface area above the former Equilibrium Line Altitude (ELA) (Cunningham et al., 2019), this study also includes a first terrain analysis of the most extensively glaciated African mountains (Osmaston and Harrison, 2005). Considering the varying hypsography of the mountains is crucial for comparing and interpreting regional differences of past glacial fluctuations and drawing conclusions about the palaeoclimate.

## 2.2 Results

### 2.2.1 Hypsography of Africa's glaciated mountains

Africa's high mountains cover less than 0.1% of the entire area of the continent and are located mainly along the East African Rift (Fig. 2.1). Exceptions are the High Atlas in northwestern, Mount Cameroon in western, and Drakensberg in southern Africa as well as the Tibesti in the Sahara and Jebel Marra in the Sahel. The afro-alpine area  $>3500$  masl equals to 0.016 % ( $5041 \text{ km}^2$ ) and the area  $>4000$  masl to 0.0028 % ( $880 \text{ km}^2$ ) of the continent's total area of  $\sim 31.6$  million  $\text{km}^2$ .

The extent, elevation range and hypsography of the Ethiopian Highlands, East African Mountains and High Atlas in northern Africa differ widely (Fig. 2.2). The Ethiopian Highlands (Arsi, Bale and Simien Mountains) reach maximum elevations between 4000 and 4500 masl. In contrast, the highest East African Mountains (Kilimanjaro, Mount Kenya and Rwenzori) rise above 5000 masl and are defined by their topographic prominence and small area-elevation ratio. Africa's highest mountain Kilimanjaro reaches almost 5900 masl and covers  $387 \text{ km}^2$   $>3500$  masl and  $190 \text{ km}^2$   $>4000$  masl. Mount Kenya and the Rwenzori Mountains also cover an area of more than  $320 \text{ km}^2$   $>3500$  masl and  $120 \text{ km}^2$   $>4000$  masl. Even though the Ethiopian Highlands are lower in elevation, they comprise the largest part of Africa's alpine environment due to the broad base of the mountains (Fig. 2.2). The hypsography of the Bale Mountains is exceptional because individual elevation bands (plateaus) protrude and its surface area does not decrease evenly with elevation (Fig. 2.2). Due to the broad base and extent of the central plateau, the Bale Mountains represent Africa's largest solitary alpine environment. They cover 8 % of the continent's area  $>3000$  masl, 22 % of the area  $>3500$  masl and 25 % of the area

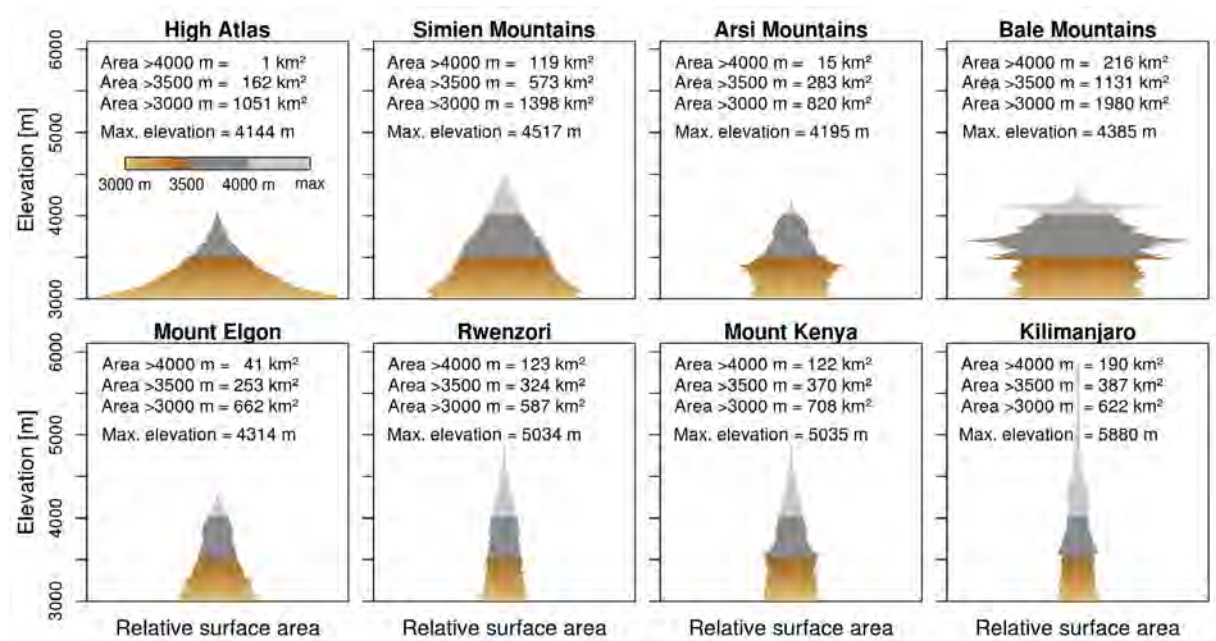


FIGURE 2.2: Hypsography of the eight African mountains that were most extensively glaciated during the Late Pleistocene. Stated maximum elevations may differ by several meters from the real height of the mountains since the entire terrain analysis is based on the evaluation of digital surface models with a pixel resolution of  $\sim 90$  m.

> 4000 masl. For the High Atlas, a broad base and exponential decrease of surface area with elevation is characteristic. While 1051 km<sup>2</sup> of the mountain range are located above 3000 masl and 162 km<sup>2</sup> above 3500 masl, only 1 km<sup>2</sup> exceeds 4000 masl.

The varying hypsography of the mountains has implications for present and past glaciations on the continent. Under present climatic conditions, the ELA is located far above the maximum elevation of most of the African mountains. Glaciers can therefore only persist in the summit areas of the three highest peaks. However, when the ELA decreases below 4000-4500 masl as during the last glaciation (Osmaston and Harrison, 2005), the potential surface area in Africa for the accumulation of snow and formation of ice increases drastically. While the entire area >5000 masl on the continent is limited to 22 km<sup>2</sup> and the area between 4500-5000 masl to 61 km<sup>2</sup>, 796 km<sup>2</sup> are available for potential glaciations between 4000-4500 masl and additional 4161 km<sup>2</sup> between 3500-4000 masl.

### 2.2.2 Glacial history of the Bale Mountains

The central Sanetti Plateau above 3800 masl in the Bale Mountains hosts several glacial and periglacial features that are remarkable for the tropics (Fig. 2.3, Fig. A.1). Large boulders (up to 8 m wide and 5 m high) encircle the highest peak (Tullu Dimtu, 4377 masl) in the central part of the plateau at a distance of about 2 and 2.5 km (Fig. 2.3, Fig. A.2). Due to their shape and distribution around the peak, it is likely that the boulders originate from a former ice cap and were deposited along the ice margin. The scatter of erratic boulders on the Sanetti Plateau has previously been defined as Big Boulder Moraine (Miehe and Miehe, 1994). Outside the Big Boulder Moraine, erratic boulders are completely lacking. Subglacial till and small depressions

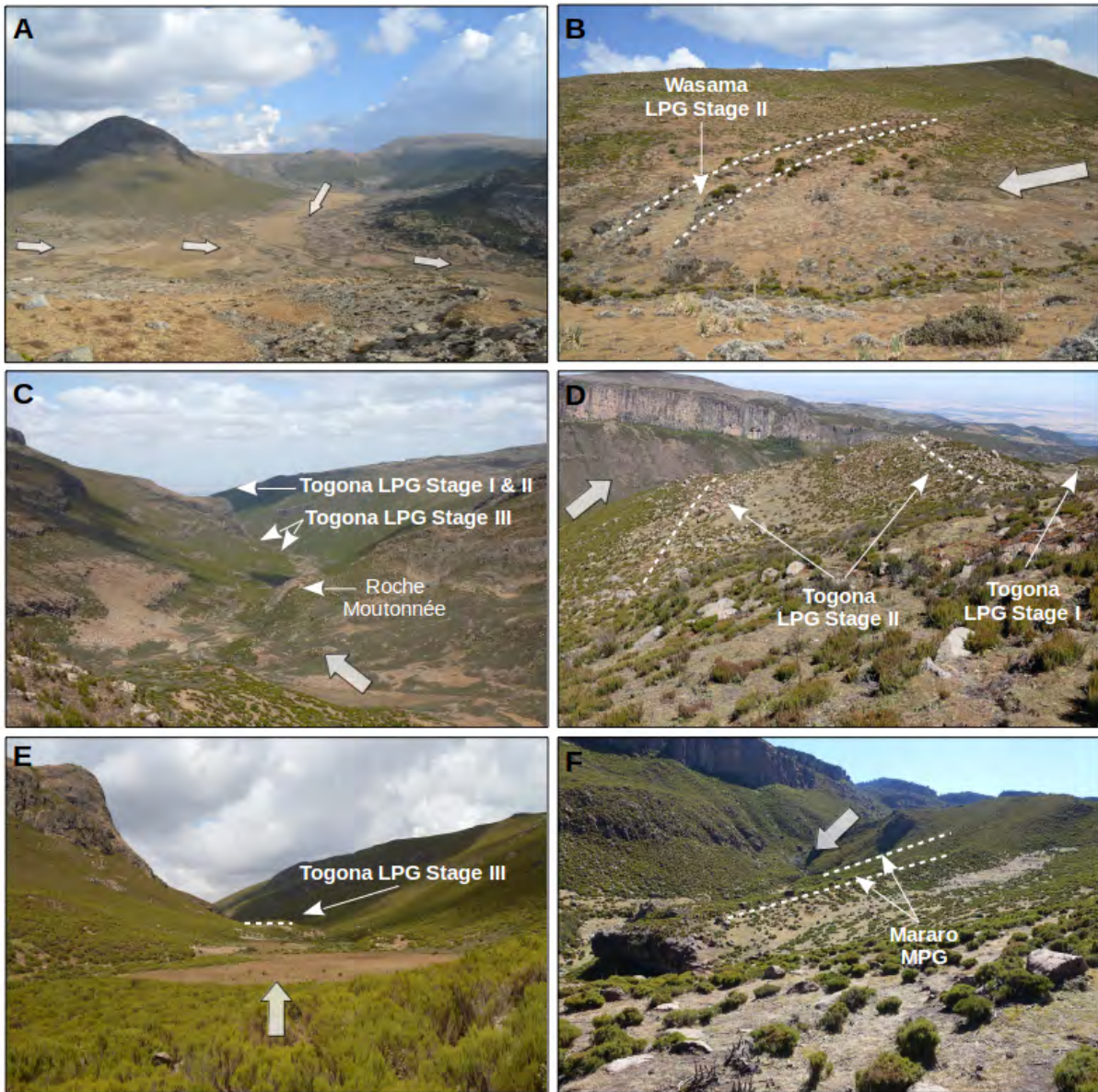


FIGURE 2.3: Glacial geomorphology of the northern valleys. (A) View into the former accumulation basin of the Wasama Valley (northern margin of the plateau in the background). (B) Terminal moraine in the Wasama Valley. (C) Moraine sequence and roche moutonnée in the Togona Valley. (D) Lateral moraines in the Togona Valley. (E) Innermost terminal moraine in the Togona Valley. (F) Two moraines in the Mararo Valley from the Mid Pleistocene.

resulting from irregular glacial erosion are typical for the northern part of the plateau. The small depressions are seasonally filled with water and desiccate during the dry season. An outstanding geomorphological feature on the plateau are large sorted stone stripes that are up to 2 m deep, 15 m wide and 200 m long (Fig. A.2). They are located at gentle slopes ( $4\text{--}8^\circ$ ) of two volcanic plugs about 3 and 5 km south of Tullu Dimtu and in the far west of the plateau (Fig. A.3). Sorted stone stripes of similar size are only known from periglacial environments in the high latitudes and their genesis requires permafrost, a deep active layer and cyclic freezing and thawing (Goldthwait, 1976; Kessler and Werner, 2003). The hardly-weathered surfaces suggest a rather young age for the formation of these features (e.g. global LGM or postglacial). Relict block fields characterise the upper part of the southern and southwestern escarpment. In contrast to the western, northern and eastern valleys, no moraines or any other glacial features were detected in the field or on high-resolution satellite images along the southern escarpment.

In the western, northern, and eastern U-shaped valleys, moraines and other glacial features like *roche moutonnées* are well-preserved (Fig. 2.3). We recorded numerous glacial features in several valleys of the Bale Mountains that were unexplored before. The terminal and lateral moraines in the valleys are mainly located between 3600–3900 masl and suggest that the glaciers in the northwest were mainly 4–5 km and those in the northeast up to 7–8 km long. The maximum ice thickness inferred from the elevation difference between the valley floors and preserved lateral moraines was about 200–300 m. Moraines consisting of fine and coarse material are rare in the Bale Mountains (Fig. A.1). Moraines made up solely of large trachytic and basaltic boulders (for the lithology see Fig. A.4) prevail. An exception are the innermost moraines in the Wasama and Togona Valley. They are formed of unsorted glacial debris and are several meters high. The lowermost glacial features are heavily-weathered boulders that are distributed unevenly between 3500–3550 masl in the plains of the northwestern Web Valley.

The 69  $^{36}\text{Cl}$ -surface-exposure-ages of moraine boulders from the Bale Mountains reveal a consistent glacial chronology for the U-shaped valleys and provide first insights into the deglaciation of the palaeo ice cap on Tullu Dimtu (Fig. 2.4). Based on exposure ages of terminal moraines from the Rafu, Harcha and Togona Valley, the local LGM is dated to  $39.6 \pm 9.9$  ka (Late Pleistocene Glaciation, LPG, Stage I). The outermost moraine in the Wasama Valley originates probably also from LPG Stage I, but no samples were taken for dating. Lateral moraines that are located  $\sim 100$  m above the valley floor in the northern Batu Gudda and eastern Badaguser Valley stem most likely also from the local LGM. However, the obtained exposure ages are equivocal. The age of the four dated boulders from the Badaguser Valley ranges from  $17.5 \pm 1.3$  to  $57.1 \pm 3.1$  ka. Characteristic for the Batu Gudda Valley are two parallel lateral moraines. The sampled boulder from the lower moraine relates to LPG Stage I, but the two boulders from the upper lateral moraine are older and both dated to  $\sim 70$  ka. Three well-preserved terminal moraines from the northwestern Harcha and Wasama Valley and two lateral moraines from the northeastern Togona Valley clearly indicate a glacial readvance at  $17.8 \pm 1.5$  ka (LPG Stage II). The innermost terminal moraines from the same valleys are dated to  $15.2 \pm 1.2$  ka (LPG Stage III) and provide a maximum age for the onset of deglaciation. Interestingly, the element composition of the boulders from the different valleys and glacial stages vary significantly (Fig. A.4). This finding suggests that the boulders originate from different

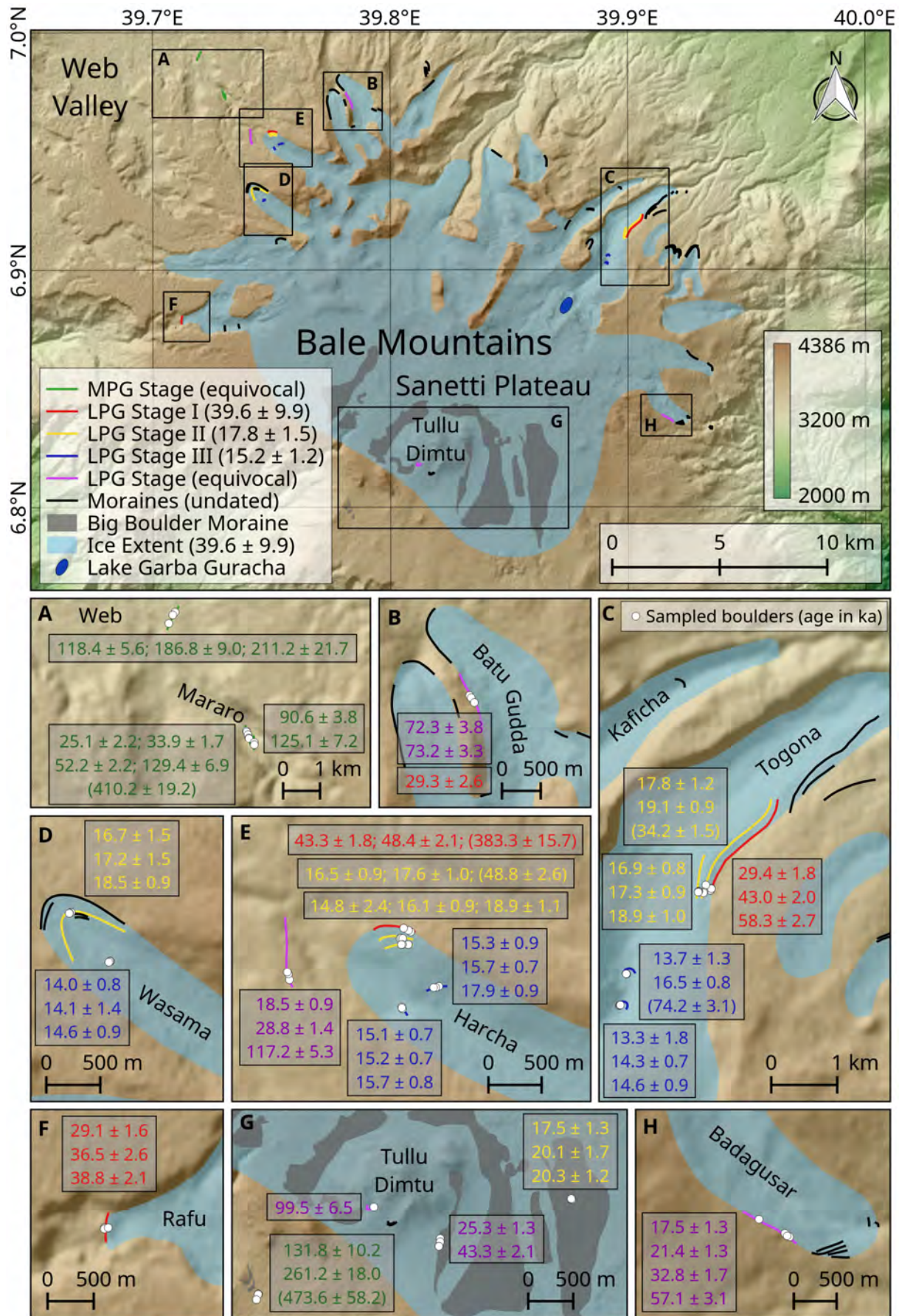


FIGURE 2.4: Glaciation map and  $^{36}\text{Cl}$  glacial chronology of the Bale Mountains. Ice extent represents LPG Stage I. One white dot may represent multiple samples due to scale.  $^{36}\text{Cl}$  ages from the Wasama and Harcha Valley are adopted from Ossendorf et al. (2019).

catchment areas. The erratic boulders from the Web Valley and moraine boulders from the Mararo Valley reveal exposure ages of  $>100$  ka and indicate a larger Mid Pleistocene Glaciation (MPG) prior to the LPG Stage I. However, the age scatter and lack of preserved glacial features from this period prevents determining the exact timing of the MPG stages.

During LPG Stage I, the plateau glaciation extended down into the western, northern and eastern valleys and formed several outlet glaciers (Fig. 2.4). Since glacial features that are suitable for dating were neither found along the southern margin of the former ice cap nor at the northern transfluence, it remains unclear when exactly the ice cap reached its maximum extent. Three boulders from the outer Big Boulder Moraine at Tullu Dimtu are dated to  $17.5 \pm 1.3$ ,  $20.1 \pm 1.7$ , and  $20.3 \pm 1.2$  ka and correlate with LPG Stage II in the valleys. In contrast, the two sampled boulders from the inner Big Boulder Moraine, which is supposed to be geomorphologically younger, are dated to  $25.3 \pm 1.3$  and  $43.3 \pm 2.1$  ka and are not in agreement with LPG Stage III in the valleys. The exposure age ( $>130$  ka) of large boulders outside the LPG Stage I ice cap extent might indicate an even larger plateau glaciation during the Mid Pleistocene, but the glacial origin of the boulders could not be verified unequivocally in the field. They could also be a product of in-situ weathering.

The exposure ages obtained from rock samples of the sorted stone stripes scatter and do not confirm a global LGM or postglacial formation age as suggested by the hardly-weathered surface of the columnar basalt and trachyte (Fig. A.1). Three samples from the stone stripes south of Tullu Dimtu reveal an age of  $84 \pm 4$  and twice of  $281 \pm 13$  ka. Even older ages were obtained for the western stone stripes (Fig. A.3). The old ages indicate that dating of permafrost features on the Sanetti Plateau is problematic since the rocks were apparently exposed to  $^{36}\text{Cl}$ -producing cosmic rays before the formation of the patterned grounds. On the contrary, the old ages and well-preserved structure of the stone stripes imply that they were never covered by thick ice for a longer period. Hence, they serve as negative evidence for the southern and western limits of the plateau glaciation during LPG Stage I.

The extent of the former ice cap on Tullu Dimtu with respect to the limits of the outer Big Boulder Moraine was in the order of  $75 \text{ km}^2$ . However, the topographic depressions across the northern plateau and smooth geomorphological transition of the plateau into the valleys suggest that the ice cap extended beyond the limits of the Big Boulder Moraine during LPG Stage I and covered up to  $155 \text{ km}^2$  of the plateau at that time. The western, northern and eastern valley glaciers contributed another  $110 \text{ km}^2$  of ice coverage. Altogether, about  $265 \text{ km}^2$  (23% of the area  $>3500$  masl) of the Bale Mountains might have been glaciated during LPG Stage I (Fig. 2.4).

### 2.2.3 Glacial history of the Arsi Mountains

Another Ethiopian mountain range that was extensively glaciated during the Pleistocene are the up to 4195 masl high Arsi Mountains, located east of the Main Ethiopian Rift and 100 km northwest of the Bale Mountains (Fig. 2.1). A large alpine plateau like the one in the Bale Mountains does not exist (Fig. 2.2). Characteristic for the Arsi Mountains is their elongated shape and the preservation of lateral and terminal moraines in most of the U-shaped valleys along the central ridge (Fig. 2.5). The terminal and lateral moraines suggest that the valley glaciers were

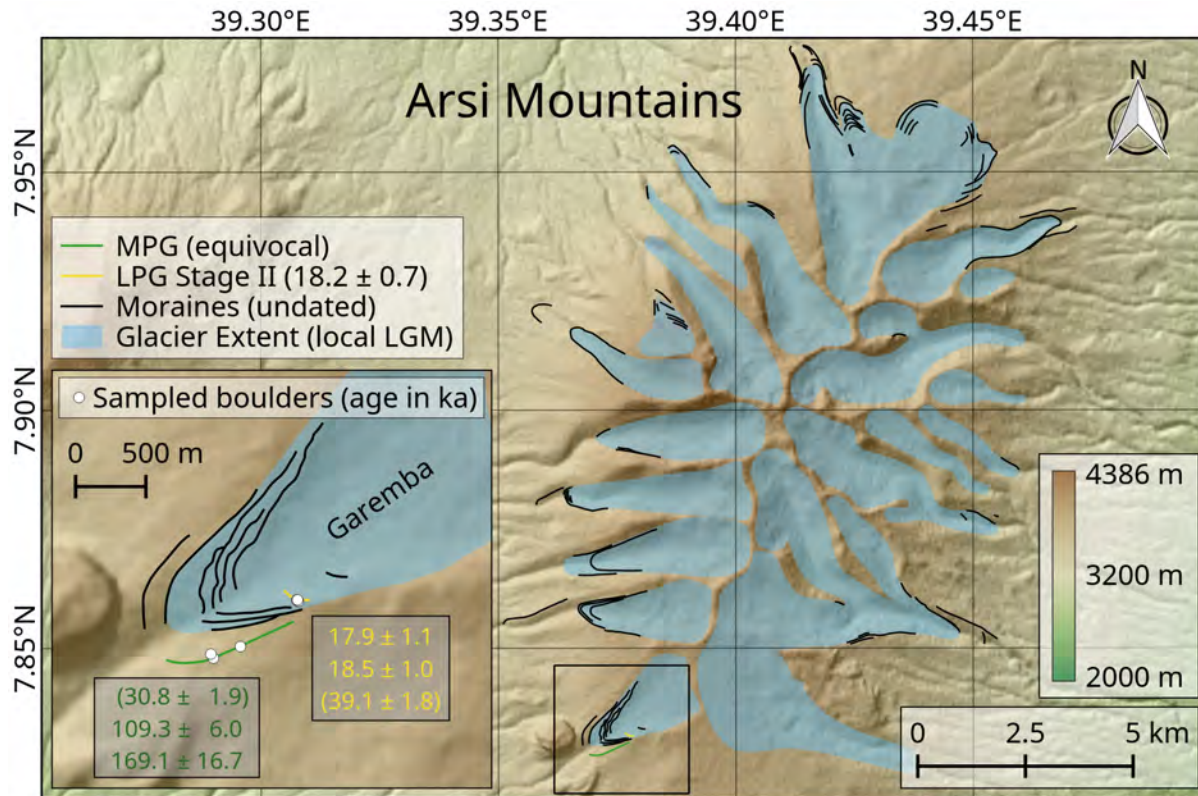


FIGURE 2.5: Glaciation map and  $^{36}\text{Cl}$  glacial chronology of the Arsi Mountains. Ice extent represents LPG Stage I. One white dot may represent multiple samples due to scale.

mainly between 2.5 and 5.5 km long and up to 200 m thick. Some of the moraine sequences comprise multiple glacial stages. The lowermost moraine in the investigated southwestern Garemba Valley is >100 ka old and originates from the largest MPG. The undated uppermost moraine in the valley originates most likely from LPG Stage III and indicates the glacial extent before the onset of deglaciation. The next outer moraine is dated to  $18.2 \pm 1.1$  ka and coincides with LPG Stage II readvance in the Bale Mountains. Three additional moraine ridges are located between LPG Stage II and the maximum MPG extent (Fig. 2.5). One of these moraines must represent LPG Stage I. At that time, about  $83 \text{ km}^2$  (29 % of the area >3500 masl) of the Arsi Mountains were glaciated.

#### 2.2.4 Reconstructed ELAs and temperature depression

The LPG Stage I moraines in the western and northwestern valleys of the Bale Mountains are mainly located between 3800 and 3850 masl. In the northern and northeastern valleys, the glaciers extended further down and reached elevations below 3500-3700 masl. The highest peaks at the glacier headwalls along the northern declivity exceed 4100-4300 masl. This translates into a relatively small vertical extent of the valley glaciers in the order of 300-800 m. A terminus-to-headwall-altitude-ratio (THAR) of 0.5 revealed an ELA for the northwestern glaciers of  $3940 \pm 40$  m ( $\text{ELA}_{\text{Harcha}} \sim 3980$  masl,  $\text{ELA}_{\text{unnamed}} \sim 3940$  masl,  $\text{ELA}_{\text{BatuGudda}} \sim 3900$  masl). These glaciers did not gain any mass input from the central ice cap and are therefore most suitable for ELA reconstructions (Fig. 2.4). The maximum elevation of lateral moraines

(MELM method) in the Harcha (~3950 masl), Batu Gudda (~3880 masl) and Togona Valley (~3800 masl) as well as remains of a former cirque glacier in the same valley (~3850-3900 masl) provide minimum values for the ELA and thus support the THAR results. The present annual 0 °C isotherm is located at 4650 masl, ~270 m above the highest peak (Tullu Dimtu), and serves as a rough proxy for the theoretical modern ELA. The difference between the theoretical modern ELA and the palaeo ELA yields an ELA lowering of 710 m. Applying a modern regional lapse rate of 7.2 °C km<sup>-1</sup> (Fig. A.5) to the calculated ELA lowering and assuming an uncertainty of ±0.5 °C for the palaeo lapse rate results in a temperature depression for the Bale Mountains of 5.1 ± 0.7 °C at LPG Stage I.

A mean LPG Stage I ELA of 3840 ± 80 m was calculated for the neighboring Arsi Mountains using the THAR method. However, the individual ELAs of the west- and east-facing palaeoglaciers differ widely (Fig. A.6). The average ELA of the east-facing glaciers (3780 ± 30 m) was about 125 m lower than that of the west-facing glaciers (3905 ± 35 m). This pattern is also supported by the lower glacial limits (3400-3500 masl vs. 3650-3750 masl) and lower maximum elevation of lateral moraines in the eastern valleys (3800 vs. 3900 masl). The reconstructed ELAs from the Arsi and Bale Mountains agree within the margin of uncertainty and demonstrate that glacial geomorphological features in the Ethiopian Highlands are a valuable proxy for assessing regional palaeoclimatic changes.

### 2.2.5 Late Pleistocene glacial fluctuations in Eastern Africa

The combined analyses of the new glacial chronologies from the Ethiopian Highlands and previously published chronologies from the Rwenzori Mountains (Kelly et al., 2014; Jackson et al., 2019), Mount Kenya, and Kilimanjaro (Shanahan and Zreda, 2000) reveals that tropical glaciers in Eastern Africa advanced asynchronously during the Late Pleistocene (Fig. 2.6). In the southern Ethiopian Highlands, the local LGM (LPG I) predated the global LGM and occurred already at 39.6 ± 9.9 ka during Marine Isotope Stage (MIS) 3. A similar pattern is also evident from the High Atlas in northwestern Africa, where glaciers reached their maximum expansion (Glacial Unit 1) at 50.2 ± 19.5 ka and therefore also prior to the global LGM (Hughes et al., 2018). On Mount Kenya, the presumed local LGM was dated to 28 ± 3 ka (Liki II moraine in the Gorges Valley) and on Kilimanjaro to 20 ± 1 ka (Mawenzi main glaciation) (Shanahan and Zreda, 2000). However, the overall large age scatter of dated moraines on Mount Kenya and Kilimanjaro hinders the comparison with other glacial chronologies and palaeoclimate proxies (Kelly et al., 2014). A consistent glacial chronology from the lower Mubuku Valley in the Rwenzori Mountains testifies major advances at 28.9 ± 1.0 (Mahoma Stage 4), 28.7 ± 0.6 (Mahoma Stage 3), 24.9 ± 0.5 (Mahoma Stage 2) and 21.5 ± 0.7 ka (Mahoma Stage 1) during or shortly before the global LGM (Kelly et al., 2014; Jackson et al., 2019). Interestingly, any evidence for a major glacier advance in the Ethiopian Highlands during the global LGM is lacking. A distinct glacier advance that is clearly recognizable in the Ethiopian Highlands (LPG Stage II) as well as Rwenzori Mountains (Mahoma Stage 0) is dated to ~18 ka. However, while the ice extent in the Ethiopian Highlands during LPG Stage II is almost similar to the local LGM extent, the Mahoma 0 moraine in the Rwenzori Mountains is located almost 5 km up the valley from the Mahoma 1 terminus (Jackson et al., 2019). Despite temporal differences of the major

glacier advances in Eastern Africa and the High Atlas, distinct glacier shrinkage after  $\sim 15$ -12 ka is verified for all studied African mountains at the end of the last glacial cycle (Shanahan and Zreda, 2000; Hughes et al., 2018; Ossendorf et al., 2019). In the Bale Mountains, the onset of deglaciation after  $15.2 \pm 1.2$  ka is in line with the basal age of a sediment core from the cirque lake Garba Guracha (3940 masl) (Umer et al., 2007), which is located in the head of the Togona Valley (Fig. 2.4).

Not only the timing, but also the reconstructed maximum ice extent and percentage of the glaciated area above the lower ice limits ( $\sim 3500$  masl) (Osmaston and Harrison, 2005) during the last glacial cycle differ widely between the individual mountains in Eastern Africa. The four most extensive Late Pleistocene glaciations occurred in the Bale Mountains, in the Rwenzori Mountains and on Mount Kenya and Kilimanjaro (Table A.1). This observation is in agreement with the mountains high maximum elevation and large area above the palaeo ELA (Fig. 2.2). When comparing the percentage of the glaciated area above the lower ice limits of the individual mountains, a distinct spatial pattern becomes apparent: the percentage of the glaciated area above 3500 masl is much higher in the East African Mountains near the equator (Rwenzori = 62-80 %, Mount Kenya = 54-65 %, Kilimanjaro = 39-52 %, Mount Elgon = 30-38 %) than in the more northern Ethiopian Highlands (Arsi = 29 %, Bale = 23 %, Simien = 2 %).

## 2.3 Discussion

Comprehensive glacial geomorphological and chronological investigations from the Bale and Arsi Mountains presented here demonstrate that extensive plateau and valley glaciers formed in the southern Ethiopian Highlands during the Mid and Late Pleistocene.  $^{36}\text{Cl}$  surface exposure ages of moraine boulders provide evidence that glaciers in the Ethiopian Highlands reached their local LGM (LPG Stage I) well before the global LGM (Shakun and Carlson, 2010) at  $39.6 \pm 9.9$  ka. Ice covered about 265 km<sup>2</sup> of the Bale Mountains and 83 km<sup>2</sup> of the neighboring Arsi Mountains at that time. The maximum glacier extent was accompanied by a mean temperature depression in the region of  $5.1 \pm 0.7$  °C. Two post-LGM readvances were dated to  $17.8 \pm 1.5$  ka (LPG Stage II) and to  $15.2 \pm 1.2$  ka (LPG Stage III). The comparison of the new  $^{36}\text{Cl}$  glacial chronologies from the southern Ethiopian Highlands with previously published  $^{36}\text{Cl}$  and  $^{10}\text{Be}$  glacial chronologies from Kilimanjaro, Mount Kenya, and the Rwenzori Mountains clearly shows that tropical glaciers in Eastern Africa responded asynchronously to Late Pleistocene climate changes. This finding challenges the persisting idea of uniform glacier expansion and shrinkage in the tropics during the Late Pleistocene and questions the role of temperature as the predominant driver of past glacier fluctuations in Eastern Africa (Kelly et al., 2014; Jackson et al., 2019).

Based on the latest reevaluation of published  $^{10}\text{Be}$  moraine ages from the Andes and new  $^{10}\text{Be}$  data from the Rwenzori Mountains, Jackson et al. (2019) concluded that tropical glaciers reached their last glacial maxima at  $\sim 29$ -20 ka and started to melt down at  $\sim 20$ -19 ka. The authors hypothesise that the supposed “early” onset of deglaciation in the tropics before the

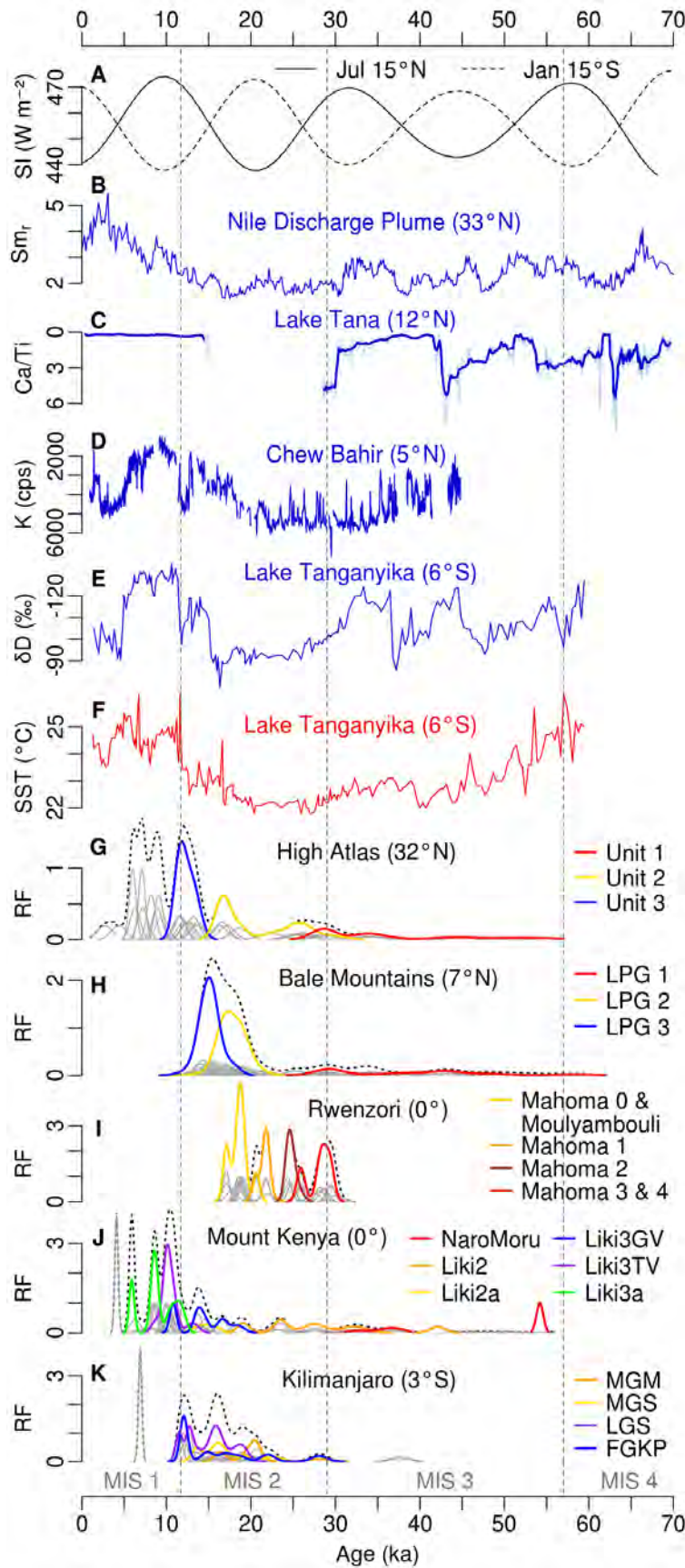


FIGURE 2.6: Comparison of different climate proxies and glacial chronologies from Eastern Africa for the last 71 ka. (A) Insolation variations at 15°N (July) and 15°S (January) (Berger and Loutre, 1991). (B) Smr record (smectite to illite + chlorite ratio) from the Nile discharge plume off Israel indicating wet (↑) and dry (↓) phases in the Northern Ethiopian Highlands (Ehrmann et al., 2016). (C) Ca/Ti record (calcium to titanium ratio) from Lake Tana (Northern Ethiopian Highlands) indicating high (↑) and low (↓) lake levels (Lamb et al., 2018). (D) Potassium record from Chew Bahir (Southern Ethiopian Rift) indicating wet (↑) and dry (↓) periods (Foerster et al., 2018). (E) Deuterium record from Lake Tanganyika (East African Rift) indicating wet (↑) and dry (↓) periods (Tierney et al., 2008). (F) Sea surface temperature proxy from Lake Tanganyika (Tierney et al., 2008). (G-K) Relative frequency (RF) of surface exposure ages from the High Atlas (<sup>36</sup>Cl and <sup>10</sup>Be) (Hughes et al., 2018), Bale Mountains (<sup>36</sup>Cl) (Ossendorf et al., 2019), Rwenzori (<sup>10</sup>Be) (Kelly et al., 2014; Jackson et al., 2019), Mount Kenya (<sup>36</sup>Cl) (Shanahan and Zreda, 2000) and Kilimanjaro (<sup>36</sup>Cl) (Shanahan and Zreda, 2000). Each gray line illustrates the age (with an analytical error of 1σ) of one dated glacial feature as a Gaussian distribution (the flatter the curve, the larger the uncertainty). Black dotted lines represent the sum of all individual ages (including outliers). Colored lines represent the sum of all ages (excluding outliers) from the same glacial stage as defined in the original publications (see Methods) (Shanahan and Zreda, 2000; Kelly et al., 2014; Hughes et al., 2018; Jackson et al., 2019; Ossendorf et al., 2019). Mount Kenya: GV = Gorges Valley, TV = Teleki Valley. Kilimanjaro: MGM = Main Glaciation Mawenzi, MGS = Main Glaciation Saddle, LGS = Little Glaciation Saddle, FGKP = Fourth Glaciation Kibo Peak.

rapid CO<sup>2</sup> rise at 18.2 ka was due to high-latitude warming, which reduced the thermal gradient between the polar regions and tropics and decreased the heat removal from the tropics towards the high latitudes. A key assumption underlying this hypothesis is that tropical glaciers are most sensitive to changes in temperature. As modern analogy and evidence that temperature is the main climatic control on glacier mass balance in the inner tropics, Jackson et al. (2019) quote a controversial study claiming rising temperatures as the dominant factor for recent glacier melting in the Rwenzori Mountains (Taylor et al., 2006). However, the detailed comment on this study by Mölg et al. (2006) elaborating the importance of other climate variables for the energy and mass balance of tropical glaciers was neglected in the discussion about climate sensitivity of tropical glaciers (Jackson et al., 2019). Several studies from Kilimanjaro and Rwenzori Mountains emphasise that climate variables related to air moisture (e.g. specific humidity affecting sublimation, cloudiness affecting incoming solar radiation, precipitation affecting glacier surface albedo and mass gain) dominate the present surface energy balance of tropical glaciers in Eastern Africa, especially at high elevations above the 0 °C isotherm (Mölg, Georges, and Kaser, 2003; Mölg and Hardy, 2004; Mölg et al., 2006; Mölg et al., 2008). In light of the modern observations, it seems highly questionable that past glacial fluctuations in Eastern Africa can be explained by temperature variations alone.

If temperature was the primary control on past glacier fluctuations in Eastern Africa, the local LGM and onset of deglaciation in the East African Mountains and Ethiopian Highlands should have occurred rather simultaneously. However, the local LGM in the Ethiopian Highlands predated the global LGM and deglaciation was not underway before ~18 ka. While the ~18 ka stage (Mahoma 0) in the Rwenzori Mountains is located about 5 km up the valley from the LGM terminus (Mahoma 1) and clearly indicates pronounced glacier shrinkage after ~20-19 ka (Jackson et al., 2019), glaciers in the southern Ethiopian Highlands reached almost the same extent at LPG Stage II ( $17.8 \pm 1.5$  ka) as during LPG Stage I ( $39.6 \pm 9.9$  ka). To discuss the potential influence of different climate variables on past glacial fluctuation in Eastern Africa, we compiled additional Late Pleistocene climate proxy records from the region (Fig. 2.6).

LPG Stage I in the Bale Mountains coincided with a climate period favouring glacier growth. Temperatures in Eastern Africa decreased continuously from the MIS 4/3 transition until ~45-35 ka and remained on a relatively low level until ~20-18 ka, as proxy data from Lake Tanganyika in the Great Rift Valley show (Fig. 2.6). A deuterium record from the same lake indicates furthermore that MIS 3 was generally wetter than MIS 2, despite several distinct drought periods (Tierney et al., 2008). Sedimentation rates from the Nile discharge plume in the Mediterranean Sea, lake level fluctuations from Lake Tana (northwestern Ethiopian Highlands), and a potassium record from Chew Bahir (southern Ethiopian Rift) confirm the alternation of longer humid periods and abrupt dry phases during MIS 3 (Ehrmann et al., 2016; Lamb et al., 2018; Foerster et al., 2018). The concurrence of low temperatures with a persistent humid period might have triggered the maximum glacier advance in the Bale Mountains prior to the global LGM. A similar scenario is likely for the High Atlas in northwestern Africa, where the local LGM ( $50.2 \pm 19.5$  ka) also coincided with a cold and relatively wet period (Hughes et al., 2018; Tjallingii et al., 2008). However, the large age spread of the local LGM stages in the Bale Mountains and High Atlas hinders the attribution of individual glacier advances to

specific climatic events. Furthermore, cold and wet conditions in Eastern Africa should have also triggered glacier expansion in the Rwenzori Mountains during MIS 3. Since the undifferentiated outermost moraines in the Rwenzori Mountains have not yet been dated (Kelly et al., 2014; Jackson et al., 2019), it can be speculated that they also originate from MIS 3. During the persistent cold and dry period from  $\sim 30$ -20 ka, when almost all African Great Lakes were nearly or completely desiccated (Johnson et al., 1996; Gasse, 2000), glaciers in the Bale Mountains were probably stagnating somewhere between LPG Stage II and III (Fig. 2.4). The contrasting glacier advances in the Rwenzori at that time (Kelly et al., 2014; Jackson et al., 2019) indicate that at least the highest elevations between the Congo Basin and African Great Lakes received enough moisture for sustaining extensive valley glaciers. The late glacial advances in the Bale Mountains at  $17.8 \pm 1.5$  and  $15.2 \pm 1.2$  ka can be explained by increasingly wetter climatic conditions in the region between  $\sim 20$ -15 ka as suggested by the potassium record from Chew Bahir (Fig. 2.6). The discrepancy between increasingly wetter conditions at Chew Bahir ( $5^\circ\text{N}$ ) and sustained dry conditions at Lake Tanganyika ( $6^\circ\text{S}$ ) between  $\sim 20$ -15 ka might explain the difference between major glacier expansion in the Ethiopian Highlands and stagnation in the Rwenzori Mountains at  $\sim 18$  ka. The onset of deglaciation in the Bale Mountains and successive glacier recession on Mount Kenya and Kilimanjaro after  $\sim 15$  ka is in line with rapidly rising temperatures after  $\sim 20$ -15 ka, depending on the reference record (Loomis et al., 2017). Nevertheless, due to the scarcity of climate proxy records from high elevations and uncertainty of palaeo precipitation simulations, our understanding of the Late Pleistocene climate in Eastern Africa is not yet sufficient to disentangle the impact of various climate variables on past glacier dynamics.

Besides the timing, also the extent of past glaciations varied among the mountains in Eastern Africa. Most extensively glaciated were the Bale Mountains, Rwenzori Mountains, Kilimanjaro and Mount Kenya (Table A.1). The ratio between the glaciated and total available surface area above the lower ice limit ( $\sim 3500$  masl) (Osmaston and Harrison, 2005; Mark and Osmaston, 2008) was much smaller in the Ethiopian Highlands (2-29 %) compared to the East African Mountains (30-80 %). The discrepancy might be due to the higher maximum elevation of the East African Mountains (Fig. 2.2), but could also indicate a negative precipitation gradient from the equator towards the outer tropics. Surprising is the extremely small LGM extent of only  $13 \text{ km}^2$  in the Simien Mountains (northern Ethiopian Highlands) (Hurni, 1989), which stands in stark contrast to the available surface area of  $573 \text{ km}^2$  above 3500 masl and  $119 \text{ km}^2$  above 4000 masl (Fig. 2.2). Provided that the glacial reconstruction is reliable, only very dry climatic conditions and the lack of sufficient accumulation basins in this rugged terrain could explain the contrast between minor glaciations in the northern and extensive glaciations in the southern Ethiopian Highlands. The Simien Mountains are located at the present northern limits of the tropical rain belt (Costa et al., 2014). A slight southward-shift of the northern limits of the tropical rain belt during a period of reduced summer insolation on the northern hemisphere might have caused a pronounced drought in the region. However, the climatic interpretation of past glaciations in Eastern Africa remains hypothetical as long as comparative studies on recent afro-alpine precipitation patterns are lacking and novel LGM rainfall simulations are not better constrained (Chevalier, Brewer, and Chase, 2017).

The presented glacial chronological and geomorphological work provides insights into the climate and glacial history of Eastern Africa, but also raises more specific questions regarding the complex plateau glaciation and discrepancy between the ice-free southern escarpment and extensively glaciated northern declivity of the Bale Mountains (Fig. 2.4). Fluvial erosion along the southern escarpment during the Holocene could theoretically explain the absence of well-preserved glacial deposits, but gullies and other erosion features are lacking. The formation of extensive glaciers in the south is unlikely because the southern plateau is less elevated and larger basins for the accumulation of snow do not exist. On the contrary, also prevailing north-westerly to northeasterly winds associated with a distinct precipitation pattern (wet northern and dry southern declivity) could explain this mismatch. The phenomenon of larger glaciers (lower ELAs) at the windward slopes and smaller glaciers (higher ELAs) in the precipitation shadow is also evident on other African mountains like Kilimanjaro (Osmaston and Harrison, 2005; Mark and Osmaston, 2008). Permafrost patterns on the southern plateau and fossil block fields along the southern escarpment of the Bale Mountains support the idea of a drier southern declivity (Fig. A.2). Dominating moisture fluxes from north to northeast associated with convection and cloud formation could also explain the lower palaeo ELAs in the northern and eastern valleys of the Arsi Mountains (Fig. A.6) (Osmaston and Harrison, 2005; Mark and Osmaston, 2008). However, it is important to note that the prevailing direction of the incoming moisture fluxes in the Ethiopian Highlands does not necessarily indicate where the moisture comes from. Moist air parcels from the Indian Ocean or Congo Basin may flow around the highlands and intrude from the north (Levin, Zipser, and Cerling, 2009; Viste and Sorteberg, 2013; Costa et al., 2014; Lemma et al., 2020). To verify whether the hypothesised high-elevation north-south precipitation discrepancy in the Bale Mountains is consistent with present climatic conditions or indicates changes in large-scale circulation patterns during the LGM, further information on the recent synoptic pattern are required.

A peculiarity of the Bale Mountains, which stands out from all other glaciated African mountains except Kilimanjaro, was the formation of an extensive plateau glaciation. Due to equivocal exposure ages and the lack of clear glacial geomorphological features outside the Big Boulder Moraine (Fig. 2.4), reconstructing the maximum extent and recession stages of the plateau glaciation is fraught with uncertainty. Dating of additional boulders from the inner Big Boulder Moraine and determining the age of glaciofluvial sediments in the northern shallow depressions would help to better constrain the deglaciation history of the plateau. The well-preserved structure and old exposures ages of the stone stripes on the southern and western plateau indicate that not the entire area of the plateau above the reconstructed palaeo ELA ( $\sim 3925$  masl) was covered by ice (Fig. 2.4). Ice free areas above the ELA could be the result of high insolation, variable precipitation and snow drift due to strong winds. The tabular ice fields with their characteristic ice walls on Kilimanjaro, which are mainly controlled by solar radiation and changes in precipitation and surface albedo, might serve as a modern analogy for the former plateau glaciation in the Bale Mountains (Kaser et al., 2010).

The reconstructed ELA lowering of  $\sim 700$  masl in the Bale Mountains during LPG Stage I and the inferred temperature depression of  $5.1 \pm 0.7^\circ\text{C}$  provides a minimum estimate for the Late Pleistocene temperature decrease and downward shift of the alpine belt in the southern

Ethiopian Highlands. Other temperature reconstructions in Eastern Africa from the same period are rare. Proxy data from Lake Rutundu, Lake Tanganyika, and the Congo Basin focus mainly on the global LGM and propose a regional cooling at that time of  $\sim 4\text{--}6^\circ\text{C}$  compared to today (Weijers et al., 2007; Tierney et al., 2008; Loomis et al., 2017). However, due to the steepened lapse rate (Loomis et al., 2017) and maximum temperature decrease during the MIS 2 (Fig. 2.6), the temperature and vegetation belt depression in the Ethiopian Highlands was probably even larger during the global LGM than LPG Stage I. Our new palaeoclimatic and environmental findings from the region have direct implications for the settlement history and ecology of the mountains in Eastern Africa. With our comprehensive glacial reconstruction, we provide further evidence that the repeated residence of Middle Stone Age foragers in the Bale Mountains 47–31 ka (Ossendorf et al., 2019) coincided with a phase of maximum glaciation and up to  $6^\circ\text{C}$  cooler temperatures. Besides the abundance of obsidian for the manufacturing of stone tools and an endemic rodent as a key food source, year-round melt water from the nearby glaciers was probably one of the important resources for attracting game and early foragers (Ossendorf et al., 2019). The end of the settlement phase at  $\sim 31$  ka might be related to drier climatic conditions and a reduction in melt water after LPG Stage I. The large ice-covered area and 700 masl downward shift of the alpine belt must have also drastically affected the habitat of endemic species like the Giant Molerat, Mountain Nyala and Ethiopian Wolf, which nowadays populate the Sanetti Plateau and Ericaceous Belt ( $\sim 3000\text{--}4300$  masl) (Miehe and Miehe, 1994). Nevertheless, the latest archeological findings (Ossendorf et al., 2019) and high percentage of endemic mammal species ( $>20\%$ ) in the Bale Mountains (Miehe and Miehe, 1994) prove the absence of glacial extinction events in the region. Middle Stone Age foragers as well as endemic plants, mammals, and rodents were coping with the harsh climatic conditions in the Ethiopian Highlands and East African Mountains during the last glacial cycle.

## 2.4 Conclusion

This contribution provides clear evidence that the Ethiopian Highlands were subject to severe climatic and environmental changes during the Late Pleistocene, with implications for the palaeoecology and early migration of hunter-gatherers into the high tropical mountains. At  $39.6 \pm 9.9$  ka, well before the global LGM, glaciers reached their maximum expansion in the Ethiopian Highlands and covered altogether about  $350\text{ km}^2$  of the Bale and adjacent Arsi Mountains. The mean annual air temperature in higher elevations at that time was  $5.1 \pm 0.7^\circ\text{C}$  lower than today and caused a downward shift of the afro-alpine belt of about 700 m. These findings along with ecological investigations and latest archaeological excavations indicate that endemic afro-alpine species (plants, mammals, rodents, etc.) and the arriving Middle Stone Age foragers adapted to the harsh environmental conditions in the highlands during the Late Pleistocene. Furthermore, the comparison of different glacial geomorphological and chronological studies from the East African Mountains and Ethiopian Highlands reveals regional differences in the timing and extent of past glaciations. The differences suggest less moist conditions from the inner to the outer tropics and demonstrate that temperature variations alone cannot explain the asynchronous Late Pleistocene glacier fluctuations in tropical Eastern

Africa. Spatial and temporal variations in precipitation, cloudiness, air humidity and insolation must also be taken into account. To unravel the complex dynamics of the palaeoglaciers and palaeoclimate in the region, reliable glacial chronologies from the northern Ethiopian Highlands and other equatorial mountains (Kilimanjaro, Mount Kenya, Mount Elgon, Aberdare), where moraine sequences are well-preserved, are urgently needed.

## **2.5 Materials and Methods**

### **2.5.1 Terrain analysis**

For our terrain analysis of Africa's alpine environment, we analysed digital elevation data of the entire continent provided by the CGIAR Consortium for Spatial Information (CGIAR-CSI). The CGIAR-CSI data set is a void-filled elevation product (Reuter, Nelson, and Jarvis, 2007; Jarvis, Reuter, and Nelson, 2008) with a spatial resolution of approximately 93 m at the equator derived from 3 arc-second data (version 2) of the NASA Shuttle Radar Topography Mission (SRTM). As recent studies have shown, SRTM elevation data are suitable for hypsometric and topographic analyses of mountains worldwide due to the product's near-global coverage and vertical accuracy (Elsen and Tingley, 2015). We downloaded ten elevation data tiles (each  $30 \times 30$  degree in size) from the CGIAR-CSI website (version 4.1, available at <http://srtm.csi.cgiar.org>). The ten tiles cover together the entire area of the continent. Along the edges, the tiles were overlapping by up to 2 km. We cut and merged the tiles properly to guaranty accurate area-elevation calculations. Since most of the Pleistocene glaciations and periglacial processes in Africa were limited to elevations  $>3000$  masl (Osmaston and Harrison, 2005; Mark and Osmaston, 2008), we neglected areas below this elevation in our analysis. We quantified the continent-wide area above 3000, 3500 and 4000 masl using the CGIAR-CSI elevation data set to specify the extent of the afro-alpine environment. Furthermore, we calculated the surface-area-distribution with increasing elevation of eight African mountains that were most extensively glaciated during the Pleistocene (Osmaston and Harrison, 2005; Mark and Osmaston, 2008). The relative and absolute surface area based on the CGIAR-CSI date set was computed for 10 m elevation bands between 3000 masl and the individual maximum mountain height.

### **2.5.2 Glacial geomorphological mapping**

Comprehensive geomorphological mapping of glacial and periglacial features is mandatory for the spatial and chronological reconstruction of past glaciations (Chandler et al., 2018). We evaluated maps and photographs of previous studies on Quaternary glaciations in the southern Ethiopian Highlands to compile geomorphological evidence of palaeoglaciations in the Bale and Arsi Mountains (Potter, 1976; Mieke and Mieke, 1994; Osmaston, Mitchell, and Osmaston, 2005; Osmaston and Harrison, 2005; Mark and Osmaston, 2008). In contrast to the Arsi Mountains, where moraines sequences are documented in almost every valley (Potter, 1976; Osmaston and Harrison, 2005; Mark and Osmaston, 2008), glacial and periglacial features in the Bale Mountains were hitherto only fragmentarily studied on the Sanetti Plateau and in

the Wasama, Harcha and Togona valley (Miehe and Miehe, 1994; Osmaston, Mitchell, and Osmaston, 2005; Ossendorf et al., 2019). During our ground reconnaissance, we mapped erratic boulders, moraines, roche moutonnées and periglacial features all over the Bale Mountains. Furthermore, we analysed high-resolution DigitalGlobe satellite imagery to identify terminal and lateral moraines in remote areas of the mountain range. If it was feasible, the remote observations were verified in the field later on. High-resolution satellite images were also used to verify and complement previous moraine mapping attempts in the Arsi Mountains (Osmaston and Harrison, 2005; Mark and Osmaston, 2008). For detailed information on the location and characteristics of each mapped moraine in the Bale and Arsi Mountains, see supplementary materials.

### 2.5.3 Surface exposure dating

To develop a robust glacial chronology for the Bale Mountains, we build upon 21 recently published  $^{36}\text{Cl}$  cosmogenic surface exposure datings from the Harcha and Wasama valley (Ossendorf et al., 2019). We analysed 48 additional erratic boulders Table A.2 on stable geomorphic surfaces at 14 different sites in the valleys and on the Sanetti Plateau following established sampling strategies (Akçar et al., 2011). Furthermore, we took six rock samples from periglacial features in the south and west of the Sanetti Plateau to determine their time of formation. In the southwestern Garemba Valley of the adjacent Arsi Mountains, three boulders from the outermost and three from the second innermost moraine were sampled to verify whether the glacial chronology of the Bale Mountains is also representative for other mountains of the southern Ethiopian Highlands. Approximately 1 kg of rock material from the upper 5 cm of each boulder was taken with hammer, chisel and angle grinder for the subsequent laboratory analysis. An inclinometer was used to measure the topographic shielding.

The 60 rock samples from the Bale and Arsi Mountains were crushed, sieved and chemically treated in the Surface Exposure Dating Laboratory at the University of Bern. 120 g of the 200-400  $\mu$  grain-size fraction was leached in 2 M  $\text{HNO}_3$  and afterwards rinsed with ultra-pure water (18.2 M $\Omega$ •cm) to remove any non-in-situ produced chlorine. From each leached sample, an aliquot of 10 g was sent to SGS Laboratories in Toronto, Canada. There, major and trace element concentrations, required for the calculation of local  $^{36}\text{Cl}$  production rates, were measured Table A.3. For the extraction of Cl-isotopes, we followed an established approach (Akçar et al., 2012) using isotope dilution (Stone et al., 1996b; Elmore et al., 1997; Ivy-Ochs et al., 2004; Desilets et al., 2006). Total Cl- and  $^{36}\text{Cl}$ -concentrations Table A.4 were measured from one target at the 6 MV AMS-facility of the ETH Zurich based on the isotope dilution technique (Ivy-Ochs et al., 2004) and the gas-filled magnet to separate  $^{36}\text{S}$  (Vockenhuber, Miltenberger, and Synal, 2019). The measured ratios of  $^{36}\text{Cl}/^{35}\text{Cl}$  were normalised to the ETH in-house standard K382/4N (Christl et al., 2013) with a  $^{36}\text{Cl}/\text{Cl}$ -value of  $17.36 \times 10^{-12}$  (calibrated against the Nishiizumi KNSTD5000 standard in 2009), whereas the stable ratio of  $^{37}\text{Cl}/^{35}\text{Cl}$  was normalised to the natural  $^{37}\text{Cl}/^{35}\text{Cl}$ -ratio, which equals to 31.98 % of the K382/4N standard and machine blank.

We calculated surface exposure ages of the boulders from the Bale and Arsi Mountains based on the measured total Cl and  $^{36}\text{Cl}$  concentrations. The applied spallogenic production rate of cosmogenic  $^{36}\text{Cl}$  at sea-level from Ca corresponds to  $48.8 \pm 1.7 \text{ atoms g}^{-1} \text{ Ca a}^{-1}$  (Stone et al., 1996a; Stone et al., 1998) and from K to  $162 \pm 24 \text{ atoms g}^{-1} \text{ K a}^{-1}$  (Evans et al., 1997). Since altitude and latitude influence the scaling of the  $^{36}\text{Cl}$  production rate, we followed the scheme described in Stone (Stone, 2000) to correct for the geographic location of the sampling sites. Muon capture contributes with  $5.3 \pm 0.5 \text{ atoms g}^{-1} \text{ Ca a}^{-1}$  to the production of  $^{36}\text{Cl}$  from Ca (Stone et al., 1996a; Stone et al., 1998). Another source for the production of  $^{36}\text{Cl}$  is the capture of thermal and epithermal neutrons by  $^{35}\text{Cl}$  near the surface in the order of  $760 \pm 150 \text{ neutrons g}^{-1} \text{ air a}^{-1}$  (Liu et al., 1994; Phillips, Stone, and Fabryka-Martin, 2001; Alfimov and Ivy-Ochs, 2009). We used major and trace element (B, Gd and Sm) concentrations to determine the fraction of low-energy neutrons available for the production of  $^{36}\text{Cl}$  from  $^{35}\text{Cl}$  (Phillips, Stone, and Fabryka-Martin, 2001; Alfimov and Ivy-Ochs, 2009). U and Th concentrations served for the quantification of non-cosmogenic  $^{36}\text{Cl}$  in the rocks. We corrected  $^{36}\text{Cl}$  production rates for sample thickness Table A.2 assuming a rock density of  $2.65 \text{ g cm}^{-3}$  and an attenuation length of  $160 \text{ g cm}^{-2}$ . Correction factors were computed to account for the topographic shielding at the sampling sites (Dunne, Elmore, and Muzikar, 1999; Tikhomirov et al., 2014). The attenuating effect of snow on the local production of  $^{36}\text{Cl}$  is neglected since snow is rare in the Bale Mountains and melts within hours or days (Miehe and Miehe, 1994). Post-depositional erosion rates of boulders have not been determined in the Ethiopian Highlands and East African mountains, but are estimated to be in the range of 0 to  $2 \text{ mm ka}^{-1}$  (a detailed discussion on the effect of erosion on  $^{36}\text{Cl}$  ages is given in Shanahan and Zreda, 2000). To account for the impact of erosion, we calculated three different  $^{36}\text{Cl}$  surface exposure ages for every boulder Table A.4 considering a minimum, medium and maximum erosion scenario ( $\varepsilon_{min} = 0 \text{ mm ka}^{-1}$ ,  $\varepsilon_{med} = 1 \text{ mm ka}^{-1}$ ,  $\varepsilon_{max} = 2 \text{ mm ka}^{-1}$ ). All exposure ages presented in Fig. 2.4 and 2.5 are stated without any erosion correction ( $\varepsilon = 0 \text{ mm ka}^{-1}$ ). The  $1\sigma$ -error given for each individual exposure age includes solely the analytical uncertainty. Recently published surface exposure ages from Rwenzori Mountains ( $^{10}\text{Be}$ ) (Kelly et al., 2014; Jackson et al., 2019) and High Atlas ( $^{10}\text{Be}$  and  $^{36}\text{Cl}$ ) (Hughes et al., 2018) were adopted without any modifications for discussion and Fig 2.6. Furthermore, it was not possible to recalculate the 20-year old  $^{36}\text{Cl}$  ages from Mount Kenya and Kilimanjaro (Shanahan and Zreda, 2000) because only  $^{36}\text{Cl}/\text{Cl}$  and no  $^{36}\text{Cl}$  concentrations or information on the blank corrections, spiking with Cl carrier etc. were made available along with the original publication. For the sake of easy reproducibility and for testing the impact of different  $^{36}\text{Cl}$  production rate scalings, we also computed the exposure ages of the boulders from the Bale and Arsi Mountains using the online version (2.0) of the CRONUS  $^{36}\text{Cl}$  Exposure Age Calculator (Marrero et al., 2016). All input data required for the CRONUS calculator (<http://cronus.cosmogenicnuclides.rocks/2.0/>) are available in Table A.5. For the results see Table A.6.

#### 2.5.4 Glacial chronology

Based on the exposure age, location and geomorphology of the investigated moraines, we distinguished between different glaciations and glacial stages in the Bale Mountains to establish a

glacial chronology. The exposure ages of moraine boulders from the upper valleys and Sanetti Plateau allow to differentiate between three glacial stages within the Late Pleistocene glaciation (LPG): I (local LGM), II (readvance) and III (readvance before onset of deglaciation). We grouped all exposure ages of moraines associated with the same glacial stage. If one of the three exposure ages of a moraine deviated from the other two in the order of more than  $3\sigma$ , it was treated as an outlier. Moraines comprising three or more inconsistent exposure ages were classified as 'equivocal'. The arithmetic mean ( $n = 9$ , outliers = 1) was used for determining the timing of LPG Stage I due to the large scatter of the moraine boulder ages. The timing of LPG Stage II ( $n = 16$ , outliers = 2) and LPG Stage III ( $n = 14$ , outliers = 1) was calculated using the weighted mean. Along with the weighted mean, we computed the internal (analytical) and external ("geomorphological") error Table A.7. The external error is defined by the standard deviation ( $1\sigma$ ) of the glacial stage and the internal error by the standard error of the weighted mean. In Fig. 2.4 and 2.5, only the larger of the two errors is reported. For the Mid Pleistocene Glaciation (MPG), it was not possible to constrain the timing of the two geomorphologically evident glacial stages because of the large scatter of the exposure ages.

### 2.5.5 Glacial extent

To assess the potential ice cover extent in the valleys of the Bale Mountains during the local LGM, we reconstructed palaeoglacier outlines based on the location of mapped and dated moraines associated with LPG Stage I. In those valleys, where no terminal moraines were detected, the elevation of the lower ice limits in the neighboring valleys served as reference for the compilation of the glaciation map. Glacial geomorphological features and landforms, but also outcrops and cliffs which lack any sign of glacial erosion, were mapped in the head of the upper valleys to delineate the former accumulation areas. In the absence of geomorphological evidence for or against glacial activity, we interpolated the palaeoglacier boundaries to the best of our knowledge, referring to the typical geometry of valley glaciers.

For the reconstruction of the geometry and extent of the plateau glaciation during LPG Stage I, we studied the distribution of erratic boulders around Tullu Dimtu, sediment-filled depressions across the northern plateau and large periglacial patterns across the southern and western plateau. The boulders encircling Tullu Dimtu were probably deposited after LPG stage I and therefore indicate the minimum extent of the former plateau glaciation. Subglacial till and numerous shallow depression across the northern plateau provide evidence for a much larger plateau glaciation extending down into the western, northern and eastern valleys. To the south and west of Tullu Dimtu, well-preserved permafrost features exist (Fig. A.2 and Fig. A.3). Due to the large dimension, undisturbed structure, barely weathered surface and old exposure age of these features, we assume that they have not, or at least not for a long time, been covered by thick ice during the local LGM. Therefore, the features serve as markers for the southern and western limit of the plateau glaciation.

The extent of the local LGM glaciation in the Arsi Mountains was reconstructed based on the well-preserved terminal and lateral moraines in the valleys following the procedure described above. The outermost (lowermost) terminal moraines in the valleys were not considered for the delineation of the glacier boundaries since they probably originate from the Mid

Pleistocene glaciation.

### 2.5.6 Equilibrium line altitude and temperature reconstruction

The climatic equilibrium line altitude (ELA) is defined as the average elevation over a 30-year period of a glacier zone where the annual net balance (accumulation vs. ablation) is zero (Singh, 2011). Since the position of the ELA responds sensitively to climatic changes, it is a useful proxy for temperature reconstructions, especially in alpine regions, where other climate records are often lacking. The most widely used methods for calculating ELAs like the accumulation-area-ratio (AAR) or area-altitude-balance-ratio (AABR) require knowledge about the geometry of palaeoglaciers (Benn et al., 2005). However, the current knowledge about the plateau glaciation in the Bale Mountains is not sufficient to draw contour lines, reconstruct the geometry of the palaeo ice cap, and quantify the ice mass turnover from the plateau into the valleys. Hence, we applied a simple terminus-to-headwall-altitude-ratio (THAR), which assumes a constant ratio between the altitude of the frontal position and headwall of the reconstructed palaeoglaciers (Benn et al., 2005). A THAR of 0.5 is appropriate for tropical valley glaciers (Osmaston, Mitchell, and Osmaston, 2005). We chose three valleys (Harcha, unnamed, and Batu Gudda) in the northwest of the Bale Mountains for the ELA reconstruction since they did not gain any mass input from the central ice cap and were fed solely by snowfall. To back up the calculations, we also determined the maximum elevation of lateral moraines (MELM) in the Harcha, Batu Gudda and Togona Valley because their upper limit provides a reliable minimum elevation for the palaeo ELA. The comparison between palaeo and modern ELAs from the same region allows calculating temperature changes relative to today. Due to the absence of present-day glaciers in the Ethiopian Highlands, we used the present mean annual 0 °C isotherm (freezing height) as a rough proxy for the modern ELA (Greene, Seager, and Broecker, 2002; Benn et al., 2005). Hourly temperature data from 1<sup>st</sup> March 2017 until 28<sup>th</sup> February 2018 of three recently installed automatic weather stations between 3848 and 4377 masl on the Sanetti Plateau served for the computation of an average modern lapse rate ( $\Gamma_{modern} = 7.2 \text{ }^\circ\text{C km}^{-1}$ ) and the determination of the present 0 °C isotherm ( $ELA_{modern} = 4650 \text{ masl}$ ). For more information, see Fig. A.5 and caption. The temperature depression at LPG Stage I ( $\Delta T$  in °C) was calculated using the following formula and assuming an uncertainty of  $\pm 40 \text{ m}$  for the palaeo ELA ( $ELA_{palaeo} = 3940 \text{ masl}$ ) and of  $\pm 0.5 \text{ }^\circ\text{C}$  for the applied lapse rate ( $\Gamma_{palaeo} = \Gamma_{modern}$ ):

$$\Delta T = (ELA_{palaeo} - ELA_{modern}) \times \Gamma_{palaeo} \quad (2.1)$$

The applied lapse rate of  $7.2 \pm 0.5 \text{ }^\circ\text{C km}^{-1}$  for translating the ELA-lowering into a temperature change is similar to the tropical paleo lapse rate of  $6.7 \pm 0.3 \text{ }^\circ\text{C km}^{-1}$  derived from global LGM surface temperatures of four East African Lakes between 474 and 3081 masl (Loomis et al., 2017). For calculating the ELA of 19 paleoglaciers in the Arsi Mountains, we applied the same procedure (THAR and MELM method) as described above.

## Acknowledgements

We thank the Ethiopian Wildlife Conservation Authority, the College of Natural and Computational Sciences (Addis Ababa University), the Department of Plant Biology and Biodiversity Management (Addis Ababa University), the Philipps University of Marburg, the Frankfurt Zoological Society, the Ethiopian Wolf Project and the Bale Mountains National Park for their cooperation and kind permission to conduct field work. We are grateful to Kemal Mohammed, Mekbib Fekadu, Wege Abebe, Katinka Thielsen, Tiziana Koch, Aschalew Gashaw, Terefe Endale, Geremew Mebratu, Beriso Kemal, Mohammed Kedir, Temame, Edris Abduku, Sabrina Erlwein, Lukas Munz, and Julian Struck for contributing to the preparation and implementation of the field work. Special thanks also go to the Digital Globe Foundation for providing high-resolution satellite images of the Bale Mountains (granted to A.R.G.).

Funding: This research was funded by the Swiss National Science Foundation (SNF, grant no. 200021E-165446/1) and the German Research Foundation (DFG) in the framework of the joint Ethio-European DFG Research Unit 2358 “The Mountain Exile Hypothesis”.

## References

- Akçar, N. et al. (2011). “Post-Depositional Impacts on ‘Findlinge’ (Erratic Boulders) and Their Implications for Surface-Exposure Dating”. In: *Swiss J. Geosci.* 104.3, pp. 445–453. DOI: 10.1007/s00015-011-0088-7.
- Akçar, N. et al. (2012). “<sup>36</sup>Cl Exposure Dating of Paleoearthquakes in the Eastern Mediterranean: First Results from the Western Anatolian Extensional Province, Manisa Fault Zone, Turkey”. In: *Geol. Soc. Am. Bull.* 124.11-12, pp. 1724–1735. DOI: 10.1130/B30614.1.
- Alfimov, V. and S. Ivy-Ochs (2009). “How Well Do We Understand Production of <sup>36</sup>Cl in Limestone and Dolomite?” In: *Quat. Geochronol.* 4.6, pp. 462–474. DOI: 10.1016/j.quageo.2009.08.005.
- Benn, D. I. et al. (2005). “Reconstruction of Equilibrium-Line Altitudes for Tropical and Sub-Tropical Glaciers”. In: *Quat. Int.* 138-139, pp. 8–21. DOI: 10.1016/j.quaint.2005.02.003.
- Berger, A. and M. F. Loutre (1991). “Insolation Values for the Climate of the Last 10 Million Years”. In: *Quat. Sci. Rev.* 10.4, pp. 297–317. DOI: 10.1016/0277-3791(91)90033-Q.
- Chandler, B. M. P. et al. (2018). “Glacial Geomorphological Mapping: A Review of Approaches and Frameworks for Best Practice”. In: *Earth-Sci. Rev.* 185, pp. 806–846. DOI: 10.1016/j.earscirev.2018.07.015.
- Chevalier, M., S. Brewer, and B. M. Chase (2017). “Qualitative Assessment of PMIP3 Rainfall Simulations across the Eastern African Monsoon Domains during the Mid-Holocene and the Last Glacial Maximum”. In: *Quat. Sci. Rev.* 156, pp. 107–120. DOI: 10.1016/j.quascirev.2016.11.028.
- Christl, M. et al. (2013). “The ETH Zurich AMS Facilities: Performance Parameters and Reference Materials”. In: *Nucl. Instrum. Methods Phys. Res. B* 294, pp. 29–38. DOI: 10.1016/j.nimb.2012.03.004.

- Costa, K. et al. (2014). "Isotopic Reconstruction of the African Humid Period and Congo Air Boundary Migration at Lake Tana, Ethiopia". In: *Quat. Sci. Rev.* 83, pp. 58–67. DOI: 10.1016/j.quascirev.2013.10.031.
- Cunningham, M. T. et al. (2019). "Glacial Limitation of Tropical Mountain Height". In: *Earth Surf. Dynam.* 7.1, pp. 147–169. DOI: 10.5194/esurf-7-147-2019.
- Desilets, D. et al. (2006). "Determination of Cosmogenic  $^{36}\text{Cl}$  in Rocks by Isotope Dilution: Innovations, Validation and Error Propagation". In: *Chemical Geology* 233.3-4, pp. 185–195. DOI: 10.1016/j.chemgeo.2006.03.001.
- Dimitrov, D., D. Nogués-Bravo, and N. Scharff (2012). "Why Do Tropical Mountains Support Exceptionally High Biodiversity? The Eastern Arc Mountains and the Drivers of Saintpaulia Diversity". In: *PLoS ONE* 7.11, pp. 1–15. DOI: 10.1371/journal.pone.0048908.
- Dunne, J., D. Elmore, and P. Muzikar (1999). "Scaling Factors for the Rates of Production of Cosmogenic Nuclides for Geometric Shielding and Attenuation at Depth on Sloped Surfaces". In: *Geomorphology* 27.1-2, pp. 3–11. DOI: 10.1016/S0169-555X(98)00086-5.
- Ehrmann, W. et al. (2016). "A Distal 140 Kyr Sediment Record of Nile Discharge and East African Monsoon Variability". In: *Clim. Past* 12.3, pp. 713–727. DOI: 10.5194/cp-12-713-2016.
- Elmore, D. et al. (1997). "Status and Plans for the PRIME Lab AMS Facility". In: *Nucl. Instrum. Methods Phys. Res. B* 123.1-4, pp. 69–72. DOI: 10.1016/S0168-583X(96)00621-0.
- Elsen, P. R. and M. W. Tingley (2015). "Global Mountain Topography and the Fate of Montane Species under Climate Change". In: *Nat. Clim. Chang.* 5.8, pp. 772–776. DOI: 10.1038/nclimate2656.
- Evans, J. M. et al. (1997). "Cosmogenic Chlorine-36 Production in K-Feldspar". In: *Nucl. Instrum. Methods Phys. Res. B* 123.1-4, pp. 334–340. DOI: 10.1016/S0168-583X(96)00714-8.
- Foerster, V. et al. (2018). "Towards an Understanding of Climate Proxy Formation in the Chew Bahir Basin, Southern Ethiopian Rift". In: *Palaeogeogr. Palaeoclimatol. Palaeoecol.* 501, pp. 111–123. DOI: 10.1016/j.palaeo.2018.04.009.
- Gasse, F. (2000). "Hydrological Changes in the African Tropics since the Last Glacial Maximum". In: *Quat. Sci. Rev.* 19.1-5, pp. 189–211. DOI: 10.1016/S0277-3791(99)00061-X.
- Goldthwait, R. P. (1976). "Frost Sorted Patterned Ground: A Review". In: *Quat. Res.* 6.1, pp. 27–35.
- Greene, A. M., R. Seager, and W. S. Broecker (2002). "Tropical Snowline Depression at the Last Glacial Maximum: Comparison with Proxy Records Using a Single-Cell Tropical Climate Model". In: *J. Geophys. Res.* 107.D8, p. 4061. DOI: 10.1029/2001JD000670.
- Hastenrath, S. (2009). "Past Glaciation in the Tropics". In: *Quat. Sci. Rev.* 28.9-10, pp. 790–798. DOI: 10.1016/j.quascirev.2008.12.004.
- Hughes, P. D. et al. (2018). "Timing of Pleistocene Glaciations in the High Atlas, Morocco: New  $^{10}\text{Be}$  and  $^{36}\text{Cl}$  Exposure Ages". In: *Quat. Sci. Rev.* 180, pp. 193–213. DOI: 10.1016/j.quascirev.2017.11.015.
- Hurni, H. (1989). "Late Quaternary of Simien and Other Mountains in Ethiopia". In: *Quaternary and Environmental Research on East African Mountains*. Rotterdam / Brookfield: Balkema, pp. 105–120.

- Ivy-Ochs, S. et al. (2004). "Initial Results from Isotope Dilution for Cl and  $^{36}\text{Cl}$  Measurements at the PSI/ETH Zurich AMS Facility". In: *Nucl. Instrum. Methods Phys. Res. B* 223-224, pp. 623–627. DOI: 10.1016/j.nimb.2004.04.115.
- Jackson, M. S. et al. (2019). "High-Latitude Warming Initiated the Onset of the Last Deglaciation in the Tropics". In: *Sci. Adv.* 5.12, pp. 1–8. DOI: 10.1126/sciadv.aaw2610.
- Jarvis, A., H. I. Reuter, and A. Nelson (2008). "Hole-filled SRTM for the globe Version 4, available from the CGIAR-CSI SRTM 90m Database, <http://srtm.csi.cgiar.org>". In:
- Johnson, T. C. et al. (1996). "Late Pleistocene Desiccation of Lake Victoria and Rapid Evolution of Cichlid Fishes". In: *Science* 273.5278, pp. 1091–1093. DOI: 10.1126/science.273.5278.1091.
- Kaser, G. (1999). "A Review of the Modern Fluctuations of Tropical Glaciers". In: *Glob. Planet. Chang.* 22.1-4, pp. 93–103. DOI: 10.1016/S0921-8181(99)00028-4.
- Kaser, G. and H. Osmaston (2002). *Tropical Glaciers*. International Hydrology Series. Cambridge University Press.
- Kaser, G. et al. (2010). "Is the Decline of Ice on Kilimanjaro Unprecedented in the Holocene?" In: *The Holocene* 20.7, pp. 1079–1091. DOI: 10.1177/0959683610369498.
- Kelly, M. A. et al. (2014). "Expanded Glaciers during a Dry and Cold Last Glacial Maximum in Equatorial East Africa". In: *Geology* 42.6, pp. 519–522. DOI: 10.1130/G35421.1.
- Kessler, M. A. and B. T. Werner (2003). "Self-Organization of Sorted Patterned Ground". In: *Science* 299.5605, pp. 380–383. DOI: 10.1126/science.1077309.
- Lamb, H. F. et al. (2018). "150,000-Year Palaeoclimate Record from Northern Ethiopia Supports Early, Multiple Dispersals of Modern Humans from Africa". In: *Sci. Rep.* 8.1. DOI: 10.1038/s41598-018-19601-w.
- Lemma, B. et al. (2020). "Spatial and Temporal  $^2\text{H}$  and  $^{18}\text{O}$  Isotope Variation of Contemporary Precipitation in the Bale Mountains, Ethiopia". In: *Isot. Environ. Health Stud.* Pp. 1–14. DOI: 10.1080/10256016.2020.1717487.
- Levin, N. E., E. J. Zipser, and T. E. Cerling (2009). "Isotopic Composition of Waters from Ethiopia and Kenya: Insights into Moisture Sources for Eastern Africa". In: *J. Geophys. Res.* 114, pp. 1–13. DOI: 10.1029/2009JD012166.
- Liu, B. et al. (1994). "Cosmogenic  $^{36}\text{Cl}$  Accumulation in Unstable Landforms: 1. Effects of the Thermal Neutron Distribution". In: *Water Resour. Res.* 30.11, pp. 3115–3125. DOI: 10.1029/94WR00761.
- Loomis, S. E. et al. (2017). "The Tropical Lapse Rate Steepened during the Last Glacial Maximum". In: *Science Advances* 3.1, pp. 1–7. DOI: 10.1126/sciadv.1600815.
- Mark, B. G. and H. A. Osmaston (2008). "Quaternary Glaciation in Africa: Key Chronologies and Climatic Implications". In: *J. Quat. Sci.* 23.6-7, pp. 589–608. DOI: 10.1002/jqs.1222.
- Marrero, S. M. et al. (2016). "Cosmogenic Nuclide Systematics and the CRONUScal Program". In: *Quat. Geochronol.* 31, pp. 160–187. DOI: 10.1016/j.quageo.2015.09.005.
- Miehe, S. and G. Miehe (1994). *Ericaceous Forests and Heathlands in the Bale Mountains of South Ethiopia - Ecology and Man's Impact*. Hamburg: Stiftung Walderhaltung in Afrika.

- Mölg, T., C. Georges, and G. Kaser (2003). "The Contribution of Increased Incoming Shortwave Radiation to the Retreat of the Rwenzori Glaciers, East Africa, during the 20th Century". In: *Int. J. Climatol.* 23.3, pp. 291–303. DOI: 10.1002/joc.877.
- Mölg, T. and D. R. Hardy (2004). "Ablation and Associated Energy Balance of a Horizontal Glacier Surface on Kilimanjaro". In: *J. Geophys. Res.* 109.D16. DOI: 10.1029/2003JD004338.
- Mölg, T. et al. (2006). "Comment on "Recent Glacial Recession in the Rwenzori Mountains of East Africa Due to Rising Air Temperature" by Richard G. Taylor, Lucinda Mileham, Callist Tindimugaya, Abushen Majugu, Andrew Muwanga, and Bob Nakileza". In: *Geophys. Res. Lett.* 33.20, pp. 1–4. DOI: 10.1029/2006GL027254.
- Mölg, T. et al. (2008). "Mass Balance of a Slope Glacier on Kilimanjaro and Its Sensitivity to Climate". In: *Int. J. Climatol.* 28.7, pp. 881–892. DOI: 10.1002/joc.1589.
- Osmaston, H. A. and S. P. Harrison (2005). "The Late Quaternary Glaciation of Africa: A Regional Synthesis". In: *Quat. Int.* 138-139, pp. 32–54. DOI: 10.1016/j.quaint.2005.02.005.
- Osmaston, H. A., W. A. Mitchell, and J. A. N. Osmaston (2005). "Quaternary Glaciation of the Bale Mountains, Ethiopia". In: *J. Quat. Sci.* 20.6, pp. 593–606. DOI: 10.1002/jqs.931.
- Ossendorf, G. et al. (2019). "Middle Stone Age Foragers Resided in High Elevations of the Glaciated Bale Mountains, Ethiopia". In: *Science* 365.6453, pp. 583–587. DOI: 10.1126/science.aaw8942.
- Phillips, F. M., W. D. Stone, and J. T. Fabryka-Martin (2001). "An Improved Approach to Calculating Low-Energy Cosmic-Ray Neutron Fluxes near the Land/Atmosphere Interface". In: *Chem. Geol.* 175, pp. 689–701.
- Potter, E. C. (1976). "Pleistocene Glaciation in Ethiopia: New Evidence". In: *J. Glaciol.* 17.75, pp. 147–150.
- Reuter, H. I., A. Nelson, and A. Jarvis (2007). "An Evaluation of Void-filling Interpolation Methods for SRTM Data". In: *Int. J. Geogr. Inf. Sci.* 21.9, pp. 983–1008. DOI: 10.1080/13658810601169899.
- Shakun, J. D. and A. E. Carlson (2010). "A Global Perspective on Last Glacial Maximum to Holocene Climate Change". In: *Quat. Sci. Rev.* 29, pp. 1801–1816. DOI: 10.1016/j.quascirev.2010.03.016.
- Shanahan, D. F. and M. Zreda (2000). "Chronology of Quaternary Glaciations in East Africa". In: *Earth Planet. Sci. Lett.* 177, pp. 23–42.
- Singh, V. P., ed. (2011). *Encyclopedia of Snow, Ice and Glaciers*. Encyclopedia of Earth Sciences Series. Dordrecht: Springer. ISBN: 978-90-481-2641-5.
- Stone, J. et al. (1998). "Cosmogenic Chlorine-36 Production in Calcite by Muons". In: *Geochim. Cosmochim. Acta* 62.3, pp. 433–454. DOI: 10.1016/S0016-7037(97)00369-4.
- Stone, J. O. H. (2000). "Air Pressure and Cosmogenic Isotope Production". In: *J. Geophys. Res.* 105.B10, pp. 23753–23759. DOI: 10.1029/2000JB900181.
- Stone, J. O. H. et al. (1996a). "Cosmogenic Chlorine-36 from Calcium Spallation". In: *Geochim. Cosmochim. Acta* 60.4, pp. 679–692. DOI: 10.1016/0016-7037(95)00429-7.
- Stone, J. O. H. et al. (1996b). "Cosmogenic chlorine-36 production rates from calcium and potassium". In: *Radiocarbon* 38, pp. 170–171. DOI: 10.1029/2006GL026484.

- Taylor, R. G. et al. (2006). "Recent Glacial Recession in the Rwenzori Mountains of East Africa Due to Rising Air Temperature". In: *Geophys. Res. Lett.* 33.10, n/a–n/a. DOI: 10.1029/2006GL025962.
- Tierney, J. E. et al. (2008). "Northern Hemisphere Controls on Tropical Southeast African Climate During the Past 60,000 Years". In: *Science* 322.6976, pp. 252–255. DOI: 10.1038/nature02251.
- Tierney, J. E. et al. (2011). "Late Quaternary Behavior of the East African Monsoon and the Importance of the Congo Air Boundary". In: *Quat. Sci. Rev.* 30.7-8, pp. 798–807. DOI: 10.1016/j.quascirev.2011.01.017.
- Tikhomirov, D. et al. (2014). "Calculation of Shielding Factors for Production of Cosmogenic Nuclides in Fault Scarps". In: *Quat. Geochronol.* 19, pp. 181–193. DOI: 10.1016/j.quageo.2013.08.004.
- Tjallingii, R. et al. (2008). "Coherent High- and Low-Latitude Control of the Northwest African Hydrological Balance". In: *Nat. Geosci.* 1.10, pp. 670–675. DOI: 10.1038/ngeo289.
- Umer, M. et al. (2007). "Late Pleistocene and Holocene Vegetation History of the Bale Mountains, Ethiopia". In: *Quat. Sci. Rev.* 26.17-18, pp. 2229–2246. DOI: 10.1016/j.quascirev.2007.05.004.
- Viste, E. and A. Sorteberg (2013). "Moisture Transport into the Ethiopian Highlands". In: *Int. J. Climatol.* 33.1, pp. 249–263. DOI: 10.1002/joc.3409.
- Vockenhuber, C., K.-U. Miltenberger, and H.-A. Synal (2019). "<sup>36</sup>Cl Measurements with a Gas-Filled Magnet at 6 MV". In: *Nucl. Instrum. Methods Phys. Res. B* 455, pp. 190–194. DOI: 10.1016/j.nimb.2018.12.046.
- Weijers, J. W. H. et al. (2007). "Coupled Thermal and Hydrological Evolution of Tropical Africa over the Last Deglaciation". In: *Science* 315.5819, pp. 1701–1704. DOI: 10.1126/science.1138131.



## Chapter 3

# Implications of present ground temperatures and relict stone stripes in the Ethiopian Highlands for the palaeoclimate of the tropics

Alexander R. Groos<sup>1</sup>, Janik Niederhauser<sup>1</sup>, Luise Wraase<sup>2</sup>, Falk Hänsel<sup>2</sup>, Thomas Naus<sup>2</sup>, Naki Akçar<sup>3</sup>, Heinz Veit<sup>1</sup>

<sup>1</sup>Institute of Geography, University of Bern, Switzerland

<sup>2</sup>Department of Geography, Philipps University of Marburg, Germany

<sup>3</sup>Institute of Geological Sciences, University of Bern, Switzerland

*Author contributions: A.R.G., N.A., and H.V. designed the research concept, conducted the geomorphological mapping, sampled the stone stripes for exposure dating, and installed the ground temperature loggers. A.R.G. and N.A. processed the rock samples in the laboratory. F.H. set up the weather stations. L.W. conducted the GPR measurements and serviced the weather stations. F.H., L.W., and T.N. processed and provided the meteorological data. A.R.G. and J.N. processed the ground temperature data, conducted the statistical analysis, and performed the ground temperature simulations. A.R.G. drafted the manuscript and figures with contributions from all authors.*

Under review in *Earth Surf. Dynam. Discuss.*

<https://doi.org/10.5194/esurf-2020-53>

Submitted: 19<sup>th</sup> June 2020

## Abstract

Large sorted patterned grounds are the most prominent features of periglacial and permafrost environments of the mid and high latitudes, but have not yet been verified for the tropics. Here, we report on relict large sorted polygons (up to 8 m in diameter) and large sorted stone stripes (up to 1000 m long, 15 m wide, and 2 m deep) on the ~4000 masl high Sanetti Plateau in the Bale Mountains, southern Ethiopian Highlands. For a systematic investigation of past and present frost-related processes and landforms in the Bale Mountains, we conducted geomorphological mapping both in the field and on satellite images. The sorted stone stripes were studied in more detail by applying aerial photogrammetry, ground-penetrating radar measurements, and  $^{36}\text{Cl}$  surface exposure dating. In addition, we installed 29 ground temperature data loggers between 3493 and 4377 masl to analyse present frost occurrence and seasonal temperature variations from 2017 to 2020. Finally, we ran a simple experiment and combined recent ground temperature measurements with meteorological data in a statistical model to assess the air temperature depression needed for the past formation of deep seasonal frost and cyclic freezing and thawing on the plateau. Our results show that relict and modern periglacial landforms are common in the Bale Mountains. Nocturnal superficial ground frost on the plateau occurs at 35-90 days per year, but the mean annual ground temperature ( $\sim 11^\circ\text{C}$ ) is far off from seasonal or permanent frost conditions. The modelling experiment suggests a minimum air temperature depression on the plateau of  $7.6 \pm 1.3^\circ\text{C}$  for the emergence of several decimetre deep seasonal frost. The stone stripes probably formed under periglacial conditions in proximity of a palaeo ice cap on the plateau during the coldest period(s) of the last glacial cycle. We hypothesise that the slightly inclined and unglaciated areas of the plateau, the coexistence of regolith and large blocks, the occurrence of deep seasonal frost, as well as relatively dry conditions beyond the ice cap provided ideal conditions for frost heave and sorting and the formation of large sorted patterned grounds. The presence of these landforms and the associated air temperature depression provide further evidence for an amplified cooling of high tropical mountains during the last glacial period that is yet not well captured in global climate models.

## 3.1 Introduction

The Earth experienced a pronounced global-mean cooling of  $5\text{-}7^\circ\text{C}$  during the global Last Glacial Maximum (LGM;  $22 \pm 4$  ka after Shakun and Carlson, 2010) compared to the pre-industrial climate, but the magnitude of cooling and expansion of ice sheets and glaciers varied considerably across the globe. While global climate models point towards a maximum cooling over the northern hemisphere ice sheets, they suggest only a moderate cooling for the tropics (Schneider von Deimling et al., 2006). A synthesis of sea surface temperatures testifies to a moderate mean zonal LGM cooling of the tropical oceans of  $\sim 2^\circ\text{C}$  (MARGO Project Members, 2009). However, terrestrial temperature reconstructions based on calculated snow line depressions on tropical mountains indicate a much stronger and more heterogeneous cooling of  $2\text{-}14^\circ\text{C}$  (Mark et al., 2005). Other terrestrial palaeoclimate data from the low-latitudes confirm the pronounced cooling over land and highlight an amplified cooling with increasing elevation

(Farrera et al., 1999; Loomis et al., 2017). Disentangling the causes for the mismatch between the reconstructed cooling of the tropical oceans and land areas, especially at high elevation, is crucial for understanding and simulating global climate changes during the last glacial period because the energy excess in the the tropics and transport towards higher latitudes drives the large-scale atmospheric and oceanic circulation (Kageyama, Harrison, and Abe-Ouchi, 2005). Model uncertainties and limitations as well as erroneous marine and terrestrial temperature reconstructions have been discussed as potential causes for the discrepancy. Climate model experiments and latest temperature reconstructions along an elevational gradient in Eastern Africa provide an alternative explanation: they support the interpretation that the amplified cooling at high elevations in the tropics during the global LGM was the result of a drier atmosphere and steeper lapse rate (Kageyama, Harrison, and Abe-Ouchi, 2005; Tripathi et al., 2014; Loomis et al., 2017). However, climate proxy data from the high tropical mountains are still sparse although they are essential for quantifying global LGM temperature changes in the middle troposphere (Farrera et al., 1999).

A promising region for high-elevation palaeoclimatic and geocological reconstructions in the tropics are the Bale Mountains in the southern Ethiopian Highlands as they comprise Africa's largest alpine environment and provide manifold evidence for past glacial and periglacial processes (Grab, 2002; Osmaston, Mitchell, and Osmaston, 2005; Hendrickx et al., 2014; Groos et al., in revision). During the Late Pleistocene, an ice cap with several outlet glaciers covered the central Sanetti Plateau and northern valleys of the Bale Mountains. The local maximum glacier expansion in the region was reached between 50-30 ka, well before the global LGM, and coincided with a temperature depression of 4-6 °C (Groos et al., in revision). In view of the gradual global cooling until  $22 \pm 4$  ka, an even stronger temperature depression ( $>6$  °C) in the Ethiopian Highlands seems likely after 50-30 ka. A conspicuous geomorphological feature beyond the glacial remains of the former ice cap on the Sanetti Plateau are large sorted stone stripes (several meters wide and hundred meters long) between 3850 and 4150 masl. They are associated with past sporadic permafrost and might indicate a severe cooling in the Bale Mountains during the Pleistocene (Miehe and Miehe, 1994; Grab, 2002). Sorted patterned grounds of similar size are typical for periglacial and permafrost environments of the mid and high latitudes (Goldthwait, 1976; André et al., 2008). Diurnal freeze-thaw cycles in tropical mountains are sufficient for the development of small-scale patterned grounds (Francou, Méhauté, and Jomelli, 2001), but the large dimension of the stone stripes on the Sanetti Plateau is unique for the low latitudes as their formation presumably requires deep ground frost and seasonal freezing and thawing (e.g. Kessler and Werner, 2003). A systematic investigation of the relict periglacial landforms and present frost patterns in the Bale Mountains is lacking. When, how, and under which environmental conditions the relict patterned grounds formed and what their occurrence implies for the palaeoclimate of the tropics is therefore still unexplored.

The aim of this study is the systematic investigation of past and present frost-related processes and landforms in the Bale Mountains to elaborate the potential of geomorphological features like the large sorted stone stripes for paleoclimatic reconstructions at high-elevations in the tropics. For gaining insights into the spatial and elevational distribution of relict and active periglacial landforms, we conducted geomorphological mapping both in the field and on

high-resolution satellite images. The sorted stone stripes on the Sanetti Plateau were studied in more detail by applying aerial photogrammetry, ground-penetrating radar (GPR) measurements, and  $^{36}\text{Cl}$  surface exposure dating. The  $^{36}\text{Cl}$  ages were originally published by Groos et al. (in revision) in a palaeoglaciological context, but we present them here again as they are also of relevance for the interpretation of the relict stone stripes. Since knowledge on present frost occurrence and ground temperature variations in the Bale Mountains is indispensable for discussing how and under which climatic and environmental conditions the relict structures may have formed, we installed a ground temperature network covering the Sanetti Plateau and northeastern declivity. In a final step, we combined the ground temperature measurements with meteorological data from nearby weather stations and applied a simple statistical model to assess the minimum air temperature depression needed for the formation of deep frost and patterned grounds in the tropical Ethiopian Highlands.

## 3.2 Study Area

The Bale Mountains (6.6–7.1 °N, 39.5–40.0 °E) are located southeast of the Main Ethiopian Rift and belong to the Bale-Arsi massif which constitutes the western part of the southern Ethiopian Highlands (Fig. 3.1). Precambrian rocks and overlying Mesozoic marine sediments form the base of the massif and are covered by Cenozoic trachytic and basaltic lava flows (Miehe and Miehe, 1994; Osmaston, Mitchell, and Osmaston, 2005; Hendrickx et al., 2014). Due to the lack of geological maps, lithological information, geochemical studies, and radiometric dating, especially in the southern Ethiopian Highlands, the exact timing of volcanic eruptions is unknown and the successive formation of the Bale-Arsi massif still poorly understood (Mohr, 1983; Osmaston, Mitchell, and Osmaston, 2005). Characteristic for the Bale Mountains is the central Sanetti Plateau with a mean elevation of ~4000 masl. It is bounded to the west by hardly weathered lava flows, to the north and east by broad U-shaped valleys, and to the south by the Haremma Escarpment. Several volcanic plugs and cinder cones like the highest peak Tullu Dimtu (4377 masl) rise above the plateau (Osmaston, Mitchell, and Osmaston, 2005). With an area of almost 2000 km<sup>2</sup> above 3000 masl, the Bale Mountains comprise Africa's most extensive alpine environment (Groos et al., in revision) and are an important fresh water source for the surrounding lowlands. The main tributaries of the only two perennial rivers in the Somali lowlands, Shebelle and Jubba, originate from the Bale Mountains.

The seasonal movement of the Intertropical Convergence Zone (ITCZ) and zonal shift of the Congo Air Boundary, which defines the confluence of air masses from the Indian Ocean and Atlantic, determines the climate and rainfall patterns of the Ethiopian Highlands (Levin, Zipser, and Cerling, 2009; Tierney et al., 2011; Costa et al., 2014). Due to the complex topography, the mean annual precipitation varies considerably across the region and is strongly linked to elevation (Gebrechorkos, Hülsmann, and Bernhofer, 2019). Three seasons characterise the current climate: The dry season (traditionally called "Bega") lasts from November to February and is followed by two rainy seasons ("Belg" and "Kiremt"). While "Belg" (March to June) is more pronounced in the southern Ethiopian Highlands, "Kiremt" (July to October) plays a

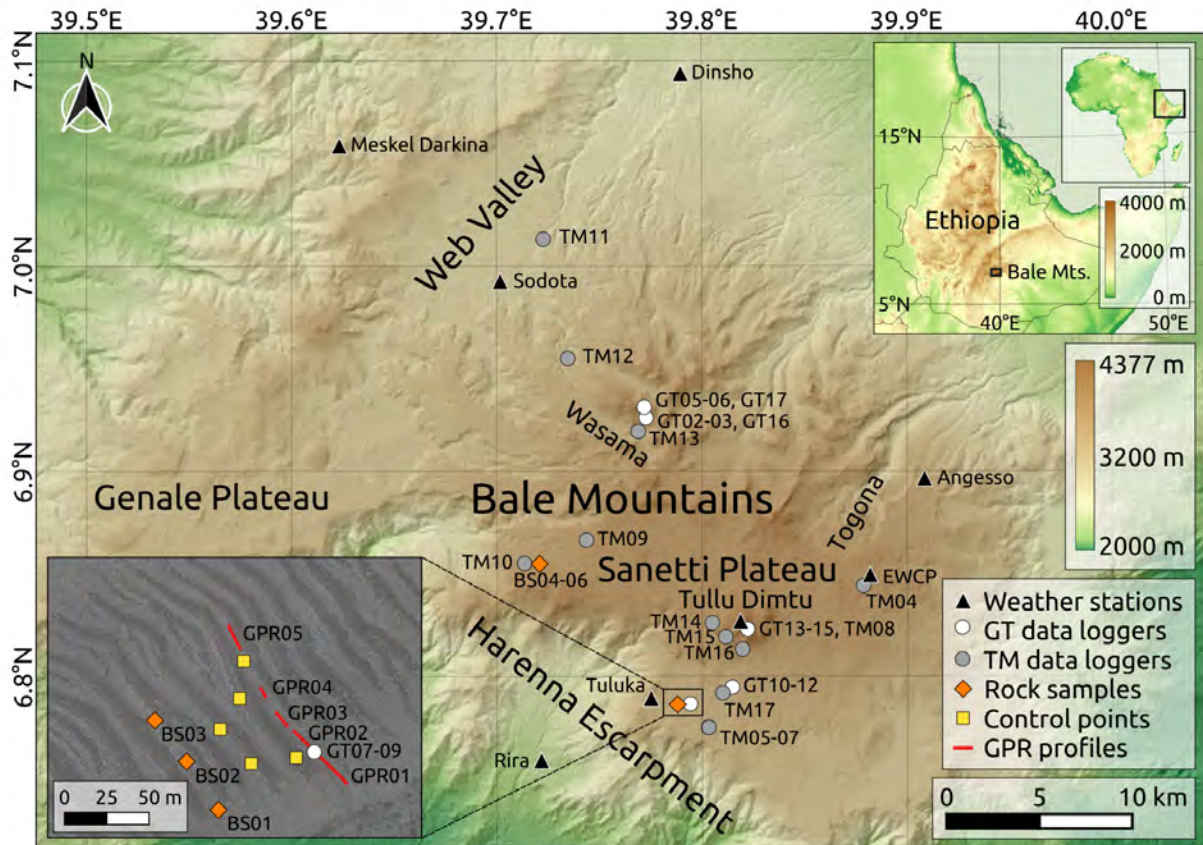


FIGURE 3.1: Overview map of the experimental setup and observation network in the Bale Mountains, southern Ethiopia. The lowest weather stations Magnete (1599 masl) and Delo Mena (1315 masl) are located 25 and 40 km south of Rira. GT: high-quality temperature data loggers. TM: low-cost temperature data loggers. Rock samples: blocks sampled for surface exposure dating. Control points: natural objects used for the georeferencing of the high-resolution orthophoto and digital surface model. GPR: ground-penetrating radar. Data basis: SRTM 1 Arc-Second Global (United States Geological Survey) and high-resolution WorldView-1 satellite image (DigitalGlobe Foundation).

major role in the northern highlands including the upper catchment area of the Blue Nile (Conway, 2000; Seleshi and Zanke, 2004). During the dry season, when the ITCZ in Eastern Africa is located south of the equator and high pressure cells have established over Western Asia and the Sahara, northeasterly trade winds from the Arabian Peninsula and Sea prevail in the Bale Mountains and cause only little precipitation. Along with the northward movement of the ITCZ from March to June, the main wind direction changes from northeast to southeast and brings moist air from the southern Indian Ocean to the Bale Mountains (Lemma et al., 2020). Although the Gulf of Guinea and Congo Basin are important moisture sources for the northern Ethiopian Highlands (Levin, Zipser, and Cerling, 2009; Viste and Sorteberg, 2013; Costa et al., 2014), they seem of minor relevance for the Bale-Arsi massif (Lemma et al., 2020). The Sanetti Plateau and highest peaks of the massif experience occasional snowfall during the rainy seasons, but the thin snowpack usually melts within hours or days (Miehe and Miehe, 1994).

Like most of the other tropical mountains in Eastern Africa, the Bale Mountains are currently unglaciated. The present mean  $0^{\circ}\text{C}$  isotherm (a rough proxy for the modern snow line in the tropics) is located at least 300 m above the highest peak Tullu Dimtu. However, latest glacial geomorphological and chronological studies provide clear evidence that the snow

line was much lower during the Late Pleistocene and favoured the formation of an extensive plateau glaciation with outlet glaciers extending down into the northern valleys. Between 50-30 ka during the local Last Glacial Maximum in the southern Ethiopian Highlands, ice covered about 265 km<sup>2</sup> of the Bale and additional 83 km<sup>2</sup> of the adjacent Arsi Mountains. Two later glacial stages were dated to ~18 and ~15 ka. At ~18 ka, the ice extent was slightly smaller than during the local LGM, but ice still covered the central part of the plateau and northern valleys. Deglaciation in the region set in after ~18-15 ka. The highlands remained probably ice-free over the entire Holocene (Ossendorf et al., 2019; Groos et al., in revision). Besides glacial landforms like moraines and roche moutonnées, also relict periglacial features have been reported from the Bale Mountains (Grab, 2002; Hendrickx et al., 2014). Among those, large sorted stone circles (several meters in diameter) and stone stripes (several meters wide and hundred meter long) on the Sanetti Plateau are the most prominent ones. The formation of such large features is associated with freeze-thaw processes and indicates decimetre to meter deep seasonal frost or sporadic permafrost with a thick active layer (see Sections 3.3.7, 3.4, and 3.5). Field observations and short-term ground temperature measurements between December 1989 and March 1990 verify that nocturnal frost near the soil-atmosphere interface still occurs. The most apparent results of the modern freeze-thaw cycles are the formation of needle ice along saturated stream banks and the presence of sorted stone nets in flat and poorly drained areas on the Sanetti Plateau (Miehe and Miehe, 1994; Grab, 2002).

Afroalpine herbs, grasses, *Helichrysum* dwarf shrubs, extrazonal patches of *Erica*, and giant lobelias cover the ice-free and barren Sanetti Plateau today (Miehe and Miehe, 1994). The plateau is home to many endemic plant species like the giant lobelia (*Lobelia rhynchopetalum*) (Chala et al., 2016) and mammal species like the Ethiopian wolf (*Canis simensis*) (e.g. Gottelli et al., 1994), giant mole-rat (*Tachyoryctes macrocephalus*) (e.g. Vlasatá et al., 2017), and mountain nyala (*Tragelaphus buxtoni*) that are restricted to the Ethiopian Highlands (Miehe and Miehe, 1994). Since these endemic species mainly populate the upper valleys and Sanetti Plateau today, palaeoclimatic and -environmental changes like a severe cooling, expansion of the ice cover and periglacial area as well as depression of altitudinal vegetation belts must have directly affected their habitat and are therefore also of relevance in a geocological context.

### 3.3 Data and Methods

#### 3.3.1 Mapping of periglacial landforms

Comprehensive and thorough geomorphological mapping of glacial and periglacial landforms provides crucial data for establishing glacial chronologies and reconstructing the palaeoclimate and palaeoenvironment of polar and alpine regions (Chandler et al., 2018). We evaluated maps, photographs, and field notes from previous studies dealing with periglacial processes and landforms in the Bale Mountains (e.g. Messerli and Winiger, 1992; Miehe and Miehe, 1994; Grab, 2002; Umer, Kebede, and Osmaston, 2004; Osmaston, Mitchell, and Osmaston, 2005) to compile evidence of relict and modern frost occurrence. Since periglacial landforms have yet not been described systematically, we performed extensive geomorphological mapping on

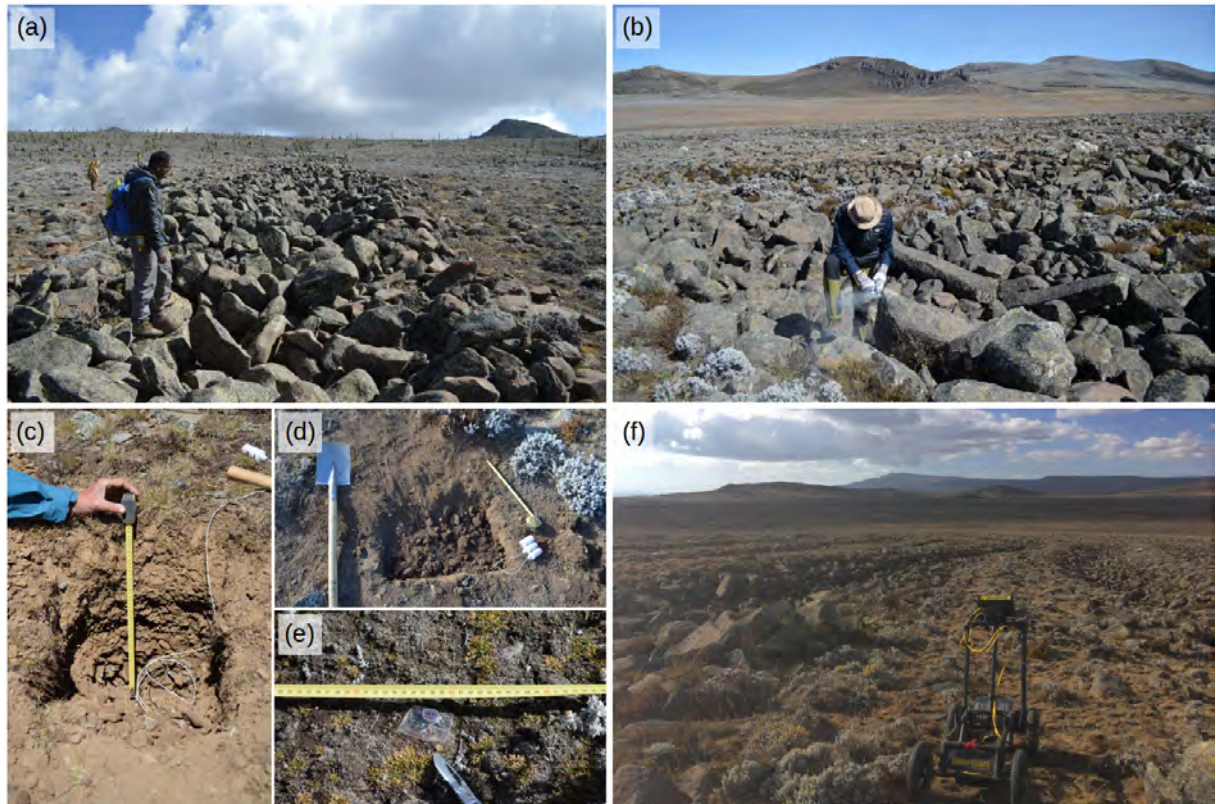


FIGURE 3.2: Field work in the Bale Mountains: (a) reconnaissance and mapping of periglacial landforms, (b) sampling of stone stripes for surface exposure dating, (c-e) installation of ground temperature loggers, and (f) ground-penetrating radar survey.

the Sanetti Plateau, along the upper Hareenna Escarpment and in the western, northern, and eastern valleys during multiple field excursions between 2016 and 2020 (Fig. 3.2). In addition, we evaluated high-resolution WorldView-1 satellite images (pixel size = 0.5 m) provided by the DigitalGlobe Foundation to identify features in remote and difficult-to-access areas of the mountain range. All periglacial features discovered in the field or on satellite images were geotagged and compiled in a catalogue (see Table B.1).

For a detailed analysis of the geomorphology, geometry, and size of the sorted stone stripes on the Sanetti Plateau, we conducted a manual aerial survey (~50 m above ground level) with a small quadcopter (DJI Mavic Pro) on the 30<sup>th</sup> January 2020 at 2 pm local time. A total of 75 aerial images were acquired during the survey and processed with the photogrammetric software OpenDroneMap (following the approach described in Groos et al., 2019) to obtain a high-resolution orthophoto (5 cm) and digital surface model (DSM, 10 cm) of the stone stripes. Five natural objects (rocks and dwarf shrubs) visible on the orthorectified WorldView-1 image and at least on three aerial images were used as ground control points (Fig. 3.1) for a rough georeferencing of the orthophoto and DSM (Groos et al., 2019). The necessary elevation information were extracted from the SRTM 1 Arc-Second Global dataset.

### 3.3.2 Ground-penetrating radar measurements

Investigating the internal structure of the sorted stone stripes by excavating a transect was not possible due to regulations. Instead, we performed a ground-penetrating radar (GPR) survey between two stripes on the southern Sanetti Plateau on the 10<sup>th</sup> February 2020 (Fig. 3.1). We made use of the Pulse EKKO PRO GPR with a 1000 MHz antenna (7.5 cm sensor width) manufactured by Sensors & Software Inc., which was originally purchased by another sub-project of the Ethio-European DFG Research Unit 2358 “The Mountain Exile Hypothesis” for geocological investigations (for system settings see Table B.2). The GPR was mounted on a compatible pushcart (Fig. 3.2). As survey setting, an exploration depth of 1 m and pulse length of 16 nanoseconds (ns) was applied for the first line and modified to 1.5 m depth and 24 ns pulse length for the following lines. The starting point of the GPR measurement was located 10 m above the position of data loggers GT07-09 since the uppermost part of the volcanic plug was not accessible with the pushcart. Due to uneven terrain and several natural obstacles like smaller stones and *Helichrysum* dwarf shrubs, the GPR profile between the two stone stripes was split into five separate lines varying between 3.8 and 38.5 m in length. The chaotic structure of the stones stripes prevented a GPR survey inside the troughs and coarse material. For analysis and visualisation of the GPR data, we used the software EKKO Project (version 5.0).

### 3.3.3 <sup>36</sup>Cl surface exposure dating of periglacial landforms

Previous studies have demonstrated that the stabilisation age of relict periglacial features like rock glaciers and block fields can be successfully dated with cosmogenic nuclides (e.g. Barrows, Stone, and Fifield, 2004; Ivy-Ochs et al., 2009; Steinemann et al., in press). In analogy, we sampled two sorted stone stripes on the Sanetti Plateau, one about 5 km south and another one about 10 km west of Tullu Dimtu (Fig. 3.1), to determine the stabilisation age of these features. The results were originally published by Groos et al. (in revision) in a palaeoglaciological context. We present them here briefly again as they are also of relevance for the discussion of the origin of the sorted stone stripes. From both ston stripes, we selected three columnar rocks for <sup>36</sup>Cl surface exposure dating (Table 3.1). To avoid distorting effects on exposure dating due to strong shielding in the trough-shaped stripes or toppling of rocks after the stabilisation phase, we only chose rocks that were sticking out a bit and were wedged between other rocks. The upper few centimetres of each target rock were sampled with hammer, chisel, and angle grinder for the subsequent laboratory analysis (Fig. 3.2). An inclinometer was used in the field for measuring the topographic shielding. For extraction of the isotope <sup>36</sup>Cl, the six samples were crushed, sieved and chemically treated in the Surface Exposure Dating Laboratory of the University of Bern. Total Cl- and <sup>36</sup>Cl-concentrations (see Table B.4) were measured from one target at the 6 MV AMS-facility of the ETH Zurich using the isotope dilution technique (Ivy-Ochs et al., 2004) and a gas-filled magnet to separate <sup>36</sup>S (Vockenhuber, Miltenberger, and Synal, 2019). For a detailed description of the sample preparation, Cl and <sup>36</sup>Cl measurements, and surface exposure age calculation see Groos et al. (in revision).

TABLE 3.1: Description of periglacial features on the Sanetti Plateau sampled for  $^{36}\text{Cl}$  surface exposure dating. TAD = Trachyandesite.

Rock sample	Lithology	Latitude (°N)	Longitude (°E)	Elevation (masl)	Boulder length (m)	Boulder width (m)	Boulder height (m)	Sample thickness (cm)	Shielding factor
BS01	Basalt	6.78634	39.79297	3874	2.1	0.6	1.0	2.5	0.9961
BS02	Basalt	6.78660	39.79280	3869	1.5	0.5	1.4	4.5	0.9961
BS03	Basalt	6.78682	39.79263	3865	0.6	0.4	1.0	3.0	0.9997
BS04	Basalt	6.85491	39.72078	4050	0.8	0.6	1.1	5.0	0.9990
BS05	TAD	6.85513	39.72074	4049	0.5	0.5	1.0	4.5	0.9990
BS06	TAD	6.85550	39.72049	4045	1.5	0.5	0.6	3.5	0.9994

### 3.3.4 Ground temperature measurements

For measuring hourly ground temperatures of the Bale Mountains, we installed high-quality UTL-3 Scientific Dataloggers (hereafter GT data loggers) in 2, 10, and 50 cm depth at five different locations with little vegetation between 3877 and 4377 masl (Fig. 3.1 and Table 3.2). The GT data loggers are developed by GEOTEST Ltd. in collaboration with the Swiss Institute for Snow and Avalanche Research. They consist of a waterproof housing, a YSI 44005 thermistor for measuring temperature, a memory for up to 65,000 readings (>7 years by hourly interval), a replaceable 3.6 V lithium battery for power supply, and a USB interface for data transfer. According to the manufacturer, the measurement accuracy is  $<0.1\text{ }^{\circ}\text{C}$  at  $0\text{ }^{\circ}\text{C}$  and the thermometric drift per 100 months is  $<0.01\text{ }^{\circ}\text{C}$  at  $0\text{ }^{\circ}\text{C}$ . At each of the five measurement sites, the upper 50 cm of the ground were removed to install the GT data loggers (Fig. 3.2). We used data loggers with an external cable and thermistor for the measurements in 10 and 50 cm depth. A standard logger without external cable was placed just below the surface in 2 cm depth. After the installation, each hole was filled in the same order as during the excavation to ensure as little disturbance of the profile as possible. Additional low-cost tempmate.-B2 temperature data loggers (hereafter TM data loggers) in the size of a button cell (Fig. 3.2) were distributed across the Bale Mountains between 3493 and 4377 masl to increase the spatial coverage of near-surface (2 cm) hourly ground temperature measurements (Fig. 3.1 and Table 3.2). The single-use TM data loggers consist of a splashproof housing (we wrapped the loggers in thin tape for better protection), an unspecified thermistor, a memory for up to 8192 readings (341 days by hourly interval), and an irreplaceable 3.0 V battery. A logger-pan-to-USB cable is needed for connecting the TM loggers to a computer and retrieving the data. The measurement accuracy is  $\pm 0.5\text{ }^{\circ}\text{C}$  at  $-10$  to  $65\text{ }^{\circ}\text{C}$  according to the manufacturer. Due to the much lower accuracy of the TM data loggers compared to the GT data loggers, we performed a comparative measurement indoor over several hours with logger GT04 as reference. Since the root-mean-square deviation of each TM data logger from the reference measurement was smaller than the stated accuracy of  $\pm 0.5\text{ }^{\circ}\text{C}$ , a calibration was unnecessary. For a direct cross-comparison in the field, data logger TM08 was installed next to GT13 in 2 cm depth on top of Tullu Dimtu. Two TM data logger (16 and 17) were buried below *Erica* in 10 cm depth for comparison with sites (TM14 and TM15) with only little vegetation.

Several issues occurred during the measurement period from January 2017 to January 2020

TABLE 3.2: Overview of the installed ground temperature data loggers (excluding six lost items).

Data logger	Latitude (°N)	Longitude (°E)	Elevation (masl)	Depth (cm)	Slope (°)	Aspect (°)	Start of measurement	Readout dates
GT16	6.92725	39.77275	4153	2 ± 1	22	140	31.12.17	14.06.18, 23.01.20
GT02	6.92725	39.77275	4153	10 ± 2	22	140	06.01.17	17.12.17, 31.12.17, 14.06.18, 23.01.20
GT03	6.92725	39.77275	4153	50 ± 5	22	140	06.01.17	17.12.17, 31.12.17, 14.06.18, 23.01.20
GT17	6.93000	39.77188	4181	2 ± 1	19	35	31.12.17	14.06.18, 23.01.20
GT05	6.93000	39.77188	4181	10 ± 2	19	35	06.01.17	17.12.17, 31.12.17, 14.06.18, 23.01.20
GT06	6.93000	39.77188	4181	50 ± 5	19	35	06.01.17	17.12.17, 31.12.17, 14.06.18, 23.01.20
GT07	6.78665	39.79342	3877	2 ± 1	8	320	21.01.17	10.12.17, 06.01.18, 25.01.20
GT08	6.78665	39.79342	3877	10 ± 2	8	320	21.01.17	10.12.17, 06.01.18, 25.01.20
GT09	6.78665	39.79342	3877	50 ± 5	8	320	21.01.17	10.12.17, 06.01.18, 25.01.20
GT10	6.79474	39.81469	3932	2 ± 1	10	130	21.01.17	11.12.17, 06.01.18, 26.01.20
GT11	6.79474	39.81469	3932	10 ± 2	10	130	21.01.17	11.12.17, 06.01.18, 26.01.20
GT12	6.79474	39.81469	3932	50 ± 5	10	130	21.01.17	11.12.17, 06.01.18, 26.01.20
GT13	6.82617	39.81897	4377	2 ± 1	0	-	21.01.17	19.12.17, 20.01.20, 26.01.20
GT14	6.82617	39.81897	4377	10 ± 2	0	-	21.01.17	19.12.17, 20.01.20
GT15	6.82617	39.81897	4377	50 ± 5	0	-	21.01.17	19.12.17, 26.01.20
TM04	6.84411	39.87876	4129	2 ± 1	0	-	18.01.17	09.12.17, 05.01.18, 10.06.18
TM05	6.77522	39.80307	3858	2 ± 1	0	-	18.01.17	09.12.17, 06.01.18, 29.12.18, 25.01.20
TM06	6.77535	39.80311	3857	2 ± 1	0	-	18.01.17	09.12.17, 06.01.18, 29.12.18
TM07	6.77521	39.80318	3856	2 ± 1	0	-	18.01.17	09.12.17, 06.01.18, 29.12.18, 25.01.20
TM08	6.82617	39.81897	4377	2 ± 1	0	-	21.01.17	19.12.17
TM09	6.86644	39.74365	4084	2 ± 1	0	-	23.01.17	12.12.17, 15.06.18, 24.01.20
TM10	6.85509	39.71345	4022	2 ± 1	0	-	23.01.17	13.12.17, 15.06.18, 24.01.20
TM11	7.01307	39.72272	3493	2 ± 1	0	-	29.12.17	14.06.18
TM12	6.95493	39.73463	3769	2 ± 1	0	-	30.12.17	14.06.18, 22.01.20
TM13	6.91937	39.76898	3930	2 ± 1	0	-	31.12.17	14.06.18, 22.01.20
TM14	6.82605	39.80496	4124	10 ± 2	0	-	06.01.18	30.12.18, 26.01.20
TM15	6.81928	39.81152	4185	10 ± 2	0	-	06.01.18	30.12.18, 16.02.20
TM16	6.81327	39.81968	4103	10 ± 2	0	-	06.01.18	30.12.18, 26.01.20
TM17	6.79197	39.81005	3880	10 ± 2	0	-	06.01.18	31.12.18, 26.01.20

and caused considerable data gaps (Fig. 3.3). The data logger positions were originally marked with four small plastic poles in 2 m distance. They were apparently too conspicuous and led to the loss of several items (GT01, GT04, GT18, TM01-03, TM08, and TM11). Therefore, we removed all poles and switched to natural markers (dwarf shrubs, stones, etc.). Data loggers GT01 and GT04 were replaced by GT16 and GT17. On Tullu Dimtu, data loggers GT13-15 were taken away in May 2017, but could be recovered and reinstalled in January 2018. Furthermore, we also noticed a relatively short battery life of just two years for some of the GT and TM data loggers leading to a substantial data loss. Two years are much shorter than the battery life stated by both manufacturers for the respective sampling interval (GT ~ 3-5 years, TM ~ 5 years). After consultation, the manufacturer of the GT data loggers adjusted the internal handling of the lithium batteries to ensure the stated battery life. The two data loggers TM05 and TM06 temporarily recorded unrealistic low values (down to -40 °C). Individual outliers and

longer periods with implausible measurements were removed from the time series. After the first reading of data logger GT07, we realised that it was accidentally placed in 6 cm depth and not in 2 cm as intended. The relocation towards the surface in December 2017 led to an abrupt increase in the temperature amplitude. Therefore, we calculated hourly ground temperature gradients between 6 and 10 cm depth from GT07 and GT08 data by applying a simple linear regression to extrapolate the GT07 measurements from 6 to 2 cm in the period 21<sup>st</sup> January to 10<sup>th</sup> December 2017. A compilation of all ground temperature time series from the Bale Mountains is provided in Table S1. Data gaps were filled using a simple linear regression and data from other GT or TM data loggers to generate a complete data set for the period 1<sup>st</sup> of February 2017 to 20<sup>th</sup> January 2020 (see Section 3.3.6). All data modifications made for each logger are listed in Table S2 (see data availability statement for Tables S1-4).

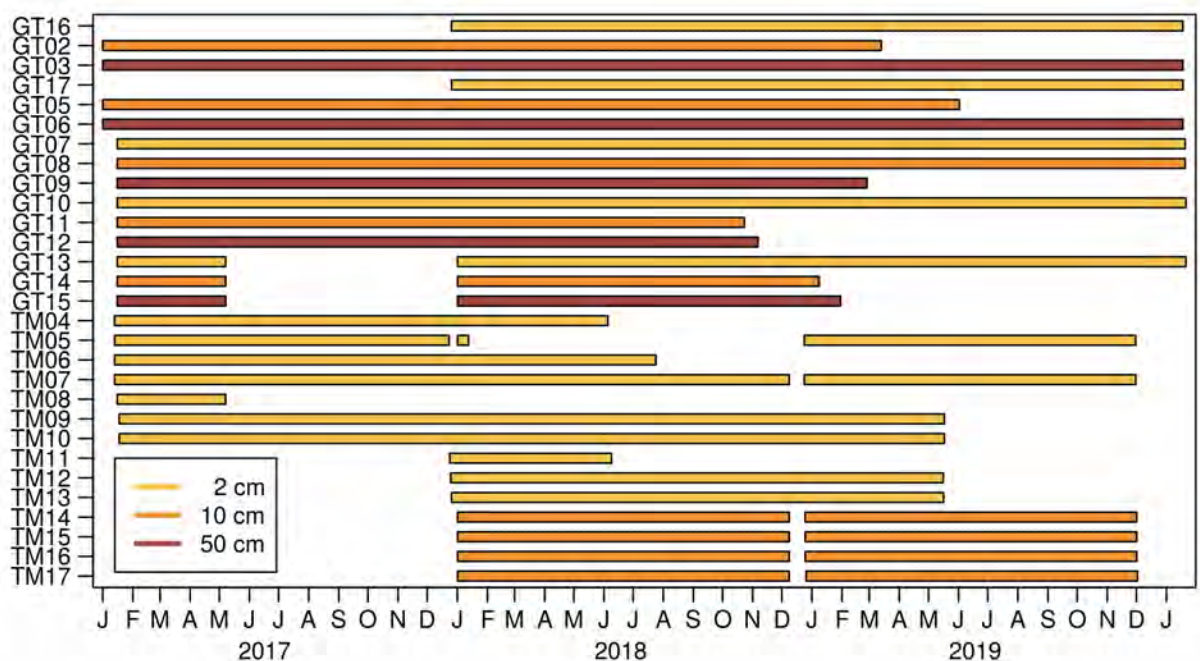


FIGURE 3.3: Measurement period(s) of each ground temperature data logger between January 2017 and January 2020. For the statistical gap-filling method applied to obtain complete time series see Section 3.6.

### 3.3.5 Meteorological measurements

Within the framework of the DFG Research Unit 2358 ten automatic weather stations (AWS) were installed in the Bale Mountains national park between 1315 and 4377 masl beginning of 2017 (Table 3.3). The AWS are manufactured by Campbell Scientific and consist of a three metre galvanised tubing tripod, a grounding kit, a weather-resistant enclosure, a measurement and control system (CR800), a solar module (SDT200), a 168 Wh battery, a charging regulator, a temperature and relative humidity probe (CS215) with radiation shield, a pyranometer (LI-200R), a two-dimensional ultrasonic anemometer from Gill Instruments, and a rain gauge from Texas Electronics (TR-525USW 8"). For protection, the AWS are wire-fenced by a 3 x 3 m compound. Air temperature, relative humidity, and global radiation are measured in 2 m height, wind

speed and wind direction in 2.6 m height, and precipitation in 1 m height. The measurement interval is 15 minutes. All measured variables are finally aggregated to hourly averages.

TABLE 3.3: Overview of the installed automatic weather stations in the Bale Mountains. \*Ratio of actual to maximum possible measurements during the respective measurement period. \*\*The weather station was abandoned after breakdown in April 2018.

Weather station	Location	Latitude (°N)	Longitude (°E)	Elevation (masl)	First measurement	Last	Data completeness (%)*
BALE001	Tullu Dimtu	6.82693	39.81871	4377	04.02.17	31.01.20	73
BALE002	Tuluka	6.78945	39.77511	3848	02.02.17	30.01.20	100
BALE003	Angesso Station	6.89642	39.90854	3949	31.01.17	30.01.20	68
BALE004	Magnete	6.51622	39.74515	1599	06.02.17	01.02.20	100
BALE005	Meskel Darkina	7.05860	39.62336	3724	09.02.17	05.10.19	97
BALE006	Rira Substation	6.75912	39.72161	2803	06.02.17	19.02.20	86
BALE007	Dinsho Head Quarter	7.09378	39.78966	3208	28.01.17	20.02.20	100
BALE008	Sodota**	6.99249	39.70171	3529	29.01.17	21.04.18	100
BALE009	EWCP Station	6.84945	39.88197	4124	01.02.17	30.01.20	100
BALE010	Delo Mena	6.41199	39.83328	1315	11.02.17	01.02.20	100

### 3.3.6 Statistical data interpolation and analysis

To obtain a complete and consistent data set of hourly ground temperatures for the Bale Mountains from 1<sup>st</sup> February 2017 until 20<sup>th</sup> January 2020, we applied a statistical gap-filling approach. Most of the ground temperature measurements from different locations or depths overlap for a certain period in time (see Fig. 3.3) and allow to establish a statistical relationship. We applied a simple linear regression model to interpolate missing data points in the time series of a logger using data from a nearby logger for which measurements were available. If multiple logger with a similar equidistance came into question for the interpolation, we chose the one that yielded the best fit (evaluated by the coefficient of determination  $R^2$ ) and lowest root-mean-square error (RMSE). The overlapping measurement period between the predicting logger and dependent logger was split into a calibration and validation part. For the interpolation of incomplete time series in 10 or 50 cm depth, we drew on available data from 2 cm depth of the same location. We used a moving average of the data from 2 cm depth to account for the time-lag response to atmospheric changes in greater depths. The number of preceding hours considered for the calculation of the moving average that yielded the best prediction (high  $R^2$ , low RMSE) of the ground temperatures in 10 or 50 cm depth was chosen. Details on the data gap-filling of each incomplete time series are provided in Table S4. The validation of the simple linear models applied for interpolation revealed an average  $R^2$  of  $0.86 \pm 0.07$  and RMSE of  $1.9 \pm 1.4$  °C. The time series of the data loggers TM05-06, TM08, and TM14-17 were not interpolated because the data served only for comparative experiments (low-cost vs. high-quality loggers, vegetated vs. unvegetated locations, etc.) and were dispensable for the temporal and elevational analysis.

Most of the AWS installed in the Bale Mountains measured continuously, but some of the time series are interrupted due to issues with the power supply (Table 3.3). The hourly meteorological data from the different AWS are stored in an online database and gaps in the time series of all variables except wind speed and direction are interpolated statistically following a workflow developed by Wöllauer et al. (in revision). Single missing values are interpolated linearly using the average of the adjacent data points. Longer gaps in a time series are filled using available data from several nearby AWS. A multiple linear regression model fitted with data from the overlapping measurement periods is applied to predict the missing values from data of those AWS that reveal a strong correlation and low RMSE. Predictor variables (AWS) with a high  $R^2$  and low error are given a higher weight in the interpolation.

We evaluated the interpolated hourly meteorological and ground temperature data statistically to quantify frost occurrence and spatio-temporal ground temperature variations in the Bale Mountains. Twelve data loggers from 2 cm depth (excluding TM05-06, TM08, and TM14-17) and five loggers from 10 and 50 cm depth were considered for calculating mean annual ground temperatures, daily ground temperature cycles, thermal gradients, number of frost days, frost penetration depth, elevational gradients, etc. To study seasonal ground temperature variations related to changes in insolation, cloudiness and humidity, we conducted the calculations separately for the entire study period, the dry season (Bega: November – February), and the two rainy seasons (Belg: March – June, Kiremt: July – October). Furthermore, comparative measurements were performed to investigate the differences in ground temperature between north- and south-facing slopes (GT16 and GT02-03 vs. GT17 and GT05-06), vegetated and un-vegetated areas (TM16-17 vs. TM14-15), and the performance of low-cost vs. high-quality data loggers (TM08 vs. GT13).

### 3.3.7 Ground temperature modelling and palaeoclimate reconstruction

The potential of periglacial landforms for paleoclimatic and environmental reconstructions has already been pointed out in pioneering studies from more than half a century ago (e.g. Galloway, 1965). Periglacial landforms are often more abundant than glacial deposits, especially in dry regions, and can be a more reliable climate proxy than palaeo glacier extents as their formation is less sensitive to changes in precipitation. Here, we explore a novel and experimental approach to infer palaeoclimatic information from relict periglacial landforms and established ground temperature modelling (e.g. MacLean and Ayres, 1985) using on-site meteorological data and present ground temperature measurements.

We make the following main assumptions for our model experiment: First, the large sorted stone stripes on the Sanetti Plateau are of periglacial origin and their formation required deep seasonal frost or sporadic permafrost with a thick active layer (see Sections 3.4 and 3.5 for arguments supporting this interpretation). Second, deep seasonal frost (or permafrost) forms when the long-term mean annual ground temperature is  $< -1$  °C. Third, the impact of the geothermal heat flux on ground temperatures near the surface is negligible in the Bale Mountain. The principal idea of the introduced method is to establish a statistical relationship between the measured ground temperatures and a set of meteorological variables for simulating under which

climatic conditions (e.g. decrease in air temperature and insolation) the mean ground temperature would approximate frost conditions. For the development of separate multiple linear regression models, we considered three locations on the Sanetti Plateau where ground temperatures and meteorological variables were measured simultaneously (Tullu Dimtu, EWCP Station, Tuluka). We chose only air temperature and global radiation as explanatory variables. The wind speed time series contains data gaps, precipitation is limited to individual rain events, and relative humidity does not show a direct linear relationship with ground temperature (see Section 3.4.3). The multiple linear regression model at each site was calibrated for the period 1<sup>st</sup> February 2017 – 31<sup>st</sup> January 2019 and validated for the period 1<sup>st</sup> February 2019 – 20<sup>th</sup> January 2020. Based on the established statistical relationship, present-day hourly ground temperatures in 2 cm ( $T_{2cm}$ ) can be modelled using measured air temperature and incoming shortwave radiation:

$$T_{2cm,i} = \beta_0 + (\beta_1 \times T_{air,i}) + (\beta_2 \times Q_{S,i}), \quad (3.1)$$

where  $T_{air,i}$  ( $i = 1, \dots, n$ ) is the hourly measured air temperature in °C,  $Q_{S,i}$  is the hourly measured incoming shortwave radiation in  $W m^{-2}$ ,  $\beta_0$  is the intercept,  $\beta_1$  is the coefficient for  $T_{air}$ , and  $\beta_2$  is the coefficient for  $Q_S$ . The coefficients and goodness of fit for each of the three linear models are provided in Table 3.4. For simulating past ground temperatures, two additional parameters,  $\Delta T_{air}$  and  $\Delta Q_S$ , were introduced:

$$T_{2cm,i} = \beta_0 + (\beta_1 \times (T_{air,i} - \Delta T_{air})) + (\beta_2 \times (Q_{S,i} - \Delta Q_S)), \quad (3.2)$$

where  $\Delta T_{air}$  is the difference between the mean present-day and past air temperature in °C and  $\Delta Q_S$  is the difference between the mean present-day and past incoming shortwave radiation in  $W m^{-2}$ . For simplicity, we set  $\Delta Q_S$  to  $30 W m^{-2}$  (the rough lowering of incoming shortwave radiation during the LGM at 15°N, see Groos et al., in revision). To infer the air temperature depression at the formation time of the periglacial landforms using Eq. 3.2, we increased  $\Delta T_{air}$  (starting with:  $\Delta T_{air} = 0^\circ C$ ) with every iteration until  $T_{2cm}$  became  $< -1^\circ C$ . We tested all three developed multiple linear regression models (Tullu Dimtu, EWCP Station, and Tuluka) to quantify the uncertainty of the approach originating from differences in the model coefficients  $\beta$  (Table 3.4). Since the lowest-situated stone stripes on the Sanetti Plateau are located at an elevation of 3870-3890 masl, we used meteorological data ( $T_{air}$  and  $Q_S$ ) from the Tuluka AWS at 3848 masl to run the three models. Alternatively, the meteorological data from the higher-situated AWS (Tullu Dimtu and ECWP Station) can be adjusted to the elevation of the stone stripes using a lapse rate of  $0.7^\circ C$  per 100 m (see Section 3.4.2). Running each model with the locally adjusted meteorological data led to the same calculated temperature depression as using the Tuluka AWS data. We rescaled the simulated ground temperatures in 2 cm depth to the maximum seasonal ground temperature variations in 10 and 50 cm depth observed today (see Section 3.4.2) to model temperature variations in these depths:

$$T_{50cm,i} = (\bar{T}_{2cm} - a) + \frac{(T_{2cm,i} - \min(T_{2cm})) \times (b - a)}{(\max(T_{2cm}) - \min(T_{2cm}))}, \quad (3.3)$$

where ( $T_{50cm,i}$ ) are the simulated ground temperatures in 50 cm depth in °C ( $i = 1, \dots, n$ ),  $\bar{T}_{2cm}$

TABLE 3.4: Coefficients and goodness of fit of the three established multiple linear regression models (MLRM) with ground temperature as dependent and air temperature and global radiation as explanatory variables. Distance means the distance between AWS and data logger,  $\beta_0$  is the intercept,  $\beta_1$  the air temperature coefficient, and  $\beta_2$  the incoming shortwave radiation coefficient.

Linear regression model	Elev. (masl)	Dist. (m)	$\beta_0$	$\beta_1$	$\beta_2$	R <sup>2</sup> cal	RMSE cal (°C)	R <sup>2</sup> val	RMSE val (°C)
MLRM Tullu Dimtu	4377	90	3.7	1.7	0.004	0.73	3.0	0.72	3.0
MLRM EWCP Station	4124	690	1.2	1.6	0.010	0.79	3.6	0.76	3.6
MLRM Tuluka	3848	2050	-0.5	1.9	0.004	0.63	4.9	0.78	4.0

is the mean air temperature in 2 cm depth in °C,  $a$  ( $= -1.25$  °C) is the predefined seasonal minimum, and  $b$  ( $= 1.25$  °C) the predefined maximum of  $T_{50cm,i}$ . For 10 cm depth ( $T_{10cm}$ ),  $a$  equals to  $-3$  °C and  $b$  to  $3$  °C. The main drawback of the presented approach is the non-consideration of ground moisture and thermal conductivity due to the lack of respective measurements. To further improve the method in the future, profile sensors measuring moisture, electrical conductivity, and temperature in 5 cm intervals between 0 and 50 cm depth have been installed at three AWS on the Sanetti Plateau in January 2020. The data are not yet available.

## 3.4 Results

### 3.4.1 Distribution and characteristics of periglacial landforms

The Bale Mountains comprise a wide range of periglacial landforms and other characteristic geomorphological features related to present and relict frost occurrence (Fig. 3.4 and Table B.1). Current frost-induced phenomena like frozen waterfalls, needle ice, patterned grounds, and solifluction lobes are limited to the upper part of the valleys ( $>3900$  masl), Sanetti Plateau, and highest peaks, even though ground temperatures below freezing can sporadically extend to much lower elevations (down to 2700-3000 masl). We observed needle ice (3-5 cm long) mainly along water-saturated stream banks at places with cold air ponding. Needle ice is a typical small-scale example for diurnal freeze-thaw cycles in the Bale Mountains as it forms at clear nights throughout the dry season. Interestingly, we also found evidence for seasonal frost phenomena. Up to 10 m high frozen water falls evolve at shaded north-exposed cliffs in the Wasama Valley during the dry season and last until the onset of the following wet season. Active small-scale polygonal stone nets occur in flat and poorly drained areas on the Sanetti Plateau and unvegetated solifluction lobes above 4100 masl at the southern slopes of Mount Wasama. Compared to the modern periglacial processes and landforms, relict geomorphological features are larger and much more pronounced in the Bale Mountains.

Most of the relict periglacial features can be found along the Harena Escarpment, on the Sanetti and Genale Plateau, and at the slopes of the highest peaks (Fig. 3.5a). Characteristic for the highest peaks of the northern declivity are bare and gentle slopes and the accumulation of scree below heavily eroded basaltic and trachytic cliffs. This type of deposits is associated inter alia with frost weathering and differs from the chaotic spread of individual boulders below elongated cliffs at lower elevations. Another conspicuous landform associated with periglacial activity are large blockfields located between 3500 and 4000 masl at the southern and western

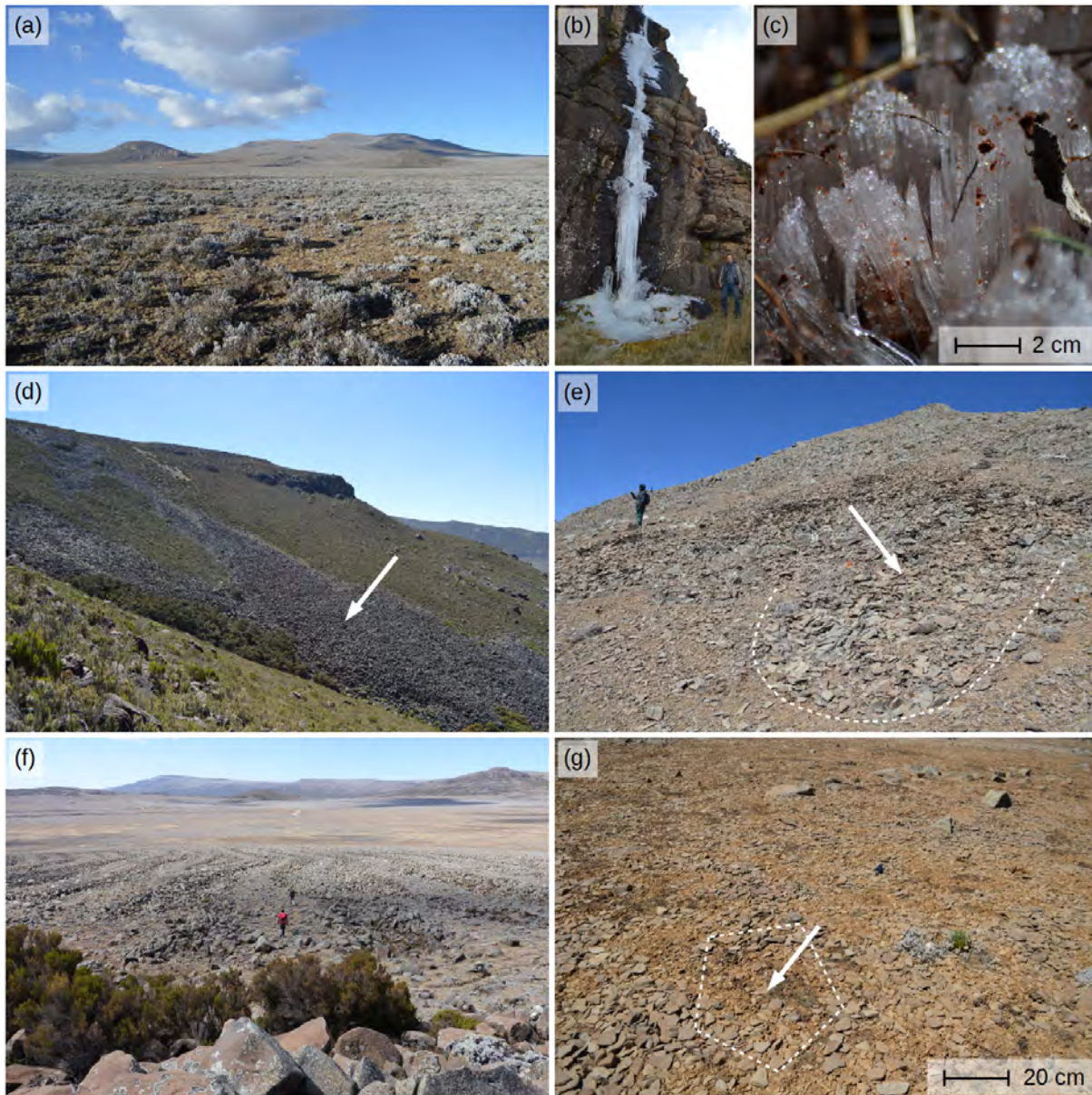


FIGURE 3.4: Periglacial environment of the Bale Mountains: (a) view from the southern Sanetti Plateau towards Tullu Dimtu, (b) frozen waterfall and (c) needle ice in the Wasama Valley, (d) relict blockfields along the southern Hareenna Escarpment, (e) active solifluction lobes at Mt. Wasama, (f) relict sorted stone stripes, and (g) active sorted polygons on the Sanetti Plateau.

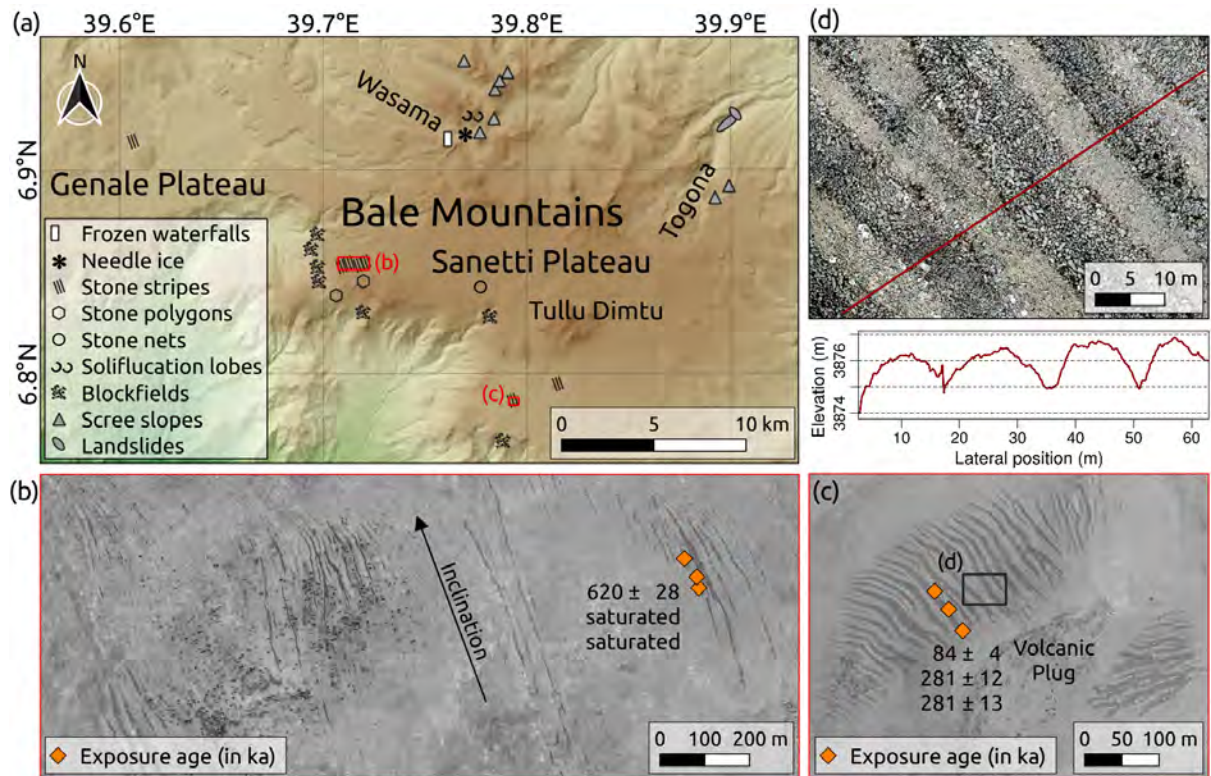


FIGURE 3.5: (a) Overview map of periglacial landforms and other characteristic geomorphological features in the Bale Mountains. (b-c) Sorted stone stripes in the western (b) and southern part (c) of the Sanetti Plateau as seen on WorldView-1 satellite images (DigitalGlobe Foundation). (d) High-resolution orthophoto and DSM cross-section profile of the stone stripes derived from the aerial images.

slopes of the Sanetti Plateau. The blockfields consist of hardly weathered angular boulders and are no longer active as the presence of lichens and partly reoccupation by *Erica* prove. Circular patterns across the Sanetti and Genale Plateau as well as elevated areas of the northern declivity are not further considered here since they are, at least in some areas, of biogenic origin related to the activity of the endemic giant mole-rat (Miehe and Miehe, 1994). The most striking geomorphological features on the Sanetti Plateau are large sorted patterned grounds comprising stone stripes and less developed stone circles.

The large sorted stone stripes occur exclusively on the southern and western Sanetti Plateau and at one site on the lower Genale Plateau (Fig. 3.5). On the southern Sanetti Plateau and on the Genale Plateau, the stone stripes formed at gentle slopes (inclination:  $2 - 9^\circ$ ) of three different volcanic plugs between 3700 and 3950 masl. The stone stripes consist of hardly weathered angular or columnar basalt boulders (Fig. 3.2 and 3.6), are partly covered by lichens, and are up to 200 m long, 15 m wide, and 2 m deep (Fig. 3.5c). While the stone stripes are trough-shaped, the areas with finer material inbetween are more rampart-like (Fig. 3.5d). The distance between the stone stripes equals in most cases to the width of the stripes. Typical for some of the stone stripes is that they split up into two narrower branches in the upper part and merge to a single wider branch in the lower part. As the GPR survey suggests, the regolith layer between the stone stripes contains no larger rocks (exceeding several decimetres) and is more than 1.5 m deep (Fig. 3.6b). The surface of the underlying solid rock was not detected. All larger rocks

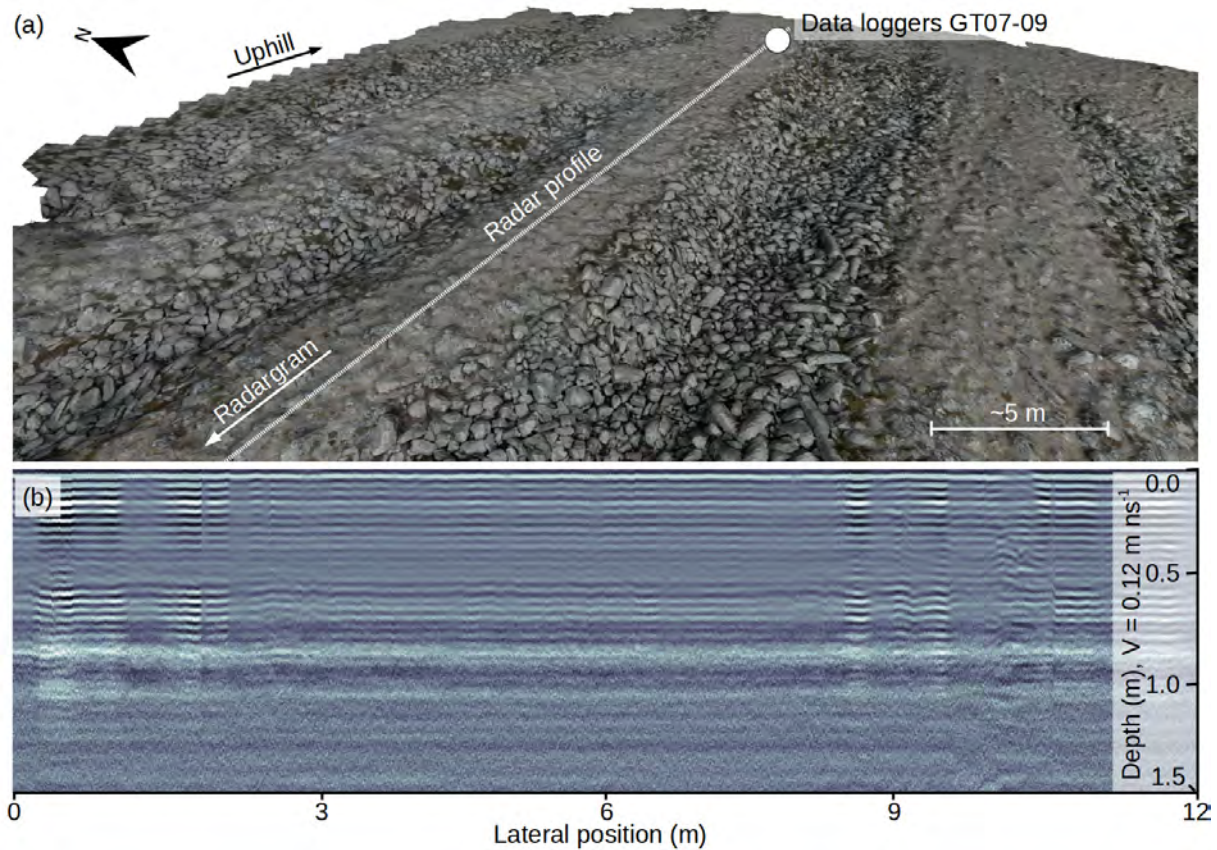


FIGURE 3.6: (a) 3D aerial view and (b) radargram of the sorted stones stripes on the southern Sanetti Plateau. For the location of the displayed radargram section (GPR05) see Fig. 3.1.

(up to 0.5 m wide and 2 m long) are located mainly in the troughs or on top of the regolith layer. On the slightly inclined ( $2 - 9^\circ$ ) western Sanetti Plateau between 3950 and 4150 masl, the stone stripes are 300 - 1000 m long and mainly 5 - 10 m wide (Fig. 3.5b). Most of the stripes are connected to heavily eroded cliffs. In the upper part, some of the stripes split up into multiple branches and where the plateau flattens, a transition from sorted stone stripes to less developed stone circles is visible in the field, but hardly recognisable on satellite images.

The six dated rock samples from two different locations on the Sanetti Plateau originate from basaltic (BS01-04) and trachytic (BS05-06) lava flows as it is indicated by the varying alkali and silica contents (Table B.3). We obtained very high  $^{36}\text{Cl}$  concentrations, especially for the two trachytic samples ( $>120 \times 10^6 \text{ At g}^{-1}$ ) from the western part of the plateau (Table B.4). In these two samples (BS05 and BS05),  $^{36}\text{Cl}$  has reached saturation. This means that the production and decay of  $^{36}\text{Cl}$  average out. Since the resulting exposure ages ( $>1000 \text{ ka}$ ) are at the limit of the method, they are not explicitly stated in the figures and tables. Based on the remaining samples, we calculated non-erosion-corrected  $^{36}\text{Cl}$  surface exposure ages of  $84 \pm 4$ ,  $281 \pm 12$ , and  $281 \pm 13 \text{ ka}$  for the southern and of  $620 \pm 13 \text{ ka}$  for the western stone stripes (Table B.4). However, due to the high  $^{36}\text{Cl}$  concentrations, an erosion rate of  $>1 \text{ mm ka}^{-1}$  would lead to considerably older exposure ages for all samples except BS01. The “old” ages conflict with a

relatively young formation age (e.g. global LGM or postglacial) as suggested by the morphology and hardly weathered surface of the investigated angular and columnar boulders. Long-term exposure of the sampled rocks to  $^{36}\text{Cl}$ -producing cosmic rays prior to the formation of the stone stripes could explain this mismatch. Despite the high  $^{36}\text{Cl}$  concentrations, a temporary ice cover overlying the stone stripes for several thousand years during the last glacial cycle cannot be entirely ruled out from the exposure dating alone. A meter-thick ice cover would reduce the production rate, but a period of several thousand years would not be sufficient to affect the  $^{36}\text{Cl}$  concentrations noticeably or zero the inheritance. However, a temporary ice cover overlying the stripes seems unlikely in light of the absent field evidence for such a scenario.

### 3.4.2 Present frost occurrence and ground temperature variations

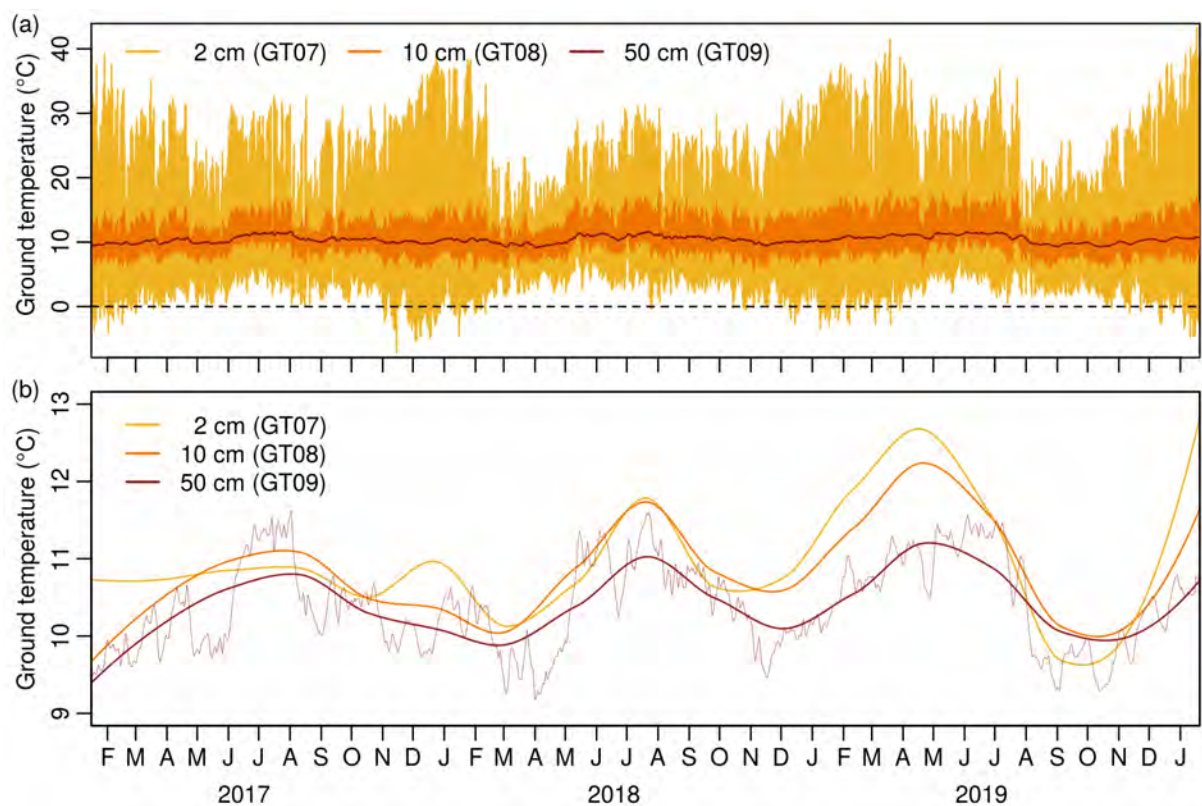


FIGURE 3.7: (a) Hourly ground temperatures and (b) seasonal ground temperature variations in 2, 10, and 50 cm depth on the southern Sanetti Plateau (3877 masl) from January 2017 to January 2020. A local regression with a smoothing span of 0.32 was applied to derive seasonal ground temperature variations from hourly measurements. Daily mean ground temperature variations in 50 cm are provided additionally (thin dark red line).

The observed present-day ground temperatures in the Bale Mountains show characteristic daily and seasonal variations, but are in general way off from permafrost conditions (Fig. 3.7). At the location of the stone stripes on the southern Sanetti Plateau, the mean multiannual ground temperature between the surface and 50 cm depth is 11 °C. On top of the highest peak Tullu Dimtu, the mean annual ground temperature is 7.5 °C. The mean air temperature at the same location is 2 °C and therefore about 5.5 °C lower than the mean ground temperature. While the daily ground temperature range is largest near the surface and decreases with depth,

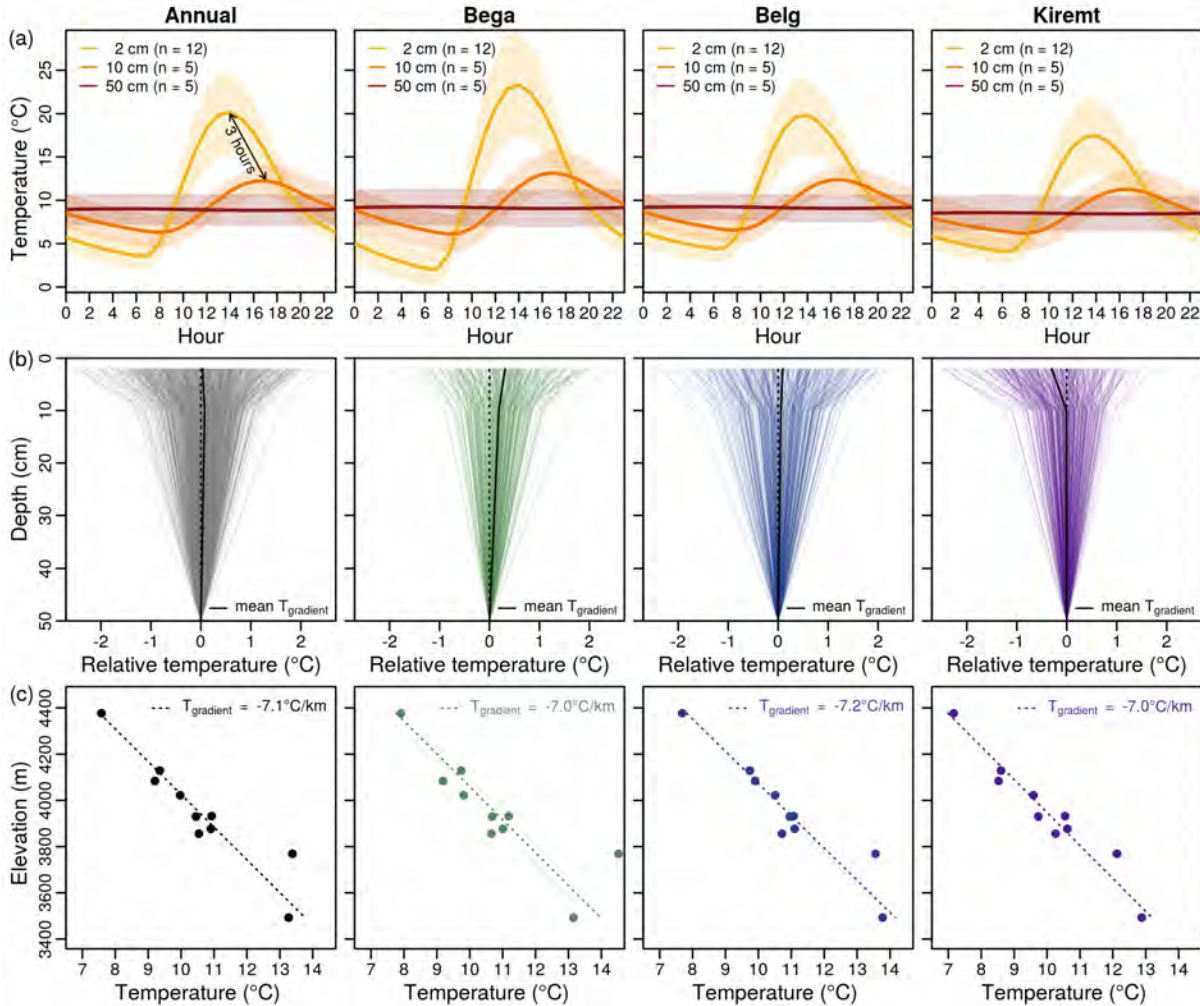


FIGURE 3.8: (a) Mean multiannual and multiseasonal diurnal ground temperature cycle in 2, 10, and 50 cm depth considering all data (as defined in Section 3.6) between February 2017 and January 2020 from the respective depths. The shaded areas display the mean diurnal ground temperature variability (as standard deviation) resulting from the different logger locations. First column: multiannual mean, second column: multiannual dry season mean (Bega: Nov/Dec/Jan/Feb), third column: multiannual wet season mean (Belg: Mar/Apr/May/June), fourth column: multiannual wet season mean (Kiremt: Jul/Aug/Sep/Oct). (b) Multiannual (black) and multiseasonal (Bega: green, Belg: blue, Kiremt: purple) daily ground temperature profiles in 2-50 cm depth between February 2017 and January 2020. Each line represents a mean daily ground temperature profile averaged over the five locations where data loggers were installed in 2, 10, and 50 cm depth. (c) Mean multiannual (black) and multiseasonal (Bega: green, Belg: blue, Kiremt: purple) ground temperature gradients in 2 cm depth between 3493 and 4377 masl considering all data (excluding the warm-biased GT16 logger from a southern slope and the cold-biased GT17 logger from a northern slope) from Feb 2017 to Jan 2020.

the seasonal variations in all depths follow a similar cycle (Fig. 3.7). On the plateau, the ground cools down during the dry season (Bega) and warms up during the wet seasons (Belg and Kiremt). The difference between the seasonal minimum and maximum of daily mean temperatures over a year is about 10 °C near the surface, 6 °C in 10 cm, and 2.5 °C in 50 cm depth (in Fig. 3.7, daily mean ground temperatures are only presented for 50 cm depth). This shows that seasonal temperature variations can also be of relevance for tropical mountains with a pronounced diurnal climate. The time series is far too short for deriving any long-term trends, but the interannual ground temperature variability observed during the three-year period (2017 – 2020) was rather low (<0.5 °C).

Near the surface, the diurnal ground temperature amplitude is well pronounced and varies on average between 10-20 °C during the wet and 20-30 °C during the dry season (Fig. 3.8a). Extreme temperatures of up to 45-50 °C during cloudless days and down to -10 °C during clear night have been observed on the Sanetti Plateau. Nocturnal ground frost on the plateau occurs at 35-90 days per year. However, the frost penetrates only the uppermost centimetres. The diurnal amplitude decreases considerably with increasing depth. At 10 cm depth, temperatures below freezing have not been measured at any of the logger locations during the entire study period. The annual ground temperature profile in the upper 50 cm is homogeneous. The daily temperature difference between the surface and 50 cm depth is rarely larger than  $\pm 2$  °C (Fig. 3.8b). Annual ground temperatures increase from Tullu Dimtu down to the lowest logger location in the Web Valley by 0.71 °C per 100 m (Fig. 3.8c), but nocturnal frost occurs in the valleys still at 5-25 days per year. The ground temperature gradient of 0.71 °C per 100 m is similar to the annual lapse rate obtained for the plateau (0.70 °C per 100 m) and northern declivity from measured air temperatures (Fig. 3.9). Interestingly, the lapse rate obtained for the Harena Escarpment is less steep (0.62 °C per 100 m) and might represent wetter conditions and pronounced cloud formation at the southern declivity between  $\sim 1500$ -3800 masl compared to the drier plateau and northern declivity. However, the number of AWS below the afro-alpine belt is not sufficient to determine unequivocally elevations where the mean annual lapse rate changes from a more or less dry adiabatic to a moist adiabatic and vice versa. Distinct elevational changes in the lapse rate could indicate the mean annual condensation level as well as the upper atmospheric storey where dry north-easterly trade winds dominate.

The comparative experiment on Mount Wasama shows clear differences between the thermal regime of the southern and northern slope (Fig. 3.10a). The southern slope is on average more than 2 °C warmer and reveals a more pronounced seasonality and larger diurnal amplitude which favours freezing and thawing and might explain the presence of solifluction lobes. While the mean daily temperature at the southern slope peaks towards the end of the dry season (January to February) when the sun is in its zenith, it reaches its maximum at the northern slope a few month later when the sun approaches its northernmost position. The ground temperature differences between vegetated and unvegetated areas on the Sanetti Plateau are less obvious (Fig. 3.10b). Small *Erica* trees and bushes buffer the diurnal temperature amplitudes of the shaded ground, but have only little impact on the seasonality. Like at Mount Wasama, both south exposed locations at Tullu Dimtu (vegetated and unvegetated) have their temperature maxima at the end of the dry season, whereas the vegetated and unvegetated locations in the

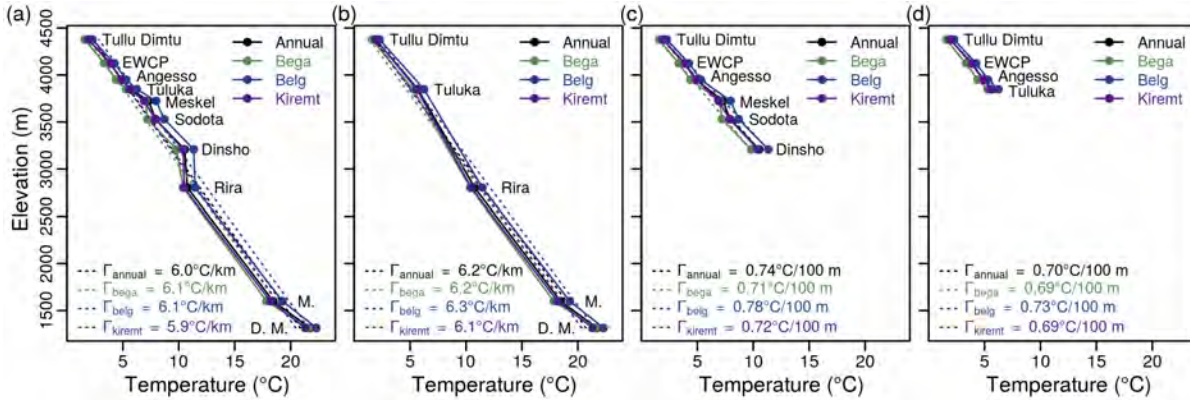


FIGURE 3.9: Mean multiannual and multiseasonal (Bega: Nov/Dec/Jan/Feb, Belg: Mar/Apr/May/June, Kiremt: Jul/Aug/Sep/Oct) lapse rate of air temperature (a) in the Bale Mountains, (b) along the Harennna Escarpment, (c) along the northern declivity, and (d) on the Sanetti Plateau between February 2017 and January 2020. The lapse rate for the northern declivity and Sanetti Plateau is given in °C per 100 m because of the relatively small elevation range (ca. 1200 and 500 m).

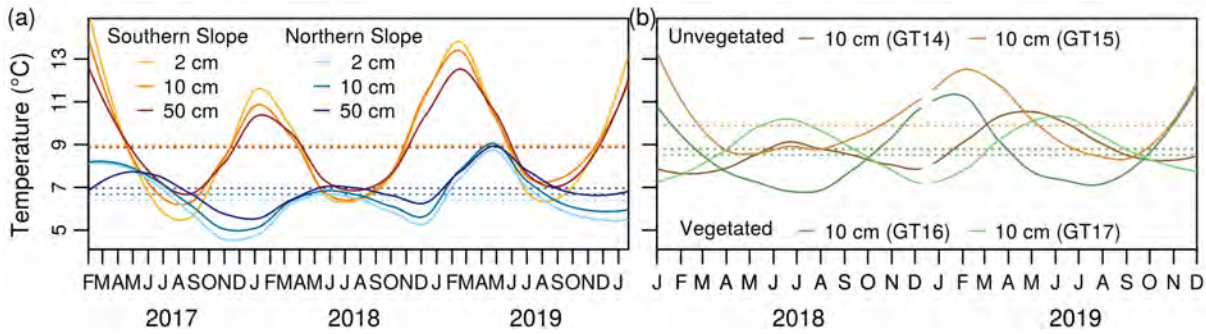


FIGURE 3.10: (a) Comparison of the seasonal ground temperature variations in 2, 10, and 50 cm depth between the northern and southern slope of Mount Wasama. Data from the southern slope at 4153 masl are from the loggers GT16/GT02/GT03, and data from the northern slope at 4181 masl are from the loggers GT17/GT05/GT06. (b) Comparison of seasonal ground temperature variations in 2, 10, and 50 cm depth between locations with and without Erica at the slopes of Tullu Dimtu. A local regression with a smoothing span of 0.32 was applied to derive seasonal ground temperature variations from hourly measurements.

plain heat up during June/July. The cross-comparison between low-cost and high-quality data loggers on top of Tullu Dimtu revealed a promising relationship ( $R^2 = 0.98$ ) and proved that the tested low-cost loggers, which have not been developed explicitly for scientific applications, are suitable for short-term (< 1 year) ground temperature measurements and experiments at high elevations. Both loggers measured nearly the same mean ground temperature (8.46 vs. 8.48 °C). Only the standard deviation of the low-cost logger was a bit larger (9.1 vs. 7.3 °C) since it was installed minimal closer to the surface.

### 3.4.3 Modelled palaeo ground temperatures

At the three locations on the Sanetti Plateau (Tullu Dimtu, EWCP Station, and Tuluka), where ground temperatures and a set of meteorological variables were measured concurrently, the ground temperature is mainly controlled by air temperature and global radiation (Fig. 3.11).

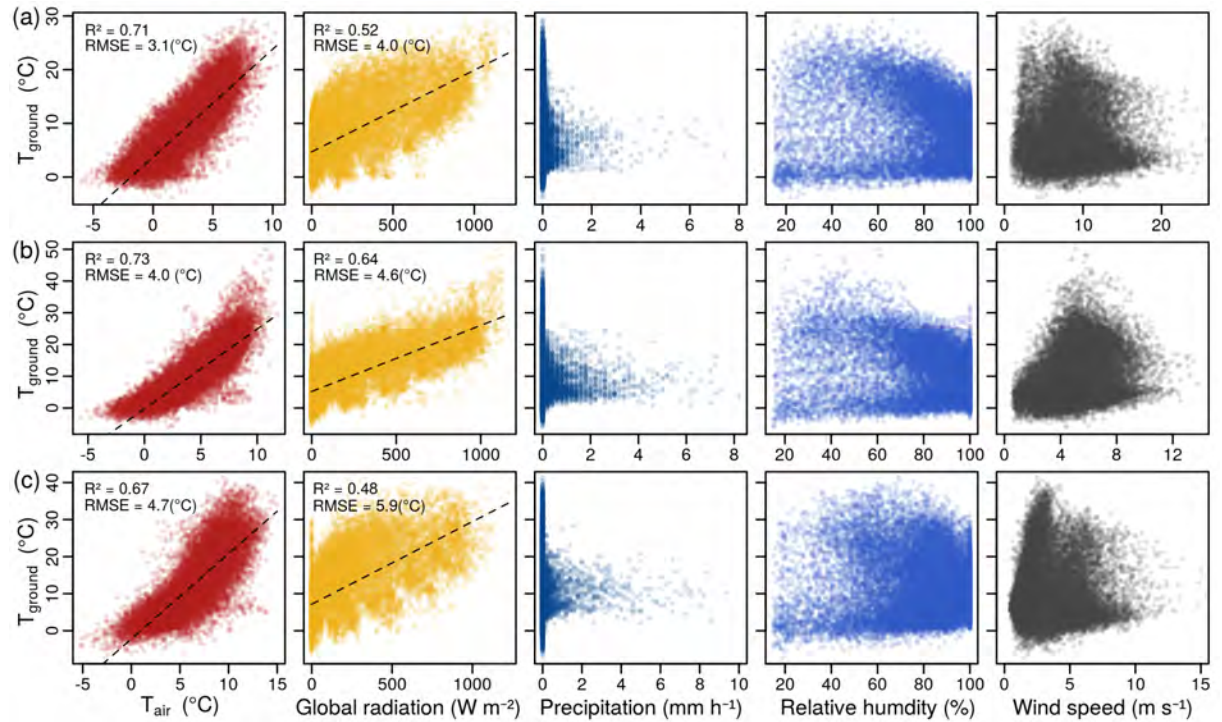


FIGURE 3.11: Relationship between hourly ground temperatures in 2 cm depth and different meteorological variables at three different locations: (a) Tullu Dimtu (GT13 vs. BALE001), (b) EWCP Station (TM04 vs. BALE009), (c) Tuluka (GT07 vs. BALE002).

The two variables can explain together about  $75 \pm 3\%$  of the ground temperature variance (Table 3.4). Ground temperature and the other meteorological variables do not show any significant linear relationship what is not surprising in view of the non-consideration of ground moisture. Precipitation, relative humidity, and wind speed affect ground moisture as well as evaporation and therefore alter the energy balance at the surface and energy transfer into the ground. Measuring and considering ground moisture (directly at the AWS) would likely help to reduce the uncertainties of the applied multiple linear regression models (RMSE of 3–4  $^{\circ}\text{C}$ ). Nevertheless, the established relationship between ground temperature and air temperature/global radiation is strong enough to use the models for a first palaeoclimatic reconstruction experiment. To obtain mean annual ground temperatures associated with deep seasonal ground frost or sporadic permafrost ( $T_{\text{ground}} < -1^{\circ}\text{C}$ ) at the elevation of the lowermost stone stripes on the southern Sanetti Plateau during their time of formation, the three tested linear models require a mean ground temperature depression of  $\sim 12^{\circ}\text{C}$ . This would translate into a mean air temperature depression of  $7.6 \pm 1.3^{\circ}\text{C}$  (the error is the standard deviation of the three model outputs) which would imply a mean annual air temperature on the southern plateau of  $-1.9 \pm 1.3^{\circ}\text{C}$ . The deduced stronger decrease of the ground temperature over the air temperature is due to the observed modern relationship. A cooling/warming of the air of  $1^{\circ}\text{C}$  relates to a decrease/increase of the ground of 1.6–1.9  $^{\circ}\text{C}$  and vice versa (see Table 3.4 and Fig. 3.11). The geophysical reason for this statistical relationship can be manifold. They are associated with the radiative forcing and energy exchange between the atmosphere and ground, which in turn is affected by many factors ranging from insolation, air pressure, relative humidity to the

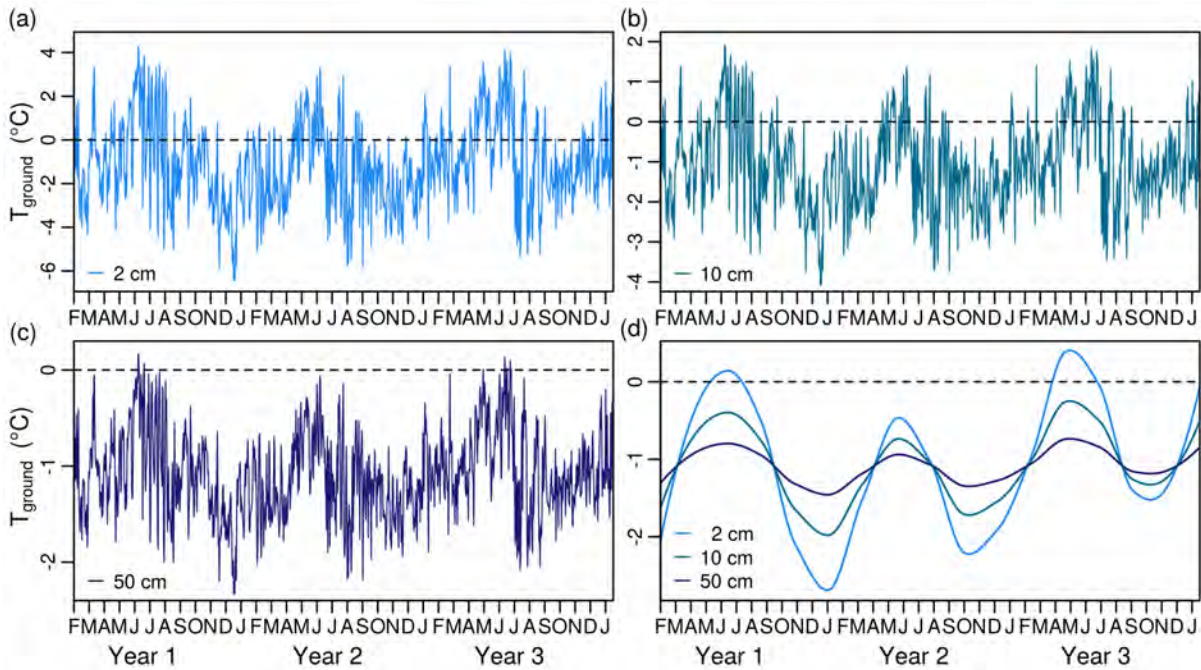


FIGURE 3.12: Simulated daily mean ground temperatures in (a) 2 cm, (b) 10 cm, and (c) 50 cm depth on the southern Sanetti Plateau (3877 masl) assuming a decrease in temperature of  $7.6 \pm 1.3^\circ\text{C}$  and decrease in global radiation of  $30 \text{ W m}^{-2}$  relative to present-day conditions. (d) A local regression with a smoothing span of 0.32 was applied to derive seasonal ground temperature variations from daily mean values.

thermal conductivity, specific heat capacity, density, humidity, albedo, etc. of the ground.

Over a year, the seasonal mean daily ground temperature fluctuations between the surface and 50 cm depth were theoretically large enough to freeze and thaw the upper half metre of the ground (Fig. 3.12). However, seasonal freezing and thawing below 50 cm depth seems unlikely in the past if the ground properties and seasonal temperature fluctuations were similar like today. A mean annual ground temperature in the order of  $-1^\circ\text{C}$  seems critical for the formation of deep seasonal frost on the Sanetti Plateau since much warmer temperatures would prevent seasonal freezing and lower temperatures seasonal thawing.

### 3.5 Discussion

Comprehensive geomorphological investigations in combination with different field measurements,  $^{36}\text{Cl}$  surface exposure dating, and statistical ground temperature modelling presented here provide novel insights in the distribution, characteristics, and palaeoclimatic implications of modern and relict periglacial landforms in the tropical Bale Mountains in the southern Ethiopian Highlands. Modern diurnal and seasonal frost phenomena like small-scale patterned grounds, solifluction lobes, frozen waterfalls, and needle ice are limited to the Sanetti Plateau, the highest peaks, and the upper part of the northern valleys above 3900 masl. Relict periglacial landforms are more abundant and much more pronounced in the Bale Mountains. Besides extensive blockfields along the southern and western Harennna Escarpment, large sorted stone stripes on the southern and western Sanetti Plateau between 3850 to 4150 masl are the most

prominent geomorphological features. These features are associated with seasonal freezing and thawing of the upper half metre of the ground. Ground temperature measurements at sixteen locations between 3493 to 4377 masl over a three-year period (2017-2020) verify seasonal temperature variations and frequent nocturnal frost on the plateau and in the valleys. However, the frost penetrates only the uppermost centimetres of the ground. The mean annual present-day ground temperature between the southern stone stripes ( $\sim 11^\circ\text{C}$ ) is way off from permafrost conditions. Experimental modelling suggests that a distinct ground temperature depression of  $\sim 12^\circ\text{C}$  and air temperature depression of  $7.6 \pm 1.3^\circ\text{C}$  would be necessary for the formation of deep seasonal frost at the elevation of the stone stripes. The main aim of the following discussion is to elaborate when and how the large structures may have formed and what their presence implies for the palaeoclimate and palaeogeocology of the tropical Ethiopian Highlands.

Patterned grounds comprising sorted stone stripes, circles, and polygons are a common feature of periglacial environments and are known from the Arctic (e.g. Nicholson, 1976; Hallet, 2013), Antarctic (e.g. Hallet, Sletten, and Whilden, 2011), mid latitudes (e.g. Richmond, 1949; Miller, Common, and Galloway, 1954; Ball and Goodier, 1968; André et al., 2008), and high mountains worldwide (e.g. Francou, Méhauté, and Jomelli, 2001; Matsuoka, 2005; Bertran et al., 2010). They have also been detected on other celestial bodies like Mars (e.g. Mangold, 2005; Balme et al., 2009). Small-scale sorted stone stripes in the order of centimetres to decimetres, which are associated with superficial diurnal freeze-thaw cycles, are typical for several mid-latitude and also high tropical mountains (e.g. Francou, Méhauté, and Jomelli, 2001; Matsuoka, 2005). However, large sorted stone stripes comparable to those on the Sanetti Plateau (10-15 m wide and 100-1000 m long) have not been reported from any other tropical mountain and seem to be a rare phenomenon in general. In contrast to small-scale features which do not necessarily require mean annual air temperatures below freezing, large sorted patterned grounds like stone circles and polygons that are well-documented for the High Arctic (e.g. Kessler and Werner, 2003; Hallet, 2013) occur commonly in permafrost areas with mean annual air temperatures of  $-4$  to  $-6^\circ\text{C}$  (Goldthwait, 1976). The only other location worldwide where stone stripes in the same order of magnitude as on the Sanetti Plateau and even larger have been described are the non-volcanic Falkland Islands in the South Atlantic (André et al., 2008).

The vernacular term for extensive blockstreams and stone stripes in the Falkland Islands is “stone runs”. Stone runs cover large parts of the eastern and western island and are linked to quartzite outcrops in the elevated areas (50-700 m). The stone stripes in the Falkland Island show some interesting similarities and differences with the features on the Sanetti Plateau. They occur in clusters at gentle slopes (inclination:  $1-10^\circ$ ), are several hundred meters long, several meters wide, consist of large angular blocks (up to 2 m wide and 5 m long), and originate in some cases from eroded ridges and summit areas. As on the Sanetti Plateau, the coarse stone stripes in the Falkland Islands run parallel downslope and alternate with stripes of fine-grained material of similar width (André et al., 2008). However, the partial emergence of stone stripes from blockfields and downslope transition into vast blockstreams as it is typical for the Falkland Islands is uncommon for the Bale Mountains where the stripes are restricted to the plateau and the blockfields to the southern and western escarpment. Also the geological

(volcanic vs. sedimentary and metamorphic rocks), climatic (continental vs. oceanic), and geographical setting (tropical mountain vs. mid-latitude island) between the Bale Mountains and Falkland Islands differs considerably. A link between both locations is the coexistence of coarse and fine-grained material (large angular blocks and regolith) and the evidence for glaciations and colder conditions during the Pleistocene (Clapperton, 1971; Clapperton and Sudgen, 1976; Groos et al., in revision).

The origin and genesis of the stone runs in the Falkland Islands has been discussed controversially over the last one hundred years and numerous theories have been proposed to explain their formation as a result of different interconnected periglacial processes (frost shattering, frost heave, frost sorting, etc.). Based on a literature review and micromorphological analyses, André et al. (2008) come to a more nuanced conclusion and consider the stone runs as complex polygenetic landform. The authors hypothesise that the parent material (blocks and regolith) formed under subtropical or temperate conditions during the Neogene/Palaeogene and interpret the stone runs as the product of subsequent frost-sorting during the cold stages of the Pleistocene. Nevertheless, the understanding of the physical processes underlying the frost-related sorting of such large blocks is still fragmentary (Aldiss and Edwards, 1999). The limited process understanding, the small number of analogies worldwide, and the lack of a cross-section profile complicate the interpretation of the stone stripes on the Sanetti Plateau in the Bale Mountains, but the following observations and findings suggest that deep seasonal frost and periglacial processes played a major role in the formation of this landform.

As aforementioned, the Bale Mountains were covered by an extensive ice cap and experienced a pronounced cooling of 4-6 °C between 50-30 ka (Ossendorf et al., 2019; Groos et al., in revision). It is important to note that the stone stripes on the western and southern Sanetti Plateau are located beyond the glacial remains and the assumed maximum extent of the former ice cap. The obtained  $^{36}\text{Cl}$  surface exposure ages of >600 ka ( $^{36}\text{Cl}$  has reached saturation in two samples) for the western and of  $84 \pm 4$ ,  $281 \pm 12$ , and  $281 \pm 13$  ka for the southern stone stripes predate the local last glacial maximum. However, the exposure ages probably do not represent the timing of formation or stagnation of the features. Since the sampled trachytic blocks and columnar basalt originate from eroded cliffs and volcanic plugs, it is likely that they were exposed to cosmic radiation during and prior to the formation of the stone stripes. The well-preserved morphology, the absence of erratic boulders in the surrounding area, and the high  $^{36}\text{Cl}$  concentrations indicate that the stone stripes have not been eroded and deformed by a dynamic and warm-based glacier. However, we cannot completely rule out that stagnant, cold-based, and relatively shallow ice covered the stripes for several thousand years. Such an ice cover would not have been sufficient to zero the inheritance (high  $^{36}\text{Cl}$  concentrations). We interpret the hardly weathered surface of the angular blocks and little reoccupation by vegetation as an indication for a younger formation stage of the stone stripes coinciding probably with the coldest and driest phase in Africa (30-15 ka) during the last glacial period (e.g. Tierney et al., 2008). The ice extent in the Bale Mountains at  $\sim 18$  ka was slightly smaller compared to the local LGM despite the general cooling trend in Eastern Africa. The lack of any evidence for a major glacier advance between the local LGM and the  $\sim 18$  ka stage might be indicative of a cold and dry climate which provides ideal conditions for periglacial processes.

A precondition for the formation of patterned grounds is cyclic freezing and thawing of a decimetre- to meter-thick layer and the coexistence of fine-grained material and larger stones or blocks (Kessler et al., 2001; Kessler and Werner, 2003). Both large blocks and fine-grained material are present on the Sanetti Plateau. A decimetre-thick regolith layer rich in silt and loam covers the underlying bedrock of the plateau (Lemma et al., 2019). Whether the regolith has developed during the Pleistocene or during warmer periods before, as suggested for the Falkland Islands, remains unclear. The accumulation of trachytic blocks and columnar basalt at some places on the plateau is probably related to intensive frost wedging at cliffs and volcanic plugs during the last glacial cycle. As our ground temperature modelling suggests, a half-meter-thick frozen layer could have formed seasonally on the plateau outside the glaciated area as the result of a pronounced air temperature cooling of  $7.6 \pm 1.3^\circ\text{C}$  during the coldest period of the last glacial cycle. Deep frozen grounds and sporadic permafrost still exist at some of the highest tropical and subtropical mountains in Africa (Kaser et al., 2004; Vieira, Mora, and Faleh, 2017). Potential evidence for past sporadic permafrost in the Bale Mountains exists in the northeastern Togona Valley, which was covered by a 8 km long valley glacier during the Late Pleistocene. During or after deglaciation of the lower part of the valley, two large landslides (0.5 and 1.5 km long; see Fig. 3.5) occurred between the  $\sim 18$  ka and  $\sim 15$  ka moraine stages and might have been triggered by slope destabilisation due to thawing permafrost.

The strongest arguments for the stone stripes being the “final” product of frost heave and sorting is their configuration as well as the presence of less-pronounced relict large sorted stone polygons in the highest flat parts of the western plateau. The width of the alternating fine-grained and coarse stone stripes (about 10-20 times larger than the average block size), the absence of larger blocks in the fine-grained stripes, the axis orientation of the stripes parallel to the greatest slope, and the convergence of individual narrower branches to wider single stripes is remarkably similar to patterned grounds at gentle slopes predicted by numerical models after several hundred freeze-thaw cycles (Werner and Hallet, 1993; Mulheran, 1994; Kessler et al., 2001; Kessler and Werner, 2003). Such numerical models can reproduce the self-organization of different sorted grounds by varying just a few parameters (mainly stone concentration, hillslope, and degree of lateral confinement) and need about 500 to 5000 freeze-thaw cycles to form similar stripe patterns as found on the southern Sanetti Plateau (Fig. 3.5). Less cycles would lead to a more random configuration and more cycles would eliminate the smaller branches and lead to a “perfect” sorting of the stripes (see Fig. 2 in Werner and Hallet, 1993). Assuming downslope displacement rates of 10-50 cm per year (or cycle) for clasts as it is observed for small-scale periglacial features in the tropics (Francou and Bertran, 1997) would require a similar number of cycles (about 400 to 2000) to form the 200 m long stone stripes on the southern plateau. In view of the length of the coldest phase of the last glacial period, the formation of the stone stripes on the plateau in proximity to the ice cap over several hundred to thousand cycles/years is a plausible scenario.

Instead of seasonal variations, longer freeze-thaw cycles could theoretically also explain the formation of the stone stripes on the Sanetti Plateau. A formation over several cold stages during the Pleistocene as proposed for the stone runs in the Falkland Islands (Wilson et al., 2008) is conceivable. This would imply the formation of sporadic permafrost during the colder

periods and complete thawing of the ground during the warmer periods of the Pleistocene. The “old” exposure ages would generally support such a scenario, although the mismatch between the high  $^{36}\text{Cl}$  concentrations of the western stone stripe compared to the lower concentrations of the southern stone stripe would remain an open question. However, due to the well-preserved morphology of the stone stripes, the verified seasonal ground temperature variations on the Sanetti Plateau, and the absence of further evidence for the formation over several cold stages, we propose seasonal freezing and thawing during the last glacial cycle as the main mechanism for the formation of the stripes.

The presence of sorted stone stripes and other relict frost-related landforms on the Sanetti Plateau and along the Hareenna Escarpment provide further evidence that the Bale Mountains underwent severe climatic and environmental changes during the Pleistocene. Both glacial and periglacial processes played a major role in shaping the afro-alpine landscape. The inferred cooling of  $7.6 \pm 1.3^\circ\text{C}$  needed for the formation of large patterned grounds on the Sanetti Plateau is much larger than the temperature decrease in the Bale Mountains of  $5.1 \pm 0.7^\circ\text{C}$  derived from the estimated snow line depression during the local last glacial maximum 50-30 ka (Groos et al., in revision). This discrepancy might indicate a further cooling in the southern Ethiopian Highlands from the time of the local maximum glacier expansion to the global LGM ( $22 \pm 4$  ka) as seen in other climate records from Eastern Africa and worldwide (e.g. Jouzel et al., 2007; Tierney et al., 2008). Moreover, the reconstructed temperature decrease from the Ethiopian Highlands in comparison with the reconstructions from the lower-situated Congo Basin and Lake Tanganyika in the order of 4 to  $4.5^\circ\text{C}$  (Weijers et al., 2007; Tierney et al., 2008) reveals an amplified tropical cooling at high elevations in Eastern Africa during the global LGM. Strong evidence for such a cooling is also provided by sea surface and air temperature reconstructions from different lakes along an elevational transect in Eastern Africa. Loomis et al. (2017) explain the observed elevational trend with a steeper tropical lapse rate ( $\Gamma_{LGM} = 6.7 \pm 0.3^\circ\text{C km}^{-1}$  vs.  $\Gamma_{modern} = 5.8 \pm 0.1^\circ\text{C km}^{-1}$ ) related to a drier atmosphere during the global LGM. The present-day mean annual lapse rate and ground temperature gradient on the Sanetti Plateau of  $0.7^\circ\text{C}$  per 100 m (Fig. 3.8 and 3.9) is larger than the palaeo ( $\Gamma_{LGM}$ ) and modern ( $\Gamma_{modern}$ ) East African lapse rate between 474 and 3081 masl. This emphasises that attention should be drawn to temporal as well as vertical changes in the lapse rate when reconstructing or simulating the palaeoclimate of the tropics. Despite improvements, global climate models still tend to underestimate the cooling at high elevations in the tropics during the last glacial cycle (Loomis et al., 2017).

The palaeoclimatic and environmental findings presented here have direct implications for the settlement history and ecology of the Bale Mountains. Latest archaeological excavations at 3469 masl in the northwestern part of the Bale Mountains along with biogeochemical, zoo-geographical, and glacial chronological investigations reveal that Middle Stone Age foragers resided in the highlands already between 47 to 31 ka and made use of the available alpine resources (Ossendorf et al., 2019). Why the residential site was abandoned after 31 ka is unclear, but might be related to a gradual cooling and dessication of the highlands until the global LGM as suggested by the large-scale periglacial landforms and lack of major glacier advances between 50-30 and  $\sim 18$  ka (Groos et al., in revision). Moreover, the temperature depression,

ice cover, and periglacial conditions must have also affected the habitat of endemic mammal species like the Ethiopian wolf, giant mole-rat, and mountain nyala that currently populate the Sanetti Plateau and upper valleys (Miehe and Miehe, 1994). Due to the absence of any evidence for glacial extinction events in the region, we conclude that endemic plants and mammals as well as Middle Stone Age foragers coped with the harsh climatic and environmental conditions in the Ethiopian Highlands during the Pleistocene.

Many questions regarding the relict periglacial processes and landforms in the Bale Mountains remain open due to the pioneering and experimental character of this study and may hopefully stimulate further research on this topic. A key challenge for better understanding the landscape evolution on the Sanetti Plateau is the development of a robust geochronology. The age of the volcanic plugs, the formation time of the regolith and stone stripes as well as the deglaciation history of the former ice cap on Tullu Dimtu are uncertain. Moreover, information on the depth and internal structure (grain size distribution, mineral composition, etc.) of the coarse and fine-grained stone stripes would provide additional insights into the genesis of the landforms. To reduce the uncertainty of the statistical model applied for ground temperature simulations and air temperature reconstructions, considering the impact of moisture on the thermal conductivity and heat capacity of the ground as well as energy fluxes into the ground is necessary. It is possible that ground moisture and stagnant water played a more important role during the Late Pleistocene than today due to (perma)frost-induced waterlogging and perennial melting of snow and ice. Why the relict patterned grounds are restricted to the southern and western Sanetti Plateau can be explained by the assumed preconditions for their formation: a relatively flat and unglaciated terrain, presence of coarse and fine grained material, deep ground frost, and absence of a thick snow layer.

### 3.6 Conclusion

This contribution provides further evidence that the tropical Bale Mountains in the southern Ethiopian Highlands were subject to severe climatic and environmental changes during the Late Pleistocene. Both glacial and periglacial processes have shaped the afro-alpine environment. Compared to the modern nocturnal and seasonal frost phenomena, relict periglacial landforms like blockfields along the Harena Escarpment and sorted stone stripes on the Sanetti Plateau are much larger and more developed. The large sorted stone stripes are exceptional for the tropics and probably formed under periglacial conditions in proximity of the palaeo ice cap on Tullu Dimtu during the coldest period(s) of the last glacial cycle. We hypothesise that the slightly inclined and unglaciated areas of the Sanetti Plateau, the coexistence of regolith and large blocks, the occurrence of deep seasonal frost, as well as relatively dry conditions beyond the ice cap provided ideal conditions for frost heave and sorting and the formation of large patterned grounds. Based on our ground temperature measurements and modelling experiment, we propose a distinct ground temperature depression of  $\sim 12^\circ\text{C}$  and air temperature depression of  $7.6 \pm 1.3^\circ\text{C}$  as precondition for the formation of deep ground frost on the Sanetti Plateau. The novel idea of using a statistical relationship between measured present-day ground temperatures and meteorological variables to assess past climatic changes through

the simulation of palaeo ground temperatures has also potential for other regions where relict frost-related periglacial landforms exist. Comparing the reconstructed air temperature depression from the Bale Mountains with climate records from lower elevations in Eastern Africa emphasises a strongly amplified cooling at high elevations that has already been outlined for many other tropical mountains. Such a cooling in tandem with the extensive glaciation and frost action must have dramatically affected the habitat of endemic mammal species like the Ethiopian wolf, giant mole-rat, and mountain nyala that currently populate the Sanetti Plateau and upper valleys of the Bale Mountains. Attention should therefore be given to the amplified middle troposphere cooling when reconstructing and modelling climatic and geocological changes in the tropical mountains of Eastern Africa.

## Data Availability

The ground temperature data (Tables S1-4) can be downloaded from the open access library PANGAEA (provisional link until data are published:

<https://filesender.switch.ch/filesender/?vid=06bf00d3-d750-e748-82f8-00006e12ef78>).

Raw data, aerial images, additional field photos, etc. are available upon request by email to the corresponding author.

## Acknowledgements

This research was funded by the Swiss National Science Foundation (SNF, grant no. 200021E-165446/1) and the German Research Foundation (DFG) in the framework of the joint Ethio-European DFG Research Unit 2358 “The Mountain Exile Hypothesis”. We thank the Ethiopian Wildlife Conservation Authority, the College of Natural and Computational Sciences (Addis Ababa University), the Department of Plant Biology and Biodiversity Management (Addis Ababa University), the Philipps University Marburg, the Frankfurt Zoological Society, the Ethiopian Wolf Project, and the Bale Mountains National Park for their cooperation and kind permission to conduct field work. We are grateful to Mekbib Fekadu, Wege Abebe, Katinka Thielsen, Tiziana Koch, Aschalew Gashaw, Terefe Endale, Geremew Mebratu, Beriso Kemal, Mohammed Kedir, Edris Abduku, Sabrina Erlwein, Lukas Munz, Julian Struck, and Bruk Lemma for contributing to the preparation and implementation of the field work, Serdar Yesilyurt for support in the lab, and Armin Rist for the fruitful discussion. Special thanks also go to the DigitalGlobe Foundation for providing high-resolution WorldView-1 satellite images of the Bale Mountains (granted to A.R.G) and to the developers and maintainers of the open-source software used in this study (R, QGIS, OpenDroneMap, MeshLab, LibreOffice, etc.).

## References

Aldiss, D. T. and E. J. Edwards (1999). *The Geology of the Falkland Islands*. British Geological Survey Technical Report WC/99110.

- André, M.-F. et al. (2008). "Stone Runs in the Falkland Islands: Periglacial or Tropical?" In: *Geomorphology* 95.3-4, pp. 524–543. DOI: 10.1016/j.geomorph.2007.07.006.
- Ball, D. F. and R. Goodier (1968). "Large Sorted Stone-Stripes in the Rhinog Mountains, North Wales". In: *Geogr. Ann. Ser. A-phys. Geogr.* 50.1, p. 54. DOI: 10.2307/520871.
- Balme, M. R. et al. (2009). "Sorted Stone Circles in Elysium Planitia, Mars: Implications for Recent Martian Climate". In: *Icarus* 200.1, pp. 30–38. DOI: 10.1016/j.icarus.2008.11.010.
- Barrows, T., J. O. Stone, and L. K. Fifield (2004). "Exposure Ages for Pleistocene Periglacial Deposits in Australia". In: *Quat. Sci. Rev.* 23.5-6, pp. 697–708. DOI: 10.1016/j.quascirev.2003.10.011.
- Bertran, P. et al. (2010). "The Impact of Periglacial Processes on Palaeolithic Sites: The Case of Sorted Patterned Grounds". In: *Quat. Int.* 214.1-2, pp. 17–29. DOI: 10.1016/j.quaint.2009.10.021.
- Chala, D. et al. (2016). "Good-Bye to Tropical Alpine Plant Giants under Warmer Climates? Loss of Range and Genetic Diversity in *Lobelia Rhynchopetalum*". In: *Ecol. Evol.* 6.24, pp. 8931–8941. DOI: 10.1002/ece3.2603.
- Chandler, B. M. P. et al. (2018). "Glacial Geomorphological Mapping: A Review of Approaches and Frameworks for Best Practice". In: *Earth-Sci. Rev.* 185, pp. 806–846. DOI: 10.1016/j.earscirev.2018.07.015.
- Clapperton, C. M. (1971). "Evidence of Cirque Glaciation in the Falkland Islands". In: *J. Glaciol.* 10.58, pp. 121–125. DOI: 10.3189/S0022143000013058.
- Clapperton, C. M. and D. E. Sudgen (1976). "The Maximum Extent of Glaciers in Part of West Falkland". In: *J. Glaciol.* 17.75, pp. 73–77. DOI: 10.3189/S0022143000030732.
- Conway, D. (2000). "The Climate and Hydrology of the Upper Blue Nile River". In: *Geogr. J.* 166.1, pp. 49–62. DOI: 10.1111/j.1475-4959.2000.tb00006.x.
- Costa, K. et al. (2014). "Isotopic Reconstruction of the African Humid Period and Congo Air Boundary Migration at Lake Tana, Ethiopia". In: *Quat. Sci. Rev.* 83, pp. 58–67. DOI: 10.1016/j.quascirev.2013.10.031.
- Farrera, I. et al. (1999). "Tropical Climates at the Last Glacial Maximum: A New Synthesis of Terrestrial Palaeoclimate Data. I. Vegetation, Lake-Levels and Geochemistry". In: *Clim. Dyn.* 15.11, pp. 823–856. DOI: 10.1007/s003820050317.
- Francou, B. and P. Bertran (1997). "A Multivariate Analysis of Clast Displacement Rates on Stone-banked Sheets, Cordillera Real, Bolivia". In: *Permafrost and Periglacial Process.* 8, p. 12.
- Francou, B., N. L. Méhauté, and V. Jomelli (2001). "Factors Controlling Spacing Distances of Sorted Stripes in a Low-Latitude, Alpine Environment (Cordillera Real, 16 °S, Bolivia): Spacing Distances of Sorted Stripes in the Cordillera Real". In: *Permafrost Periglacial Process.* 12.4, pp. 367–377. DOI: 10.1002/ppp.398.
- Galloway, R. W. (1965). "Late Quaternary Climates in Australia". In: *J. Geol.* 73.4, pp. 603–618. DOI: 10.1086/627096.
- Gebrechorkos, S. H., S. Hülsmann, and C. Bernhofer (2019). "Long-Term Trends in Rainfall and Temperature Using High-Resolution Climate Datasets in East Africa". In: *Sci. Rep.* 9.1, pp. 1–9. DOI: 10.1038/s41598-019-47933-8.

- Goldthwait, R. P. (1976). "Frost Sorted Patterned Ground: A Review". In: *Quat. Res.* 6.1, pp. 27–35.
- Gottelli, D. et al. (1994). "Molecular Genetics of the Most Endangered Canid: The Ethiopian Wolf *Canis Simensis*". In: *Mol. Ecol.* 3.4, pp. 301–312. DOI: 10.1111/j.1365-294X.1994.tb00070.x.
- Grab, S. (2002). "Glacial and Periglacial Phenomena in Ethiopia: A Review". In: *Permafrost Periglacial Process.* 13.1, pp. 71–76. DOI: 10.1002/ppp.405.
- Groos, A. R. et al. (2019). "The Potential of Low-Cost UAVs and Open-Source Photogrammetry Software for High-Resolution Monitoring of Alpine Glaciers: A Case Study from the Kanderfirn (Swiss Alps)". In: *Geosciences* 9.8, pp. 1–21. DOI: 10.3390/geosciences9080356.
- Groos, A. R. et al. (in revision). "Asynchronous Late Pleistocene glacier fluctuations in tropical Eastern Africa". In: *Science Advances*.
- Hallet, B. (2013). "Stone Circles: Form and Soil Kinematics". In: *Proc. R. Soc. A* 371.2004, p. 20120357. DOI: 10.1098/rsta.2012.0357.
- Hallet, B., R. Sletten, and K. Whilden (2011). "Micro-Relief Development in Polygonal Patterned Ground in the Dry Valleys of Antarctica". In: *Quat. res.* 75, pp. 347–355. DOI: 10.1016/j.yqres.2010.12.009.
- Hendrickx, H. et al. (2014). "Quaternary Glacial and Periglacial Processes in the Ethiopian Highlands in Relation to the Current Afro-Alpine Vegetation". In: *Z. Geomorphol.* 59.1, pp. 37–57. DOI: 10.1127/0372-8854/2014/0128.
- Ivy-Ochs, S. et al. (2004). "Initial Results from Isotope Dilution for Cl and <sup>36</sup>Cl Measurements at the PSI/ETH Zurich AMS Facility". In: *Nucl. Instrum. Methods Phys. Res. B* 223-224, pp. 623–627. DOI: 10.1016/j.nimb.2004.04.115.
- Ivy-Ochs, S. et al. (2009). "Latest Pleistocene and Holocene Glacier Variations in the European Alps". In: *Quat. Sci. Rev.* 28.21-22, pp. 2137–2149. DOI: 10.1016/j.quascirev.2009.03.009.
- Jouzel, J. et al. (2007). "Orbital and Millennial Antarctic Climate Variability over the Past 800,000 Years". In: *Science* 317.5839, pp. 793–796. DOI: 10.1126/science.1141038.
- Kageyama, M., S. P. Harrison, and A. Abe-Ouchi (2005). "The Depression of Tropical Snowlines at the Last Glacial Maximum: What Can We Learn from Climate Model Experiments?" In: *Quat. Int.* 138-139, pp. 202–219. DOI: 10.1016/j.quaint.2005.02.013.
- Kaser, G. et al. (2004). "Modern Glacier Retreat on Kilimanjaro as Evidence of Climate Change: Observations and Facts". In: *Int. J. Climatol.* 24.3, pp. 329–339. DOI: 10.1002/joc.1008.
- Kessler, M. A. and B. T. Werner (2003). "Self-Organization of Sorted Patterned Ground". In: *Science* 299.5605, pp. 380–383. DOI: 10.1126/science.1077309.
- Kessler, M. A. et al. (2001). "A Model for Sorted Circles as Self-Organized Patterns". In: *J. Geophys. Res.* 106.B7, pp. 13287–13306. DOI: 10.1029/2001JB000279.
- Lemma, B. et al. (2019). "Chemotaxonomic Patterns of Vegetation and Soils along Altitudinal Transects of the Bale Mountains, Ethiopia, and Implications for Paleovegetation Reconstructions – Part II: Lignin-Derived Phenols and Leaf-Wax-Derived n-Alkanes". In: *E&G Quaternary Sci. J.* 68.2, pp. 189–200. DOI: 10.5194/egqsj-68-189-2019.

- Lemma, B. et al. (2020). "Spatial and Temporal  $^2\text{H}$  and  $^{18}\text{O}$  Isotope Variation of Contemporary Precipitation in the Bale Mountains, Ethiopia". In: *Isot. Environ. Health Stud.* Pp. 1–14. DOI: 10.1080/10256016.2020.1717487.
- Levin, N. E., E. J. Zipser, and T. E. Cerling (2009). "Isotopic Composition of Waters from Ethiopia and Kenya: Insights into Moisture Sources for Eastern Africa". In: *J. Geophys. Res.* 114, pp. 1–13. DOI: 10.1029/2009JD012166.
- Loomis, S. E. et al. (2017). "The Tropical Lapse Rate Steepened during the Last Glacial Maximum". In: *Science Advances* 3.1, pp. 1–7. DOI: 10.1126/sciadv.1600815.
- MacLean, S. F. and M. P. Ayres (1985). "Estimation of Soil Temperature from Climatic Variables at Barrow, Alaska, U.S.A." In: *Arct. Alp. Res.* 17.4, p. 425. DOI: 10.2307/1550867.
- Mangold, N. (2005). "High Latitude Patterned Grounds on Mars: Classification, Distribution and Climatic Control". In: *Icarus* 174.2, pp. 336–359. DOI: 10.1016/j.icarus.2004.07.030.
- MARGO Project Members (2009). "Constraints on the Magnitude and Patterns of Ocean Cooling at the Last Glacial Maximum". In: *Nat. Geosci.* 2.2, pp. 127–132. DOI: 10.1038/ngeo411.
- Mark, B. G. et al. (2005). "Tropical Snowline Changes at the Last Glacial Maximum: A Global Assessment". In: *Quat. Int.* 138-139, pp. 168–201. DOI: 10.1016/j.quaint.2005.02.012.
- Matsuoka, N. (2005). "Temporal and Spatial Variations in Periglacial Soil Movements on Alpine Crest Slopes". In: *Earth Surf. Process. Landforms* 30.1, pp. 41–58. DOI: 10.1002/esp.1125.
- Messerli, B. and M. Winiger (1992). "Climate, Environmental Change, and Resources of the African Mountains from the Mediterranean to the Equator". In: *Mt. Res. Dev.* 12.4, pp. 315–336. DOI: 10.2307/3673683.
- Miehe, S. and G. Miehe (1994). *Ericaceous Forests and Heathlands in the Bale Mountains of South Ethiopia - Ecology and Man's Impact*. Hamburg: Stiftung Walderhaltung in Afrika.
- Miller, R., R. Common, and R. W. Galloway (1954). "Stone Stripes and Other Surface Features of Tinto Hill". In: *Geogr. J.* 120.2, p. 216. DOI: 10.2307/1791537.
- Mohr, P. (1983). "Ethiopian Flood Basalt Province". In: *Nature* 303, pp. 577–584. DOI: 10.1038/303577a0.
- Mulheran, P. A. (1994). "Theory of Self-Organisation in Sorted Stone Stripes". In: *J Phys* 4.1, pp. 1–5.
- Nicholson, F. H. (1976). "Patterned Ground Formation and Description as Suggested by Low Arctic and Subarctic Examples". In: *Arctic and Alpine Research* 8, p. 329. DOI: 10.2307/1550437.
- Osmaston, H. A., W. A. Mitchell, and J. A. N. Osmaston (2005). "Quaternary Glaciation of the Bale Mountains, Ethiopia". In: *J. Quat. Sci.* 20.6, pp. 593–606. DOI: 10.1002/jqs.931.
- Ossendorf, G. et al. (2019). "Middle Stone Age Foragers Resided in High Elevations of the Glaciated Bale Mountains, Ethiopia". In: *Science* 365.6453, pp. 583–587. DOI: 10.1126/science.aaw8942.
- Richmond, Gerald M. (1949). "Stone Nets, Stone Stripes, and Soil Stripes in the Wind River Mountains, Wyoming". In: *Geol. J.* Pp. 143–153.
- Schneider von Deimling, T. et al. (2006). "How Cold Was the Last Glacial Maximum?" In: *Geophys. Res. Lett.* 33.14, pp. 1–5. DOI: 10.1029/2006GL026484.

- Seleshi, Y. and U. Zanke (June 2004). "Recent Changes in Rainfall and Rainy Days in Ethiopia". In: *Int. J. Climatol.* 24.8, pp. 973–983. DOI: 10.1002/joc.1052.
- Shakun, J. D. and A. E. Carlson (2010). "A Global Perspective on Last Glacial Maximum to Holocene Climate Change". In: *Quat. Sci. Rev.* 29, pp. 1801–1816. DOI: 10.1016/j.quascirev.2010.03.016.
- Steinemann, O. et al. (in press). "Tracking rockglacier evolution in the Eastern Alps from the Lateglacial to the early Holocene". In: *Quat. Sci. Rev.*
- Tierney, J. E. et al. (2008). "Northern Hemisphere Controls on Tropical Southeast African Climate During the Past 60,000 Years". In: *Science* 322.6976, pp. 252–255. DOI: 10.1038/nature02251.
- Tierney, J. E. et al. (2011). "Late Quaternary Behavior of the East African Monsoon and the Importance of the Congo Air Boundary". In: *Quat. Sci. Rev.* 30.7-8, pp. 798–807. DOI: 10.1016/j.quascirev.2011.01.017.
- Tripathi, A. K. et al. (2014). "Modern and Glacial Tropical Snowlines Controlled by Sea Surface Temperature and Atmospheric Mixing". In: *Nat. Geosci.* 7.3, pp. 205–209. DOI: 10.1038/ngeo2082.
- Umer, M., Seifu Kebede, and Henry A. Osmaston (2004). "Quaternary Glacial Activity on the Ethiopian Mountains". In: *Developments in Quaternary Sciences*. Ehlers, J., Gibbard, P. L. Vol. 2. Quaternary Glaciations - Extent and Chronology, Part III. Amsterdam: Elsevier, pp. 171–174. DOI: 10.1016/S1571-0866(04)80122-2.
- Vieira, G., C. Mora, and A. Faleh (2017). "New Observations Indicate the Possible Presence of Permafrost in North Africa (Djebel Toubkal, High Atlas, Morocco)". In: *Cryosphere* 11.4, pp. 1691–1705. DOI: 10.5194/tc-11-1691-2017.
- Viste, E. and A. Sorteberg (2013). "Moisture Transport into the Ethiopian Highlands". In: *Int. J. Climatol.* 33.1, pp. 249–263. DOI: 10.1002/joc.3409.
- Vlasatá, T. et al. (2017). "Daily Activity Patterns in the Giant Root Rat (*Tachyoryctes Macrocephalus*), a Fossorial Rodent from the Afro-Alpine Zone of the Bale Mountains, Ethiopia". In: *J. Zool.* 302.3, pp. 157–163. DOI: 10.1111/jzo.12441.
- Vockenhuber, C., K.-U. Miltenberger, and H.-A. Synal (2019). "<sup>36</sup>Cl Measurements with a Gas-Filled Magnet at 6 MV". In: *Nucl. Instrum. Methods Phys. Res. B* 455, pp. 190–194. DOI: 10.1016/j.nimb.2018.12.046.
- Weijers, J. W. H. et al. (2007). "Coupled Thermal and Hydrological Evolution of Tropical Africa over the Last Deglaciation". In: *Science* 315.5819, pp. 1701–1704. DOI: 10.1126/science.1138131.
- Werner, B.T. and B. Hallet (1993). "Numerical Simulation of Self-Organized Stone Stripes". In: *Nature* 361.
- Wilson, P. et al. (2008). "Stone Run (Block Stream) Formation in the Falkland Islands over Several Cold Stages, Deduced from Cosmogenic Isotope (<sup>10</sup>Be and <sup>26</sup>Al) Surface Exposure Dating". In: *J. Quat. Sci.* 23.5, pp. 461–473. DOI: 10.1002/jqs.1156.
- Wöllauer, S. et al. (in revision). "TubeDB: an on-demand processing database system for climate data". In: *Computers & Geosciences*.

## Chapter 4

# Middle Stone Age foragers resided in high elevations of the glaciated Bale Mountains, Ethiopia

Götz Ossendorf <sup>1</sup>, Alexander R. Groos <sup>2</sup>, Tobias Bromm <sup>3</sup>, Minassie Girma Tekelemariam <sup>1</sup>, Bruno Glaser <sup>3</sup>, Joséphine Lesur <sup>4</sup>, Joachim Schmidt <sup>5</sup>, Naki Akçar <sup>6</sup>, Tamrat Bekele <sup>7</sup>, Alem-seged Beldados <sup>8</sup>, Sebsebe Demissew <sup>7</sup>, Trhas Hadush Kahsay <sup>9</sup>, Barbara P. Nash <sup>10</sup>, Thomas Nauss <sup>11</sup>, Agazi Negash <sup>12</sup>, Sileshi Nemomissa <sup>7</sup>, Heinz Veit <sup>2</sup>, Ralf Vogelsang <sup>1</sup>, Zerihun Woldu <sup>7</sup>, Wolfgang Zech <sup>13</sup>, Lars Opgenoorth <sup>14,15</sup>, Georg Mieke <sup>11</sup>

<sup>1</sup>Institute of Prehistoric Archaeology, University of Cologne, Germany; <sup>2</sup>Institute of Geography, University of Bern, Switzerland; <sup>3</sup>Department of Soil Biogeochemistry, Martin Luther University Halle-Wittenberg, Germany; <sup>4</sup>MNHN/CNRS-UMR 7209 Archaeozoology, Archaeobotany Laboratory, France; <sup>5</sup>Institute of Biosciences, University of Rostock, Germany; <sup>6</sup>Institute of Geological Sciences, University of Bern, Switzerland; <sup>7</sup>Department of Plant Biology and Biodiversity Management, Addis Ababa University, Ethiopia; <sup>8</sup>Department of Archaeology and Heritage Management, Addis Ababa University, Ethiopia; <sup>9</sup>School of Earth Science, Addis Ababa University, Ethiopia; <sup>10</sup>Department of Geology and Geophysics, University of Utah, USA; <sup>11</sup>Department of Geography, Philipps University of Marburg, Germany, <sup>12</sup>Paleoanthropology and Paleoenvironment Program, Addis Ababa University, Ethiopia; <sup>13</sup>Institute of Soil Science and Soil Geography, University of Bayreuth, Germany; <sup>14</sup>Department of Ecology, Philipps University Marburg, Germany; <sup>15</sup>Swiss Federal Research Institute WSL, Switzerland

*Author contributions:* G.O., A.R.G., T.Br., M.G.T., B.G., and R.V.: manuscript conceptualization; G.O., A.R.G., T.Br., and B.G.: writing original draft; J.L., B.P.N., and J.S.: writing specialist contributions; G.O., A.R.G., T.Br., M.G.T., J. S., N.A., A.B., T.H.K., H.V., R.V., W.Z., and G.M.: field work, excavation, mapping, sampling, and data collection; G.O. and M.G.T.: lithic analysis; A.R.G.: glacial chronological analysis; T.Br. and B.G.: anthrosol analysis; B.P.N. and A.N.: electron microprobe analysis; J.L.: faunal analysis; J.S.: ground beetle analysis; R.V., A.B., A.N., N.A., H.V., T.Be., S.N., and W.Z.: supervision; S.D., T.N., L.O., Z.W., and G.M.: project administration and funding acquisition. All authors reviewed and edited the first draft of the paper.

*Science*, 2019, 365 (6453), 583-587, <https://doi.org/10.1126/science.aaw8942>

## Abstract

Studies of early human settlement in alpine environments provide insights into human physiological, genetic, and cultural adaptation potentials. Although Late and even Middle Pleistocene human presence has been recently documented on the Tibetan Plateau, little is known regarding the nature and context of early persistent human settlement in high elevations. Here, we report the earliest evidence of a prehistoric high-altitude residential site. Located in Africa's largest alpine ecosystem, the repeated occupation of Fincha Habera rock shelter is dated to 47 to 31 thousand years ago. The available resources in cold and glaciated environments included the exploitation of an endemic rodent as a key food source, and this played a pivotal role in facilitating the occupation of this site by Late Pleistocene hunter-gatherers.

## 4.1 Main Text

The occupation of the world's high mountains and plateaus has long been thought to have occurred rather late in human history (Aldenderfer, 2014; Rademaker et al., 2014; Chen et al., 2015; Meyer et al., 2017). High-altitude hypoxia severely limits every aspect of human life, especially when combined with other stressors such as low and oscillating temperatures, aridity, and higher levels of ultraviolet radiation (Beall, 2001; Aldenderfer, 2006; Alkorta-Aranburu et al., 2012). However, recent studies have revealed the presence of a Denisova hominin as early as 160 thousand years (ka) ago on the outer eastern slope of the Tibetan Plateau (Chen et al., 2019), and at 4600 m above sea level (masl), short-term stays for raw material procurement and artefact manufacturing have been dated to 30 to 40 ka ago (Zhang et al., 2018). Here, we describe the world's oldest occupation of a residential site at high elevation, which was repeatedly inhabited by humans who exploited a glaciated African ecosystem.

Past human adaptations to African highlands are poorly known despite the considerable amount of evidence of cultural and behavioural flexibility documented for Middle Stone Age (MSA) populations in Africa (Barham and Mitchell, 2008; Brooks et al., 2018). Palaeoenvironmental and archaeological data on alpine settlements are needed to assess the modes of past human biological responses, such as short-term acclimatization (e.g., via epigenetic modifications), or longer-term genetic changes (Beall, 2014; Julian, 2017). We suggest that the ecological stability of the humid African mountains provided refugia not only for plants and animals but also for humans during times when the lowland climates were arid (Basell, 2008; Brandt et al., 2012; Stewart and Stringer, 2012). The Bale Mountains are ideal for testing this hypothesis, as the endemic species richness of this largest Afro-alpine ecosystem testifies to its ecological stability. Moreover, this area yields palaeoecological and archaeological records that enable the reconstruction of landscape and human history (Miehe and Miehe, 1994).

Here, we present the results of combined archaeological, soil biogeochemical, glacial chronological, and zoogeographical analyses. Archaeological excavations were conducted at the MSA site Fincha Habera, and intensive surveys were conducted to locate related human activities in the landscape. This led to the identification of five obsidian outcrops at ~4200 masl (Fig. 4.1 and Fig. C.1), the highest currently known in Ethiopia. Abundant surface scatters of flaked

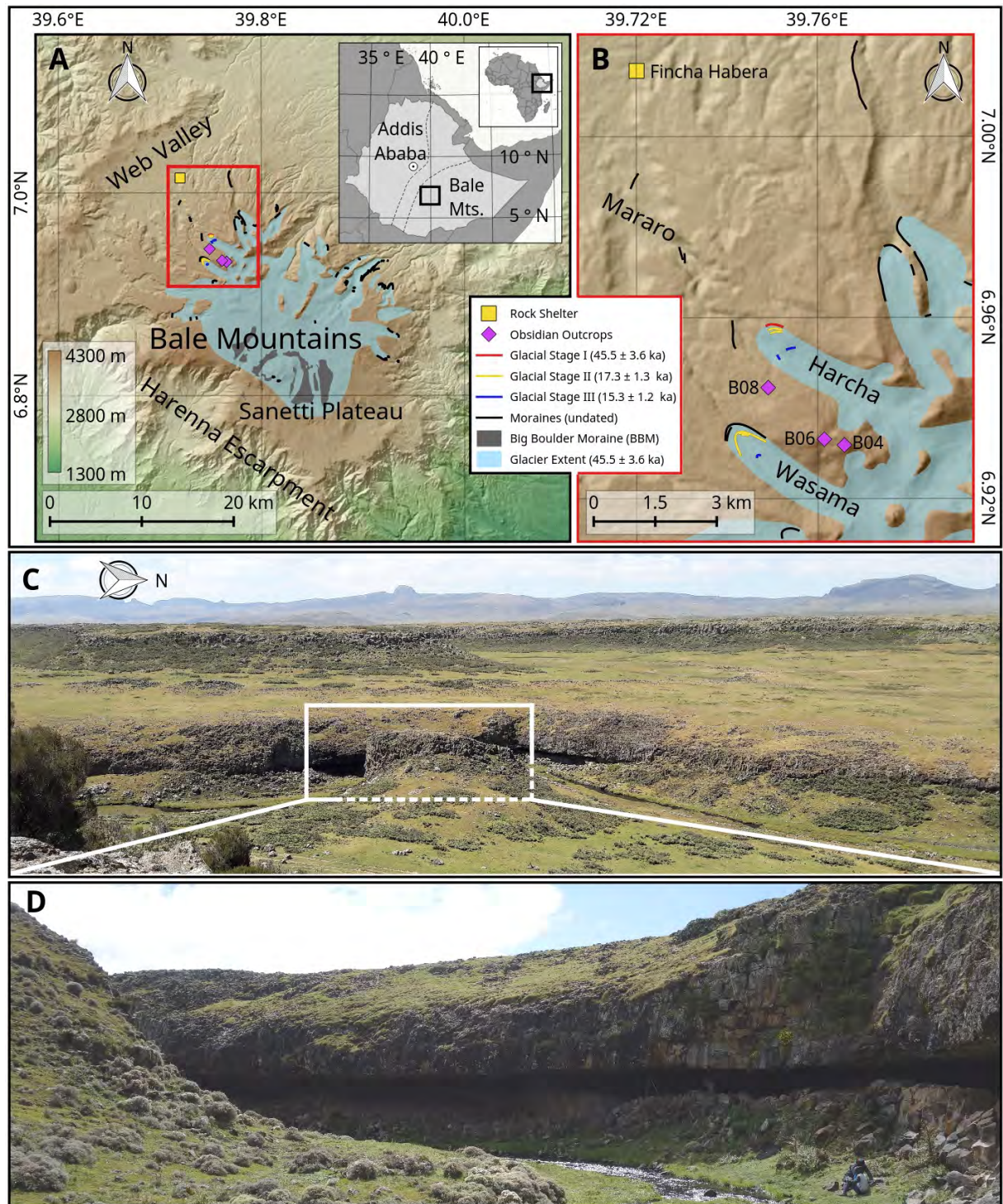


FIGURE 4.1: Geographic location and setting of the study area. (A) Overview map of the glaciated Bale Mountains in southern Ethiopia during the local Last Glacial Maximum ( $45.5 \pm 3.6$  ka ago). (B) Detailed map showing the glacial chronology of the northwestern valleys, the location of the MSA site Fincha Habera rock shelter and the location of natural obsidian sources (B04, B06, and B08) along the ridge between the glaciated Harcha and Wasama Valleys. (C) Setting and (D) close-up view of Fincha Habera rock shelter in the Web Valley.



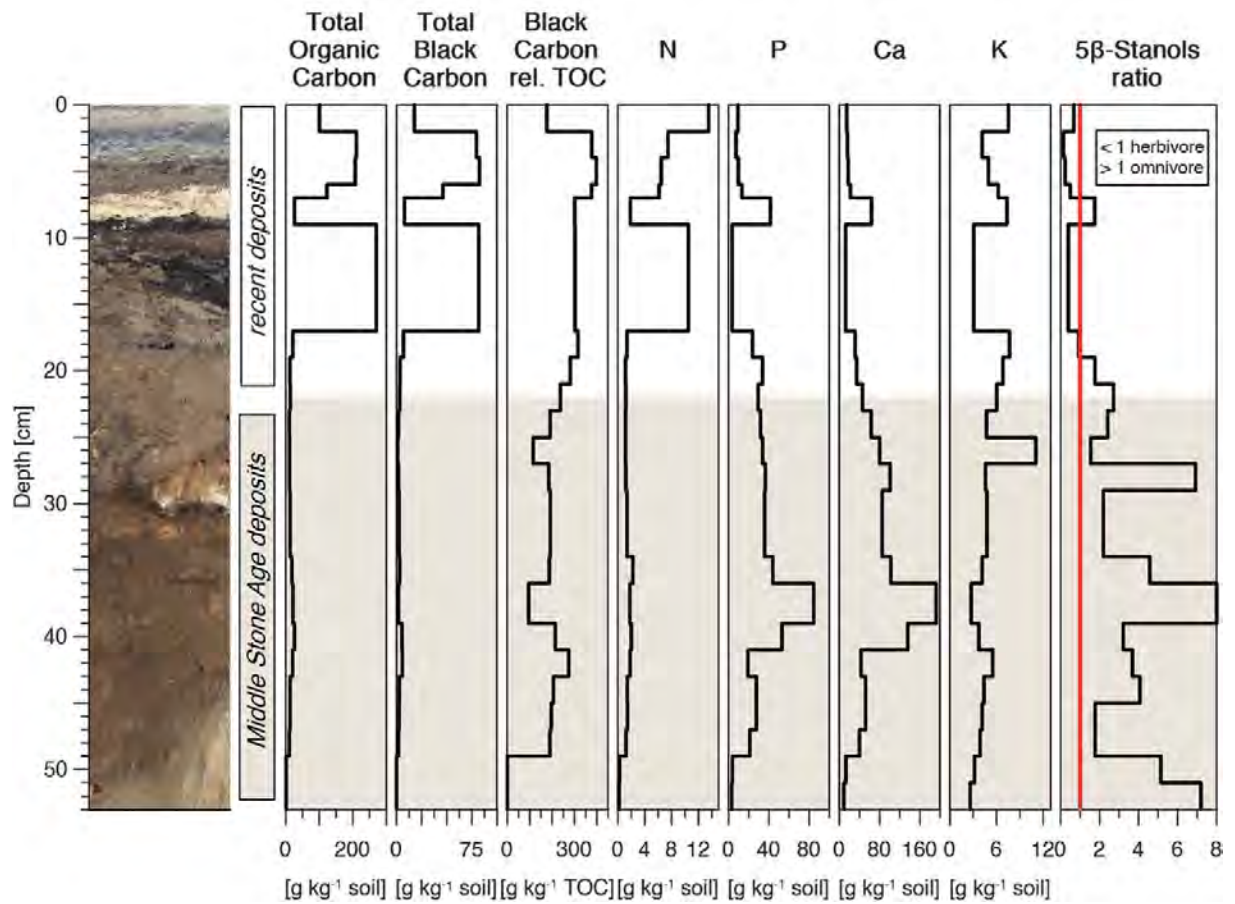


FIGURE 4.3: Soil profile and depth functions of biogeochemical proxies representing soil organic matter quantity [total organic carbon (TOC) and nitrogen] and human influence (black carbon content, element contents, and steroid pattern). Plot on the far right shows the ratio of  $5\beta$ -stanols (coprostanol + epicoprostanol)/( $5\beta$ -stigmastanol + epi- $5\beta$ -stigmastanol). The red line differentiates major input of herbivore feces (<1) and omnivore feces (>1).

nitrogen in the lower deposits, indicating less input of organic material and only remnants of former hearths. The quantities of phosphorus and calcium were much higher compared with the upper part (Fig. 4.3), which is consistent with the increased number of bones. The ratios of  $5\beta$ -stanols indicated a major contribution of omnivore faeces (Fig. 4.3). Although the assessment for  $5\beta$ -stanols does not allow differentiation between human faeces and that of other omnivores (see Section 4.2), the faecal depositions throughout the lower part of the profile are very likely to be of human origin because of the high  $5\beta$ -stanol ratios, the high P values, the abundance of lithic artefacts and human-accumulated fauna (see analysis below), and the low  $5\beta$ -stanol ratios of directly analysed hyena coprolites (Table C.1).

Twenty-one accelerator mass spectrometry (AMS) radiocarbon dates were obtained to perform a chronological classification of the deposits (Table C.2). Charcoal and burnt faunal remains were used to date the human occupations, and hyena coprolite samples were used to derive the coeval human and carnivore presence. The objective of  $^{14}\text{C}$  dating of black carbon was to test the sediment integrity of the deposits (Fig. 4.2). Eight dates from the lower deposits supported a Late Pleistocene occupation, bracketing the MSA settlement between 47 and 31 ka ago. Very young results, exclusively derived from charcoal samples, fell within the last 800

years and also occurred in the MSA-bearing layers (Table C.2). Accordingly, the black carbon dates prove that mixing of the sediments had occurred, as they represent averaged ages from their respective levels. This might most likely be associated with the digging of pits by humans (Fig. 4.2A) or with herbivores enclosed in the shelter as mentioned above. In the lower deposits, postdepositional disturbances can be attributed to hyenas. Their presence was confirmed by corresponding coprolites and by nearly 200 gnawing and digestion marks visible on large mammal bones (Fig. 4.4D). The dating results of two coprolites confirmed that hyenas were present during and after the MSA occupation (Table C.3). Correspondingly, the vertical distribution of coprolites (Fig. C.4) and bones with hyena marks (Fig. C.5) was largely restricted to the upper parts of the MSA-bearing layers.



FIGURE 4.4: Selected findings from the MSA deposits. (A) Drawings of obsidian lithic artifacts: unifacial points (1 and 3), laterally retouched blade with alternate edge retouch (2), scraper (4), point with basal thinning (5), and photograph of a tested cortical nodule (6). (B) Photograph of hyena (*C. crocuta*) coprolite with included rodent bone fragment. (C) Photograph of ostrich eggshell fragment. (D) Photograph of digested bovid phalanges. (E) Photograph of left mandible from a giant mole-rat (*T. macrocephalus*) that shows extremity burning marks. Scale bars indicate 1 cm.

The MSA lithic assemblage from Fincha Habera clearly exhibits several similarities to broadly coeval Ethiopian late MSA occurrences from the lowlands (Pleurdeau, 2006; Gossa, Sahle, and Negash, 2012; Ménard et al., 2014; Pleurdeau et al., 2014; Leplongeon, Pleurdeau, and Hovers,

2017) dating to the late Marine Isotope Stage (MIS) 3. These included the presence of prepared core technologies, uni-facial points (Fig. 4.4, A1 and A3), laterally retouched blades (Fig. 4.4, A2), scrapers (Fig. 4.4, A4), and points (Fig. 4.4, A5), and the assemblage composition (Table C.3) and reduction sequences (see Section 4.2) were also similar. Obsidian was the nearly exclusively used raw material at Fincha Habera. Electron microprobe analysis of 14 obsidian artefacts (Fig. C.4) corroborated an identical chemical composition with samples from the local obsidian outcrops at 4200 masl (Data S1). A different composition was only noted for a single artefact (sample 17/2-14), which also differed from more than 30 known obsidian sources in the Afar and Main Ethiopian Rift (Negash, Brown, and Nash, 2011). The lithic analysis of the assemblage revealed homogeneous techno-economic behaviours beginning from the acquisition to the discard of the artefacts (see Section 4.2). The assemblage is characterised by the following features throughout the MSA deposits: high artefact density, presence of all reduction stages of the manufacturing process, a large amount of cortex, and a high proportion of utilised artefacts (Data S2). In addition, the high number of unworked or only initially tested nodules (Fig. 4.4, A6) hints at a “provisioning of places” strategy (Kuhn, 1995) applied by humans, which is usually associated with resource predictability.

The prehistoric inhabitants of Fincha Habera rock shelter consumed the endemic Afro-alpine giant mole-rat (*Tachyoryctes macrocephalus*). The abundant faunal assemblage (Table C.4) of the MSA deposits consisted almost exclusively (93.5%) of this rodent (Fig. 4.4E). Roasting was the predominant method of preparation, as indicated by the high number of burnt bones and the location of the burn marks at the extremities, especially in the lowermost MSA deposits (Fig. C.5). No digestion or gnawing marks that would suggest consumption by hyenas could be identified on the rodent bones. Giant mole-rats have a current density of at least 29 individuals per hectare in the local environment, with the adults weighing  $\sim 1$  kg (Bekele and Yalden, 2013). Hunting and consumption of rodents with similar life-history traits are well documented in tropical regions worldwide (see Section 4.2). The remaining fauna at Fincha Habera included bovids, especially the endemic mountain nyala; baboons; and a small carnivore (probably a fox), which still occur at these altitudes today. A single fragment of ostrich eggshell (Fig. 4.4C) must have been imported from the lowlands. All of the coprolites (Fig. 4.4B) were probably produced by spotted hyenas (*Crocuta crocuta*) on the basis of their size and morphology. Hyena digestion and gnawing marks were only visible on the large mammal remains, particularly bovids. However, several coprolites were found to contain mole-rat bones and incisors (Fig. 4.4B), thus indicating that hyenas and humans competed for this food source.

To reconstruct the climate and environment that the prehistoric inhabitants experienced, glacial chronological and zoogeographical studies were conducted (see Section 4.2). The extensive glaciation periods on the Bale Mountains have been corroborated by glacial landforms and deposits in the western, northern, and eastern valleys, as well as in the central highland (Fig. 4.1 and Fig. C.6). Even though the valley glaciers advanced multiple times, they never reached the MSA site and its surroundings during the Quaternary (Fig. 4.1). The local Last Glacial Maximum (Glacial Stage I,  $45.5 \pm 3.6$  ka ago) occurred during MIS 3 (Figs. C.7 and C.8), before the global Last Glacial Maximum (Shakun and Carlson, 2010). Glacial Stage I coincided

with a generally cold and slightly wetter period in eastern Africa that followed the sustained dry climate during MIS 4 (Tierney, deMenocal, and Zander, 2017; Foerster et al., 2018). This likely favoured the advance of glaciers in the region, covering  $\sim 265 \text{ km}^2$  of the mountain range at that time. Ice was flowing from a central ice cap down into the northern valleys and formed several outlet glaciers. Meltwater from the Harcha and Wasama Glaciers drained through the Web Valley and supplied fresh water to the MSA foragers given that glacial melt occurs in the tropics throughout the year. The glacier extent at Glacial Stage II ( $17.3 \pm 1.3 \text{ ka ago}$ ) was slightly smaller compared with Glacial Stage I (Fig. 4.1). The ages of the innermost moraines (Glacial Stage III) suggest that deglaciation started after  $15.3 \pm 1.2 \text{ ka ago}$  (Figs. C.7 and C.8). Moraines from the period in between are lacking, but because of the persistent cold conditions during MIS 3 and 2 (Tierney et al., 2008), it is likely that the terminal position of the northern valley glaciers oscillated between the positions of Glacial Stage II and III. Thus, prehistoric foragers in the Bale Mountains must have been very familiar with cold, glaciated environments, especially while accessing the ice-free ridge to extract obsidian (Fig. 4.1).

Another proxy, micro-areal endemic wingless ground beetle species strictly adapted to the forest zone and to permanently humid, humus-rich soil conditions (Table C.8), also corroborate the availability of fresh water as a reliable and persistent resource during the MSA occupation. In addition, based on their large diversity and geographical distribution (C.9), as well as their known phylogenetic age, these beetles confirm that permanent surface water drainage systems across the Bale Mountains are considerably older than the last glacial cycle (see Section 4.2). Therefore, gallery forests should have occurred in close vicinity to the MSA site during the last glacial period, thus forming a habitat for the mountain nyala and other prey species of the MSA foragers. Because this applies to all valley systems of the Bale Mountains, the ground beetle data are clear evidence of the widespread and simultaneous presence of more moderate Pleistocene environments downslope of the central highland (Fig. C.9).

The above results reveal substantial strategic decisions made by MSA foragers in high elevations. Over several millennia, Fincha Habera was repeatedly used as a residential site. This function is indicated by the density of archaeological materials, the existence of hearth remains and the use of fire, the massive presence of human faeces, the simultaneous manufacture and intense use of predominantly locally derived lithic artefacts, and the preparation and consumption of food. Moreover, the location of Fincha Habera in more moderate climatic contexts was optimally placed at elevations 500 to 700 m below the glaciers, but still in proximity to available resources. The practice of importing predictable resources to a residential site from logistical forays into the Afro-alpine zone included the gathering of obsidian and giant mole-rats. By focusing on the latter as a sustainable key food source, two essential requirements for high-altitude living – higher caloric demands and a reduction of physical strain – were met. This prey was available year-round, occurred in large numbers within a restricted habitat, and was easy to catch (Yalden and Largen, 1992; Sillero-Zubiri, Tattersall, and Macdonald, 1995). These factors enabled long-term stays at Fincha Habera within a potential annual subsistence circuit. The identification of additional coeval residential sites would be needed to prove permanent human residence in the Bale Mountains, which can currently be neither proven nor refuted.

Past connections with lowland areas are indicated by the presence at Fincha Habera of an

ostrich eggshell fragment and artefacts made of obsidian and quartz of unknown provenance. Although only a few late MIS 3 dates are available from the Main Ethiopian Rift and beyond, coeval human presence during this period at lower elevations is likely (Ménard et al., 2014; Pleurdeau et al., 2014; Brandt et al., 2017) and does not favour an interpretation of the Bale Mountains as a climate-driven human refuge.

## **4.2 Materials and Methods**

### **4.2.1 Archaeological survey and excavation**

Extensive archaeological surveys (2015-2018) were carried out by foot and pack horse to map, document and investigate the spatio-temporal distribution of past human settlement activities and strategies. Aimed at covering the six major landscape and distinct mesoclimatic units of the Bale Mountains, as defined by Mieke and Mieke (Mieke and Mieke, 1994), this was primarily based on the distribution of rock shelter sites recorded by Reber et al. (2018). The exploration of rock shelters with signs of prehistoric human use was accompanied by intensive surveys in the vicinity to identify associated open-air activities, e.g. at former quarrying sites. The only obsidian outcrops were identified and sampled on Wasama Ridge (Fig. 4.1, Figs. C.1, C.2) and include sites B04 (4240 masl: 6.931790 °N, 39.765835 °E), B05 (4188 masl: 6.933269 °N, 39.761610 °E), B06 (4187 masl: 6.933269 °N, 39.761613 °E), B07 (4185 masl: 6.932819 °N, 39.761227 °E) and B08 (3959 masl: 6.944482 °N, 39.749015 °E). Further primary or secondary obsidian occurrences in the Bale Mountains have never been detected, neither by our research unit nor during many years of previous field work by some members. Extensive fluvial transport of obsidian can therefore be ruled out.

Test excavations were carried out at Fincha Habera rock shelter at the eastern flank of the Web Valley, in immediate proximity to a small stream (Fig. 4.1). The site designation in our catalogue is A45 (3469 masl: 7.014577 °N, 39.720068 °E). Previous palaeoecological studies at this site focused on the analysis of zoogenic dung deposits (Kuzmicheva et al., 2013; Kuzmicheva et al., 2014). Signs of recent use include hearth remains and boulders piled at the entrance to enclose livestock. The shelter was formed by erosion of conglomeratic deposits embedded between two aphanatic basalt flows. With a lateral extent of more than 70 m, it is composed of several compartments, only one of which (25 m in width) preserved sufficient amounts of sediments to allow for the excavation of two test squares. A grid in relation to fixed points was established within the shelter (Fig. C.3). The height of the ceiling is ~150 cm at the entrance and steadily reduces towards the back of the shelter (~100 cm in grid squares F4 to F20; ~50 cm in grid squares I8 to I17). Two test squares (1 x 1 m) were chosen for excavation (E8 and H11), which were further subdivided into (0.25 x 0.25 m) quarter squares according to their compass direction. These were independently excavated following the visible stratigraphic units. Where natural strata were greater than 5 cm thick, these were subdivided into artificial spits of a maximum of 5 cm depth (Fig. C.4). In a few instances this was not possible due to the presence of larger rocks. All sediments were dry sieved through 5-, 2.5- and 1-mm mesh sizes.

Sorting and labelling of the archaeological material recovered by excavation and sieving – including faunal and botanical remains – was carried out according to squares, quarter squares and excavation levels. After reaching bedrock, profile walls were drawn and photographically documented (Fig. 4.2). A total of 22 sediment samples (for subsequent anthrosol and sedimentological analyses) was removed at 1-2 cm intervals from a 7 cm wide column on the north wall of square E8 (Fig. 4.2).

## 4.2.2 Anthrosol analyses

### Background

Human activities such as burning of organic material (i.e. fire pits), food preparation, storage of organic materials and disposal of organic waste (plant and animal tissue), metabolic by-products (faeces of humans and livestock), processing of non-food organic and inorganic materials (wood, bone, chipped stone tools etc.) result in the enrichment of a multitude of residues in soils (Middleton, 2004). These residues are incorporated into the sediment of the present surface, either due to the exceedingly small particle size of some physical residues or their decomposition by-products, or through complexation and adsorption of free ions in liquid residues into a variety of compounds within the sediment (Middleton, 2004). If leaching, disturbance or alteration of any other kind can be excluded the residues incorporated in the compounds are preserved and can be chemically detected and identified (Middleton and Price, 1996; Middleton, 1998).

Steroids, including  $5\beta$ -stanols, are not moved through the soil by leaching due to their low water solubility and good adsorption to particulate organic matter, making them an ideal biomarker to trace human and animal faeces (Lloyd et al., 2012). While  $5\beta$ -stigmastanol is produced from stigmasterol in the gut of herbivores, coprostanol is produced from cholesterol in the gut of omnivores – e. g. humans and pigs. Both, coprostanol and  $5\beta$ -stigmastanol are altered to their epimers by microbial degradation over time. The ratio of (coprostanol + epi-coprostanol) / ( $5\beta$ -stigmastanol + epi- $5\beta$ -stigmastanol) as proposed by Bull et al. (2002) can be used as a marker for the distinction of the main input of faeces. Values smaller than 1 indicate faeces of herbivores as major input, while omnivore faeces as main input results in values greater than 1. Based on the results of the faunal analysis (Table C.4), baboons and hyenas are possible contributors to the input omnivore faeces, apart from humans. Hyenas can be excluded to have significantly contributed to the faeces in the deposits, based on the low  $5\beta$ -stanols ratio of their coprolites (Table C.1). Currently, we cannot exclude baboons as contributors, but given the dense accumulation of MSA lithic artefacts, charcoals and faunal remains, and the presence of exotic items – all undeniably accumulated by humans – we rather attribute the omnivorous signal to the repeated presence of humans.

### Fecal biomarker analysis

Steroid analysis followed the method described by Birk et al. (2012). In brief, air-dried and finely ground soils and two coprolites (see Fig. C.4 for provenance) were spiked with an internal standard ( $5\alpha$ -pregnan- $3\beta$ -ol) and total lipids were Soxhlet-extracted with dichloromethane/

methanol (2:1, v/v). After drying under a gentle stream of nitrogen, total lipids extracts were saponified with 5% KOH in methanol overnight (10–14 hours). Subsequently, extracts were separated by sequential liquid-liquid extraction into a neutral fraction (including the sterols, stanols and stanones) and an acidic fraction (including the bile acids).

The neutral fraction was then further fractionated by solid phase extraction (SPE) using 5% deactivated silica gel preconditioned with hexane. Non-polar substances (aliphatic and aromatic compounds) were eluted with hexane and discarded. The fraction containing the  $\Delta^5$ -sterols, stanols and stanones was eluted with dichloromethane followed by dichloromethane/acetone (2:1, v/v) and dried.

$\Delta^5$ -sterols, stanols, and stanones were silylated with a mixture of 1,1,3,3,3-Hexamethyl-disilazane (HMDS), Trimethylchlorosilane (TMCS) and pyridine (3:1:9, w/w/v; Sylon HTP).  $\alpha$ -cholestane was added as a second internal standard.

All samples were analysed with a GC/MS QP 2010 (Shimadzu Corporation, Kyoto, Japan). Gas chromatographic separation of the  $\Delta^5$ -sterols, stanols and stanones was carried out with a HP-5MS column (30 m  $\times$  0.25 mm  $\times$  0.25  $\mu$ m; Agilent, Santa Clara, CA, USA) and electron ionisation mode at electron energy of 70 eV. The ion source temperature was set to 260 °C, interface to 290 °C and the injection port to 290 °C. Helium was used as carrier gas and linear velocity was kept constant at 35 cm sec<sup>-1</sup>. 1  $\mu$ l of each sample was injected in split-less mode. For the sterol, stanol and stanone separation the column temperature program was: 80 °C (held 1.5 min) to 265 °C at 12 °C min<sup>-1</sup>, to 288 °C at 0.60 °C min<sup>-1</sup>, to 320 °C at 20 °C min<sup>-1</sup> (held 10 min). Measurement in Scan mode and comparison with external standards were used to verify peak identity, and measurements in selected ion monitoring mode (SIM) were carried out for quantification. The quantification of steroids was done using an external standard series with six concentrations for each compound. For sterols, stanols, and stanones the recovery of the first internal standard 5 $\alpha$ -pregnan-3 $\beta$ -ol averaged 71  $\pm$  19% (mean  $\pm$  standard deviation).

### 4.2.3 Total element analysis

Total element concentration of soil and coprolite samples was analysed by aqua regia extraction according to 11466 (1995). 3 g of dried, sieved soil was weighed in a glass tube and digested with hydrochloric acid (37%) and nitric acid (65%) (3:1, v/v). The extracts were filtered through ashless cellulose filters into volumetric flasks and quantitatively filled with deionised water. Further diluted samples were analysed using an inductively-coupled plasma optical emission spectrometer (ICP-OES, ULTIMA 2, HORIBA Scientific S.A.S, Jubin-Yvon, France).

Total organic carbon (TOC) and Total nitrogen (TN) content were measured using a EURO EA Elemental Analyzer (EuroVector, Hekatech, Germany) coupled via a Conflo III Interface to an isotope ratio mass spectrometer (IRMS; Finnigen Delta V Advantage, Thermo Scientific, Bremen, Germany).

### 4.2.4 Black carbon analysis

Black carbon content was determined by extracting and measuring the benzene polycarboxylic acid (BPCA) contents following the revised (Brodowski et al., 2005) method of Glaser et al.

(1998). Polyvalent cations were removed by hydrolysing 500 mg of soil with 4M trifluoroacetic acid at 105 °C for 4 hours. The residue after filtration and washing was digested with 65 % nitric acid at 170 °C for 8 hours in a high pressure digestion apparatus. After filtration, a diluted aliquot was dropped on to a cation exchange resin (Dowex 50 W X 8, 200–400 mesh, Fluka, Steinheim, Germany) to remove remaining polyvalent cations. The eluates were freeze-dried, re-dissolved with Methanol and transferred to micro reaction vessels with Teflon-coated septum screw caps. After evaporation to dryness under a gentle stream of nitrogen, BPCA were derivatised with BSTFA and TSIM (98:2, v/v) at 90 °C for 2 hours. Separation of individual BPCAs was carried out by GC-FID (GC-2010, Shimadzu Corporation, Kyoto, Japan) using an SPB-5 column (30 m × 0.25 mm × 0.25 μm; Supelco, Sigma-Aldrich, St. Louis, MO, USA). The quantification of BPCAs was done using an external standard series with five concentrations for each analyte. Measured BPCA concentrations of samples were corrected by the recovery of the internal standard (phthalic acid) following the calculation of carbon content of BPCAs. The sum of BPCA-carbon was converted to charcoal equivalents using a factor of 2.27 as suggested by Glaser et al. (1998). Results are given as total Black Carbon content in soil ( $\text{g } C_{BC} \text{ kg}^{-1} \text{ soil}$ ) and normalised to TOC ( $\text{g } C_{BC} \text{ kg}^{-1} \text{ TOC}$ ).

#### 4.2.5 Electron microprobe analysis of obsidian

Analyses were performed with a Cameca (Gennevilliers, France) SX-50 instrument at the University of Utah using natural and synthetic standards and utilizing Probe for EMPA software. For each sample, three points were analyzed on each of two obsidian fragments. Analytical conditions were 15 kV accelerating voltage, 25 nA beam current and a 10–25 μm beam diameter. Oxygen was determined directly such that the analytical total provides a measure of the quality of the analysis together with an estimate of the water content (MP H<sub>2</sub>O in Data S1) (Nash, 1992). Details of the analytical method, instrument conditions and standards are provided in Kuehn, Froese, and Shane (2011); the Utah microprobe facility is laboratory #5 therein. Results of the analysis are summarised in Data S1.

#### 4.2.6 Radiocarbon dating and calibration

Radiocarbon dating was carried out by two independent laboratories (Beta Analytic, Miami, FL, USA and CologneAMS, Cologne, Germany) and included four different sample materials. Dating results,  $\delta^{13}\text{C}$  and details on the provenance of all samples are provided in Table C.2. Calibrated radiocarbon ages were given as  $2\sigma$  probability calendar year ages calculated with OxCal v. 4.3.2 at CologneAMS and with BetaCal v. 3.21 at Beta Analytic, based on the probability method by Ramsey (2009), using the IntCal13 calibration curve (Reimer et al., 2013). For full preparation method, see Rethemeyer et al. (2013).

Coprolite samples (Beta-506527 and Beta-506526) only underwent acid washing pretreatment. Bone collagen extraction (Beta-522263 and Beta-522264) took place with alkali. For Beta-522263, the C:N ratio is 3.55, the %C is 22.67 and the %N is 7.45. For Beta-522264, the C:N ratio is 3.3, %C is 38.27 and the %N is 13.49. Black carbon was extracted by hydrolysing four replicates of 250 mg of soil with 4M trifluoroacetic acid at 105 °C for 4 hours following a

pressure digestion with nitric acid at 170 °C for 8 hours. After filtration, the replicates were combined and dried to remove excess nitric acid.

#### 4.2.7 Lithic analysis

Terminology of lithic analysis generally follows Inizan et al. (1999) and lithic studies of Ethiopian late MSA assemblages in particular (Pleurdeau, 2006; Brandt et al., 2012; Gossa, Sahle, and Negash, 2012; Ménard et al., 2014; Pleurdeau et al., 2014; Leplongeon, Pleurdeau, and Hovers, 2017). A detailed and standardised attribute analysis of all flaked material (excluding angular waste and chips) was carried out in 2017 and 2018 at the National Museum of Ethiopia. The recorded data on the 1019 artefacts recovered at Fincha Habera rock shelter was not only to allow for comparison with well-documented assemblages, but also serves to add a quantitative dimension to the more qualitative recognition of reduction sequences by identifying marker pieces within the assemblage. Basic attributes recorded on all artefacts include data on raw material, coverage, position and nature of patinated/cortical surfaces, completeness and thermal damage. Cores were studied by metric data, type and surface condition of striking platforms, number of negative scars and direction and location of debitage surfaces relative to each other. Debitage products were analysed by recording data on their metrics, angle of impact, nature, shape and metrics of striking platform remnants, location of fracture impact point, obliquity, bulb, bulb scars, lips, general shape, number and direction of dorsal negative scars, and edge contours. Modified pieces (retouched tools as well as utilised pieces) were additionally studied by location, type and extent of retouch and/or utilization (Data S2).

The assemblage composition is summarised in Table C.3. Raw materials other than obsidian include chert varieties ( $n = 40$ , 3.9% total assemblage), basalt ( $n = 28$ , 2.7%), quartz ( $n = 1$ , 0.1%), and indeterminate raw materials ( $n = 35$ , 3.4%). The reduction sequence – from acquisition to discard – present in the analysed assemblage can be summarised as follows: shown by the electron microprobe analysis, the sampled obsidian artefacts almost exclusively derive from the local obsidian outcrops. Local acquisition is also evidenced by a large number of small (<5 cm), but unworked or only initially tested cortical obsidian nodules (Fig. 4.4, A6). After decortification on site, the reduction sequence continued with a unipolar exploitation of cores with two, either opposing or perpendicular platforms. Faceting of platforms and numerous overshots and core tablets indicate the preparation and maintenance of cores. Subsequent bipolar reduction is confirmed by two highly reduced cores and the presence of eight characteristic debitage products (Data S2). Flakes are the major blank category of the assemblage (Table C.3), but the infrequent blades were more commonly chosen for retouch. Common modifications include alternate edge retouch (Fig. 4.4, A2) and basal thinning (Fig. 4.4, A5). Macroscopic traces of utilization regularly occur both on retouched and unretouched artifacts (Data S2). Finished tools are mainly uni-facial points (Fig. 4.4, A1, A3) and laterally retouched points and blades (Fig. 4.4, A2, A5), while scrapers (Fig. 4.4, A4) and borers are present but rare (Data S2).

Additional data on numbers and percentages of marker pieces of the MSA assemblage mentioned in the main text include: unworked or tested cortical obsidian nodules ( $n = 31$ ,

3.1 % total assemblage), debitage products with cortex remnants (n = 222, 37.0 % total debitage products), debitage products with rounded cortex remnants suggesting fluvial transport (n = 12, 5.4 % total cortical artefacts), cores with opposing (n = 8, 66.7 % total cores) or perpendicular platforms (n = 4, 33.3 % total cores), faceted platforms (n = 23, 27.7 % total retouched/utilised artefacts), bipolar debitage products (n = 8, 1.3 % total debitage products), retouched and/or utilised artefacts (n = 83, 8.3 % total assemblage), uni-facial points (n = 10, 12.1 % total retouched/utilised artefacts), laterally retouched points (n = 16, 19.3 %), laterally retouched blades (n = 17, 20.5 % total retouched/utilised artefacts), artefacts with alternate edge retouch (n = 4, 4.8 % total retouched/utilised artefacts), artefacts with proximal thinning (n = 6, 7.2 % total retouched/utilised artefacts), scrapers (n = 6, 7.2 % total retouched/utilised artefacts), notched pieces (n = 5, 6.0 %), and borers (n = 3, 3.6 % total retouched/utilised artefacts).

#### 4.2.8 Faunal analysis

A total of 3655 bones were recovered from the excavation at Fincha Habera rock shelter. Large fragments were collected directly from the excavation grids and all the sediment was sieved (5, 2.5 and 1 mm mesh) to recover the smallest fragments. Faunal remains were analysed at the National Museum of Ethiopia in 2017 and 2018. Most of the remains (n=2305) originated from square H11 on which this analysis focuses (Table C.4). While preservation is good, the bones are highly fragmented and only 66 % could be identified. Most of the large mammal limb bones are broken in a spiral-shape and present splinters indicating that breakage occurred on fresh bones and was done by human or carnivore activities (Lyman, 1994). Bone surfaces are well preserved and present mainly two kinds of traces: digestion and gnawing marks by a large carnivore (< 200) and burn marks suggesting human processing (vertical distribution shown in Fig. C.5). As the location of the latter (only extremities in direct contact with the flame) is representative of roasting (Lyman, 1994) and no gnawing and/or digestion marks were identified on burnt bones, and given the high number of burnt giant mole-rat bones (> 500), we favour human exploitation of giant mole-rats. The almost total absence of cut marks (only once) might be due to the small size of the prey. The colour of the burning marks and the absence of calcinated pieces suggest a low degree of burning. The method of cooking and eating can be well compared to the MSA bird exploitation at Sibudu Cave (Val, de la Peña, and Wadley, 2016). Hunting and consumption of rodents with similar lifeways is archaeologically known in southern African MSA and LSA contexts (Henshilwood, 1997). For an overview on worldwide documented cases of rodent consumption, see Fiedler (1990). However, we currently have no means to infer the hunting practices on *Tachyoryctes macrocephalus* in the present MSA context.

Identifications were made using the osteological reference collection of the Ethiopian National Museum. Moreover, we also used the morphological and osteometric criteria for taxonomic distinctions Gentry (1978), Walker (1985), and Peters (1988). The identification of the coprolites as being produced by spotted hyena (*Crocuta crocuta*) was based on their size and morphology, but this remains to be confirmed by genetic analyses. Species identification of *Tachyoryctes macrocephalus* is based on the measurements of the lower molar rows. Because of the great diversity of wild bovids in Ethiopia (Bekele and Yalden, 2013) and the high degree of

fragmentation of the bones, we could not always take our identifications as far as the species, genus or even sub-family level. We then divided these unidentified remains into five categories (Table C.4), mainly determined by the size of the bones (Lesur, Vigne, and Gutherz, 2007). For quantification, numbers of identified specimens were counted (NISPs) and whenever possible, mammal bones were measured according to the standard system developed by von den Driesch (1976).

### **4.2.9 Glacial chronology of the Harcha and Wasama Valleys**

#### **Background**

Even though the Bale Mountains in the southern Ethiopian Highlands represent the largest afro-alpine environment above 4000 masl, ice caps and valley glaciers are absent nowadays. However, typical glacial geomorphological features like moraines, cirques and roche moutonnées are recorded from the northern valleys and indicate different periods of glaciation (Miehe and Miehe, 1994; Osmaston, Mitchell, and Osmaston, 2005). Studying the extent and timing of Quaternary glaciations in this region is of particular interest since variations of glacier extent related to temperature changes, precipitation and insolation are a sophisticated proxy for the reconstruction of the palaeoclimate and -environment during the early phase of human occupation (Rademaker et al., 2014). Comprehensive mapping and dating of moraines is a prerequisite for the analysis of glacier and climate variations, but such information is still lacking for the Bale Mountains. Therefore, we chose the Harcha and Wasama Valleys in the vicinity of the archaeological site Fincha Habera rock shelter (Fig. 4.1) to study the regional glacial history and palaeoenvironment of Middle Stone Age foragers.

#### **Mapping**

We mapped glacial geomorphological features in the western, northern and eastern valleys of the Bale Mountains as well as on the central Sanetti Plateau during multiple field surveys between 2016 and 2018. In addition, we evaluated high-resolution DigitalGlobe satellite imagery and detected terminal and lateral moraines in remote and difficult to access areas of the mountain range. Where possible, these observations were verified in the field later on. Moraine sequences covering several glacial stages were discovered in the Harcha and Wasama Valleys and were used to establish a glacial chronology. No glacial deposits were found along the steep and intensively eroded Haremma Escarpment in the south. On the Sanetti Plateau, clusters of erratic boulders encircling the highest peak (Tullu Dimtu, 4377 masl) at a distance of ca. 2 and 5.5 km were mapped. These clusters are interpreted as remnants of a former ice cap (Miehe and Miehe, 1994; Osmaston, Mitchell, and Osmaston, 2005).

#### **Glacial extent**

To estimate the extent of the former ice cover in the valleys during the local LGM, glacier outlines was reconstructed from the location of the terminal and lateral moraines. In those valleys where no terminal moraines were preserved, the lower ice limit in the neighbouring valleys

served as a reference for the compilation of the glaciation map. Outcrops and cliffs, which did not show any signs of glacial erosion, were used to determine the glacier boundaries in the former accumulation areas. In valleys where glacial morphological evidence was completely missing, palaeo glacier boundaries were interpolated by referring to the typical geometry of valley glaciers. In total, glaciers in the western, northern and eastern valleys covered about 110 km<sup>2</sup> of the Bale Mountains during the maximum extent of the last glacial cycle. Estimating the extent of even older glaciations was not possible due to very few preserved moraines.

On the Sanetti Plateau, the Tullu Dimtu boulders are most likely remnants of a former ice cap and might indicate the limits of two different glacial stages, which are marked by the inner and outer Big Boulder Moraine (BBM) (Fig. 4.1). Large periglacial features like linear and polygonal areas of sorted stone cover the western and southern plateau and probably evolved under permafrost conditions. These well-preserved structures indicate that these areas have not been covered and intensively eroded by thick ice. Indirectly, these patterns indicate the southern and western limits of the central ice cap (Osmaston, Mitchell, and Osmaston, 2005). Direct and indirect geomorphological evidence for the northern and eastern boundaries of the ice cap is lacking. However, numerous small depressions across the northern plateau linked to irregular subglacial erosion suggest a much larger ice cap than indicated by the BBM. The extent of the central ice cap on the Sanetti Plateau with respect to the location of the outer BBM was about 75 km<sup>2</sup>. However, based on the tentative outline of the maximum extent, it is likely that an additional 80 km<sup>2</sup> of the plateau were covered by ice extending down into the northern valleys. Altogether, about 265 km<sup>2</sup> of the Bale Mountains were glaciated at the maximum stage of the last glacial cycle.

### Sampling strategy

To establish a glacial chronology through cosmogenic <sup>36</sup>Cl surface exposure dating, we selected fifteen trachytic boulders on stable geomorphic surfaces from five moraines in the Harcha Valley and six trachytic boulders from two moraines in the Wasama Valley (Fig. C.6 and Table C.5) following established sampling strategies. The height of the boulders varied from 0.7 to 5.1 m (average of 2.4 m). The topographic shielding was determined using an inclinometer. Between 0.5 and 1 kg of rock material from the upper 5 cm of each boulder was removed using hammer, chisel and angle grinder for laboratory analysis.

### Laboratory procedure

All 21 samples from the Bale Mountains were prepared in the Surface Exposure Dating Laboratory at the University of Bern. Before chemical treatment, every rock sample was crushed and sieved. In order to remove any chlorine not produced in situ, 120 g of the 200 – 400 μm grain-size fraction was leached in 2 M HNO<sub>3</sub> and rinsed afterwards with ultrapure water (18.2 MΩ-cm). For the extraction of Cl isotopes, we followed the laboratory procedure described by Akçar et al. (2012, and references therein), which is based on the method introduced by Stone et al. (1996b), using isotope dilution. Major and trace element data of all samples (Table C.6) are required for the calculation of local <sup>36</sup>Cl production rates. An aliquot of ca. 10 g from each

leached sample was sent to SGS Laboratories in Toronto, Canada, where the elemental analysis was performed. Total Cl- and  $^{36}\text{Cl}$ -concentrations were measured from one target at the 6 MV AMS-facility of the ETH Zurich using the isotope dilution technique. The measured ratios of  $^{36}\text{Cl}/^{35}\text{Cl}$  were normalised to the ETH in-house standard K382/4N (Christl et al., 2013) with a  $^{36}\text{Cl}/\text{Cl}$ -value of  $17.36 \times 10^{-12}$  (normalised to the Nishiizumi standard of 2009), whereas the stable ratio of  $^{37}\text{Cl}/^{35}\text{Cl}$  was normalised to the natural  $^{37}\text{Cl}/^{35}\text{Cl}$ -ratio, which equals to 31.98 % of the K382/4N standard and machine blank.

### Surface exposure age calculation

Based on the measured total Cl and  $^{36}\text{Cl}$  concentrations, surface exposure ages were calculated for the boulders from the Harcha and Wasama Valley following the description in Akçar et al. (2012, and references therein). The applied spallogenic production rate of cosmogenic  $^{36}\text{Cl}$  at sea-level from Ca corresponds to  $48.8 \pm 1.7$  atoms  $\text{g}^{-1} \text{Ca a}^{-1}$  and from K to  $162 \pm 24$  atoms  $\text{g}^{-1} \text{K a}^{-1}$ . Altitude and latitude of the sampling sites influence the scaling of the  $^{36}\text{Cl}$  production rate following the scheme of Stone (2000). Muon capture contributes  $5.3 \pm 0.5$  atoms  $\text{g}^{-1} \text{Ca a}^{-1}$  to the production of  $^{36}\text{Cl}$  from Ca. The capture of thermal and epithermal neutrons near the surface in the order of  $760 \pm 150$  neutrons  $\text{g}^{-1} \text{air a}^{-1}$  is another source for the production of  $^{36}\text{Cl}$ . Major and trace element (B, Gd, and Sm) concentrations are considered in order to determine the fraction of low-energy neutrons available for producing  $^{36}\text{Cl}$  from  $^{35}\text{Cl}$ , while U and Th concentrations served for the quantification of non-cosmogenic  $^{36}\text{Cl}$  in the rocks. We corrected  $^{36}\text{Cl}$  production rates for sample thickness (Table C.5) assuming a rock density of  $2.65 \text{ g cm}^{-3}$  and an attenuation length of  $160 \text{ g cm}^{-2}$ . To account for the topographic shielding at the sampling sites (Table C.5), correction factors were computed using the program of Tikhomirov et al. (2014). The impact of snow cover on the production of  $^{36}\text{Cl}$  is negligible in the Bale Mountains since the rarity of snowfall events and the rapid melting of snow within hours or days (Miehe and Miehe, 1994) prevents snow from accumulating on the boulders. Independent information on post-depositional erosion rates are not available neither for the Ethiopian Highlands nor the other East African mountains, but are estimated to be in the range of  $0 - 2 \text{ mm ka}^{-1}$ . For a detailed discussion on the effect of erosion on  $^{36}\text{Cl}$  ages see (Shanahan and Zreda, 2000). To account for the impact of variable erosion rates, we calculated three different  $^{36}\text{Cl}$  surface exposure ages for every boulder (Table C.7) considering a minimum, medium and maximum erosion scenario ( $\varepsilon_{\min} = 0 \text{ mm ka}^{-1}$ ,  $\varepsilon_{\text{med}} = 1 \text{ mm ka}^{-1}$ ,  $\varepsilon_{\max} = 2 \text{ mm ka}^{-1}$ ), as suggested by Shanahan and Zreda (2000). Exposure ages in Figs. 4.1, C.7, and C.8 are stated without erosion correction ( $\varepsilon = 0 \text{ mm ka}^{-1}$ ). The  $1\sigma$ -error given for each individual exposure age includes solely the analytical uncertainty.

### Glacial chronology

To establish a glacial chronology for the Bale Mountains, we discriminated between three Glacial Stages (I, II, III) in the Harcha and Wasama Valleys based on the geomorphology, location and age of the terminal moraines (Figs. C.6, C.7). All exposure ages of moraines from both valleys associated with the same glacial stage were grouped, except of boulders HA02 ( $383.3 \pm$

15.7 ka BP) and HA06 ( $48.8 \pm 2.6$  ka BP). They were excluded from further calculations because they do not overlap in age with the other two boulders of the respective moraine (Fig. C.7, Table C.7) within a  $3\sigma$  limit. The differing ages probably result from a complex exposure history of the two boulders including an inherited cosmogenic  $^{36}\text{Cl}$  signal from pre-depositional exposure(s). We considered all remaining exposure ages ( $n_I = 2$ ,  $n_{II} = 8$ ,  $n_{III} = 9$ ) for the calculation of the weighted average of Glacial Stage I, II and III. Since the mean internal (analytical) error of the exposure ages is smaller than the external (geomorphological) uncertainty defined by the standard deviation ( $1\sigma$ ) of each glacial stage, we report the weighted average with the external error (Fig. 4.1).

#### 4.2.10 Derivation of palaeoenvironmental conditions from ground beetle data

##### Background

Ground beetles have exceptional proxy properties both for extant and palaeoecological environments (Elias, 2007; Kotze et al., 2011). Extensive comparative analyses of Late Quaternary fossil beetle associations with extant associations have proven that the ecological requirements of beetle species have not changed but have been constant on palaeoecological time scales (Coope, 1986; Coope, 2004; Elias, 2007; Elias, 2010). Furthermore, ground beetles show exceptionally high micro-areal endemic species richness in mountains of the mid and lower latitudes. E.g., the Ethiopian Highlands are characterised by a very high number of wingless species each with a very small distributional area which usually not exceeds a single mountain or even valley system (Brühl, 1997; Schmidt and Faille, 2018). The only plausible explanation for such distribution patterns is in situ speciation: Low dispersal capacity and strict adaptation to certain environmental conditions, of which first of all are soil humidity and temperature (Lindroth, 1949; Thiele, 1974; Coope, 1986; Atkinson, Briffa, and Coope, 1987), result in geographic separation of the populations in the course of the geomorphological and climatic development of the mountainous environment and consequently, in the geographic radiation of the lineages (evolution of swarms of allopatric species which are highly endemic to certain parts of the mountains). Finally, ground beetle's high phylogenetic age (species age) easily extends hundreds of thousands years (Sota and Nagata, 2008; Andújar, Serrano, and Gómez-Zurita, 2012; Faille et al., 2014). As a consequence, distributional patterns of extant wingless beetle species strictly adapted to specific habitat conditions therefore allow reconstructing location and palaeoenvironmental conditions of the respective species-specific glacial refuges, particularly due to the markedly reduced dispersal ability even on evolutionary time scales (Holdhaus, 1954; Schmidt et al., 2011).

Here, we concentrate on the reconstruction of humidity and temperature patterns since these climatic factors markedly determine the suitability of a given area for residence of Middle Stone Age foragers. We use distributional data of extant wingless humidity adapted beetle species according to a method introduced by Schmidt et al., 2011 and successfully used to reconstruct the LGM temperature depression of South Tibet.

### Data collection

Distributional and ecological data of the ground beetles of the Bale Mountains were collected during six years of field work (2013-2019). To answer the question of whether environmental conditions suitable for human occupations persisted in the area during the last glaciation period we selected data from tiny wingless ground beetles of the genus *Trechus* Clairville. These beetles are strictly adapted to high soil humidity and to the temperate or colder climate, exclusively alpine species were excluded from the analysis. Consequently, selected *Trechus* species only occur in the forest zone along slopes of the Bale Mountains, in humus-rich soils near brooks shadowed by trees and bushes, at altitudes above 2000 m. Most of these species are found to be micro-areal endemics, meaning that they are endemic to a single valley system on one of the slopes of the Bale Mountains (Schmidt et al., 2011). Thus far, 39 micro-areal endemic species could be discovered in the area, with seven species endemic to the Web Valley system, of which four species were found to be endemic to the lower (Fincha Habera) and upper Wasama Valley near the residential site of the Middle Stone Age foragers (Fig. C.9, Table C.8).

### Reconstruction of palaeoenvironmental conditions

Each of the investigated valley systems along the slopes of the Bale Mountains was found to be characterised by the presence of 2-11 micro-areal endemic non-alpine *Trechus* beetle species strictly adapted to permanently humid and humus-rich soil conditions and to the temperate or colder climate (Fig. C.9, Table C.8). Vertical distributions of all of these species are confined to the Montane Forest and *Ericaceous* belts (Miehe and Miehe, 1994). These findings mandate the long-term uninterrupted presence and contemporary presence of permanent surface water drainage and temperate and colder but non-alpine climate, and thus support forest habitats, at least gallery forests, in these valleys. Due to the long-term presence of these species in the area, the humid and forested habitat conditions must have existed locally since well before the last glacial period. Consequently, within this period and thereafter, the respective valley systems have never undergone a complete desiccation, not even for a few years. Freshwater brooks and forests have thus been a characteristic landscape feature at least during the MSA occupations in the Bale Mountains.

### Acknowledgements

We thank the Ethiopian Authority for Research and Conservation of Cultural Heritage, the Ethiopian Wildlife Conservation Authority, the Ethiopian Biodiversity Institute, the College of Natural and Computational Sciences, Addis Ababa University, the Department of Plant Biology and Biodiversity Management, Addis Ababa University (DPBBM/CNS/092/2009/ 2016), the Frankfurt Zoological Society, and the Bale Mountains National Park for their cooperation and kind permission to conduct field work. For supporting or organizing field work, we are grateful to M. Fekadu, K. Thielsen, T. Koch, Z. Kefyalew, J. Hagge, Y. Merene, W. Abebe, T. Endale, G. Mebratu, B. Kemal, S. Erlwein, L. Munz, J. Struck, B. Tagane, Dejene, Bisrat, Habtam, Fitsum, Mudassir, Worku, Techete, Awel, Baye, Burka, Hassan, Mama, Salomon, Muzien,

Mukhtar, Tamam, Sultan, Abel, Mohammed, Hussein, and Neguse. We thank C. Vockenhuber and the AMS team of the ETH Zurich for conducting the  $^{36}\text{Cl}$  measurements and J. Rethemeyer and team (CologneAMS) and C. Patrick and team (Beta Analytic) for performing the radiocarbon datings. We also acknowledge the DigitalGlobe Foundation for providing high-resolution satellite imagery of the Bale Mountains granted to A.R.G. Thanks are also due to L. Wraase for providing base maps, to N. Schneid for the drawings of the lithic artefacts, and to E. Stoetzel and C. Denys for their contribution to the rodent identification. We are much indebted to J. Orton (ASHA Consulting) for his meticulous proofreading. The paper benefited from very constructive and insightful comments from three anonymous reviewers.

This research was funded by the German Research Foundation (DFG) in the framework of the joint Ethio-European DFG Research Unit 2358 “The Mountain Exile Hypothesis.” Additional funding was provided by the Swiss National Science Foundation (SNF grant no. 200021E-165446/1).

## References

- 11466, ISO (1995). *Soil Quality – Extraction of Trace Elements Soluble in Aqua Regia*. International Organization for Standardization, Geneva.
- Akçar, N. et al. (2012). “ $^{36}\text{Cl}$  Exposure Dating of Paleoearthquakes in the Eastern Mediterranean: First Results from the Western Anatolian Extensional Province, Manisa Fault Zone, Turkey”. In: *Geol. Soc. Am. Bull.* 124.11-12, pp. 1724–1735. DOI: 10.1130/B30614.1.
- Aldenderfer, M. (2006). “Modelling plateau peoples: the early human use of the world’s high plateaux”. In: *World Archeol.* 38.3, pp. 357–370. DOI: 10.1080/00438240600813285.
- Aldenderfer, M. (2014). *Altitude Environments in Archaeology*. Ed. by C. Smith. Springer New York, pp. 163–168. DOI: 10.1007/978-1-4419-0465-2\_2012.
- Alkorta-Aranburu, G. et al. (2012). “The Genetic Architecture of Adaptations to High Altitude in Ethiopia”. In: *PLoS Genet.* 8.12, pp. 1–13. DOI: 10.1371/journal.pgen.1003110.
- Andújar, C., J. Serrano, and J. Gómez-Zurita (2012). “Winding up the Molecular Clock in the Genus *Carabus* (Coleoptera: Carabidae): Assessment of Methodological Decisions on Rate and Node Age Estimation”. In: *BMC Evol. Biol.* 12.1, p. 40. DOI: 10.1186/1471-2148-12-40.
- Atkinson, T. C., K. R. Briffa, and G. R. Coope (1987). “Seasonal Temperatures in Britain during the Past 22,000 Years, Reconstructed Using Beetle Remains”. In: *Nature* 325.6105, pp. 587–592. DOI: 10.1038/325587a0.
- Barham, L. and P. Mitchell (2008). *The First Africans: African Archaeology from the Earliest Tool-makers to Most Recent Foragers*. Cambridge World Archaeology. Cambridge University Press. DOI: 10.1017/CB09780511817830.
- Basell, L. (2008). “Middle Stone Age (MSA) Site Distributions in Eastern Africa and Their Relationship to Quaternary Environmental Change, Refugia and the Evolution of *Homo Sapiens*”. In: *Quat. Sci. Rev.* 27.27-28, pp. 2484–2498. DOI: 10.1016/j.quascirev.2008.09.010.
- Beall, C. M. (2001). “Adaptations to Altitude: A Current Assessment”. In: *Annu. Rev. Anthropol.* 30.1, pp. 423–456. DOI: 10.1146/annurev.anthro.30.1.423.

- Beall, C. M. (2014). "Adaptation to High Altitude: Phenotypes and Genotypes". In: *Annu. Rev. Anthropol.* 43.1, pp. 251–272. DOI: 10.1146/annurev-anthro-102313-030000.
- Bekele, A. and D. W. Yalden (2013). *The Mammals of Ethiopia and Eritrea*. Addis Ababa Univ. Press.
- Birk, J. J. et al. (2012). "Combined Quantification of Faecal Sterols, Stanols, Stanones and Bile Acids in Soils and Terrestrial Sediments by Gas Chromatography–Mass Spectrometry". In: *J. Chromatogr. A* 1242, pp. 1–10. DOI: 10.1016/j.chroma.2012.04.027.
- Brandt, S. A. et al. (2012). "Early MIS 3 Occupation of Mochena Borago Rockshelter, Southwest Ethiopian Highlands: Implications for Late Pleistocene Archaeology, Paleoenvironments and Modern Human Dispersals". In: *Quat. Int.* 274, pp. 38–54. DOI: 10.1016/j.quaint.2012.03.047.
- Brandt, S. A. et al. (2017). "A New MIS 3 Radiocarbon Chronology for Mochena Borago Rockshelter, SW Ethiopia: Implications for the Interpretation of Late Pleistocene Chronostratigraphy and Human Behavior". In: *J. Archaeol. Sci.* 11, pp. 352–369. DOI: 10.1016/j.jasrep.2016.09.013.
- Brodowski, S. et al. (2005). "Revised Black Carbon Assessment Using Benzene Polycarboxylic Acids". In: *Org. Geochem.* 36.9, pp. 1299–1310. DOI: 10.1016/j.orggeochem.2005.03.011.
- Brooks, A. S. et al. (2018). "Long-Distance Stone Transport and Pigment Use in the Earliest Middle Stone Age". In: *Science* 360.6384, pp. 90–94. DOI: 10.1126/science.aao2646.
- Brühl, C. (1997). "Flightless Insects: A Test Case for Historical Relationships of African Mountains". In: *J. Biogeogr.* 24.2, pp. 233–250. DOI: 10.1046/j.1365-2699.1997.00073.x.
- Bull, I. D. et al. (2002). "The Origin of Faeces by Means of Biomarker Detection". In: *Environ. Int.* 27.8, pp. 647–654. DOI: 10.1016/S0160-4120(01)00124-6.
- Chen, F. et al. (2019). "A Late Middle Pleistocene Denisovan Mandible from the Tibetan Plateau". In: *Nature* 569.7756, pp. 409–412. DOI: 10.1038/s41586-019-1139-x.
- Chen, F. H. et al. (2015). "Agriculture Facilitated Permanent Human Occupation of the Tibetan Plateau after 3600 B.P." In: *Science* 347.6219, pp. 248–250. DOI: 10.1126/science.1259172.
- Christl, M. et al. (2013). "The ETH Zurich AMS Facilities: Performance Parameters and Reference Materials". In: *Nucl. Instrum. Methods Phys. Res. B* 294, pp. 29–38. DOI: 10.1016/j.nimb.2012.03.004.
- Coope, G. R. (1986). *Coleoptera analysis*. Ed. by B. E. Berglund. Wiley, pp. 703–713.
- Coope, G. R. (2004). "Several Million Years of Stability among Insect Species Because of, or in Spite of, Ice Age Climatic Instability?" In: *Phil. Trans. R. Soc. Lond. B* 359.1442, pp. 209–214. DOI: 10.1098/rstb.2003.1393.
- Elias, S. A. (2007). *Beetle records*. Ed. by S. A. Elias and C. J. Mock. Elsevier, pp. 153–163.
- Elias, S. A. (2010). *Advances in Quaternary Entomology*. Elsevier.
- Faille, A. et al. (2014). "Late Miocene Origin of an Ibero-Maghrebian Clade of Ground Beetles with Multiple Colonizations of the Subterranean Environment". In: *J. Biogeogr.* 41.10, pp. 1979–1990. DOI: 10.1111/jbi.12349.
- Fiedler, L. A. (1990). "Rodents as a Food Source". In: *Proc. Vertebr. Pest C.* 30, pp. 149–155.

- Foerster, V. et al. (2018). "Towards an Understanding of Climate Proxy Formation in the Chew Bahir Basin, Southern Ethiopian Rift". In: *Palaeogeogr. Palaeoclimatol. Palaeoecol.* 501, pp. 111–123. DOI: 10.1016/j.palaeo.2018.04.009.
- Gentry, A. W. (1978). "Bovidae" in *Evolution of African Mammals*. Ed. by V. J. Maglio and H. B. S. Cooke. Cambridge Univ. Press, pp. 540–572.
- Glaser, B. et al. (1998). "Black Carbon in Soils: The Use of Benzenecarboxylic Acids as Specific Markers". In: *Org. Geochem.* 29.4, pp. 811–819. DOI: doi:10.1016/S0146-6380(98)00194-6.
- Gossa, T., Y. Sahle, and A. Negash (2012). "A reassessment of the Middle and Later Stone Age lithic assemblages from Aladi Springs, Southern Afar Rift, Ethiopia". In: *Azania* 47.2, pp. 210–222. DOI: 10.1080/0067270X.2012.676314.
- Henshilwood, C.S. (1997). "Identifying the Collector: Evidence for Human Processing of the Cape Dune Mole-Rat, *Bathyergus Suillus*, from Blombos Cave, Southern Cape, South Africa". In: *J. Archaeol. Sci.* 24.7, pp. 659–662. DOI: 10.1006/jasc.1996.0148.
- Holdhaus, K. (1954). *Die Spuren der Eiszeit in der Tierwelt Europas*. Wagner.
- Inizan, M.-L. et al. (1999). *Technology and Terminology of Knapped Stone*.
- Julian, C. G. (2017). "Epigenomics and Human Adaptation to High Altitude". In: *J. Appl. Physiol.* 123.5, pp. 1362–1370. DOI: 10.1152/jappphysiol.00351.2017.
- Kotze, D. J. et al. (2011). "Forty Years of Carabid Beetle Research in Europe – from Taxonomy, Biology, Ecology and Population Studies to Bioindication, Habitat Assessment and Conservation". In: *ZooKeys* 100, pp. 55–148. DOI: 10.3897/zookeys.100.1523.
- Kuehn, S. C., D. G. Froese, and P. A. R. Shane (2011). "The INTAV Intercomparison of Electron-Beam Microanalysis of Glass by Tephrochronology Laboratories: Results and Recommendations". In: *Quat. Int.* 246.1-2, pp. 19–47. DOI: 10.1016/j.quaint.2011.08.022.
- Kuhn, S. L. (1995). *Mousterian Lithic Technology*. Princeton Univ. Press.
- Kuzmicheva, E. A. et al. (2013). "Holocene Hyrax Dung Deposits in the Afroalpine Belt of the Bale Mountains (Ethiopia) and Their Palaeoclimatic Implication". In: *Environ. Archaeol.* 18.1, pp. 72–81. DOI: 10.1179/1461410313Z.00000000018.
- Kuzmicheva, E. A. et al. (2014). "Vegetation and Climate Reconstruction for the Bale Mountains (Ethiopia) in the Holocene According to the Pollen Analysis and Radiocarbon Dating of Zoogenic Deposits". In: *Dokl. Biol. Sci.* 458.1, pp. 281–285. DOI: 10.1134/S0012496614050019.
- Leplongeon, A., D. Pleurdeau, and E. Hovers (2017). "Late Pleistocene and Holocene Lithic Variability at Goda Buticha (Southeastern Ethiopia): Implications for the Understanding of the Middle and Late Stone Age of the Horn of Africa". In: *J. Afr. Archaeol.* 15.2, pp. 202–233. DOI: 10.1163/21915784-12340010.
- Lesur, J., J.-D. Vigne, and X. Gutherz (2007). "Exploitation of wild mammals in South-west Ethiopia during the Holocene (4000 BC–500 AD): the finds from Moche Borago shelter (Wolayta)". In: *Environ. Archaeol.* 12.2, pp. 139–159. DOI: 10.1179/174963107x226417.
- Lindroth, C. H. (1949). *Die fennoskandischen Carabidae. Eine tiergeographische Studie. III Allgemeiner Teil*. Göteborgs Kungl.
- Lloyd, C. E. M. et al. (2012). "Tracing the Flow-Driven Vertical Transport of Livestock-Derived Organic Matter through Soil Using Biomarkers". In: *Org. Geochem.* 43, pp. 56–66. DOI: 10.1016/j.orggeochem.2011.11.001.

- Lyman, R. L. (1994). *Vertebrate Taphonomy*. Cambridge Manuals in Archaeology. Cambridge University Press. DOI: 10.1017/CB09781139878302.
- Ménard, C. et al. (2014). "Late Stone Age Variability in the Main Ethiopian Rift: New Data from the Bulbula River, Ziway–Shala Basin". In: *Quat. Int.* 343, pp. 53–68. DOI: 10.1016/j.quaint.2014.07.019.
- Meyer, M. C. et al. (2017). "Permanent Human Occupation of the Central Tibetan Plateau in the Early Holocene". In: *Science* 355.6320, pp. 64–67. DOI: 10.1126/science.aag0357.
- Middleton, W. D. (1998). *Craft specialization at Ejutla, Oaxaca, Mexico: an archaeometric study of the organization of household craft production*. University of Wisconsin, Madison, WI.
- Middleton, W. D. (2004). "Identifying Chemical Activity Residues on Prehistoric House Floors: A Methodology And Rationale For Multi-Elemental Characterization of a Mild Acid Extract of Anthropogenic Sediments". In: *Archaeometry* 46.1, pp. 47–65. DOI: 10.1111/j.1475-4754.2004.00143.x.
- Middleton, W. D. and D. T. Price (1996). "Identification of Activity Areas by Multi-Element Characterization of Sediments from Modern and Archaeological House Floors Using Inductively Coupled Plasma-Atomic Emission Spectroscopy". In: *J. Archaeol. Sci.* 23.5, pp. 673–687. DOI: 10.1006/jasc.1996.0064.
- Miehe, S. and G. Miehe (1994). *Ericaceous Forests and Heathlands in the Bale Mountains of South Ethiopia - Ecology and Man's Impact*. Hamburg: Stiftung Walderhaltung in Afrika.
- Nash, B. (1992). "Analysis of Oxygen with the Electron Microprobe: Applications to Hydrous Glass and Minerals". In: *Am. Mineral.* 77, pp. 453–457.
- Negash, A., F. Brown, and B. Nash (2011). "Varieties and Sources of Artefactual Obsidian in the Middle Stone Age of the Middle Awash, Ethiopia". In: *Archaeometry* 53.4, pp. 661–673. DOI: 10.1111/j.1475-4754.2010.00579.x.
- Osmaston, H. A., W. A. Mitchell, and J. A. N. Osmaston (2005). "Quaternary Glaciation of the Bale Mountains, Ethiopia". In: *J. Quat. Sci.* 20.6, pp. 593–606. DOI: 10.1002/jqs.931.
- Peters, J. (1988). "Osteomorphological features of the appendicular skeleton of African buffalo, *Syncerus caffer* (Sparman, 1779) and of domestic cattle, *Bos Primigenius f. taurus* Bojanus, 1827". In: *Z. Saugetierkd.* 53, pp. 108–123.
- Pleurdeau, D. (2006). "Human Technical Behavior in the African Middle Stone Age: The Lithic Assemblage of Porc-Epic Cave (Dire Dawa, Ethiopia)". In: *Afr. Archaeol. Rev.* 22.4, pp. 177–197. DOI: 10.1007/s10437-006-9000-7.
- Pleurdeau, D. et al. (2014). "Cultural Change or Continuity in the Late MSA/Early LSA of Southeastern Ethiopia? The Site of Goda Buticha, Dire Dawa Area". In: *Quat. Int.* 343, pp. 117–135. DOI: 10.1016/j.quaint.2014.02.001.
- Rademaker, K. et al. (2014). "Paleoindian Settlement of the High-Altitude Peruvian Andes". In: *Science* 346.6208, pp. 466–469. DOI: doi:10.1126/science.1258260.
- Ramsey, C. B. (2009). "Bayesian Analysis of Radiocarbon Dates". In: *Radiocarbon* 51.1, pp. 337–360. DOI: 10.1017/S0033822200033865.
- Reber, D. et al. (2018). "High-Altitude Rock Shelters and Settlements in an African Alpine Ecosystem: The Bale Mountains National Park, Ethiopia". In: *Hum. Ecol.* DOI: 10.1007/s10745-018-9999-5.

- Reimer, P. J. et al. (2013). "IntCal13 and Marine13 Radiocarbon Age Calibration Curves 0–50,000 Years cal BP". In: *Radiocarbon* 55.4, pp. 1869–1887. DOI: 10.2458/azu\_js\_rc.55.16947.
- Rethemeyer, J. et al. (2013). "Status Report on Sample Preparation Facilities for <sup>14</sup>C Analysis at the New CologneAMS Center". In: *Nucl. Instrum. Meth. B* 294, pp. 168–172. DOI: 10.1016/j.nimb.2012.02.012.
- Schmidt, J. and A. Faille (2018). "Revision of *Trechus Clairville*, 1806 of the Bale Mountains and Adjacent Volcanos, Ethiopia (Coleoptera, Carabidae, Trechini)". In: *Eur. J. Taxon.* 446. DOI: 10.5852/ejt.2018.446.
- Schmidt, J. et al. (2011). "Neoendemic Ground Beetles and Private Tree Haplotypes: Two Independent Proxies Attest a Moderate Last Glacial Maximum Summer Temperature Depression of 3–°C for the Southern Tibetan Plateau". In: *Quat. Sci. Rev.* 30.15–16, pp. 1918–1925. DOI: 10.1016/j.quascirev.2011.04.014.
- Shakun, J. D. and A. E. Carlson (2010). "A Global Perspective on Last Glacial Maximum to Holocene Climate Change". In: *Quat. Sci. Rev.* 29, pp. 1801–1816. DOI: 10.1016/j.quascirev.2010.03.016.
- Shanahan, D. F. and M. Zreda (2000). "Chronology of Quaternary Glaciations in East Africa". In: *Earth Planet. Sci. Lett.* 177, pp. 23–42.
- Sillero-Zubiri, C., F. H. Tattersall, and D. W. Macdonald (1995). "Habitat Selection and Daily Activity of Giant Molerats *Tachyoryctes Macrocephalus*: Significance to the Ethiopian Wolf *Canis Simensis* in the Afroalpine Ecosystem". In: *Biol. Conserv.* 72, pp. 77–84. DOI: doi : 10.1016/0006-3207(94)00067-Z.
- Sota, T. and N. Nagata (2008). "Diversification in a Fluctuating Island Setting: Rapid Radiation of Ohomopterus Ground Beetles in the Japanese Islands". In: *Phil. Trans. R. Soc. B* 363.1508, pp. 3377–3390. DOI: 10.1098/rstb.2008.0111.
- Stewart, J. R. and C. B. Stringer (2012). "Human Evolution Out of Africa: The Role of Refugia and Climate Change". In: *Science* 335.6074, pp. 1317–1321. DOI: 10.1126/science.1215627.
- Stone, J. O. H. (2000). "Air Pressure and Cosmogenic Isotope Production". In: *J. Geophys. Res.* 105.B10, pp. 23753–23759. DOI: 10.1029/2000JB900181.
- Stone, J. O. H. et al. (1996b). "Cosmogenic chlorine-36 production rates from calcium and potassium". In: *Radiocarbon* 38, pp. 170–171. DOI: 10.1029/2006GL026484.
- Thiele, H. U. (1974). "Physiologisch-ökologische Studien an Laufkäfern zur Kausalanalyse ihrer Habitatbindung". In: *Verh. Ges. Ökol.* 1973, pp. 39–54.
- Tierney, J. E., P. B. deMenocal, and P. D. Zander (2017). "A Climatic Context for the Out-of-Africa Migration". In: *Geology* 45.11, pp. 1023–1026. DOI: 10.1130/G39457.1.
- Tierney, J. E. et al. (2008). "Northern Hemisphere Controls on Tropical Southeast African Climate During the Past 60,000 Years". In: *Science* 322.6976, pp. 252–255. DOI: 10.1038/nature02251.
- Tikhomirov, D. et al. (2014). "Calculation of Shielding Factors for Production of Cosmogenic Nuclides in Fault Scarps". In: *Quat. Geochronol.* 19, pp. 181–193. DOI: 10.1016/j.quageo.2013.08.004.
- Val, A., P. de la Peña, and L. Wadley (2016). "Direct Evidence for Human Exploitation of Birds in the Middle Stone Age of South Africa: The Example of Sibudu Cave, KwaZulu-Natal". In: *J. Hum. Evol.* 99, pp. 107–123. DOI: 10.1016/j.jhevol.2016.07.007.

- von den Driesch, A. (1976). *A Guide to the Measurement of Animal Bones from Archaeological Sites*. Harvard Univ. Press.
- Walker, R. (1985). *A Guide to Post-Cranial Bones of East African Animals*. Hylochoerus.
- Yalden, D. W. and M. J. Lagen (1992). "The Endemic Mammals of Ethiopia". In: *Mammal Rev.* 22.3-4, pp. 115–150. DOI: 10.1111/j.1365-2907.1992.tb00128.x.
- Zhang, X. L. et al. (2018). "The Earliest Human Occupation of the High-Altitude Tibetan Plateau 40 Thousand to 30 Thousand Years Ago". In: *Science* 362.6418, pp. 1049–1051. DOI: doi : 10.1126/science.aat8824.



## Chapter 5

# Synthesis

The magnitude of cooling in the equatorial East African mountains and Ethiopian Highlands during the last glacial period and its impact on the afro-alpine environment and human expansion into higher elevations is still poorly understood. Quasi-continuous archives like ice or sediment cores that provide insights into palaeoclimatic and -environmental changes at high elevations in Eastern Africa are extremely rare and cover mainly the Holocene (e.g. Thompson et al., 2002; Tiercelin et al., 2008). Glacial deposits and periglacial landforms are often the only remaining evidence of Pleistocene climatic and environmental changes in the tropical mountains of Eastern Africa (e.g. Grab, 2002; Osmaston and Harrison, 2005; Mark and Osmaston, 2008; Hastenrath, 2009). One of the least studied alpine regions in Eastern Africa with respect to the glacial and periglacial history are the Bale Mountains in the southern Ethiopian Highlands, although they comprise the continent's largest area above 4000 m (Miehe and Miehe, 1994) and testify to an extensive former plateau glaciation (Messerli et al., 1977; Osmaston, Mitchell, and Osmaston, 2005). Glacial and periglacial landforms have been reported from the Bale Mountains (Messerli et al., 1977; Miehe and Miehe, 1994; Umer, Kebede, and Osmaston, 2004; Osmaston, Mitchell, and Osmaston, 2005), but they have never been systematically mapped, dated, and investigated. To close this gap and explore the potential of this afro-alpine archive for the reconstruction of past glacier fluctuations and regional high-altitude climate and -environmental changes, is therefore the goal of this thesis. The following synthesis chapter aims to (1) combine and discuss the main findings from the three presented research articles, to (2) elaborate their broader implication for the natural and anthropogenic history of tropical mountains in Eastern Africa, and (3) to outline new research questions arising from the thesis and collaborations within the interdisciplinary research unit. The five specific research questions defined at the beginning (Chapter 1.3) serve as guidance for the synthesis:

1. What was the extent of the ice cover in the Bale Mountains during the last glacial period?
2. When were the Bale Mountains glaciated? When did the glaciers reach their maximum expansion? When did deglaciation set in?
3. When, how, and under which climatic and environmental conditions did the relict large sorted stone stripes and polygons on the Sanetti Plateau form?
4. Which cooling can be inferred from the presence of glacial and periglacial landforms and what does it imply for the palaeoclimate and -ecology of tropical mountains?
5. How did the palaeoclimate and -environment look like at the time when humans started to colonise the Bale Mountains?

**What was the extent of the ice cover in the Bale Mountains during the last glacial period?**

Accurate mapping of preserved glacial and periglacial landforms is the prerequisite for reconstructing the extent of past glaciations, estimating ELAs, and selecting appropriate sites for dating (e.g. Chandler et al., 2018). The fact that the Bale Mountains consist of a large plateau above 4000 masl, individual higher peaks, and numerous alpine valleys, is both an advantage and disadvantage in this respect. On the one hand, the Bale Mountains provide a large repertoire of glacial and periglacial landforms, but on the other hand this archive is difficult to explore due to its size and remoteness. This is also the reason why field mapping has so far been concentrated to areas along the dirt-road, crossing the central Sanetti Plateau (Osmaston, Mitchell, and Osmaston, 2005). Most of the sites in the valleys and on the plateau can only be reached on foot or horseback and require multiple days of trekking. During four months of field work, split into several expeditions between 2016 and 2020, extensive geomorphological mapping of glacial and periglacial features has been performed in the Bale Mountains as part of the dissertation. In addition, WorldView-1 satellite images with a pixel resolution of  $0.5 \times 0.5$  m (provided through DigitalGlobe Foundation) were visually evaluated to identify distinct geomorphological features in remote and difficult-to-access areas. Two complementary field trips were organised in 2017 and 2020 to the Arsi Mountains, which are located about 100 km northwest of the Bale Mountains and also provide evidence of past glaciations (Potter, 1976; Osmaston and Harrison, 2005).

The main outcome of the geomorphological field mapping and evaluation of satellite images and older reports are two glaciation maps (presented in Chapters 2 and 4), showing the local LGM (LPG Stage I, 50-30 ka) ice extent in the Bale and adjacent Arsi Mountains. For the Arsi Mountains, the reconstructed ice extent of 83 km<sup>2</sup> is very similar to the estimate of 85 km<sup>2</sup> by Osmaston and Harrison (2005). This agreement reflects the good preservation and accurate mapping of lateral and terminal moraines in most of the valleys descending from the central ridge. In contrast to the Arsi Mountains, where the catchment of the palaeo valley glaciers is well defined by the local topography, the reconstruction of the former plateau glaciation in the Bale Mountains is fraught with larger uncertainty. Based on the mapping of lateral and terminal moraines, the local LGM ice extent in the Bale Mountains, including the ice cap and valley glaciers, was constrained to 265 km<sup>2</sup>. This estimate is significantly lower than the one of  $\sim 600$  km<sup>2</sup> by Messerli et al. (1977), but larger than the one of 180 km<sup>2</sup> by Osmaston, Mitchell, and Osmaston (2005). The difference between the new estimate and the one by Osmaston, Mitchell, and Osmaston (2005) can be explained by the verification of additional glaciers in the western and eastern valleys that were unexplored before. In view of the absence of erratic boulders and other distinct glacial remains along the western, southern, and eastern plateau margins, a complete plateau glaciation as postulated by Messerli et al. (1977) and rebutted by Osmaston, Mitchell, and Osmaston (2005) seems unlikely. The presence of apparently unglaciated features on the southern and western plateau like hardly eroded volcanic plugs and relict large sorted stone stripes (addressed in Chapter 3) support the postulation of a restricted ice cap that just extended into the northern valleys.

Despite the detailed mapping of erratic boulders, our understanding of the evolution of the ice cap on the Sanetti Plateau remains unsatisfying. This is mainly due to the hardly preserved

glacial geomorphological evidence for the maximum ice extent and the poor dating control on the plateau (discussed in Chapter 2). Based on all what we can infer from the geomorphology, a transfluence of ice from the plateau into the northern valleys during the local LGM seems the most likely scenario. The fact that areas like the elevated western part (>4100 masl) on the plateau were probably ice free during the local LGM, although located far above the palaeo ELA, indicates that insolation as well as variable snow accumulation and snow redistribution by wind played a major role for the glacier mass balance on the plateau. A dry and cold climate beyond the limits of the palaeo ice cap would have provided ideal conditions for the formation of the large sorted patterned grounds as found on the southern and western plateau (see Chapter 3). Even though the present topographic and climatic conditions on the plateau differ fundamentally from those during the local LGM, a yet missing analysis of the present-day precipitation and wind flow patterns could help to develop a better understanding of the past snow accumulation on the plateau. In contrast to the valley glaciers, for which a maximum length of 4-8 km and ice thickness of 200-300 m can be inferred from the location of terminal and lateral moraines, the ice thickness and geometry of the plateau glaciation is difficult to assess. The partial overdeepening (indicated by seasonal lakes) across the northern plateau and the probable ice flow into the northern valleys argues for an ice cap on the central peak Tullu Dimtu that was thick enough (several tens to a few hundred meters) to cause glacier flow through ice deformation and sliding (see also Osmaston, Mitchell, and Osmaston, 2005). Furthermore, it can be speculated that tabular ice fields like those found today on Kilimanjaro's summit plateau (e.g. Kaser et al., 2010) formed in the flat part of the southern and western Sanetti Plateau.

Another important aspect of the glacial history of the Bale Mountains is the evolution of the ice cover after the local LGM (see Chapter 2). The surface exposure dating of moraines in the northern valleys shows that the ice expansion before 19-17 ka (LPG Stage II) was only slightly smaller than that during the local LGM. The same applies to the plateau, where the dating of the outer Big Boulder Moraines suggests a minor shrinkage of the ice cap between the local LGM and LPG Stage II. However, it remains unclear when the plateau glacier started to disintegrate and separate from the valley glaciers. As already pointed out by Osmaston, Mitchell, and Osmaston (2005), the ice cap and valley glaciers might have coexisted separately for a while; similar to the present condition on Kilimanjaro (Cullen et al., 2013). Such a scenario is likely for the time between 19-14 ka, when deglaciation in the valleys and probably also on the plateau set in. The inner Big Boulder Moraine on the plateau indicates an isolated and relatively small ice cap on Tullu Dimtu after 19-17 ka, but due to ambiguous exposure ages, it was not possible to determine when the Sanetti Plateau became finally ice-free.

Independent of the uncertainties regarding the delineation of the former ice expansion, it is evident that the Bale Mountains as well as the adjacent Arsi Mountains were extensively glaciated during the Late Pleistocene (Chapter 2). The maximum ice cover of 265 km<sup>2</sup> delineated for the Bale Mountains is in the same order like that estimated for Mount Kenya (200-240 km<sup>2</sup>), Kilimanjaro (150-200 km<sup>2</sup>), and the Rwenzori Mountains (200-260 km<sup>2</sup>) (see Kaser and Osmaston, 2002; Hastenrath, 2009). Within the Ethiopian Highlands, the difference between the larger ice covers in the southern Ethiopian Highlands and the much smaller glaciated

area of 13 km<sup>2</sup> in the Simien Mountains (Hurni, 1982; Hurni, 1989) is remarkable. The Simien Mountains are slightly higher than the Bale and Arsi Mountains and comprise a large, but very rugged, afro-alpine area (Hurni, 1982; Hurni, 1989). However, the comparison and climatic interpretation of regional differences in the ice covered area of mountains is meaningless as long as other factors like the mountain height, size, and topography are neglected. Therefore, the hypsography of all mountains in Eastern Africa that were extensively glaciated was analysed in this thesis.

The results of the hypsometric analysis (Chapter 2) shows that the plateau-like Bale Mountains comprise a much larger afro-alpine area above 4000 masl than the higher equatorial mountains. Furthermore, the analysis revealed that the ratio of glaciated to total available surface area above the lower ice limits (~3500 masl) in Eastern Africa during the last glacial cycle was much higher in the equatorial mountains (Rwenzori = 62-80 %, Mount Kenya = 54-65 %, Kilimanjaro = 39-52 %) compared to the more northern Ethiopian Highlands (Arsi = 29 %, Bale = 23 %, Simien = 2 %). Although this simplified approach ignores variations in the height, topography, and ELAs between the different mountains, the distinct difference in the ratio of glaciated area could be interpreted in terms of a negative precipitation gradient from the equator towards the outer tropics. This observations is of particular interest as the Simien Mountains are located at the present northern margin of the tropical rain belt (Costa et al., 2014). A slight south-ward shift of the tropical rain belt during the last glacial period due to reduced summer insolation on the northern hemisphere might have contributed to a dry climate in this region, limiting the glacier expansion. However, such palaeoclimatic interpretations as well as the consideration of changes in large-scale circulation patterns are challenged by the limited understanding of present-day climatic differences between the various tropical mountains in Eastern Africa. Hydroclimatic maps exists for individual mountains like Kilimanjaro (Appelhans et al., 2016) and also for the entire region (e.g. Gebrechorkos, Hülsmann, and Bernhofer, 2019), but elevational and regional precipitation variations have so far not been investigated across tropical Eastern Africa.

The previous discussion regarding the extent of past glaciations in the Ethiopian Highlands and equatorial mountains in Eastern Africa leads to the following new research questions:

- Specific: What was the mass turnover from the ice cap into the northern valleys?
- Specific: How variable was the snow accumulation on the plateau?
- Specific: How did the ice cap on the Sanetti Plateau in the Bale Mountains evolve after the local LGM? Did the ice cap and valley glaciers coexisted separately during the late-glacial period (19-14 ka)?
- General: Does a modern precipitation gradient exist between the southern and northern Ethiopian Highlands as well as between the mountains in the inner and outer tropics in Eastern Africa? If yes, how pronounced is it? Could such a gradient theoretically explain the observed differences in the reconstructed ice extents? Or do the observations indeed argue for changes in the large scale atmospheric circulation (e.g. shift of tropical rain belt) in Eastern Africa during the last glacial period?

**When were the Bale Mountains glaciated? When did the glaciers reach their maximum expansion? When did deglaciation set in?**

Although a reliable glacial chronology is the basis for studying past glacier fluctuations, moraines and other glacial landforms have so far not been dated in the entire Ethiopian Highlands. The timing of the local LGM is therefore unknown and the onset of deglaciation poorly constrained.  $^{14}\text{C}$  dating of organic material from the base of afro-alpine sediment cores suggests a minimum deglaciation age of 4.1 ka BP for the Simien Mountains (Hurni, 1982), of 11.5 ka BP for the Arsi Mountains (Hamilton, 1982), and of 16.7 ka cal BP for the Togona Valley in the Bale Mountains (Tiercelin et al., 2008). Due to the lack of previous studies, potential challenges related to the cosmogenic nuclide dating of glacial landforms in the Ethiopian Highlands have so far not been addressed. As part of the dissertation, a first glacial chronology has been established for the Bale Mountains based on  $^{36}\text{Cl}$  surface exposure dating of 68 erratic boulders from different valleys and the Sanetti Plateau. Six moraine boulders from one valley in the Arsi Mountains have been additionally exposure dated for comparison and as preparation for future explorations. The obtained exposure ages from the Bale and Arsi Mountains provide first insights into past glacier fluctuations in the southern Ethiopian Highlands (presented in Chapters 2 and 4).

The lowest and geomorphologically oldest moraines and erratic boulders in the Bale Mountains were found in the northwestern valleys below 3600 masl. Most dated boulders from these locations yielded an  $^{36}\text{Cl}$  exposure age of >120 ka and suggest that the most extensive glaciation in the Bale Mountains occurred during the Mid Pleistocene (presumably during MIS 6). However, the interpretation of the oldest landforms is uncertain for various reasons: First, additional remains from the oldest glaciation have yet not been verified for other valleys in the Bale Mountains. Second, as the initial glaciation erodes the old geological surfaces, pre-exposure to cosmic radiation of the dated rocks prior to their deposition is more likely than during later glaciations and could lead to an overestimation of the exposure age (e.g. Heyman et al., 2011). Third, the age scatter of the lowermost moraines is relatively large (125-25 ka). Three younger exposure ages (52-25 ka) could also be interpreted in favour of a maximum expansion during MIS 4 or 3. Fourth, the choice of scaling and  $^{36}\text{Cl}$  production rate has the largest effect on the age calculation of the oldest samples (older than ~100 ka).

Well preserved moraines further up in the valleys consisting mainly of large erratic boulders determine the limits of the local maximum glacier expansion during the last glacial period. The obtained  $^{36}\text{Cl}$  exposure ages from four dated moraines in the valleys constrain the timing of the local LGM (LPG Stage I) in the Bale Mountains to the period 50-30 ka. The age range suggests that the glaciers persisted in a relatively stable position during MIS 3, allowing the deposition of boulders and formation of moraines over a longer time span. The next inner moraine sequence in several valleys was dated to 19-17 ka (LPG Stage II) and indicates a smaller, but similar ice extent as during LPG Stage I. This implies that the glaciers in the Bale Mountains reached their last local maximum prior to the global LGM ( $22 \pm 4$  ka after Shakun and Carlson, 2010). A maximum advance during MIS 3 and smaller expansion during MIS 2 has also been reported from other mountains (e.g. Mackintosh et al., 2006; Hughes et al., 2018) and can be explained by the climate during the global LGM, which was probably too dry for major glacier advances in some regions. The innermost moraines in the valleys were dated to 16-14 ka and represent the

last ice extent before deglaciation. The basal radiocarbon age of a new core from Lake Garba Guracha, situated at 3950 masl in the head of the formerly glaciated Togona Valleys, suggests that sedimentation started earliest at  $\sim 16$  ka and therefore confirms that the valleys in the Bale Mountains were probably ice free by 16-14 ka .

In contrast to the valleys, the glacial chronology on the Sanetti Plateau is less understood. Exposure ages of  $>130$  ka were obtained for a cluster of erratic boulders at the southern margin of the plateau. These boulder ages might support the hypothesis that the plateau glaciation reached its maximum extent during the Mid Pleistocene (e.g. MIS 6), but the dating uncertainties as discussed for the oldest glacial features in the lowest valleys apply here as well. Determining the local LGM on the plateau was not possible since the area of the assumed former ice cap margin was not reached during field work. The outer Big Boulder Moraine (BBM) encircling the highest peak Tullu Dimtu was dated to 21-16 ka and therefore relates to LPG Stage II in the valleys. However, it remains unclear whether the ice cap and valley glaciers were still connected at that time. Within the research unit, several of the seasonal lakes on the northern plateau were drilled for palaeoclimatic and -environmental investigation. The records have not yet been fully analysed and dated, but the basal age of these cores indicating the onset of sedimentation could help to elaborate when the northern part of the plateau became ice-free and disintegration of the ice cap set in. From a geomorphological and glaciological point of view, the inner BBM should be younger than the outer BBM. However, the obtained exposure ages for the inner BBM vary between 100-25 ka. A reasonable explanation for the inconsistent ages would be an inherited  $^{36}\text{Cl}$  signal in the boulders resulting from exposure prior to the last glaciation. The very short ( $<500$  m) transport of the boulders downslope of Tullu Dimtu probably prevented sufficient erosion of their surface and the complete removal of inherited  $^{36}\text{Cl}$ . Hence, it remains unclear how long an isolated ice cap persisted on Tullu Dimtu.

The preliminary and incomplete glacial chronology established for the adjacent Arsi Mountains is in line with the findings from the Bale Mountains. The lowest moraine in the studied southwestern valley of the Arsi Mountains yielded an age of 160-110 ka and indicates a potential maximum glacier advance during MIS 6. Another moraine, located further up the valley, was dated to  $\sim 18$  ka and therefore likely correlates with LPG II in the Bale Mountains. However, the number of dated moraines and boulders is too small to verify conclusively whether glaciers at different locations in the southern Ethiopian Highlands responded synchronously to past climatic changes. Since the Arsi Mountains lack a complex plateau and comprise well preserved moraine sequences in almost every valley descending from the central ridge, it is an ideal future study site for investigating the regional climate and glacier variability in cross-comparison with the Bale Mountains.

The interpretation of the inferred glacier fluctuations in the southern Ethiopian Highlands is complicated by the lack of nearby climate records, especially from higher elevations, that date back to MIS 3 or 4. Reconstructed sea surface temperatures of Lake Tanganyika in the East African Rift testify to a cooling trend in the region after the MIS 4/3 transition until  $\sim 20$  ka (Tierney et al., 2008). If the cooling trend is representative for the high mountains, the temperature depression both during MIS 3 and 2 would have been in favour of glacier expansion. However, such a cooling trend alone could not explain an early local LGM (50-30 ka) in the

Bale Mountains during MIS 3. Hydroclimatic proxy data from Lake Tanganyika and Chew Bahir (southwest Ethiopia, Foerster et al., 2018) suggest that the period 45-35 ka during MIS 3 was generally wetter than MIS 2. This means that a larger moisture input during MIS 3 might have been one of the main drivers causing an early LGM in the Bale Mountains. The glacier expansion or stagnation before 19-17 ka, defined by LPG Stage II, coincided probably with the coldest and driest phase of the last ~60 ka (e.g. Gasse, 2000; Tierney et al., 2008). However, the climate record from Chew Bahir indicates a wetter phase starting from ~20 ka (Foerster et al., 2018), which might explain a final advance before 19-17 ka. The step-wise retreat of the valley glaciers in the Bale Mountains between 19-14 ka is in line with a general warming trend (in Eastern Africa) during the Late Glacial (e.g. Tierney et al., 2008; Loomis et al., 2017).

In combination with previously published data (Shanahan and Zreda, 2000; Kelly et al., 2014) and new  $^{10}\text{Be}$  surface exposure ages of moraine boulders from the Rwenzori Mountains (Jackson et al., 2019), the presented findings from the southern Ethiopian Highlands allow a first regional comparison of glacier fluctuations in tropical Eastern Africa (see Chapter 2). The local LGM was dated to ~20 ka on Kilimanjaro, to ~28 ka on Mount Kenya, and to ~29 ka in the Rwenzori Mountains (Shanahan and Zreda, 2000; Jackson et al., 2019). Based on  $^{10}\text{Be}$  ages from the Rwenzori Mountains and recalculated  $^{10}\text{Be}$  ages from South America, Jackson et al. (2019) conclude that glaciers in the tropics reached their local LGM between 29-20 ka. Furthermore, they hypothesise that high-latitude warming led to a uniform glacial recession across the tropics, which was underway by ~20 ka. However, the results from the Bale Mountains (local LGM during MIS 3 and onset of deglaciation after 19-17 ka) highlight two things: first, in some tropical mountains the local LGM occurred prior to MIS 2 and second, glacial recession was not underway everywhere by ~20 ka. These findings from the thesis contradict a postulated uniform pantropical glacial response to global climate changes and show that changes in temperature cannot explain past glacial fluctuations in tropical Eastern Africa alone. Spatial and temporal hydroclimatic variations as well as topographic differences should therefore be given greater consideration to better understand palaeo glacier dynamics across Eastern Africa.

The following new research questions arose out of the discussion on glacier fluctuations in the southern Ethiopian Highlands and equatorial East African mountains:

- Specific: When did the oldest and maximum glaciation occur in the Bale and Arsi Mountains?
- Specific: Which climatic conditions caused the “early” maximum glacier expansion in the Bale Mountains during MIS 3?
- Specific: How long did the ice cap persist on Tullu Dimtu?
- General: Did the palaeo glaciers in the Ethiopian Highlands respond synchronously to past climate changes?
- General: How sensitive did tropical glacier in Eastern Africa respond to changes of different climate variables? Which role did spatial and temporal hydroclimatic variations play regarding past glacier fluctuations across tropical Eastern Africa?

**When, how, and under which climatic and environmental conditions did the relict large sorted stone stripes and polygons on the Sanetti Plateau form?**

Large sorted stone polygons and stripes (several meters wide and hundred meters long) between 3850 and 4150 masl on the southern and western Sanetti Plateau in the Bale Mountains were first mentioned by Miehe and Miehe (1994), but never systemically mapped and investigated. In a review paper about glacial and periglacial phenomena in Ethiopia, Grab (2002) interpreted the large dimension of these patterns as potential evidence for local permafrost in the Bale Mountains during the LGM, but did not provide any discussion on their genesis. So far, patterns of similar dimension have not been verified for any other tropical mountain. The only known analogue of similar dimension are the blockstreams and stone stripes in the Falkland Islands (see André et al., 2008). The occurrence of the large sorted polygons and stripes on the Sanetti Plateau is enigmatic for a tropical afro-alpine environment as such geomorphological forms have so far only been associated with permafrost environments and seasonal climate variations in the mid and high latitude (e.g. Goldthwait, 1976; Hallet, 2013). To better understand the present-day periglacial processes and the genesis of the relict sorted stone stripes in the Bale Mountains, ground temperatures have been measured and periglacial landforms been mapped and investigated as part of this thesis (see Chapter 3).

The three-year measurements in the Bale Mountains revealed a typical diurnal ground temperature cycle near the surface ranging from minimum  $-10^{\circ}\text{C}$  at night up to maximum  $40^{\circ}\text{C}$  during daytime. Moreover, the data show that superficial nocturnal frost occurs frequently on the Sanetti Plateau (at 35-90 days per year), but penetrates only the upper few centimetres. Below this depth, ground temperatures are continuously above the freezing point. The diurnal temperature amplitude decreases rapidly with increasing depth and below 50 cm depth temperatures are rather constant. However, the long-term measurements show that even in tropical mountains with a pronounced diurnal climate seasonal ground temperature variations of  $2.5^{\circ}\text{C}$  at 50 cm depth and up to  $10^{\circ}\text{C}$  near the surface can occur. Even though superficial frost was verified for the Sanetti Plateau, the mean annual ground temperature across depths in the order of  $11^{\circ}\text{C}$  at  $\sim 3900$  masl is way off from seasonal or permanent frost conditions.

Characteristic modern frost-related phenomena in the Bale Mountains related to diurnal or seasonal temperature variations are inter alia small-scale patterned grounds, seasonally frozen waterfalls, and nocturnal needle ice. In contrast to the modern small-scale periglacial landforms, the relict features, including extensive blockfields along the southern escarpment and the prominent sorted stone stripes on the plateau, consist of larger clasts (up to 2 m in diameter). The detailed mapping of periglacial landforms led to the discovery of undocumented stone stripes on the western plateau above 4000 masl, which are up to 15 m wide and 1000 m long. Beside the blockstreams and stone stripes in the Falkland Islands (see André et al., 2008), these are the largest described structures of their kind worldwide. The structures on the western and southern plateau have in common that they are located at slightly inclined areas and consist of alternating stripes of coarse angular blocks and regolith. The width of the coarse (trough-shaped) and fine-grained (rampart-like) stripes varies between 5 and 15 m and their axis is oriented parallel to the greatest slope. Another important detail is that some of the stone stripes split up into two narrower branches in the upper part and merge to a single wider

branch in the lower part. All these observations are very similar to the characteristics of patterned grounds at gentle slopes predicted by numerical models after several hundred freeze-thaw cycles (Mulheran, 1994; Werner and Hallet, 1993; Kessler et al., 2001; Kessler and Werner, 2003). The similarities between observed and modelled stone stripes, their geomorphological characteristics as well as the concurrence of sorted polygons and stripes on the plateau suggest that these patterns are most likely the result of frost heave and sorting related to several decimetre deep seasonal frost (or sporadic permafrost) and cycling freezing and thawing.

The formation of sporadic permafrost or deep seasonal frost on the Sanetti Plateau would require a past ground temperature depression of at least 11 °C (relative to the present-day conditions). Such an extreme cooling is unprecedented in the tropics and would imply considerable environmental change. Very cold and dry conditions beyond the limits of the former ice cap on Tullu Dimtu (see Chapter 2) during the Pleistocene might have provided suitable conditions for the formation of large patterned grounds due to frost heave and sorting over hundreds of freeze-thaw cycles. Interestingly, the large blockstreams and stone stripes in the Falkland Islands are also located outside the local Pleistocene glacier limits (Clapperton, 1971; Clapperton and Sudgen, 1976) and are interpreted as composite landforms that formed over several cold stages (Wilson et al., 2008) (see Chapter 3 for a more detailed comparison). However, to corroborate the hypothesis that the stone stripes on the Sanetti Plateau formed under periglacial conditions in proximity of the former ice cap, it would be necessary to constrain the time when these forms became geomorphologically inactive. The attempt to date the stabilisation period of the stripes with  $^{36}\text{Cl}$  was not successful due to the probable exposure of the blocks to cosmic radiation prior to and during the formation period. The well preserved morphology and hardly weathered surface of the blocks generally support a formation of the stripes during MIS 2, the coldest and driest period of the last glacial period (e.g. Tierney, deMenocal, and Zander, 2017), but a sorting over several cold stages during the Pleistocene cannot be completely ruled out.

The thesis provides a first detailed analysis and interpretation of the relict large sorted stone stripes and polygons on the Sanetti Plateau, but several questions regarding their genesis remain inadequately answered and thus lay the foundation for future research:

- Specific: What are the climatic, geological, geomorphological, and sedimentological pre-conditions for the sorting of large clasts (e.g. >2 m in diameter) and the formation of patterned grounds of this dimension? What is the minimum freeze and thaw depth required to heave large angular blocks?
- Specific: When did the stone stripes form: during the coldest period of the last glacial cycle due to seasonal freezing and thawing or over several glacial interglacial cycles during the Pleistocene?
- General: Is there further geomorphological evidence from the Ethiopian Highlands or equatorial East African mountains for relict large periglacial landforms and a severe high-altitude cooling in the region during the Quaternary?
- General: What predestines the Sanetti Plateau and Falkland Islands for the formation of large sorted stone stripes?

**Which cooling can be inferred from the presence of glacial and periglacial landforms and what does it imply for the palaeoclimate and -ecology of tropical mountains?**

Glacial and periglacial landforms like the investigated moraines, erratic boulders, and patterned grounds in the Bale Mountains provide by their presence alone clear evidence for past climatic and environmental changes at high elevations. However, to determine the magnitude of cooling during the last glacial period and to elaborate regional and elevational variations, a quantitative assessment is necessary. As long as no older (>16 ka) high-altitude lake sediment cores have been recovered from the Ethiopian Highlands, glacial and periglacial landforms are one of the few proxies that can be used for last glacial temperature reconstructions. An established method, especially in formerly unglaciated mountain areas, uses the altitude difference between past and present lower limits of the periglacial belt along with an assumed lapse rate to infer past changes in temperature. Based on this approach, Hurni (1982) and Hurni (1989) estimated a LGM air temperature depression of  $7.0 \pm 1.5^\circ\text{C}$  for the Simien Mountains and Hendrickx et al. (2015) of  $\sim 6^\circ\text{C}$  for three isolated mountains in the northern Ethiopian Highlands. The challenge with this method is that the lower periglacial limits are often difficult to determine if the respective landforms are eroded or covered by vegetation or sediments. Moreover, the period to which the estimated cooling refers is often not well constrained. In the Bale Mountains, the comparison of relict and modern periglacial landforms is further complicated by their fundamentally different morphology (large vs. small-scale phenomena) originating probably from different periglacial processes (e.g. several decimetre deep vs. superficial frost). To reconstruct the last glacial temperature depression in the Bale Mountains, two approaches – one classical and one experimental – based on the former ice extent and occurrence of the relict stone stripes were explored in the thesis (see Chapters 2 and 3).

Similar to the depression of the lower limits of the periglacial belt, vertical changes of a glacier's ELA over time can be translated into relative temperature changes using a specific lapse rate (e.g. Benn et al., 2005; Mark et al., 2005). Due to the preservation of lateral and terminal moraines in the valleys and the relatively small vertical extent (300-800 m) of the palaeo valley glaciers, the ELA in the Bale Mountains during the local LGM (LPG Stage I, 50-30 ka) could be constrained to  $3940 \pm 40$  m. In the absence of modern glaciers, the present-day  $0^\circ\text{C}$  isotherm (located at  $\sim 4650$  masl) inferred from meteorological measurements on the plateau served as approximation for the modern ELA. Applying the modern lapse on the Sanetti Plateau of  $7.2 \pm 0.5^\circ\text{C km}^{-1}$  to the ELA lowering of  $710 \pm 40$  m yielded a local LGM temperature depression of  $5.1 \pm 0.7^\circ\text{C}$ . Considering that the lapse rate during the last glacial period was probably steeper due to a drier atmosphere (e.g. Loomis et al., 2017), the reconstructed temperature decrease indicates rather a minimum than maximum threshold for the local LGM cooling in the Bale Mountains.

If we assume (based on the evidence and arguments provided in Chapter 3) that the large sorted stripes on the southern and western Sanetti Plateau are the product of frost heave and sorting due to cyclic freezing and thawing of the upper decimetres of the ground, we can use them as reference for palaeoclimatic reconstructions. Patterned grounds consisting of large clasts (>2 m in diameter) occur commonly in permafrost areas with mean annual ground and air temperatures below  $0^\circ\text{C}$  (e.g. Goldthwait, 1976). This would imply a minimum depression

of the ground temperature on the Sanetti Plateau in the order of  $>11\text{ }^{\circ}\text{C}$  as precondition for the formation of the stone stripes and polygons. A multiple linear regression model built upon the relationship between measured ground temperatures and a set of meteorological variables was applied to simulate under which climatic conditions (e.g. decrease in temperature) the mean annual ground temperature would approximate frost conditions. The results of this statistical model experiment suggest that a minimum decrease in air temperature of  $7.6 \pm 1.3\text{ }^{\circ}\text{C}$  would be required for seasonal or permanent ground frost on the plateau. Such a strong cooling would be another argument for the formation of the stone stripes and polygons during MIS 2.

Both temperature reconstructions are in the order of the estimates from the northern Ethiopian Highlands (Hurni, 1982; Hurni, 1989; Hendrickx et al., 2015) and indicate a strong regional high-altitude cooling during the last glacial cycle. The advantage of the ELA-approach in the Bale Mountains is that the inferred cooling of  $5.1 \pm 0.7\text{ }^{\circ}\text{C}$  can be directly linked to a glacial and climatic period (local LGM, 50-30 ka). Assuming that the stone stripes and polygons formed during MIS 2, the cooling of  $7.6 \pm 1.3\text{ }^{\circ}\text{C}$  would reflect a further temperature decrease after the local LGM, which is in line with regional climate proxy data from Eastern Africa (e.g. Tierney et al., 2008). The comparison between the reconstructed temperature decrease in the Ethiopian Highlands and the lower-situated Congo Basin and Lake Tanganyika in the order of 4 to  $4.5\text{ }^{\circ}\text{C}$  (Weijers et al., 2007; Tierney et al., 2008) support previous findings from the tropics indicating an amplified cooling with increasing elevation during the last glacial period. A drier atmosphere and steeper lapse rate are discussed as potential causes for the anomalous high-altitude cooling (e.g. Kageyama, Harrison, and Abe-Ouchi, 2005; Loomis et al., 2017).

A questions, which is beyond the scope of this thesis, but relevant for the understanding of the Quaternary evolution of afro-alpine ecosystems is how the distinct climatic and environmental changes during the last glacial cycle affected the habitat, distribution, and migration of (endemic) afro-alpine species in the Ethiopian Highlands (Miehe and Miehe, 1994). The glacial and periglacial investigations show that the upper valleys, the highest peaks, and large areas on the Sanetti Plateau in the Bale Mountains were covered by ice or affected by ground frost during the last glacial period. Furthermore, the ELA-lowering and temperature reconstructions suggest a depression of altitudinal vegetation belts in the order of a few hundred metres. How the endemic afro-alpine plant and mammal species like the giant lobelia (Chala et al., 2016), Ethiopian wolf (e.g. Gottelli et al., 1994), giant mole-rat (e.g Vlasatá et al., 2017), and mountain nyala, that currently populate the plateau and upper valleys, adapted to the environmental changes, is therefore one of the questions arising out of this research:

- Specific: Which areas of the Bale Mountains served as glacial refuge for the afro-alpine plant and mammal species that currently populate the plateau and upper valleys?
- Specific: Did the ice expansion, ground frost, and cooling in the Bale Mountains led to the local extinction of afro-alpine species during the last glacial period?
- General: What are additional causes beside the postulated steepened lapse rate for the amplified high-altitude cooling in tropical Eastern Africa during the last glacial period? Was the glaciated area on the highest mountains large enough to reinforce the local cooling due to a positive ice-albedo feedback?

### **How did the palaeoclimate and -environment look like at the time when humans started to colonise the Bale Mountains?**

Relatively little has been known until recently about the human colonisation of the world's highest mountains and the adaptation of humans to high-altitude climates and environments associated with low-oxygen conditions, low and fluctuating temperatures as well as higher levels of ultraviolet radiation (e.g. Beall, 2001; Aldenderfer, 2006; Alkorta-Aranburu et al., 2012). It has long been assumed that the advance of hunter-gatherers into the high mountains occurred rather late in human history. However, archaeological excavations from the Peruvian Andes revealed that hunter-gatherers already started to colonise high-altitude environments (~4500 masl) at the Pleistocene-Holocene transition (Rademaker et al., 2014). Located in proximity to the oldest known hominid sites in the Main Ethiopian Rift (e.g. Asfaw et al., 2002), the Ethiopian Highlands and equatorial East African mountains seem predestined for an even earlier human occupation. Within the framework of the interdisciplinary research unit, in which this thesis is embedded, it has therefore been hypothesised that the Bale Mountains in the Ethiopian Highlands were colonised already during the Late Pleistocene. Furthermore, it was postulated that the mountains served as glacial refuge for humans during periods (e.g. MIS 2) when the surrounding lowlands were very dry and presumably uninhabitable (Basell, 2008; Brandt et al., 2012; Stewart and Stringer, 2012). To unravel the human and environmental history of the Bale Mountains, findings from different subprojects of the research unit comprising the fields of archaeology, soil biogeochemistry, zoogeography, and Quaternary geology, were combined (see Chapter 4). The contribution of the glacial geomorphological and chronological investigations from this thesis was to embed the archaeological research in a climatic and environmental context.

Archaeological excavations at the Fincha Habera rock shelter (~3500 masl) in the Web Valley in the northwestern part of the Bale Mountains led to the discovery of the world's oldest yet known prehistoric high-altitude residential site. Typical Middle Stone Age (MSA) lithic artefacts, faunal remains like bones from the endemic giant mole-rat as well as non-local fragments of quartz and ostrich eggshell were found in the deposits of the rock shelter. Based on the radiocarbon dating of charcoal, giant mole-rat bones, coprolites, and black carbon in the MSA layer, the settlement period was constrained to 47-31 ka cal BP. The nature of the lithic artefacts shows similarities with MSA findings from the surrounding lowlands that originate from the late MIS 3 (Pleurdeau, 2006; Gossa, Sahle, and Negash, 2012; Ménard et al., 2014; Pleurdeau et al., 2014; Leplongeon, Pleurdeau, and Hovers, 2017) and therefore corroborate the radiocarbon dates. One of the key findings from the analysis of the faunal remains was that the abundant giant mole-rat, which weighs ~1 kg and is endemic to the Bale Mountains, was a key food source of the prehistoric inhabitants. Moreover, the analysis of the lithic obsidian artefacts from the rock shelter revealed an identical chemical composition with the comparison samples from the local obsidian outcrops at ~4200 masl. This suggests that the MSA foragers accessed repeatedly the obsidian outcrops, which are located ~700 m higher and ~10 km away from the residential site, for the procurement of this almost exclusively used raw material.

The glacial geomorphological and chronological findings of the thesis show that the MSA

settlement phase (47-31 ka cal BP) in the Bale Mountains coincided with the local LGM (50-30 ka), a period of extensive glaciation and colder conditions. At that time, an ice cap covered large parts of the Sanetti Plateau and 4-5 km long glaciers filled the northwestern valleys, just 7-9 km upstream of the MSA site, which was apparently never glaciated. The ridge with the obsidian outcrops between two glaciated valleys was probably ice-free. As inferred from the reconstructed ELA-lowering, the mean annual air temperature was reduced by 4-6 °C (compared to today). All these findings together indicate that the prehistoric foragers were familiar with the cold and glaciated environment of the Bale Mountains. Beside the obsidian as raw material and the giant mole-rat as food source, the perennial meltwater from the glaciers was probably one of the important afro-alpine resources for the MSA foragers. The initial hypothesis of the research unit, claiming a controversial early human occupation of the Ethiopian Highlands during the last glacial period, could be successfully corroborated in the framework of the interdisciplinary approach. Along with new evidence for short-term stays of humans at elevations up to ~4600 masl on the Tibetan Plateau (Zhang et al., 2018) and the findings from the Peruvian Andes (Rademaker et al., 2014), the discovery of the oldest residential site in the Bale Mountains demonstrates that the resources in the world's highest mountains have already been accessed by humans during the Late Pleistocene.

What drove the people into the mountains, is one of the challenging questions arising from the interdisciplinary research. The ostrich eggshell fragment as well as the artefacts made of obsidian and quartz of unknown provenance suggest a past connection between the Fincha Habera MSA site and the surrounding lowlands. A coeval presence of humans in the high- and lowlands is also supported by the few archaeological assemblages from the Main Ethiopian Rift dated to MIS 3 (Ménard et al., 2014; Pleurdeau et al., 2014; Brandt et al., 2017). This does not favour the interpretation of the Bale Mountains as climate-driven human refuge during the last glacial period and thus addresses both old and new research questions:

- Specific: Why was the Fincha Habera MSA site in the Bale Mountains abandoned after ~31 ka? Did the climate in the mountains get too cold and dry during MIS 2 (as possibly indicated by the large-scale patterned grounds on the Sanetti Plateau)?
- General: Where did humans reside during the dry phases of the last glacial cycle in Eastern Africa?
- General: What were potential push and pull factors – beside the presence of obsidian, abundant prey, and meltwater – leading to the early occupation of the highlands?
- General: To what extent did the Stone Age hunters shape the afro-alpine environment?

## References

- Aldenderfer, M. (2006). "Modelling plateau peoples: the early human use of the world's high plateaux". In: *World Archeol.* 38.3, pp. 357–370. DOI: 10.1080/00438240600813285.
- Alkorta-Aranburu, G. et al. (2012). "The Genetic Architecture of Adaptations to High Altitude in Ethiopia". In: *PLoS Genet.* 8.12, pp. 1–13. DOI: 10.1371/journal.pgen.1003110.
- André, M.-F. et al. (2008). "Stone Runs in the Falkland Islands: Periglacial or Tropical?" In: *Geomorphology* 95.3-4, pp. 524–543. DOI: 10.1016/j.geomorph.2007.07.006.
- Appelhans, T. et al. (2016). "Eco-Meteorological Characteristics of the Southern Slopes of Kilimanjaro". In: *Int. J. Climatol.* 36.9, pp. 3245–3258. DOI: 10.1002/joc.4552.
- Asfaw, B. et al. (2002). "Remains of Homo Erectus from Bouri, Middle Awash, Ethiopia". In: *Nature* 416.6878, pp. 317–320. DOI: 10.1038/416317a.
- Basell, L. (2008). "Middle Stone Age (MSA) Site Distributions in Eastern Africa and Their Relationship to Quaternary Environmental Change, Refugia and the Evolution of Homo Sapiens". In: *Quat. Sci. Rev.* 27.27-28, pp. 2484–2498. DOI: 10.1016/j.quascirev.2008.09.010.
- Beall, C. M. (2001). "Adaptations to Altitude: A Current Assessment". In: *Annu. Rev. Anthropol.* 30.1, pp. 423–456. DOI: 10.1146/annurev.anthro.30.1.423.
- Benn, D. I. et al. (2005). "Reconstruction of Equilibrium-Line Altitudes for Tropical and Sub-Tropical Glaciers". In: *Quat. Int.* 138-139, pp. 8–21. DOI: 10.1016/j.quaint.2005.02.003.
- Brandt, S. A. et al. (2012). "Early MIS 3 Occupation of Mochena Borago Rockshelter, Southwest Ethiopian Highlands: Implications for Late Pleistocene Archaeology, Paleoenvironments and Modern Human Dispersals". In: *Quat. Int.* 274, pp. 38–54. DOI: 10.1016/j.quaint.2012.03.047.
- Brandt, S. A. et al. (2017). "A New MIS 3 Radiocarbon Chronology for Mochena Borago Rockshelter, SW Ethiopia: Implications for the Interpretation of Late Pleistocene Chronostratigraphy and Human Behavior". In: *J. Archaeol. Sci.* 11, pp. 352–369. DOI: 10.1016/j.jasrep.2016.09.013.
- Chala, D. et al. (2016). "Good-Bye to Tropical Alpine Plant Giants under Warmer Climates? Loss of Range and Genetic Diversity in *Lobelia Rhynchopetalum*". In: *Ecol. Evol.* 6.24, pp. 8931–8941. DOI: 10.1002/ece3.2603.
- Chandler, B. M. P. et al. (2018). "Glacial Geomorphological Mapping: A Review of Approaches and Frameworks for Best Practice". In: *Earth-Sci. Rev.* 185, pp. 806–846. DOI: 10.1016/j.earscirev.2018.07.015.
- Clapperton, C. M. (1971). "Evidence of Cirque Glaciation in the Falkland Islands". In: *J. Glaciol.* 10.58, pp. 121–125. DOI: 10.3189/S0022143000013058.
- Clapperton, C. M. and D. E. Sudgen (1976). "The Maximum Extent of Glaciers in Part of West Falkland". In: *J. Glaciol.* 17.75, pp. 73–77. DOI: 10.3189/S0022143000030732.
- Costa, K. et al. (2014). "Isotopic Reconstruction of the African Humid Period and Congo Air Boundary Migration at Lake Tana, Ethiopia". In: *Quat. Sci. Rev.* 83, pp. 58–67. DOI: 10.1016/j.quascirev.2013.10.031.
- Cullen, N. J. et al. (2013). "A Century of Ice Retreat on Kilimanjaro: The Mapping Reloaded". In: *The Cryosphere* 7.2, pp. 419–431. DOI: 10.5194/tc-7-419-2013.

- Foerster, V. et al. (2018). "Towards an Understanding of Climate Proxy Formation in the Chew Bahir Basin, Southern Ethiopian Rift". In: *Palaeogeogr. Palaeoclimatol. Palaeoecol.* 501, pp. 111–123. DOI: 10.1016/j.palaeo.2018.04.009.
- Gasse, F. (2000). "Hydrological Changes in the African Tropics since the Last Glacial Maximum". In: *Quat. Sci. Rev.* 19.1-5, pp. 189–211. DOI: 10.1016/S0277-3791(99)00061-X.
- Gebrechorkos, S. H., S. Hülsmann, and C. Bernhofer (2019). "Long-Term Trends in Rainfall and Temperature Using High-Resolution Climate Datasets in East Africa". In: *Sci. Rep.* 9.1, pp. 1–9. DOI: 10.1038/s41598-019-47933-8.
- Goldthwait, R. P. (1976). "Frost Sorted Patterned Ground: A Review". In: *Quat. Res.* 6.1, pp. 27–35.
- Gossa, T., Y. Sahle, and A. Negash (2012). "A reassessment of the Middle and Later Stone Age lithic assemblages from Aladi Springs, Southern Afar Rift, Ethiopia". In: *Azania* 47.2, pp. 210–222. DOI: 10.1080/0067270X.2012.676314.
- Gottelli, D. et al. (1994). "Molecular Genetics of the Most Endangered Canid: The Ethiopian Wolf *Canis Simensis*". In: *Mol. Ecol.* 3.4, pp. 301–312. DOI: 10.1111/j.1365-294X.1994.tb00070.x.
- Grab, S. (2002). "Glacial and Periglacial Phenomena in Ethiopia: A Review". In: *Permafrost Periglacial Process.* 13.1, pp. 71–76. DOI: 10.1002/ppp.405.
- Hallet, B. (2013). "Stone Circles: Form and Soil Kinematics". In: *Proc. R. Soc. A* 371.2004, p. 20120357. DOI: 10.1098/rsta.2012.0357.
- Hamilton, A.C. (1982). *Environmental History of East Africa: a Study of the Quaternary*. London. DOI: 10.2307/2259986.
- Hastenrath, S. (2009). "Past Glaciation in the Tropics". In: *Quat. Sci. Rev.* 28.9-10, pp. 790–798. DOI: 10.1016/j.quascirev.2008.12.004.
- Hendrickx, H. et al. (2015). "Glacial and Periglacial Geomorphology and Its Paleoclimatological Significance in Three North Ethiopian Mountains, Including a Detailed Geomorphological Map". In: *Geomorphology* 246, pp. 156–167. DOI: 10.1016/j.geomorph.2015.05.005.
- Heyman, J. et al. (2011). "Too Young or Too Old: Evaluating Cosmogenic Exposure Dating Based on an Analysis of Compiled Boulder Exposure Ages". In: *Earth Planet. Sci. Lett.* 302.1-2, pp. 71–80. DOI: 10.1016/j.epsl.2010.11.040.
- Hughes, P. D. et al. (2018). "Timing of Pleistocene Glaciations in the High Atlas, Morocco: New <sup>10</sup>Be and <sup>36</sup>Cl Exposure Ages". In: *Quat. Sci. Rev.* 180, pp. 193–213. DOI: 10.1016/j.quascirev.2017.11.015.
- Hurni, H. (1982). "Simen Mountains - Ethiopia, Vol II (in German): Climate and Dynamics of Altitudinal Belts from the Last Cold Period to the Present Day (Part II in Co-Authorship with Peter Staehli)". In: *Geographica Bernensia* G 13, pp. 4–196.
- Hurni, H. (1989). "Late Quaternary of Simien and Other Mountains in Ethiopia". In: *Quaternary and Environmental Research on East African Mountains*. Rotterdam / Brookfield: Balkema, pp. 105–120.
- Jackson, M. S. et al. (2019). "High-Latitude Warming Initiated the Onset of the Last Deglaciation in the Tropics". In: *Sci. Adv.* 5.12, pp. 1–8. DOI: 10.1126/sciadv.aaw2610.

- Kageyama, M., S. P. Harrison, and A. Abe-Ouchi (2005). "The Depression of Tropical Snowlines at the Last Glacial Maximum: What Can We Learn from Climate Model Experiments?" In: *Quat. Int.* 138-139, pp. 202–219. DOI: 10.1016/j.quaint.2005.02.013.
- Kaser, G. and H. Osmaston (2002). *Tropical Glaciers*. International Hydrology Series. Cambridge University Press.
- Kaser, G. et al. (2010). "Is the Decline of Ice on Kilimanjaro Unprecedented in the Holocene?" In: *The Holocene* 20.7, pp. 1079–1091. DOI: 10.1177/0959683610369498.
- Kelly, M. A. et al. (2014). "Expanded Glaciers during a Dry and Cold Last Glacial Maximum in Equatorial East Africa". In: *Geology* 42.6, pp. 519–522. DOI: 10.1130/G35421.1.
- Kessler, M. A. and B. T. Werner (2003). "Self-Organization of Sorted Patterned Ground". In: *Science* 299.5605, pp. 380–383. DOI: 10.1126/science.1077309.
- Kessler, M. A. et al. (2001). "A Model for Sorted Circles as Self-Organized Patterns". In: *J. Geophys. Res.* 106.B7, pp. 13287–13306. DOI: 10.1029/2001JB000279.
- Lepplongeon, A., D. Pleurdeau, and E. Hovers (2017). "Late Pleistocene and Holocene Lithic Variability at Goda Buticha (Southeastern Ethiopia): Implications for the Understanding of the Middle and Late Stone Age of the Horn of Africa". In: *J. Afr. Archaeol.* 15.2, pp. 202–233. DOI: 10.1163/21915784-12340010.
- Loomis, S. E. et al. (2017). "The Tropical Lapse Rate Steepened during the Last Glacial Maximum". In: *Science Advances* 3.1, pp. 1–7. DOI: 10.1126/sciadv.1600815.
- Mackintosh, A. N. et al. (2006). "Exposure Dating and Glacial Reconstruction at Mt. Field, Tasmania, Australia, Identifies MIS 3 and MIS 2 Glacial Advances and Climatic Variability". In: *J. Quat. Sci.* 21.4. ISSN: 0267-8179, 1099-1417. DOI: 10.1002/jqs.989.
- Mark, B. G. and H. A. Osmaston (2008). "Quaternary Glaciation in Africa: Key Chronologies and Climatic Implications". In: *J. Quat. Sci.* 23.6-7, pp. 589–608. DOI: 10.1002/jqs.1222.
- Mark, B. G. et al. (2005). "Tropical Snowline Changes at the Last Glacial Maximum: A Global Assessment". In: *Quat. Int.* 138-139, pp. 168–201. DOI: 10.1016/j.quaint.2005.02.012.
- Ménard, C. et al. (2014). "Late Stone Age Variability in the Main Ethiopian Rift: New Data from the Bulbula River, Ziway–Shala Basin". In: *Quat. Int.* 343, pp. 53–68. DOI: 10.1016/j.quaint.2014.07.019.
- Messerli, B. et al. (1977). "Bale Mountains, the Largest Pleistocene Mountain Glacier System of Ethiopia". In: *INQUA abstracts*.
- Miehe, S. and G. Miehe (1994). *Ericaceous Forests and Heathlands in the Bale Mountains of South Ethiopia - Ecology and Man's Impact*. Hamburg: Stiftung Walderhaltung in Afrika.
- Mulheran, P. A. (1994). "Theory of Self-Organisation in Sorted Stone Stripes". In: *J Phys* 4.1, pp. 1–5.
- Osmaston, H. A. and S. P. Harrison (2005). "The Late Quaternary Glaciation of Africa: A Regional Synthesis". In: *Quat. Int.* 138-139, pp. 32–54. DOI: 10.1016/j.quaint.2005.02.005.
- Osmaston, H. A., W. A. Mitchell, and J. A. N. Osmaston (2005). "Quaternary Glaciation of the Bale Mountains, Ethiopia". In: *J. Quat. Sci.* 20.6, pp. 593–606. DOI: 10.1002/jqs.931.
- Pleurdeau, D. (2006). "Human Technical Behavior in the African Middle Stone Age: The Lithic Assemblage of Porc-Epic Cave (Dire Dawa, Ethiopia)". In: *Afr. Archaeol. Rev.* 22.4, pp. 177–197. DOI: 10.1007/s10437-006-9000-7.

- Pleurdeau, D. et al. (2014). "Cultural Change or Continuity in the Late MSA/Early LSA of Southeastern Ethiopia? The Site of Goda Buticha, Dire Dawa Area". In: *Quat. Int.* 343, pp. 117–135. DOI: 10.1016/j.quaint.2014.02.001.
- Potter, E. C. (1976). "Pleistocene Glaciation in Ethiopia: New Evidence". In: *J. Glaciol.* 17.75, pp. 147–150.
- Rademaker, K. et al. (2014). "Paleoindian Settlement of the High-Altitude Peruvian Andes". In: *Science* 346.6208, pp. 466–469. DOI: doi:10.1126/science.1258260.
- Shakun, J. D. and A. E. Carlson (2010). "A Global Perspective on Last Glacial Maximum to Holocene Climate Change". In: *Quat. Sci. Rev.* 29, pp. 1801–1816. DOI: 10.1016/j.quascirev.2010.03.016.
- Shanahan, D. F. and M. Zreda (2000). "Chronology of Quaternary Glaciations in East Africa". In: *Earth Planet. Sci. Lett.* 177, pp. 23–42.
- Stewart, J. R. and C. B. Stringer (2012). "Human Evolution Out of Africa: The Role of Refugia and Climate Change". In: *Science* 335.6074, pp. 1317–1321. DOI: 10.1126/science.1215627.
- Thompson, L. G. et al. (2002). "Kilimanjaro Ice Core Records: Evidence of Holocene Climate Change in Tropical Africa". In: *Science* 298.5593, pp. 589–593. DOI: 10.1126/science.1073198.
- Tiercelin, J.-J. et al. (2008). "High-Resolution Sedimentary Record of the Last Deglaciation from a High-Altitude Lake in Ethiopia". In: *Quaternary Science Reviews* 27.5, pp. 449–467.
- Tierney, J. E., P. B. deMenocal, and P. D. Zander (2017). "A Climatic Context for the Out-of-Africa Migration". In: *Geology* 45.11, pp. 1023–1026. DOI: 10.1130/G39457.1.
- Tierney, J. E. et al. (2008). "Northern Hemisphere Controls on Tropical Southeast African Climate During the Past 60,000 Years". In: *Science* 322.6976, pp. 252–255. DOI: 10.1038/nature02251.
- Umer, M., S. Kebede, and H. Ostmaston (2004). "Quaternary Glacial Activity on the Ethiopian Mountains". In: *Quaternary Glaciations*, pp. 171–174.
- Vlasatá, T. et al. (2017). "Daily Activity Patterns in the Giant Root Rat (*Tachyoryctes Macrocephalus*), a Fossorial Rodent from the Afro-Alpine Zone of the Bale Mountains, Ethiopia". In: *J. Zool.* 302.3, pp. 157–163. DOI: 10.1111/jzo.12441.
- Weijers, J. W. H. et al. (2007). "Coupled Thermal and Hydrological Evolution of Tropical Africa over the Last Deglaciation". In: *Science* 315.5819, pp. 1701–1704. DOI: 10.1126/science.1138131.
- Werner, B.T. and B. Hallet (1993). "Numerical Simulation of Self-Organized Stone Stripes". In: *Nature* 361.
- Wilson, P. et al. (2008). "Stone Run (Block Stream) Formation in the Falkland Islands over Several Cold Stages, Deduced from Cosmogenic Isotope ( $^{10}\text{Be}$  and  $^{26}\text{Al}$ ) Surface Exposure Dating". In: *J. Quat. Sci.* 23.5, pp. 461–473. DOI: 10.1002/jqs.1156.
- Zhang, X. L. et al. (2018). "The Earliest Human Occupation of the High-Altitude Tibetan Plateau 40 Thousand to 30 Thousand Years Ago". In: *Science* 362.6418, pp. 1049–1051. DOI: doi:10.1126/science.aat8824.

## Chapter 6

# Conclusions

Glacial and periglacial landforms in the valleys and on the central Sanetti Plateau of the Bale Mountains in the southern Ethiopian Highlands constitute a valuable archive for reconstructing past glacier fluctuations as well as climate and environmental changes at high elevations in the tropics. Based on a first systematic investigation of these landforms, this thesis provides pioneering insights into the glacial and periglacial history of the Bale Mountains. The gained insights into past glacial and periglacial processes in turn contribute to a better understanding of the magnitude and manifestation of cooling in the Ethiopian Highlands during the last glacial period and its impact on the afro-alpine ecosystem and human advance into higher elevations. From the main findings discussed in the synthesis, the following conclusions can be drawn:

1. The geomorphological mapping and interpretation of well preserved glacial and periglacial landforms enables the reconstruction of past ice extents and periglacial areas in the Bale Mountains. Furthermore, by developing a first glacial chronology for the region, it has been shown that the stabilisation age of moraines in the volcanic Ethiopian Highlands can be successfully determined using  $^{36}\text{Cl}$  surface exposure dating. The combined glacial geomorphological and chronological analysis demonstrates that an extensive plateau glaciation extending down into the northern valleys formed in the Bale Mountains during the Pleistocene. The dating of moraines in the valleys and of erratic boulders on the plateau testifies to an initial glaciation during the Mid Pleistocene (presumably MIS 6), an early local LGM lasting from 50 to 30 ka, a glacier extent at 19-17 ka similar to the local LGM, and the disintegration of the valley glaciers after 16-14 ka. One of the central questions arising from the glacial chronology is why the local LGM in the Bale Mountains occurred already during MIS 3 and therefore much earlier than the global LGM. Wetter climatic conditions during MIS 3 compared to a very dry MIS 2 may explain the “early” local glacier advance. However, whether the glacial chronology of the Bale Mountains in general and a local LGM during MIS 3 in particular are representative for the entire Ethiopian Highlands, needs to be verified by future studies from other locations bearing evidence of past glaciations (see Chapter 7).
2. Glacial landforms like moraines and periglacial features like relict large sorted patterned grounds provide clear evidence for a strong cooling and pronounced climate and environmental changes in the Bale Mountains during the last glacial period. The comparison of the postulated local temperature depression (4-6 °C during the local LGM and 6-8 °C during MIS 2) with temperature reconstructions from lower sites supports previous findings arguing for an amplified cooling with increasing elevation in tropical Eastern Africa during the Late Pleistocene. A steeper lapse rate due to a drier atmosphere during MIS 3/2 is discussed as a potential cause for the amplified high-altitude cooling. The glaciated mountains in turn might have reinforced the local cooling due to a positive ice-albedo feedback – an effect that has not yet been considered in the region. Independent of the causes, the strong cooling that led to the formation of the plateau glaciation and probably also to the genesis of the large sorted patterned grounds in the Bale Mountains must have had a considerable impact on the afro-alpine ecosystem and endemic species. To identify

potential glacial refuges of the afro-alpine plant and mammal species that currently populate the Sanetti Plateau and upper valleys, is a challenge for future palaeoecological research in the Bale Mountains.

3. The glacial history provides essential information on the climate and environmental conditions during the early human occupation of the Bale Mountains. By combining archaeological, soil biogeochemical, zoogeographical, and glacial chronological findings, the central hypothesis of the research unit – an advance of humans into the high mountains already during the last glacial period – could be corroborated. It was shown that the early colonisation of the Bale Mountains (47-31 ka cal BP) coincided with the local LGM (50-30 ka) and therefore with a relatively cold period. Beside obsidian as raw material and an abundant rodent as key food source, perennial melt water from the glaciers was probably one of the afro-alpine key resources, which might have attracted the prehistoric foragers. The interdisciplinary findings therefore not only prove that the resources of the world's high mountains have already been accessed by humans during the Late Pleistocene, but also that MSA foragers in the Bale Mountains were familiar with cold and glaciated environments.
4. In cross-comparison with available glacial chronologies and reconstructions from other tropical mountains in the region, the new data from the Bale Mountains contribute to a better understanding of past glacier fluctuations and climate variations across Eastern Africa. The comparison of glacial chronologies from the Bale Mountains, Rwenzori Mountains, Mount Kenya, and Kilimanjaro indicates differences in the timing of the local LGM and subsequent re-advances that have not been pointed out before. This asynchronicity suggests that regional hydroclimatic variations as well as topographic differences were important drivers of the palaeo glacier dynamics across Eastern Africa and should therefore be given greater attention. Another pattern emerging from the comparison is a decrease in the past ice covered area (relative to the mountain size) from the equator over the southern towards the northern Ethiopian Highlands, suggesting a negative high-altitude humidity gradient from the inner to the outer tropics. Whether such a gradient reflects present-day hydroclimatic conditions or required changes in the large-scale atmospheric circulation (e.g. southward shift of the tropical rain belt), is a potential subject of future research (see Chapter 7).



## Chapter 7

# Outlook

This thesis has elaborated the potential of glacial and periglacial landforms in the Ethiopian Highlands for the reconstruction of Pleistocene glacier fluctuations as well as climate and environmental changes. One important methodological finding emerging from the thesis is that the stabilisation age of moraines in the volcanic highlands can be successfully determined by applying  $^{36}\text{Cl}$  surface exposure dating. Therefore, the thesis lays the foundation for future glacial chronological research in other parts of the Ethiopian Highlands. Although our general understanding of the extent and timing of past glaciations in the Bale Mountains has improved considerably over the last years, many aspects of the local glacial history like the evolution of the plateau glaciation or the climatic drivers of the “early” local LGM are still poorly understood (see Chapter 5). Moreover, little is known about regional palaeoclimatic variations and past glacier fluctuations in other parts of the highlands. With the aim to refine the understanding of past glaciations and palaeoclimatic variations across the Ethiopian Highlands, this project has received additional funding from the DFG and SNSF in the course of the extension of the Ethio-European research unit “The Mountain Exile Hypothesis”. Three specific research ideas, which are partly linked to the objectives and working packages of the project’s second phase, are briefly outlined below.

### **Evolution of the plateau glaciation in the Bale Mountains**

As discussed in detail in the synthesis chapter, the reconstruction of the former plateau glaciation in the Bale Mountains is hampered by the lack of unambiguous glacial geomorphological evidence for the exact expansion of the former ice cap and a missing robust glacial chronology. However, a sound understanding of the evolution of the extensive ice cap on the Sanetti Plateau is worthwhile since it provides fundamental insights into the formation of a glacier type that was rare in Eastern Africa. Apart from the Bale Mountains and Kilimanjaro (e.g. Kaser et al., 2010), an extensive ice cap probably did not form on any of the other tropical mountains in the region. Valley glaciers were predominating (e.g. Mark and Osmaston, 2008). Furthermore, profound knowledge on the former extent of the ice cap on the Sanetti Plateau is a prerequisite for drawing conclusions about the afro-alpine palaeoclimate and -environment (see Chapters 2, 3, and 5). To elaborate more on the glacial chronology of the Sanetti Plateau, eleven additional boulders from the inner and outer big boulder moraine (BBM) have been sampled in January 2020 for  $^{36}\text{Cl}$  surface exposure dating. In addition, unpublished exposure ages of twelve erratic boulders spanning from the inner BBM to the eastern margin of the plateau were recently made available by Prof. Dr. Tim Barrows (University of Wollongong). The samples were originally taken by Osmaston, Mitchell, and Osmaston (2005) during their field trip to the Bale Mountains in 2003 and later processed and analysed by Tim Barrows. Furthermore, the basal age of sediment cores from seasonal lakes across the northern part of the plateau that were drilled by other members of the research unit will be evaluated regarding the deglaciation history of the ice cap. The basal age of these cores indicates the onset of sedimentation and could therefore help to elucidate when the northern part of the plateau became ice-free and disintegration of the ice cap began. In the long-term, applying a combined ice flow-mass balance model to the Bale Mountains would be desirable to gain additional insights into the formation and dynamics of the former plateau glaciation (e.g. Zekollari et al., 2017; Seguinot et al., 2018).

### **Glacial and climate history of the Arsi Mountains**

The more than 4000 masl high Arsi Mountains (see Fig. 2.1) in the southern Ethiopian Highlands represent an ideal research area to study the regional palaeoclimate and past glacier fluctuations in cross-comparison with the Bale Mountains. Characteristic for the Arsi Mountains is their simple elongated geometry and the absence of a vast plateau. About twenty U-shaped valleys descend to the west, north, and east from the central ridge. Moraine sequences are well preserved in most of the valleys (see Fig. 2.5) and provide a solid basis for geomorphological mapping and cosmogenic nuclide dating. Interestingly, the palaeo glaciers in the eastern valleys reached on average about 150 m further down than those in the western valleys (see Fig. A.6). This indicates pronounced differences in the mass balance of the western and eastern palaeo glaciers, which might have been caused by orographic effects and increased precipitation/cloudiness along the eastern declivity. In view of the hypothesised small-scale hydroclimatic gradients in tandem with the preservation of moraines in many valleys, the Arsi Mountains are a promising location for studying local Late Pleistocene precipitation and wind flow patterns on the basis of past glacier variations. However, a robust, but yet lacking, glacial chronology is a precondition for verifying that the moraines from the eastern and western valleys originate from the same stage and therefore support palaeoclimatic interpretation. Furthermore, an independent glacial chronology from the Arsi Mountains is essential to assess whether the findings from the Bale Mountains including a local LGM during MIS 3 is representative for the southern Ethiopian Highlands.

To develop a glacial chronology for the Arsi Mountains, 43 moraine boulders (in addition to the previous six) have been sampled in four different valley in February 2020 with the support of Serdar Yesilyurt and Beriso Kemal for surface exposure dating. As soon as a chronology is established, the different dated glacier extents will be used in combination with an advanced version of the open-source glacier surface mass balance model glacierSMBM (Groos et al., 2017; Groos and Mayer, 2017) to reconstruct spatio-temporal precipitation and temperature changes in the region. The approach is based on the assumption that glaciers were close to equilibrium (accumulation  $\sim$  ablation) at the determined glacial stages. In a first step, the model calculates the mass balance of the reconstructed palaeo glaciers using current meteorological data from the region. Based on this, a model ensemble with various combinations of adjusted (increased/decreased) temperature and precipitation data will be performed to identify the meteorological pattern which results in a steady state between accumulation and ablation (mass balance  $\sim$  0). The mean annual temperature and precipitation at steady state are finally compared with the present-day climatic conditions to quantify past temperature and precipitation changes in the southern Ethiopian Highlands. In addition to this, the amount of melt water released by the palaeo glaciers can be inferred from the modelled ablation at steady state.

### **Hydroclimatic analysis of the tropical mountains in Eastern**

The interpretation of past glacier fluctuations in the Bale Mountains and in comparison with other locations across tropical Eastern Africa has not only been hampered by the common challenges related the reconstruction and dating of past glaciations, but also by the limited understanding of present-day hydroclimatic variations at high elevation (see Chapters 2, and 5).

Without knowing for example the current differences in the amount and distribution of precipitation between the northern and southern Ethiopian Highlands, the interpretation of the discrepancy between a past glaciation of 13 km<sup>2</sup> in the Simien compared to an ice cover of 85 km<sup>2</sup> in the Arsi Mountains, which only comprise 13% of the area above 4000 masl of the former, remains highly speculative. For a better understanding of current hydroclimatic variations at high elevation across the region, a spatial assessment would be necessary. One of the most reliable datasets for studying regional rainfall distributions in the region is CHIRPS, a product combining rainfall estimates from rain gauge and satellite observations (Gebrechorkos, Hülsmann, and Bernhofer, 2019). This dataset has already been evaluated by Gebrechorkos, Hülsmann, and Bernhofer (2019) for Eastern Africa, but not with respect to elevation. To have a modern reference for palaeoclimatic interpretations and to better understand the current role of tropical mountains in Eastern Africa as “water towers” for the region, it would be worthwhile to combine the CHIRPS rainfall dataset with the hypsographic analysis presented in Chapter 2 (see Fig. 2.2). The weather stations in the Bale Mountains installed within the framework of the research unit as well as observational data from Kilimanjaro (Appelhans et al., 2016) could serve for the validation of the product’s quality at high elevations.

## References

- Gebrechorkos, S. H., S. Hülsmann, and C. Bernhofer (2019). “Long-Term Trends in Rainfall and Temperature Using High-Resolution Climate Datasets in East Africa”. In: *Sci. Rep.* 9.1, pp. 1–9. DOI: 10.1038/s41598-019-47933-8.
- Groos, A. R. and C. Mayer (2017). “glacierSMBM: Glacier Surface Mass Balance Model. R package version 0.1.” In: URL: <https://CRAN.R-project.org/package=glacierSMBM>.
- Groos, A. R. et al. (2017). “A First Attempt to Model Region-Wide Glacier Surface Mass Balances in the Karakoram: Findings and Future Challenges”. In: *Geogr. Fis. Dinam. Quat.* 40.2, pp. 137–159. DOI: 10.4461/GFDQ.2017.40.10.
- Kaser, G. et al. (2010). “Is the Decline of Ice on Kilimanjaro Unprecedented in the Holocene?” In: *The Holocene* 20.7, pp. 1079–1091. DOI: 10.1177/0959683610369498.
- Mark, B. G. and H. A. Osmaston (2008). “Quaternary Glaciation in Africa: Key Chronologies and Climatic Implications”. In: *J. Quat. Sci.* 23.6-7, pp. 589–608. DOI: 10.1002/jqs.1222.
- Osmaston, H. A., W. A. Mitchell, and J. A. N. Osmaston (2005). “Quaternary Glaciation of the Bale Mountains, Ethiopia”. In: *J. Quat. Sci.* 20.6, pp. 593–606. DOI: 10.1002/jqs.931.
- Seguinot, J. et al. (2018). “Modelling Last Glacial Cycle Ice Dynamics in the Alps”. In: *Cryosphere* 12.10, pp. 3265–3285. DOI: 10.5194/tc-12-3265-2018.
- Zekollari, H. et al. (2017). “Sensitivity, Stability and Future Evolution of the World’s Northernmost Ice Cap, Hans Tausen Iskappe (Greenland)”. In: *Cryosphere* 11.2, pp. 805–825. DOI: 10.5194/tc-11-805-2017.

## Appendix A

# Supplements to Chapter 2



FIGURE A.1: Photographs of all 81 sampled and dated glacial and periglacial features from the Bale and Arsi Mountains. Color coding of the different stages is the same as in Fig. 2.4 and Fig. 2.5. Green = MPG Stage (equivocal), violet = LPG Stage (equivocal), red = LPG Stage I, yellow = LPG Stage II, blue = LPG Stage III. White arrows indicate the approximate flow direction of the paleo-glaciers.



Fig. A.1 continued...



Fig. A.1 continued...

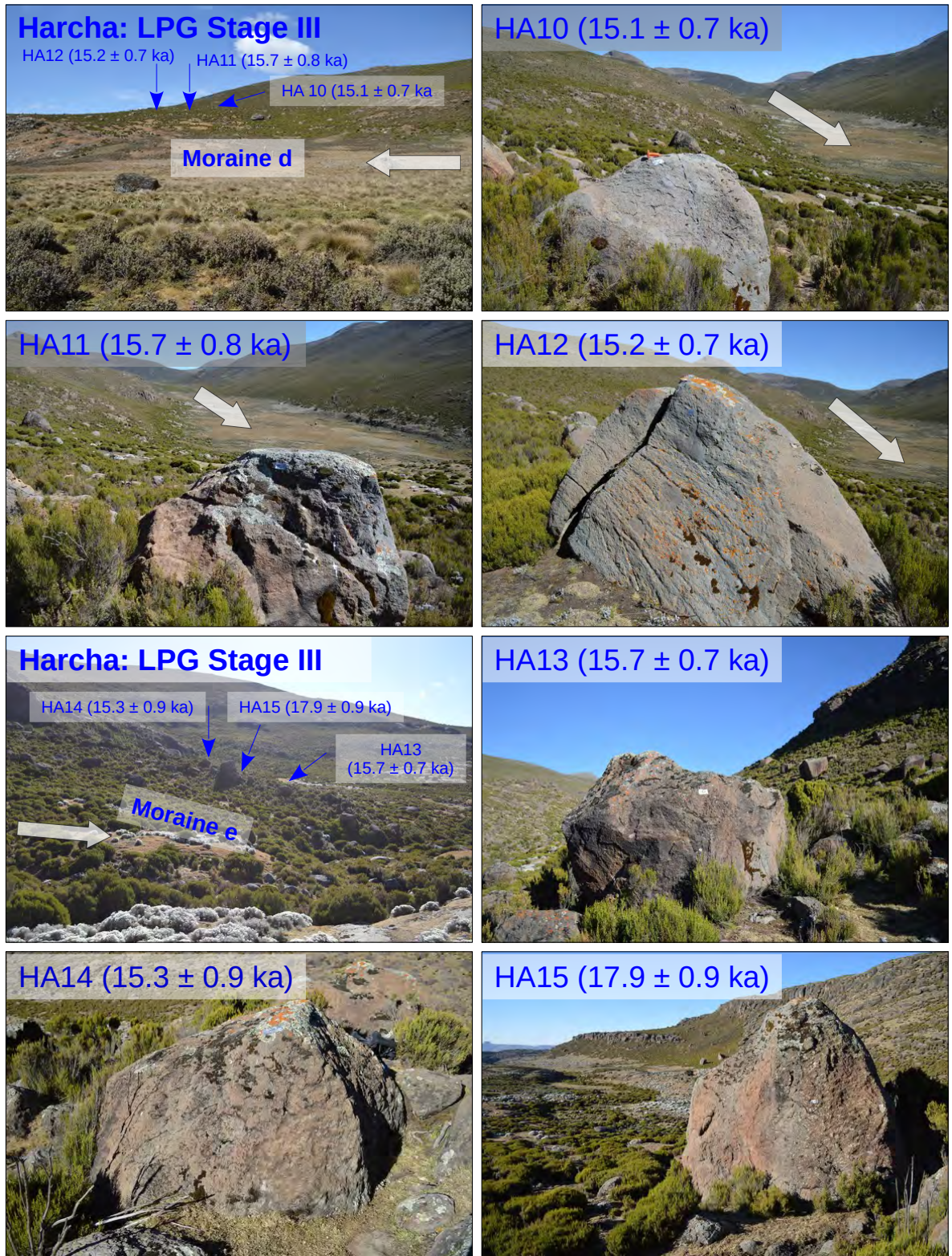


Fig. A.1 continued...



Fig. A.1 continued...

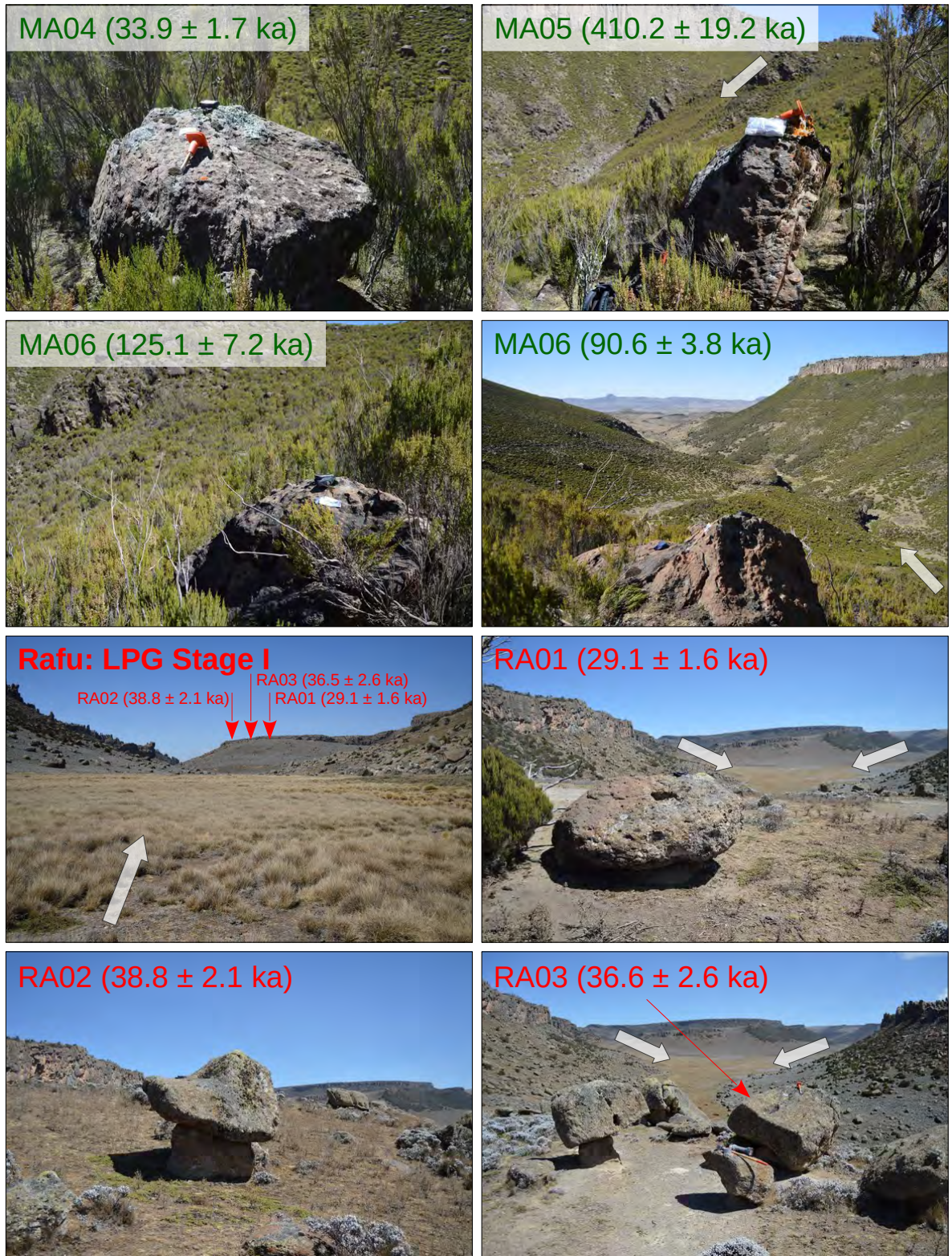


Fig. A.1 continued...

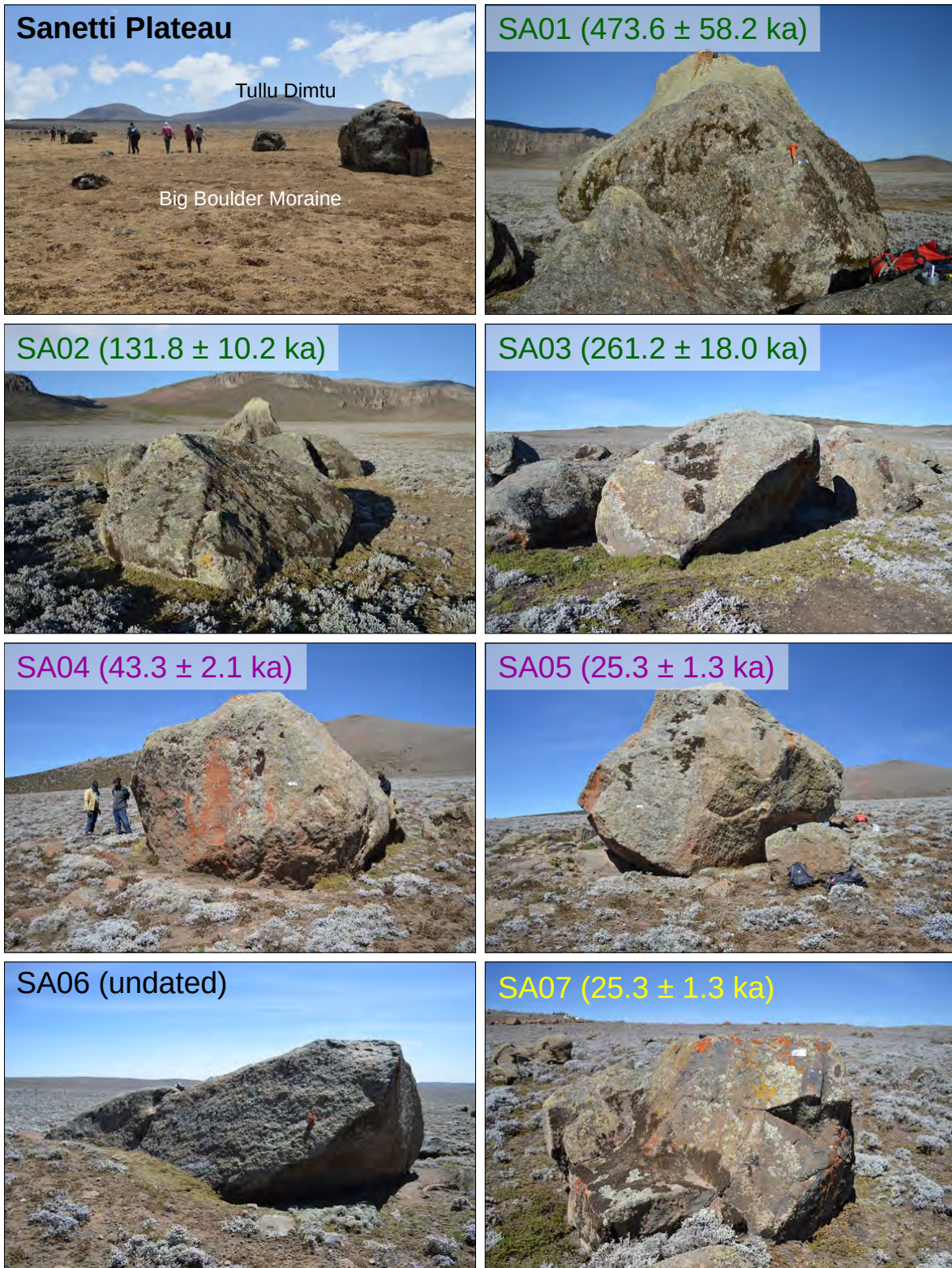


Fig. A.1 continued...

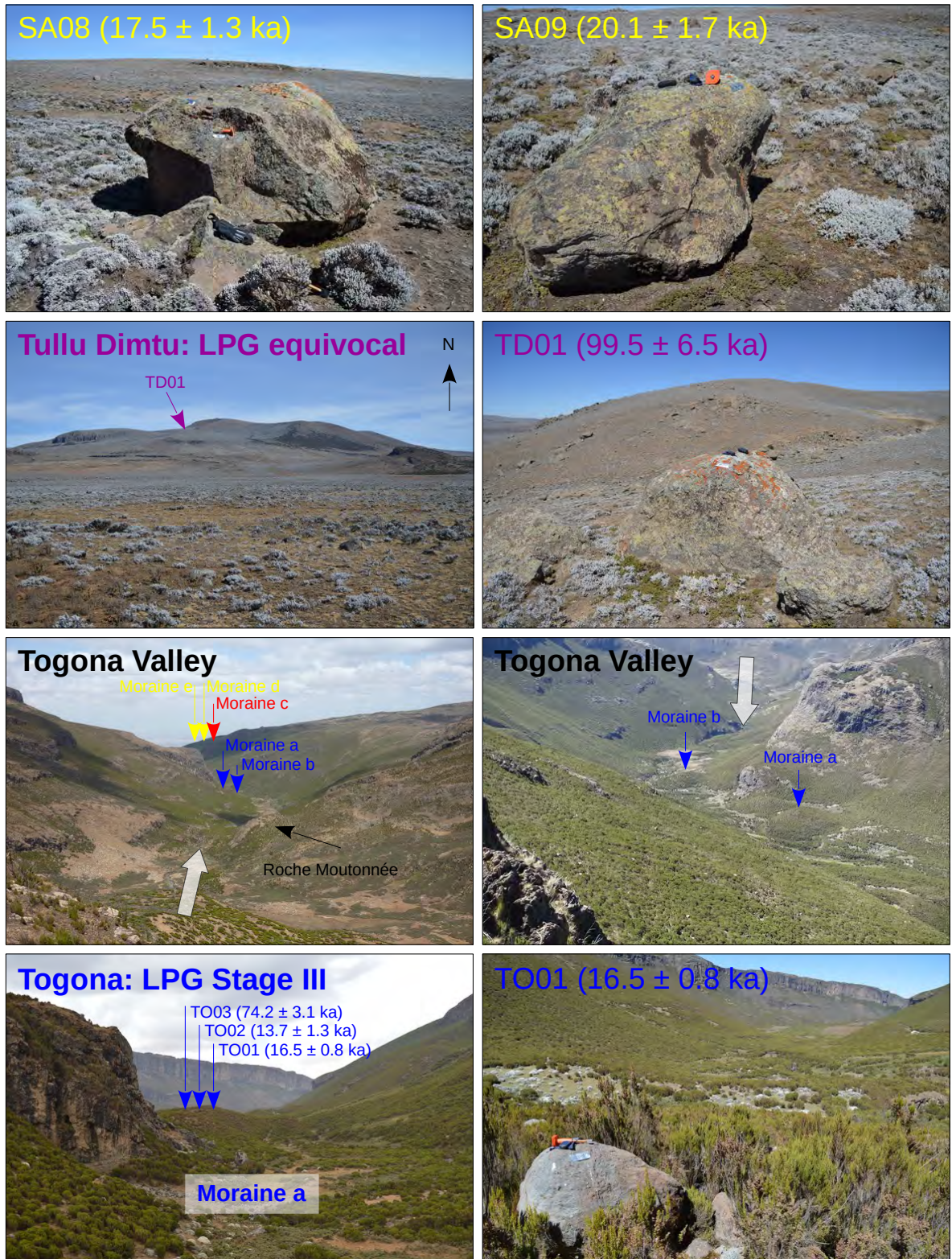


Fig. A.1 continued...

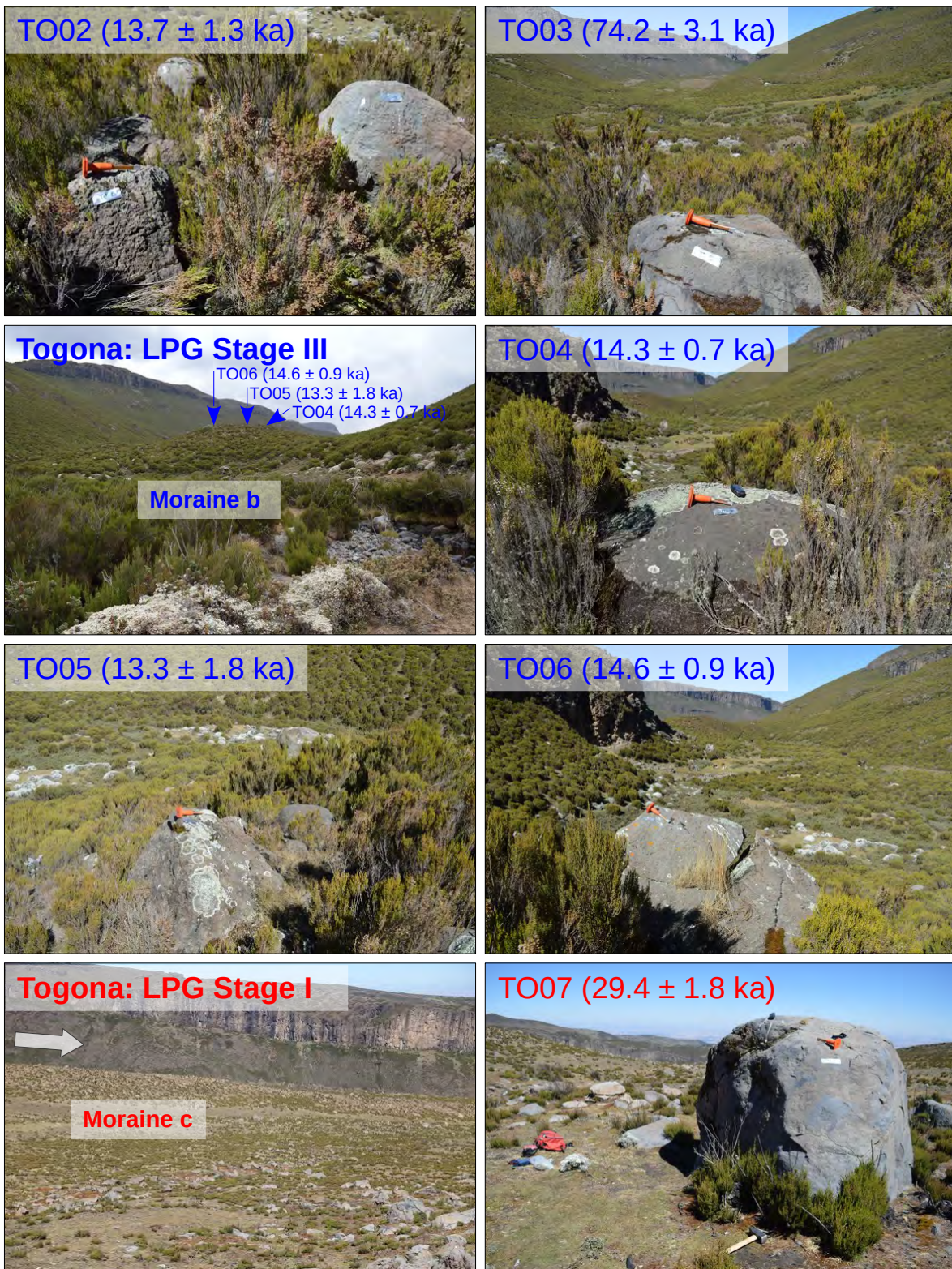


Fig. A.1 continued...



Fig. A.1 continued...

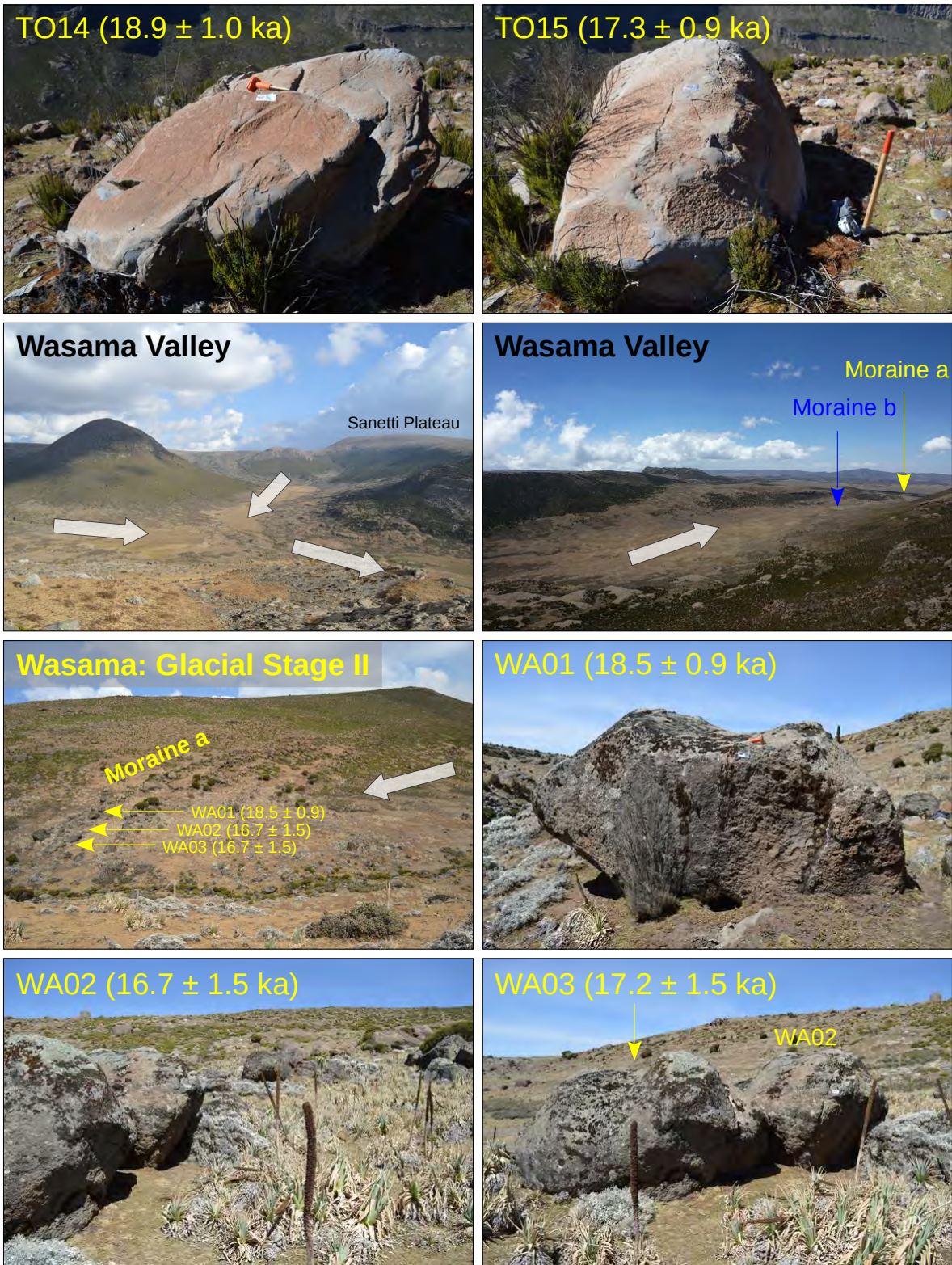


Fig. A.1 continued...

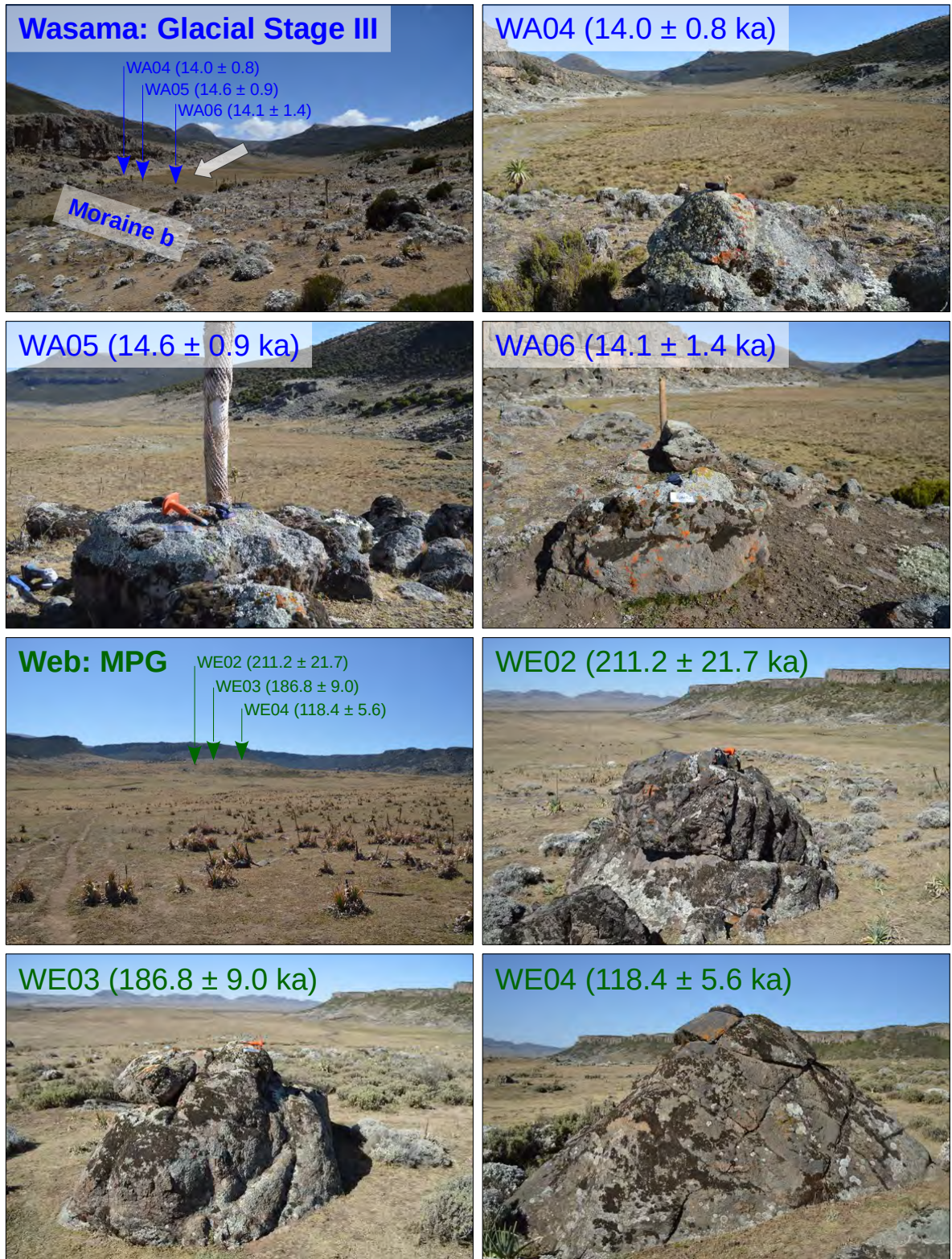


Fig. A.1 continued...



Fig. A.1 continued...



Fig. A.1 continued...

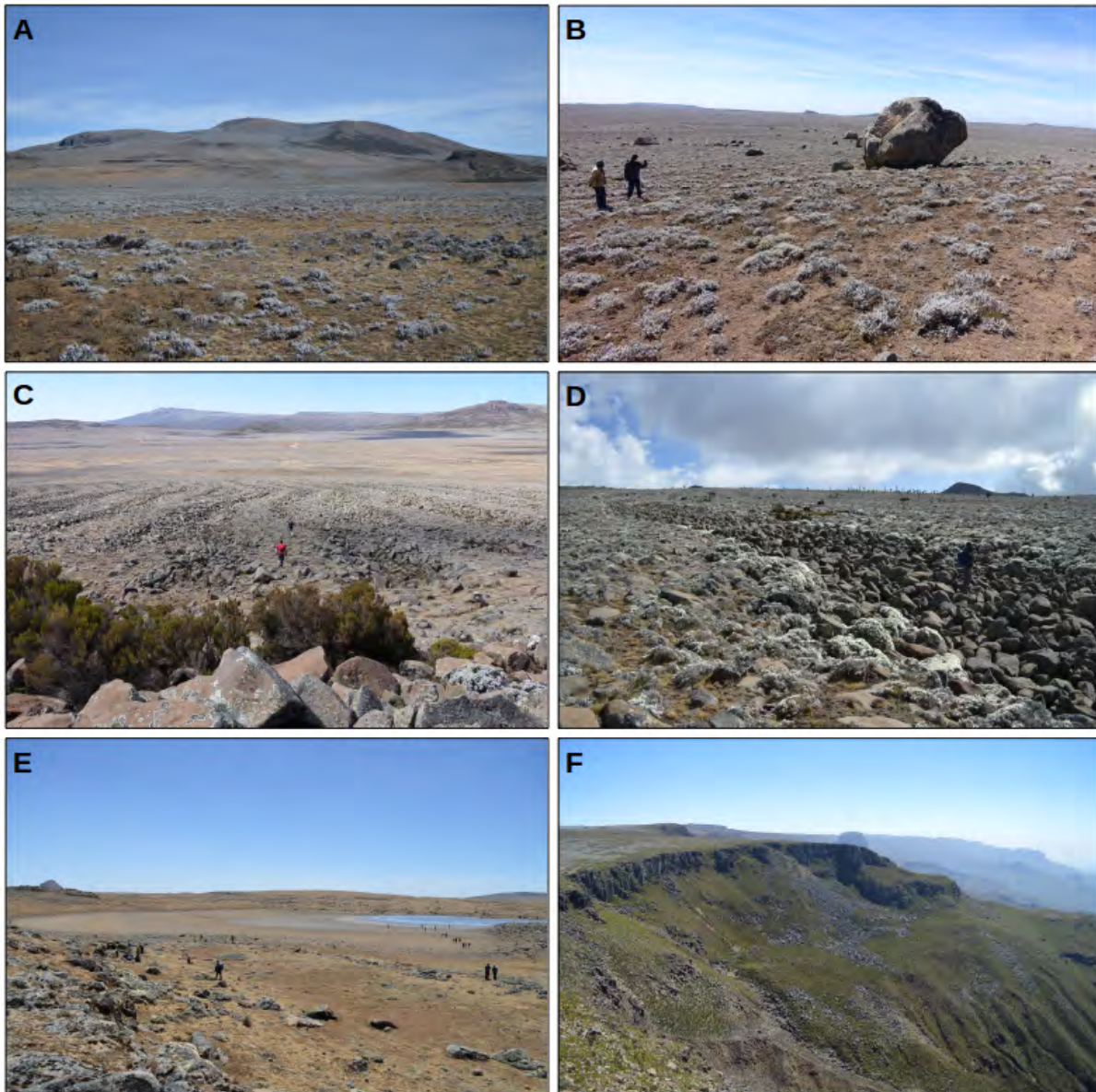


FIGURE A.2: Glacial and periglacial geomorphology of the Sanetti Plateau. (A) View from the southern plateau towards Tullu Dimtu (4377 m), the highest peak of the Bale Mountains. (B) Big boulder (5 m high) at the eastern slope of Tullu Dimtu. (C) Sorted stone stripes (up to 2 m deep, 15 m wide and 200 m long) located at the western slope of a volcanic plug 5 km south of Tullu Dimtu. (D) Sorted stone stripes at the western margin of the plateau (12 km west of Tullu Dimtu). (E) Shallow depression and seasonal lake at the northern margin of the plateau. (F) Hardly-weathered relict block fields along the southern Haremma Escarpment.

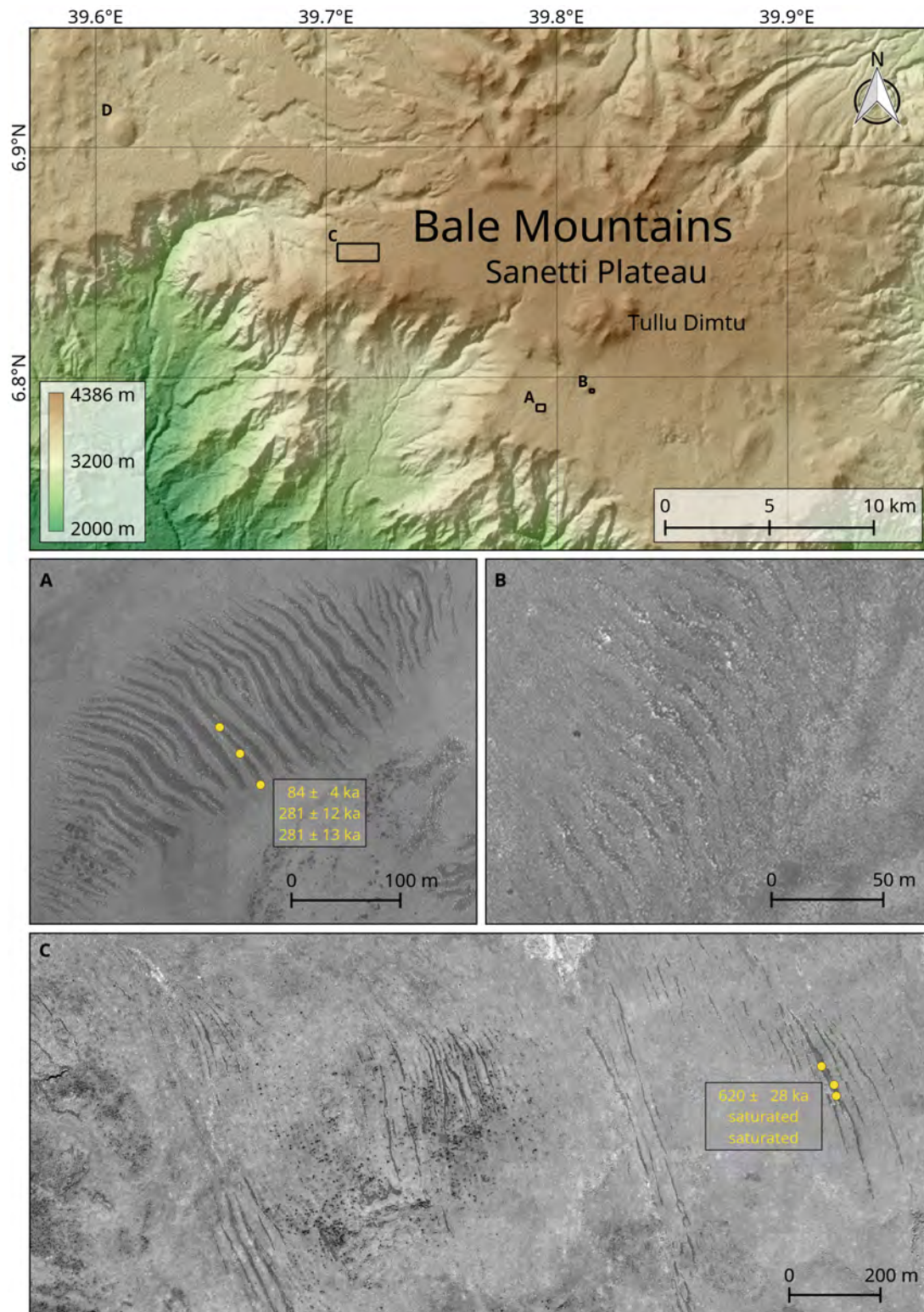


FIGURE A.3:  $^{36}\text{Cl}$  surface exposure age and location of the large sorted stone stripes. (A, B) Southern Sanetti Plateau. (C) Western Sanetti Plateau. (D) Stone stripes were also discovered on satellite images on a lower plateau ( $\sim 3700 \text{ m}$ ) in the west of the Bale Mountains. However, a field visit of these structures is still pending. High-resolution satellite images for mapping were kindly provided by the Digital Globe Foundation through an imagery grant. For field images see Fig. A.1 and A.2. The obtained old  $^{36}\text{Cl}$  surface exposure ages probably do not represent the formation age of the sorted stone stripes and are rather the result of pre-exposure to cosmic radiation. Since  $^{36}\text{Cl}$  has reached saturation (the concentration where production and decay are balanced) in samples BS05 and BS06, the resulting age ( $>1 \text{ Ma}$ ) lies at the limit of the method and is therefore not stated explicitly.

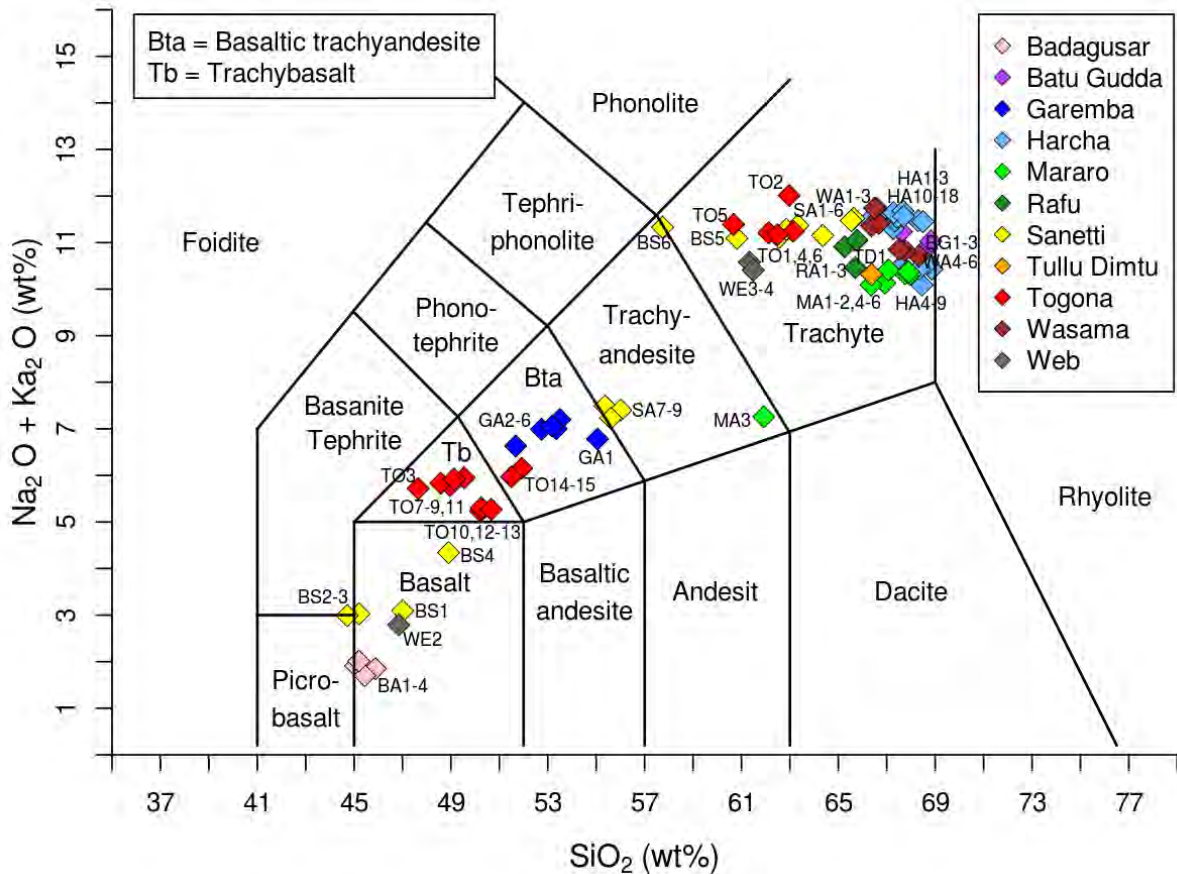


FIGURE A.4: TAS (total alkali versus silica) classification of all sampled boulders from the Bale and Arsi Mountains. The diagram shows that most of the sampled rocks are trachytes and basalts. Interestingly, the chemical signature of boulders from LPG Stage III and from LPG Stage I/II in the Togona Valley differ and indicate that they originate from two different catchments. The only outlier (TO03, 74.2 ka) of LPG Stage III in the Togona Valley (see Fig. 2.4) has the same chemical signature like the boulders from the upper lateral LPG Stage I/II moraines, suggesting that this boulder stems from an older glaciation and was reworked during LPG Stage III. In combination with a geologic map, which yet does not exist for the Bale Mountains, the chemical signature of the boulders would help to trace the ice flow and prove the transfluence of ice from the plateau into the valleys.

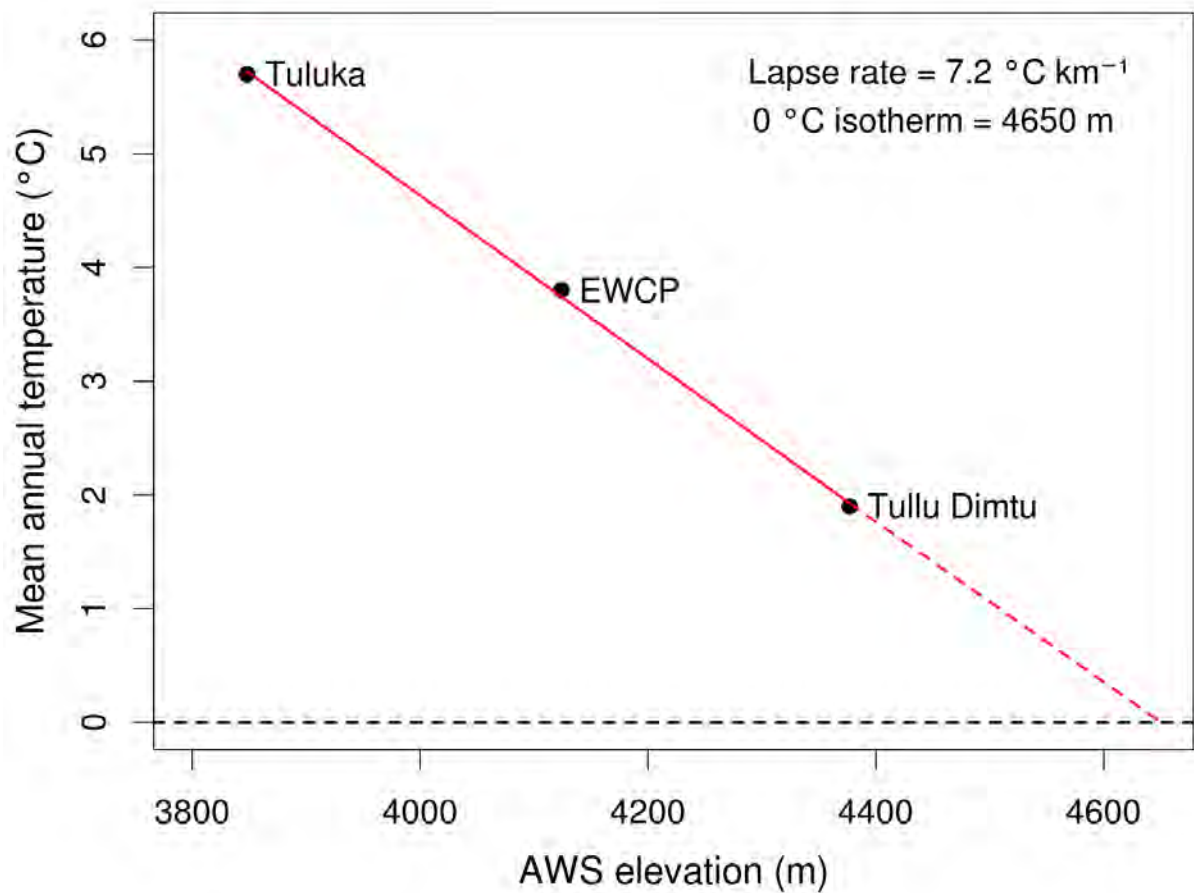


FIGURE A.5: Mean annual air temperature for three different locations and elevations in the Bale Mountains. The mean annual temperature was calculated from hourly values measured between 1<sup>st</sup> March 2017 and 28<sup>th</sup> February 2018 (the only period without longer data gaps) at three different automatic weather stations on the Sanetti Plateau: Tuluka (3848 m), EWCP – Ethiopian Wildlife Conservation Project (4124 m), Tullu Dimtu (4377 m). A linear regression was applied to calculate an annual lapse rate and determine the mean 0 °C isotherm. Due to the short measurement period, it was not possible to assess the inter-annual variability of the lapse rate and 0 °C isotherm.

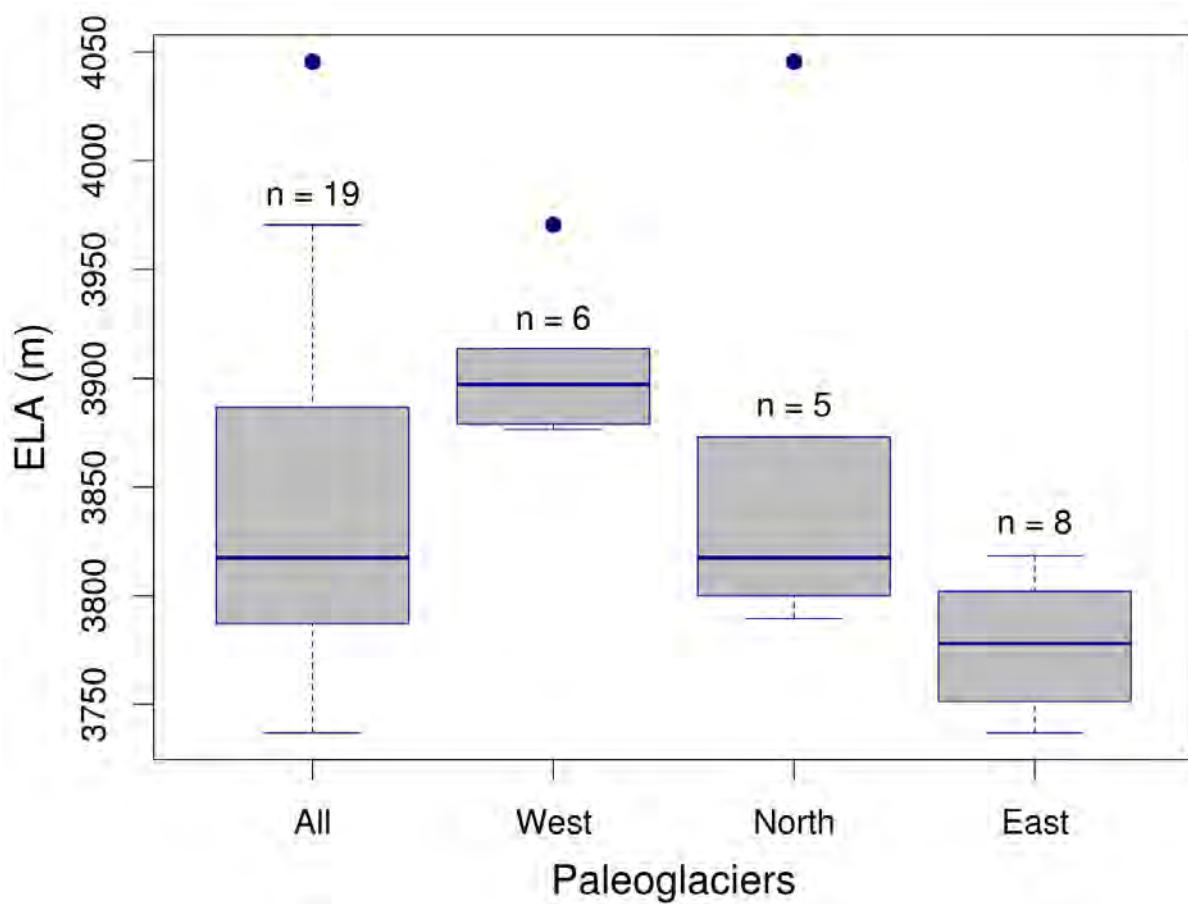


FIGURE A.6: Equilibrium line altitudes calculated for the palaeoglaciers in the western (aspect = 225-315°), northern (aspect = 315-360° and 0-45°), eastern (aspect = 45-135°), and all valleys in the Arsi Mountains based on the terminus-to-headwall-altitude-ratio (THAR).

TABLE A.1: Quaternary glaciations in Africa and estimated LGM extent.

Mountain	Country	LGM Extent (km <sup>2</sup> )	Reference
Aberdare Range	Kenya	10	Kaser and Osmaston (2002)
		23	Hastenrath (2009)
Arsi Mountains	Ethiopia	85	Osmaston and Harrison (2005)
Bale Mountains	Ethiopia	180	Osmaston, Mitchell, and Osmaston (2005)
		265	Ossendorf et al. (2019)
Kilimanjaro	Tanzania	150	Kaser and Osmaston (2002)
		200	Hastenrath (2009)
Mount Elgon	Uganda / Kenya	75	Kaser and Osmaston (2002)
		95	Hastenrath (2009)
Mount Kenya	Kenya	200	Kaser and Osmaston (2002)
		240	Hastenrath (2009)
Rwenzori	Uganda / Congo	200	Hastenrath (2009)
		260	Kaser and Osmaston (2002)
Simien Mountains	Ethiopia	13	Hurni (1989)

TABLE A.2: Geographic location and description of the sampled glacial and periglacial features from the Bale and Arsi Mountains.

Sample Name	Lithology	Location	Latitude °N (DD.DD)	Longitude °E (DD.DD)	Altitude (m a.s.l.)	Boulder Length (m)	Boulder Width (m)	Boulder Height (m)	Sample Thickness (cm)	Shielding Factor
<b>Bale Mountains (Moraine Boulders)</b>										
BA01	Basalt	Badagusar Valley	6.83809	39.91578	3919	1.3	1.2	1.0	1.0	0.9960
BA02	Basalt	Badagusar Valley	6.83691	39.91795	3886	2.6	1.8	1.7	2.5	0.9897
BA03	Basalt	Badagusar Valley	6.83661	39.91834	3887	1.0	0.9	1.1	5.0	0.9967
BA04	Basalt	Badagusar Valley	6.83670	39.91814	3883	1.4	1.0	1.2	3.5	0.9897
BG01	Trachyte	Batu Gudda Valley	6.97199	39.78252	3892	2.7	0.9	2.2	1.5	0.9568
BG02	Trachyte	Batu Gudda Valley	6.97173	39.78271	3830	2.4	2.3	1.8	2.5	0.9568
BG03	Trachyte	Batu Gudda Valley	6.97117	39.78308	3830	6.0	5.3	6.0	1.5	0.9568
HA01	Trachyte	Harcha Valley	6.95792	39.75181	3903	3.2	2.6	2.4	3.0	0.9996
HA02	Trachyte	Harcha Valley	6.95805	39.75163	3901	3.4	2.2	1.7	3.0	0.9993
HA03	Trachyte	Harcha Valley	6.95824	39.75121	3892	8.0	5.2	5.1	3.0	0.9994
HA04	Trachyte	Harcha Valley	6.95737	39.75089	3893	4.6	4.3	3.2	3.0	0.9996
HA05	Trachyte	Harcha Valley	6.95740	39.75099	3892	4.8	3.2	2.2	5.0	0.9996
HA06	Trachyte	Harcha Valley	6.95737	39.75113	3893	2.7	2.3	2.3	3.0	0.9996
HA07	Trachyte	Harcha Valley	6.95684	39.75160	3893	2.7	2.5	2.0	2.0	0.9989
HA08	Trachyte	Harcha Valley	6.95685	39.75111	3890	2.8	2.3	1.9	3.0	0.9989
HA09	Trachyte	Harcha Valley	6.95684	39.75102	3889	2.0	1.5	1.5	5.0	0.9989
HA10	Trachyte	Harcha Valley	6.95328	39.75420	3859	2.3	2.0	1.9	4.0	0.9970
HA11	Trachyte	Harcha Valley	6.95318	39.75395	3859	2.6	2.6	2.2	2.0	0.9970
HA12	Trachyte	Harcha Valley	6.95317	39.75376	3863	3.6	2.6	2.1	4.0	0.9970
HA13	Trachyte	Harcha Valley	6.95152	39.75104	3786	2.0	2.0	1.8	4.0	0.9822
HA14	Trachyte	Harcha Valley	6.95135	39.75110	3796	2.0	1.6	1.3	3.0	0.9822
HA15	Trachyte	Harcha Valley	6.95144	39.75105	3799	5.6	5.1	4.6	4.0	0.9822
HA16	Trachyte	Harcha Valley	6.95386	39.74147	3825	4.6	4.0	3.7	4.0	0.9993

HA17	Trachyte	Harcha Valley	6.95435	39.74138	3822	4.5	4.4	2.6	4.0	0.9993
HA18	Trachyte	Harcha Valley	6.95451	39.74129	3817	3.1	2.2	1.9	2.0	0.9993
MA01	Trachyte	Mararo Valley	6.97470	39.72957	3556	2.6	1.9	1.3	3.0	0.9692
MA02	Trachyte	Mararo Valley	6.97456	39.72962	3561	3.4	2.2	1.6	2.0	0.9692
MA03	Trachyandesite	Mararo Valley	6.97420	39.72977	3565	2.2	1.3	1.1	5.0	0.9709
MA04	Trachyte	Mararo Valley	6.97375	39.72987	3571	1.6	1.4	1.2	4.0	0.9663
MA05	Trachyte	Mararo Valley	6.97367	39.72992	3575	1.6	1.5	1.5	5.0	0.9663
MA06	Trachyte	Mararo Valley	6.97313	39.73064	3595	2.3	1.2	1.7	5.0	0.9759
MA07	Trachyte	Mararo Valley	6.97281	39.73064	3607	1.6	1.2	1.3	5.0	0.9759
RA01	Trachyte	Rafuy Valley	6.87894	39.71193	3866	2.0	1.4	1.0	4.5	0.9991
RA02	Trachyte	Rafuy Valley	6.87882	39.71190	3865	1.9	1.4	1.9	5.0	0.9991
RA03	Trachyte	Rafuy Valley	6.87894	39.71230	3862	2.0	1.9	1.6	4.0	0.9991
SA01	Trachyte	Sanetti Plateau	6.79694	39.78439	3857	3.8	2.7	3.3	5.0	0.9998
SA02	Trachyte	Sanetti Plateau	6.79684	39.78432	3857	4.3	3.9	1.9	5.0	0.9998
SA03	Trachyte	Sanetti Plateau	6.79556	39.78391	3858	3.2	3.0	2.0	5.0	0.9998
SA04	Trachyte	Sanetti Plateau	6.81049	39.82898	4058	7.1	7.0	3.4	5.0	0.9982
SA05	Trachyte	Sanetti Plateau	6.80966	39.82898	4047	8.4	8.1	4.8	4.0	0.9982
SA06	Trachyte	Sanetti Plateau	6.80858	39.82868	4032	8.3	5.2	3.0	5.0	0.9982
SA07	Trachyandesite	Sanetti Plateau	6.82009	39.86117	4062	2.4	2.1	1.5	4.0	1.0000
SA08	Trachyandesite	Sanetti Plateau	6.81999	39.86131	4064	4.1	3.6	2.2	4.0	1.0000
SA09	Trachyandesite	Sanetti Plateau	6.82018	39.86113	4063	1.8	1.6	1.1	5.0	1.0000
TD01	Trachyte	Tullu Dimtu	6.81821	39.81273	4192	2.9	2.7	1.5	3.0	0.9994
TO01	Trachyte	Togona Valley	6.90581	39.89138	3609	1.6	1.2	1.1	4.0	0.9740
TO02	Trachyte	Togona Valley	6.90581	39.89138	3609	0.9	0.8	0.6	5.0	0.9740
TO03	Trachybasalt	Togona Valley	6.90582	39.89135	3607	0.9	0.9	0.9	4.0	0.9740
TO04	Trachyte	Togona Valley	6.90271	39.89067	3616	2.0	1.2	0.9	3.0	0.9626
TO05	Trachyte	Togona Valley	6.90274	39.89072	3617	1.8	1.5	1.3	4.0	0.9626

TO06	Trachyte	Togona Valley	6.90276	39.89077	3614	2.4	2.3	1.6	4.0	0.9626
TO07	Trachybasalt	Togona Valley	6.91424	39.89972	3766	3.9	2.9	2.1	3.0	0.9987
TO08	Trachybasalt	Togona Valley	6.91401	39.89963	3766	2.9	2.6	1.7	4.0	0.9987
TO09	Trachybasalt	Togona Valley	6.91418	39.89973	3764	2.7	2.2	1.2	4.0	0.9987
TO10	Trachybasalt	Togona Valley	6.91455	39.89919	3772	3.3	2.7	2.1	5.0	0.9995
TO11	Trachybasalt	Togona Valley	6.91386	39.89901	3774	1.6	1.4	1.0	5.0	0.9995
TO12	Trachybasalt	Togona Valley	6.91378	39.89896	3775	2.1	2.1	1.3	4.0	0.9995
TO13	Trachybasalt	Togona Valley	6.91394	39.89850	3762	2.0	2.0	1.1	5.0	0.9989
TO14	Bas.Trachyand.	Togona Valley	6.91389	39.89846	3768	2.2	2.1	1.2	3.0	0.9910
TO15	Bas.Trachyand.	Togona Valley	6.91385	39.89845	3764	2.9	2.0	1.3	4.0	0.9989
WA01	Trachyte	Wasama Valley	6.93461	39.74273	3843	4.1	3.2	2.3	4.0	0.9971
WA02	Trachyte	Wasama Valley	6.93455	39.74256	3849	2.9	1.9	2.0	4.0	0.9971
WA03	Trachyte	Wasama Valley	6.93453	39.74254	3848	4.6	3.0	2.4	4.0	0.9971
WA04	Trachyte	Wasama Valley	6.92945	39.74686	3871	1.3	0.9	0.8	5.0	0.9946
WA05	Trachyte	Wasama Valley	6.92944	39.74683	3868	1.2	0.7	0.7	5.0	0.9946
WA06	Trachyte	Wasama Valley	6.92935	39.74671	3866	1.4	1.1	0.7	5.0	0.9946
WE02	Basalt	Weyib Valley	6.99097	39.71980	3532	3.0	2.6	1.4	5.0	0.9997
WE03	Trachyte	Weyib Valley	6.99059	39.71948	3532	5.3	2.6	1.4	3.0	0.9997
WE04	Trachyte	Weyib Valley	6.98943	39.71894	3534	6.1	4.2	1.9	5.0	0.9997
<b>Bale Mountains (Stone Stripes)</b>										
BS01	Basalt	Sanetti Plateau	6.78634	39.79297	3874	2.1	0.6	1.0	2.5	0.9961
BS02	Basalt	Sanetti Plateau	6.78660	39.79280	3869	1.5	0.5	1.4	4.5	0.9961
BS03	Basalt	Sanetti Plateau	6.78682	39.79263	3865	0.6	0.4	1.0	3.0	0.9997
BS04	Basalt	Sanetti Plateau	6.85491	39.72078	4050	0.8	0.6	1.1	5.0	0.9990
BS05	Trachyandesite	Sanetti Plateau	6.85513	39.72074	4049	0.5	0.5	1.0	4.5	0.9990
BS06	Trachyandesite	Sanetti Plateau	6.85550	39.72049	4045	1.5	0.5	0.6	3.5	0.9994

<b>Arsi Mountains (Moraine Boulders)</b>	
GA01 Bas.-Trachyand. Garembe Range	7.82859 39.37390 3810 1.5 1.1 0.9 4.0 0.9998
GA02 Bas.-Trachyand. Garembe Range	7.82785 39.37216 3787 2.0 1.7 1.6 5.0 0.9998
GA03 Bas.-Trachyand. Garembe Range	7.82811 39.37199 3783 1.3 1.3 1.0 5.0 0.9998
GA04 Bas.-Trachyand. Garembe Range	7.83150 39.37764 3874 3.3 3.0 1.9 4.0 1.0000
GA05 Bas.-Trachyand. Garembe Range	7.83158 39.37754 3873 3.4 3.3 2.1 4.0 1.0000
GA06 Bas.-Trachyand. Garembe Range	7.83159 39.37759 3872 2.9 1.5 1.6 4.0 1.0000

TABLE A.3: Major and trace element data of the rock samples from the Bale and Arsi Mountains.

Sample Name	O (wt.%)	C (wt.%)	Na (wt.%)	Mg (wt.%)	Al (wt.%)	Si (wt.%)	P (wt.%)	K (wt.%)	Ca (wt.%)	Ti (wt.%)	Mn (wt.%)	Fe (wt.%)	B (ppm)	Sm (ppm)	Gd (ppm)	U (ppm)	Th (ppm)
<b>Bale Mountains (Moraine Boulders)</b>																	
BA01	62.46	7.15	1.14	8.15	5.02	21.45	0.09	0.26	10.41	1.20	0.14	8.35	6	4.4	4.4	0.5	2.3
BA02	61.43	6.95	1.20	7.89	5.14	21.06	0.10	0.24	10.17	1.23	0.14	8.48	13	4.7	4.5	0.4	2.1
BA03	62.18	7.14	1.07	8.16	4.92	21.24	0.08	0.22	10.37	1.21	0.14	8.62	1	4.4	4.2	0.4	1.9
BA04	61.15	6.84	1.25	7.63	5.19	21.12	0.10	0.27	10.23	1.23	0.13	8.53	19	4.6	4.6	0.5	2.2
BG01	47.75	0.21	4.52	0.23	7.17	31.60	0.03	4.27	0.33	0.37	0.16	4.06	13	3.0	1.8	1.1	16.8
BG02	47.56	0.16	4.47	0.18	6.41	32.09	0.02	4.03	0.25	0.34	0.19	4.53	15	4.4	2.3	1.4	24.1
BG03	47.83	0.18	4.54	0.19	6.45	32.17	0.02	4.08	0.29	0.35	0.20	4.63	20	10.7	9.3	3.0	21.9
HA01	47.28	0.20	4.50	0.19	7.46	31.44	0.01	4.35	0.34	0.27	0.11	3.18	15	6.2	5.2	2.0	16.4
HA02	47.56	0.21	4.60	0.19	7.73	31.23	0.03	4.47	0.38	0.31	0.12	3.43	4	3.9	2.8	0.7	15.8
HA03	47.62	0.21	4.67	0.20	7.89	31.13	0.03	4.51	0.39	0.31	0.11	3.37	18	3.4	2.5	1.0	15.1
HA04	47.53	0.15	4.14	0.11	6.34	32.19	0.07	4.03	0.31	0.28	0.16	4.74	8	12.6	10.6	4.5	31.8
HA05	47.47	0.15	4.25	0.11	6.14	32.12	0.06	4.01	0.31	0.29	0.18	5.15	17	8.4	6.9	2.2	30.6
HA06	47.05	0.16	3.98	0.14	5.92	32.00	0.02	3.92	0.31	0.29	0.18	5.15	8	10.9	9.5	4.3	30.4
HA07	47.19	0.15	4.17	0.11	6.40	31.67	0.13	3.99	0.32	0.31	0.16	4.92	9	9.1	7.5	3.5	32.8
HA08	46.86	0.15	4.16	0.11	6.22	31.58	0.10	4.03	0.31	0.29	0.17	4.90	5	7.1	6.1	2.6	29.8
HA09	47.48	0.15	4.16	0.12	6.33	31.95	0.09	4.01	0.31	0.32	0.16	5.10	3	10.4	8.2	2.2	29.8
HA10	47.98	0.18	4.56	0.21	7.46	31.93	0.04	4.42	0.28	0.34	0.12	3.32	13	6.7	6.3	2.9	17.3
HA11	47.51	0.22	4.64	0.25	7.44	31.42	0.03	4.43	0.31	0.33	0.12	3.29	4	6.4	5.7	3.5	19.0
HA12	47.95	0.17	4.56	0.18	7.43	32.02	0.01	4.40	0.26	0.33	0.12	3.35	10	6.1	6.0	4.4	12.5
HA13	47.09	0.19	4.58	0.17	7.68	30.98	0.04	4.40	0.34	0.31	0.11	3.29	9	2.5	1.9	0.4	15.5
HA14	47.65	0.19	4.58	0.17	7.57	31.48	0.04	4.39	0.36	0.30	0.12	3.47	15	4.2	3.6	0.9	17.3
HA15	47.81	0.19	4.60	0.18	7.64	31.52	0.05	4.43	0.35	0.32	0.12	3.49	16	3.6	2.9	1.2	16.2
HA16	47.71	0.19	4.68	0.17	7.64	31.45	0.03	4.42	0.36	0.30	0.12	3.48	1	4.1	3.5	1.4	17.6

HAI7	47.89	0.19	4.67	0.17	7.68	31.63	0.04	4.47	0.36	0.31	0.12	3.29	17	3.9	3.1	1.5	16.4
HA18	47.88	0.19	4.62	0.17	7.62	31.65	0.05	4.43	0.34	0.30	0.12	3.46	10	2.8	2.3	0.7	16.5
MA01	46.83	0.18	4.01	0.18	6.61	31.28	0.02	3.92	0.31	0.39	0.17	4.76	4	8.3	5.7	1.7	23.4
MA02	47.43	0.20	4.15	0.18	6.72	31.67	0.04	3.93	0.36	0.36	0.19	4.64	16	6.0	4.1	1.9	26.0
MA03	43.37	0.16	1.94	0.14	7.11	28.94	0.08	3.86	0.29	0.25	0.10	3.90	2	16.8	14.0	4.1	22.9
MA04	47.02	0.16	4.17	0.15	6.81	31.35	0.07	3.98	0.29	0.32	0.18	4.62	7	9.4	6.6	2.2	31.4
MA05	46.45	0.19	4.00	0.18	6.56	31.01	0.05	3.90	0.33	0.35	0.18	4.63	6	11.4	7.5	3.2	29.8
MA06	47.47	0.19	4.12	0.19	6.58	31.77	0.04	3.95	0.33	0.35	0.18	4.83	1	7.9	5.2	1.8	27.6
MA07	47.59	0.19	4.15	0.18	6.77	31.73	0.07	3.97	0.35	0.35	0.18	4.67	15	11.2	8.1	1.8	29.6
RA01	47.37	0.22	4.24	0.16	8.79	30.71	0.04	3.94	0.45	0.33	0.07	2.62	6	8.6	7.5	1.6	10.1
RA02	46.88	0.20	4.28	0.16	8.28	30.50	0.07	4.27	0.41	0.40	0.07	2.84	7	7.6	6.5	1.7	10.1
RA03	47.44	0.21	4.33	0.18	8.48	30.74	0.04	4.33	0.41	0.39	0.09	2.98	14	7.6	5.7	1.7	10.9
SA01	47.01	0.19	4.58	0.17	8.12	30.68	0.03	4.44	0.36	0.37	0.08	2.90	13	7.5	6.4	2.8	12.6
SA02	46.66	0.18	4.39	0.14	8.46	30.08	0.04	4.34	0.36	0.43	0.08	3.16	18	11.0	9.3	2.5	11.4
SA03	47.00	0.21	4.56	0.19	8.11	30.63	0.02	4.42	0.37	0.38	0.09	2.94	15	7.7	6.7	2.8	12.2
SA04	48.69	0.68	4.83	0.55	9.36	29.24	0.02	3.82	1.37	0.46	0.10	3.48	18	2.7	2.5	1.1	8.2
SA05	48.24	0.53	4.83	0.40	9.20	29.60	0.04	4.03	1.10	0.40	0.10	3.18	10	2.8	2.4	0.9	8.2
SA06	47.92	0.58	4.78	0.46	8.88	29.38	0.02	4.01	1.18	0.42	0.10	3.29	7	2.6	2.3	1.0	7.1
SA07	50.91	1.92	4.08	1.41	9.66	25.88	0.03	1.65	4.07	1.17	0.10	5.98	12	2.9	2.9	0.4	1.0
SA08	51.04	1.89	4.01	1.33	9.92	26.18	0.01	1.66	4.10	1.15	0.09	5.34	14	2.3	2.4	0.4	1.1
SA09	50.68	1.96	3.94	1.43	9.50	25.99	0.01	1.59	4.17	1.17	0.09	5.30	13	2.3	2.5	0.4	1.1
TD01	48.08	0.46	4.44	0.39	7.70	31.02	0.04	3.60	0.91	0.27	0.11	3.43	12	4.4	3.5	1.7	34.7
TO01	47.46	0.35	4.79	0.27	9.15	29.43	0.01	4.61	0.74	0.38	0.12	3.38	15	3.1	2.7	0.8	9.0
TO02	46.70	0.44	4.54	0.35	8.38	29.04	0.01	4.23	0.90	0.32	0.16	3.88	10	6.2	5.1	1.5	15.2
TO03	52.32	2.86	3.20	2.84	8.51	22.89	0.13	1.21	4.85	2.12	0.16	9.95	10	3.8	3.5	0.6	2.5
TO04	47.24	0.42	4.56	0.32	8.48	29.51	0.01	4.23	0.87	0.30	0.15	3.93	12	4.1	3.6	0.8	12.7
TO05	46.01	0.34	4.54	0.28	8.69	28.36	0.01	4.37	0.69	0.23	0.20	4.41	7	11.6	10.3	4.1	28.6

TO06	46.81	0.41	4.47	0.28	8.63	29.21	0.00	4.27	0.89	0.29	0.19	3.62	10	5.1	4.9	2.9	14.3
TO07	52.03	2.89	3.18	2.99	8.41	22.27	0.10	1.19	4.70	2.29	0.17	10.69	13	3.4	3.2	0.5	2.1
TO08	52.25	2.84	3.29	2.82	8.53	22.71	0.18	1.16	4.81	2.08	0.16	10.26	14	4.8	4.6	0.5	2.3
TO09	44.68	0.00	3.26	2.68	8.39	23.16	0.20	1.30	4.54	1.98	0.16	9.85	1	4.1	3.9	0.6	2.8
TO10	52.75	3.00	2.91	2.57	9.23	23.47	0.06	1.09	5.76	1.37	0.12	8.29	1	2.9	3.0	0.5	1.9
TO11	51.93	2.79	3.26	2.80	8.44	22.96	0.20	1.27	4.71	1.94	0.15	9.55	5	4.5	4.2	0.7	2.7
TO12	52.94	3.13	2.89	2.81	9.33	23.49	0.02	1.16	5.80	1.36	0.12	7.41	13	2.2	2.4	0.5	2.0
TO13	52.65	2.97	2.86	2.51	9.49	23.68	0.04	1.17	5.77	1.34	0.12	7.28	3	2.8	2.8	0.5	1.8
TO14	52.21	2.69	3.23	2.33	9.04	24.27	0.06	1.49	5.14	1.49	0.13	7.51	5	3.1	3.2	0.6	2.3
TO15	52.41	2.76	3.13	2.40	9.24	24.07	0.02	1.45	5.26	1.47	0.12	7.67	7	2.9	2.8	0.6	1.9
WA01	47.44	0.22	4.50	0.21	7.64	31.02	0.04	4.40	0.39	0.36	0.13	3.79	12	7.3	6.3	1.1	16.6
WA02	47.65	0.22	4.52	0.22	7.68	31.16	0.03	4.42	0.37	0.38	0.13	3.76	7	5.9	5.7	2.2	16.9
WA03	47.48	0.18	4.62	0.17	8.15	31.08	0.01	4.57	0.32	0.35	0.09	2.98	1	3.0	3.1	1.3	10.0
WA04	47.41	0.15	4.22	0.16	6.92	31.94	0.01	4.17	0.24	0.31	0.13	3.88	9	13.4	12.6	4.6	22.4
WA05	47.31	0.14	4.26	0.15	7.36	31.67	0.02	4.23	0.22	0.29	0.12	3.54	6	14.1	11.9	3.6	21.8
WA06	47.22	0.17	4.31	0.17	7.05	31.56	0.01	4.18	0.26	0.32	0.14	3.98	17	16.9	14.9	4.1	26.0
WE02	55.83	4.85	1.44	4.77	6.62	21.89	0.18	0.71	8.32	1.45	0.14	8.68	1	6.4	5.6	0.6	3.4
WE03	47.06	0.52	4.32	0.34	9.12	28.67	0.03	3.95	1.17	0.41	0.17	3.59	11	4.2	3.3	1.0	8.0
WE04	47.09	0.52	4.25	0.34	9.20	28.74	0.03	3.89	1.17	0.40	0.15	3.43	8	4.1	3.6	0.6	7.8
<b>Bale Mountains (Stone Stripes)</b>																	
BS01	57.88	5.13	1.74	5.61	7.40	21.97	0.09	0.62	7.86	1.44	0.15	9.10	3	3.3	3.6	0.3	1.1
BS02	56.64	5.09	1.70	5.50	7.23	21.13	0.14	0.61	7.90	1.41	0.15	9.13	11	3.8	4.1	0.3	1.3
BS03	56.17	4.98	1.68	5.23	7.52	20.90	0.15	0.60	8.00	1.44	0.14	8.97	12	3.8	4.1	0.3	1.2
BS04	54.79	3.85	2.50	3.56	8.30	22.86	0.14	0.81	6.96	1.42	0.15	8.81	6	4.3	4.4	0.4	1.7
BS05	47.82	0.68	5.01	0.21	9.09	28.42	0.05	3.59	1.92	0.24	0.19	4.39	1	6.4	4.8	2.9	14.8
BS06	46.47	0.66	5.16	0.18	9.42	26.99	0.05	3.64	1.90	0.24	0.19	4.41	15	6.7	4.9	1.9	15.5

<b>Arsi Mountains (Moraine Boulders)</b>																	
GA01	49.76	1.71	3.52	1.15	9.30	25.73	0.06	1.69	3.80	1.41	0.12	6.35	10	3.9	3.8	0.9	3.1
GA02	49.75	1.79	3.56	1.45	8.71	24.65	0.07	1.82	3.60	1.65	0.16	9.06	8	4.3	4.3	1.6	3.5
GA03	49.20	1.64	3.55	1.25	8.38	24.94	0.05	1.84	3.43	1.77	0.14	8.97	19	4.1	4.0	1.7	4.8
GA04	49.07	1.75	3.28	1.57	8.33	24.15	0.04	1.83	3.25	1.67	0.17	10.27	17	3.2	3.0	1.1	4.0
GA05	50.05	1.79	3.66	1.46	8.55	25.01	0.05	1.88	3.58	1.80	0.16	8.88	3	4.4	4.5	1.6	6.0
GA06	49.86	1.77	3.61	1.37	8.80	24.86	0.05	1.83	3.62	1.72	0.15	8.77	13	4.5	4.5	1.6	5.4

TABLE A.4: Cosmogenic  $^{36}\text{Cl}$  data and surface exposure ages of the rock samples from the Bale and Arsi Mountains for three different erosion scenarios ( $\epsilon_{min} = 0 \text{ mm ka}^{-1}$ ,  $\epsilon_{med} = 1 \text{ mm ka}^{-1}$ ,  $\epsilon_{max} = 2 \text{ mm ka}^{-1}$ ).

Sample Name	Rock Dissolved (g)	$^{35}\text{Cl}$ Spike (mg)	Cl (ppm)	$^{36}\text{Cl}$ ( $10^5 \text{ At g}^{-1}$ )	Surface Exposure Age (ka)			Glacial Stage
					$\epsilon_{min}$	$\epsilon_{med}$	$\epsilon_{max}$	
<b>Bale Mountains (Stone Stripes)</b>								
BA01	30.0135	2.5652	36.9 ± 0.19	15.25 ± 0.56	32.8 ± 1.7	32.6 ± 1.8	32.5 ± 1.8	LPG E
BA02	29.9999	2.5633	58.5 ± 0.16	10.51 ± 0.47	21.4 ± 1.3	21.1 ± 1.4	20.9 ± 1.4	LPG E
BA03	30.1888	2.5615	53.1 ± 0.07	27.57 ± 0.79	57.1 ± 3.1	56.2 ± 3.4	56.5 ± 3.6	LPG E
BA04	30.0666	2.5676	85.4 ± 0.19	9.68 ± 0.49	17.5 ± 1.3	17.2 ± 1.3	17.0 ± 1.3	LPG E
BG01	29.9986	2.5732	42.5 ± 0.14	37.74 ± 0.96	73.2 ± 3.3	73.9 ± 3.5	75.4 ± 3.8	LPG E
BG02	29.9703	2.5652	69.8 ± 0.23	38.01 ± 1.03	72.3 ± 3.8	71.1 ± 4.1	71.7 ± 4.4	LPG E
BG03	30.0311	2.5664	270.8 ± 0.99	25.65 ± 1.18	29.3 ± 2.6	28.0 ± 2.6	27.2 ± 2.6	LPG I
HA01	60.5755	3.0107	35.6 ± 0.07	23.83 ± 0.52	43.3 ± 1.8	43.8 ± 1.9	44.4 ± 2.0	LPG I
HA02	60.4857	3.0107	32.2 ± 0.06	150.38 ± 3.00	383.3 ± 15.7	571.3 ± 27.3	-	LPG I
HA03	60.5238	3.0132	29.6 ± 0.04	26.61 ± 0.70	48.4 ± 2.1	49.1 ± 2.2	50.2 ± 2.3	LPG I
HA04	60.5447	3.0126	63.5 ± 0.05	10.27 ± 0.40	17.6 ± 1.0	17.6 ± 1.0	17.5 ± 1.0	LPG II
HA05	60.5077	2.9980	54.8 ± 0.08	9.30 ± 0.36	16.5 ± 0.9	16.6 ± 0.9	16.6 ± 1.0	LPG II
HA06	60.5178	3.0047	65.2 ± 0.21	27.11 ± 0.85	48.8 ± 2.6	48.5 ± 2.7	48.7 ± 2.9	LPG II
HA07	60.5397	3.0041	63.1 ± 0.12	9.37 ± 0.37	16.1 ± 0.9	16.0 ± 0.9	16.0 ± 1.0	LPG II
HA08	60.5506	3.0223	47.2 ± 2.24	8.25 ± 1.31	14.8 ± 2.4	14.8 ± 2.4	14.8 ± 2.4	LPG II
HA09	60.5300	3.6327	60.9 ± 0.17	10.98 ± 0.38	18.9 ± 1.1	18.9 ± 1.1	18.9 ± 1.1	LPG II
HA10	60.5738	3.0156	29.9 ± 0.08	8.25 ± 0.28	15.1 ± 0.7	15.2 ± 0.7	15.3 ± 0.7	LPG II
HA11	60.5264	3.0217	30.5 ± 0.06	8.74 ± 0.33	15.7 ± 0.8	15.8 ± 0.8	15.9 ± 0.8	LPG II
HA12	60.5535	3.0186	28.8 ± 0.08	8.26 ± 0.27	15.2 ± 0.7	15.3 ± 0.7	15.4 ± 0.7	LPG II
HA13	60.5224	3.0162	25.0 ± 0.07	8.07 ± 0.26	15.7 ± 0.7	15.8 ± 0.8	15.9 ± 0.8	LPG II
HA14	60.5082	3.0211	39.3 ± 0.05	8.36 ± 0.38	15.3 ± 0.9	15.4 ± 0.9	15.4 ± 0.9	LPG II
HA15	60.5255	3.0186	28.4 ± 0.06	9.34 ± 0.31	17.9 ± 0.9	18.0 ± 0.9	18.1 ± 0.9	LPG II

HA16	60.5193	3.0217	36.5 ± 0.05	58.76 ± 1.53	117.2 ± 5.3	121.5 ± 5.9	-	LPG E
HA17	60.5007	3.0156	32.4 ± 0.07	15.70 ± 0.48	28.8 ± 1.4	29.1 ± 1.4	29.4 ± 1.4	LPG E
HA18	60.5051	3.0107	31.1 ± 0.04	10.11 ± 0.33	18.5 ± 0.9	18.5 ± 0.9	18.6 ± 0.9	LPG E
MA01	60.5416	3.0393	15.3 ± 0.05	19.62 ± 0.53	52.2 ± 2.2	53.7 ± 2.3	55.5 ± 2.4	MPG
MA02	60.5580	3.0356	37.4 ± 0.41	49.38 ± 1.92	129.4 ± 6.9	134.3 ± 7.6	-	MPG
MA03	60.5647	3.0344	106.1 ± 0.85	13.81 ± 0.91	25.1 ± 2.2	24.8 ± 2.2	24.6 ± 2.2	MPG
MA04	60.5459	3.0277	41.1 ± 0.36	14.71 ± 0.46	33.9 ± 1.7	34.0 ± 1.7	34.3 ± 1.8	MPG
MA05	60.5503	3.0247	37.3 ± 0.41	116.08 ± 3.28	410.2 ± 19.2	673.8 ± 36.1	-	MPG
MA06	60.5519	3.0174	38.8 ± 0.50	49.72 ± 2.14	125.1 ± 7.2	130.0 ± 7.9	-	MPG
MA07	60.6295	3.0059	37.0 ± 0.03	36.94 ± 0.72	90.6 ± 3.8	93.4 ± 4.1	98.9 ± 4.5	MPG
RA01	30.1107	2.5707	52.2 ± 0.25	16.05 ± 0.52	29.1 ± 1.6	29.1 ± 1.6	29.1 ± 1.6	LPG I
RA02	29.4731	2.5639	68.4 ± 0.29	23.76 ± 0.71	38.8 ± 2.1	38.5 ± 2.2	38.5 ± 2.3	LPG I
RA03	30.0051	2.5799	71.7 ± 0.30	22.69 ± 1.23	36.5 ± 2.6	36.2 ± 2.6	36.2 ± 2.7	LPG I
SA01	60.5384	3.0004	450.2 ± 2.51	439.65 ± 30.17	473.6 ± 58.2	397.9 ± 54.5	-	MPG
SA02	60.5202	2.5652	205.4 ± 0.57	105.46 ± 2.50	131.8 ± 10.2	122.7 ± 10.7	125.1 ± 11.6	MPG
SA03	60.5345	2.5646	153.2 ± 0.53	165.22 ± 3.35	261.2 ± 18.0	251.5 ± 21.1	317.4 ± 28.2	MPG
SA04	60.5336	2.5695	36.3 ± 0.18	24.68 ± 0.76	43.3 ± 2.1	43.8 ± 2.2	44.6 ± 2.3	LPG E
SA05	60.5069	2.5682	40.5 ± 0.22	15.37 ± 0.56	25.3 ± 1.3	25.3 ± 1.4	25.5 ± 1.4	LPG E
SA06	60.4793	2.5689	38.0 ± 0.07	high S conc.		-	-	LPG E
SA07	60.5363	3.0356	22.3 ± 0.08	8.24 ± 0.40	20.3 ± 1.2	20.4 ± 1.2	20.5 ± 1.2	LPG II
SA08	60.5399	3.0235	5.9 ± 0.01	6.45 ± 0.42	17.5 ± 1.3	17.7 ± 1.3	17.9 ± 1.3	LPG II
SA09	60.5447	3.0265	4.7 ± 0.00	7.21 ± 0.55	20.1 ± 1.7	20.4 ± 1.7	20.8 ± 1.7	LPG II
TD01	60.5158	3.0077	34.9 ± 0.05	52.74 ± 2.85	99.5 ± 6.5	101.6 ± 6.9	106.8 ± 7.5	LPG E
TO01	60.5615	3.0276	7.0 ± 0.00	7.55 ± 0.26	16.5 ± 0.8	16.7 ± 0.8	16.9 ± 0.8	LPG III
TO02	60.5408	3.0307	104.7 ± 0.21	8.53 ± 0.68	13.7 ± 1.3	13.7 ± 1.3	13.6 ± 1.3	LPG III
TO03	60.5154	3.0227	19.7 ± 0.06	21.04 ± 0.53	74.2 ± 3.1	76.6 ± 3.3	80.3 ± 3.6	LPG III
TO04	60.5085	3.0227	3.9 ± 0.01	6.07 ± 0.23	14.3 ± 0.7	14.5 ± 0.7	14.6 ± 0.7	LPG III

TO05	60.5389	3.0264	895.1 ± 2.80	26.22 ± 1.70	13.3 ± 1.8	12.9 ± 1.7	12.6 ± 1.7	LPG III
TO06	60.5240	3.0350	1.9 ± 0.01	6.11 ± 0.33	14.6 ± 0.9	14.8 ± 1.0	15.0 ± 1.0	LPG III
TO07	60.5392	3.0363	16.3 ± 0.03	9.39 ± 0.48	29.4 ± 1.8	29.8 ± 1.8	30.2 ± 1.9	LPG I
TO08	60.5400	3.0313	31.7 ± 0.05	14.59 ± 0.43	43.0 ± 2.0	43.3 ± 2.1	43.9 ± 2.2	LPG I
TO09	60.4811	3.0313	30.6 ± 0.07	19.69 ± 0.53	58.3 ± 2.7	58.9 ± 2.8	60.1 ± 3.0	LPG I
TO10	60.5454	3.0387	5.0 ± 0.01	10.60 ± 0.31	34.2 ± 1.5	34.9 ± 1.5	35.9 ± 1.6	LPG II
TO11	60.3487	3.0356	31.1 ± 0.08	6.38 ± 0.37	17.8 ± 1.2	17.9 ± 1.3	17.9 ± 1.3	LPG II
TO12	60.4879	3.0449	8.0 ± 0.02	6.32 ± 0.20	19.1 ± 0.9	19.3 ± 0.9	19.5 ± 0.9	LPG II
TO13	60.5126	3.0178	5.3 ± 0.01	5.47 ± 0.18	16.9 ± 0.8	17.2 ± 0.8	17.3 ± 0.8	LPG II
TO14	60.5428	3.0750	14.3 ± 0.04	6.75 ± 0.26	18.9 ± 1.0	19.1 ± 1.0	19.2 ± 1.0	LPG II
TO15	60.8434	3.0775	17.5 ± 0.04	6.30 ± 0.24	17.3 ± 0.9	17.5 ± 0.9	17.6 ± 0.9	LPG II
WA01	60.5263	3.0107	27.5 ± 0.07	9.88 ± 0.37	18.5 ± 0.9	18.5 ± 1.0	18.7 ± 1.0	LPG II
WA02	60.5224	3.0132	29.7 ± 0.07	9.13 ± 0.73	16.7 ± 1.5	16.8 ± 1.5	16.9 ± 1.5	LPG II
WA03	60.5252	3.0059	18.6 ± 0.10	9.30 ± 0.77	17.2 ± 1.5	17.4 ± 1.6	17.5 ± 1.6	LPG II
WA04	60.5443	3.0071	33.7 ± 0.02	7.34 ± 0.35	14.0 ± 0.8	14.1 ± 0.8	14.1 ± 0.8	LPG III
WA05	60.5295	3.0029	30.3 ± 0.08	7.64 ± 0.40	14.6 ± 0.9	14.7 ± 0.9	14.8 ± 0.9	LPG III
WA06	60.5531	3.0041	45.9 ± 0.13	7.67 ± 0.71	14.1 ± 1.4	14.1 ± 1.4	14.2 ± 1.4	LPG III
WE02	60.4661	3.0302	308.5 ± 1.23	151.38 ± 3.63	211.2 ± 21.7	175.8 ± 20.7	-	MPG
WE03	60.5847	2.5719	61.5 ± 0.16	79.23 ± 1.74	186.8 ± 9.0	190.4 ± 11.0	219.7 ± 13.7	MPG
WE04	60.5897	3.0538	4.6 ± 0.08	41.55 ± 1.41	118.4 ± 5.6	131.2 ± 6.2	-	MPG
<b>Bale Mountains (Stone Stripes)</b>								
BS01	30.0307	2.5682	20.7 ± 0.08	30.44 ± 0.82	84.2 ± 3.7	86.7 ± 3.9	90.9 ± 4.3	
BS02	30.0068	2.5584	31.5 ± 0.07	85.93 ± 1.63	280.8 ± 11.8	332.0 ± 16.5	781.3 ± 40.0	
BS03	29.9887	2.5584	29.1 ± 0.04	85.66 ± 2.45	280.8 ± 13.0	334.5 ± 17.6	859.4 ± 46.2	
BS04	29.9982	2.5652	40.9 ± 0.22	153.56 ± 2.58	620.1 ± 28.0	-	-	
BS05	30.0349	2.5719	1027.6 ± 11.19	1268.53 ± 25.03	-	-	-	
BS06	30.0705	2.5682	1228.0 ± 13.43	1394.82 ± 46.40	-	-	-	

**Arsi Mountains (Moraine Boulders)**

GA01	60.5219	3.0259	26.4 ± 0.13	49.89 ± 4.47	158.7 ± 15.4	169.1 ± 16.7	-	MPG
GA02	60.5596	3.0344	59.2 ± 0.07	13.27 ± 0.48	31.0 ± 1.8	30.8 ± 1.9	30.7 ± 1.9	MPG
GA03	60.5121	3.0270	46.0 ± 0.15	39.06 ± 1.11	107.1 ± 5.4	109.3 ± 6.0	-	MPG
GA04	60.5172	3.0356	20.8 ± 0.05	13.79 ± 0.39	38.6 ± 1.7	39.1 ± 1.8	40.0 ± 1.8	LPG II
GA05	60.5320	3.0369	33.1 ± 0.06	7.53 ± 0.29	18.5 ± 1.0	18.5 ± 1.0	18.5 ± 1.0	LPG II
GA06	60.4944	3.0412	34.4 ± 0.08	7.21 ± 0.34	17.9 ± 1.1	17.9 ± 1.1	18.0 ± 1.1	LPG II

TABLE A.5: Input data table for easy reproducibility of the  $^{36}\text{Cl}$  surface exposure ages using the latest version of the CRONUS web calculator (Marrero et al., 2016). The combined table is too large for display. All data are available in Tables A.2, A.3, and A.4.

TABLE A.6:  $^{36}\text{Cl}$  surface exposure ages (in ka) of the rock samples from the Bale and Arsi Mountains using different  $^{36}\text{Cl}$  production rate scalings (for more information see Marrero et al., 2016).

Sample	Present study	ST	LM	SA	SF	DE	DU	LI
BA01	32.8	33.3	29.3	28.6	28.3	24.8	26.3	25.5
BA02	21.4	22.0	20.7	20.4	20.3	18.0	18.4	18.4
BA03	57.1	60.1	47.8	45.5	45.1	40.2	43.1	40.9
BA04	17.5	18.0	18.0	17.7	17.6	15.0	15.5	15.7
BG01	73.2	79.7	63.3	63.3	63.4	63.0	68.0	62.6
BG02	72.3	77.8	62.1	62.0	62.0	60.0	65.0	60.6
BG03	29.3	29.6	26.4	26.3	26.3	24.5	25.7	25.0
HA01	43.3	46.8	38.3	38.4	38.5	38.0	40.4	38.1
HA02	383.3	439.0	300.0	298.0	299.0	298.0	340.0	300.0
HA03	48.4	52.5	41.7	41.7	41.7	41.6	44.4	41.5
HA04	17.6	18.1	17.6	17.9	17.9	17.1	18.0	17.5
HA05	16.5	17.2	16.7	17.0	17.1	16.3	16.7	16.7
HA06	48.8	51.9	41.4	41.2	41.3	40.5	43.0	40.6
HA07	16.1	16.5	16.1	16.4	16.5	15.6	16.0	16.0
HA08	14.8	15.0	15.1	15.4	15.4	14.8	15.0	15.1
HA09	18.9	20.0	18.9	19.2	19.2	18.4	19.0	18.7
HA10	15.1	16.1	15.8	16.2	16.2	16.0	16.0	16.0
HA11	15.7	16.7	16.3	16.7	16.8	16.2	16.6	16.6
HA12	15.2	16.2	15.9	16.3	16.3	16.0	16.1	16.1
HA13	15.7	16.8	16.4	16.9	16.9	16.4	16.8	16.8
HA14	15.3	16.3	16.0	16.4	16.4	16.0	16.2	16.2
HA15	17.9	19.1	18.5	18.9	18.9	18.4	18.9	18.7
HA16	117.2	128.0	100.9	101.2	101.4	100.0	110.0	100.0
HA17	28.8	31.0	27.4	27.7	27.8	27.3	28.8	27.5
HA18	18.5	19.8	19.0	19.4	19.4	18.9	19.5	19.2
MA01	52.2	56.8	44.7	45.0	45.3	50.0	50.0	45.9
MA02	129.4	142.0	110.0	110.9	111.3	111.0	121.0	111.0
MA03	25.1	25.4	23.2	23.5	23.5	22.4	23.0	22.8
MA04	33.9	36.0	31.2	31.6	31.7	31.3	33.2	31.5
MA05	410.2	467.0	320.0	319.0	321.0	320.0	370.0	321.0
MA06	125.1	136.0	106.6	107.2	107.5	107.0	116.0	107.0
MA07	90.6	100.0	78.7	79.4	79.8	79.0	87.0	79.0
RA01	29.1	31.2	27.5	27.7	28.0	26.8	28.3	27.1
RA02	38.8	41.4	34.8	34.9	34.9	33.9	36.0	34.1
RA03	36.5	39.0	33.2	33.4	33.4	32.3	34.4	32.6
SA01	473.6	520.0	350.0	336.0	333.0	294.0	340.0	300.0
SA02	131.8	141.0	109.0	108.0	108.0	101.0	110.0	102.0
SA03	261.2	285.0	207.0	200.0	201.0	192.0	212.0	193.0
SA04	43.3	46.7	38.2	38.1	38.1	36.9	39.4	37.1

---

SA05	25.3	27.1	24.4	24.6	24.6	23.6	24.7	23.9
SA07	20.3	21.3	20.1	20.0	20.0	18.4	19.0	18.9
SA08	17.5	18.4	17.9	17.9	17.8	16.2	16.6	16.7
SA09	20.1	21.1	20.0	19.9	19.9	18.3	18.9	18.8
TD01	99.5	108.0	90.0	84.9	84.9	81.0	90.0	81.0
TO01	16.5	17.8	17.3	17.9	18.0	17.7	18.2	18.0
TO02	13.7	13.8	13.8	14.1	14.1	13.2	13.4	13.6
TO03	74.2	78.0	63.2	61.6	62.1	56.8	62.0	57.8
TO04	14.3	15.5	15.2	15.7	15.8	15.6	15.9	15.9
TO05	13.3	10.2	10.1	10.2	10.1	8.7	9.0	9.2
TO06	14.6	15.8	15.5	16.0	16.1	15.9	16.2	16.0
TO07	29.4	31.1	27.6	27.1	27.3	25.0	26.4	25.6
TO08	43.0	45.3	37.6	36.8	37.0	34.1	36.4	34.8
TO09	58.3	61.5	48.8	46.9	47.3	43.4	47.3	44.0
TO10	34.2	35.3	30.7	30.2	30.2	28.0	29.3	28.1
TO11	17.8	18.6	18.2	18.1	18.2	16.3	16.8	16.9
TO12	19.1	19.7	19.0	19.0	18.9	17.0	17.6	17.6
TO13	16.9	17.5	17.1	17.1	17.0	15.3	15.7	15.8
TO14	18.9	19.8	19.1	19.1	19.1	17.3	17.9	17.9
TO15	17.3	18.1	17.7	17.7	17.7	15.9	16.4	16.5
WA01	18.5	19.8	19.0	19.3	19.4	18.9	19.4	19.2
WA02	16.7	17.8	17.3	17.7	17.8	17.2	17.7	17.6
WA03	17.2	18.6	18.0	18.5	18.5	18.1	18.6	18.4
WA04	14.0	14.7	14.6	14.9	14.9	14.4	14.7	14.7
WA05	14.6	15.5	15.2	15.6	15.6	15.1	15.4	15.4
WA06	14.1	15.0	14.5	14.8	14.9	14.3	14.5	14.6
WE02	211.2	243.0	185.0	181.0	180.0	154.0	170.0	158.0
WE03	186.8	203.0	156.0	157.0	157.0	153.0	171.0	153.0
WE04	118.4	129.0	102.3	103.6	103.8	100.0	113.0	104.0
BS01	84.2	86.7	69.2	66.4	66.2	58.0	64.0	59.6
BS02	280.8	292.0	213.0	201.0	200.0	179.0	195.0	183.0
BS03	280.8	292.0	212.0	201.0	200.0	179.0	194.0	182.0
BS04	620.1	660.0	430.0	399.0	398.0	321.0	400.0	330.0
BS05	-	-	730.0	670.0	700.0	510.0	600.0	520.0
BS06	-	-	780.0	700.0	690.0	530.0	630.0	540.0
GA01	158.7	169.0	128.0	125.0	126.0	120.0	129.0	118.0
GA02	31.0	32.6	28.6	28.4	28.5	26.4	27.9	27.0
GA03	107.1	115.0	92.2	90.6	91.2	84.0	92.0	85.1
GA04	38.6	41.1	34.7	34.3	34.6	32.5	34.6	33.0
GA05	18.5	19.5	18.8	19.0	19.0	17.4	17.9	17.9
GA06	17.9	18.8	18.3	18.3	18.4	16.8	17.3	17.3

---

TABLE A.7: Age and uncertainty of the different LPG Stages in the Bale Mountains (for further information on the age and error calculation see Chapter 2.5).

Glacial Stage	Age <sub>mean</sub> (ka)	Age <sub>weighted-mean</sub> (ka)	Error <sub>internal</sub> (ka)	Error <sub>external</sub> (ka)	Boulders	Outliers
<b>Bale Mountains</b>						
LPG I	39.6	-	-	9.9	9	1
LPG II	17.8	17.8	0.3	1.5	16	2
LPG III	15.0	15.2	0.2	1.2	14	1
<b>Arsi Mountains</b>						
LPG II	18.2	18.2	0.7	0.4	2	1

TABLE A.8: Input data for the TAS diagram (Fig. A.4).

Sample Name	Na <sub>2</sub> O [%]	K <sub>2</sub> O [%]	SiO <sub>2</sub> [%]
BA01	1.54	0.31	45.88
BA02	1.62	0.29	45.06
BA03	1.44	0.26	45.44
BA04	1.68	0.33	45.19
BG01	6.09	5.14	67.61
BG02	6.03	4.85	68.65
BG03	6.12	4.91	68.82
BS01	2.34	0.75	47.01
BS02	2.29	0.74	45.20
BS03	2.27	0.72	44.71
BS04	3.37	0.97	48.90
BS05	6.76	4.33	60.81
BS06	6.95	4.38	57.74
GA01	4.75	2.03	55.05
GA02	4.80	2.19	52.74
GA03	4.78	2.22	53.35
GA04	4.42	2.21	51.67
GA05	4.93	2.27	53.50
GA06	4.86	2.20	53.18
HA01	6.06	5.24	67.27
HA02	6.20	5.39	66.81
HA03	6.30	5.43	66.60
HA04	5.58	4.85	68.87
HA05	5.73	4.83	68.71
HA06	5.37	4.72	68.46
HA07	5.62	4.81	67.75
HA08	5.61	4.86	67.56
HA09	5.61	4.83	68.35
HA10	6.15	5.32	68.30
HA11	6.26	5.34	67.22
HA12	6.15	5.30	68.50
HA13	6.18	5.30	66.28
HA14	6.17	5.29	67.35
HA15	6.20	5.34	67.43
HA16	6.31	5.33	67.28
HA17	6.30	5.38	67.67
HA18	6.23	5.34	67.70
MA01	5.41	4.72	66.92
MA02	5.60	4.73	67.76
MA03	2.61	4.65	61.92

---

MA04	5.62	4.79	67.07
MA05	5.39	4.70	66.35
MA06	5.56	4.76	67.96
MA07	5.59	4.78	67.89
RA01	5.71	4.75	65.70
RA02	5.77	5.14	65.26
RA03	5.83	5.22	65.77
SA01	6.17	5.35	65.64
SA02	5.92	5.23	64.36
SA03	6.14	5.33	65.53
SA04	6.51	4.60	62.55
SA05	6.51	4.86	63.33
SA06	6.45	4.83	62.85
SA07	5.50	1.99	55.36
SA08	5.40	2.00	56.00
SA09	5.31	1.92	55.60
TD01	5.98	4.34	66.37
TO01	6.46	5.55	62.97
TO02	6.12	5.09	62.13
TO03	4.32	1.46	48.96
TO04	6.14	5.10	63.14
TO05	6.12	5.27	60.67
TO06	6.03	5.14	62.48
TO07	4.29	1.43	47.64
TO08	4.43	1.40	48.58
TO09	4.39	1.56	49.54
TO10	3.92	1.31	50.22
TO11	4.39	1.53	49.12
TO12	3.90	1.40	50.25
TO13	3.86	1.41	50.66
TO14	4.35	1.80	51.92
TO15	4.22	1.75	51.50
WA01	6.06	5.30	66.37
WA02	6.09	5.32	66.67
WA03	6.23	5.51	66.50
WA04	5.69	5.02	68.33
WA05	5.74	5.09	67.76
WA06	5.81	5.04	67.51
WE02	1.94	0.85	46.84
WE03	5.82	4.76	61.33
WE04	5.73	4.68	61.48

---



## **Appendix B**

# **Supplements to Chapter 3**

TABLE B.1: Overview of periglacial landforms and other characteristic geomorphological features in the Bale Mountains mapped in the field and on satellite images. A compilation of glacial landforms in the Bale Mountains is provided by Groos et al. (in revision).

ID	Landform / Feature	Status	Latitude (°N)	Longitude (°E)	Elevation (m)	Slope (°)	Aspect (°)
1	Frozen waterfalls	active	6.91508	39.76298	3980 – 4000	32 – 37	350 – 10
2	Needle ice	active	6.91784	39.76978	3925 – 3935	0	-
3	Sorted stone nets	active	6.84253	39.77714	4110 – 4140	0	-
4	Scree slope	active	6.92509	39.78395	3930 – 4090	18 – 37	110 – 120
5	Solifluction lobes	active	6.92699	39.77194	4130 – 4190	20 – 22	150 – 170
6	Sorted stone stripes	relict	6.78692	39.79278	3865 – 3880	3 – 9	290 – 70
7	Sorted stone stripes	relict	6.79496	39.81503	3880 – 3940	3 – 7	70 – 180
8	Sorted stone stripes	relict	6.85486	39.72071	4020 – 4100	2 – 9	330 – 350
9	Sorted stone stripes	relict	6.85336	39.71750	4020 – 4140	2 – 9	330 – 350
10	Sorted stone stripes	relict	6.85432	39.71263	4000 – 4070	2 – 9	330 – 350
11	Sorted stone stripes	relict	6.85264	39.70884	3940 – 4100	2 – 9	330 – 350
12	Sorted stone stripes	relict	6.91414	39.60676	3715 – 3730	2 – 9	270 – 290
13	Sorted stone polygons	relict	6.83843	39.70631	4000 – 4100	0 – 4	180 – 200
14	Sorted stone polygons	relict	6.84533	39.71969	4120 – 4170	0 – 4	330 – 350
15	Blockfield	relict	6.76713	39.78794	3690 – 3800	19 – 25	240 – 250
16	Blockfield	relict	6.82818	39.78168	3970 – 4030	12 – 15	260 – 270
17	Blockfield	relict	6.83016	39.71949	3700 – 3940	17 – 19	200 – 220
18	Blockfield	relict	6.84541	39.69772	3800 – 3880	9 – 11	300 – 310
19	Blockfield	relict	6.85245	39.69704	3700 – 3830	12 – 14	260 – 270
20	Blockfield	relict	6.86119	39.69388	3550 – 3820	20 – 24	250 – 270
21	Blockfield	relict	6.86848	39.69701	3600 – 3880	20 – 24	320 – 330
22	Scree slope	relict	6.89194	39.89919	3890 – 3940	20 – 23	300 – 320
23	Scree slope	relict	6.88617	39.89236	3930 – 3980	20 – 26	350 – 360
24	Scree slope	relict	6.91829	39.77699	4070 – 4110	24 – 25	350 – 360
25	Scree slope	relict	6.95343	39.76925	4045 – 4065	24 – 25	290 – 310
26	Scree slope	relict	6.93937	39.78443	4080 – 4110	21 – 25	290 – 310
27	Scree slope	relict	6.94363	39.78672	4055 – 4100	23 – 25	350 – 360
28	Scree slope	relict	6.94764	39.79058	4080 – 4150	24 – 27	10 – 20
29	Landslide	relict	6.92268	39.89833	3490 – 3720	2 – 30	60 – 70
30	Landslide	relict	6.92644	39.90251	3490 – 3650	2 – 40	160 – 170

TABLE B.2: System settings of the used PulseEKKO PRO GPR.

Setting type	Setting	Setting type	Setting	Setting type	Setting
Frequency:	1000 MHz	Survey type:	Reflection	Start offset:	0 m
Time window:	30 ns (1.6 m)	Step size:	0.010 m	GPR trigger:	Odometer
Sampling Interval:	Normal (100 ps)	Calibration:	1080.0	Antenna separation:	0.15 m
Stacks:	4	Transmitter:	pE Pro Auto	Antenna polarization:	broadside
Velocity:	0.12 m ns <sup>-1</sup>	Receiver:	pulseEKKO Pro	Antenna orientation:	Perpendicular

TABLE B.3: Major and trace element data of the six rock samples from the Sanetti Plateau. Data from Groos et al. (in revision).

Rock sample	O	C	Na	Mg	Al	Si	P	K	Ca	Ti	Mn	Fe	B	Sm	Gd	U	Th
	% w/w.	ppm	ppm	ppm	ppm	ppm											
BS01	57.88	5.13	1.74	5.61	7.40	21.97	0.09	0.62	7.86	1.44	0.15	9.10	3	3.3	3.6	0.3	1.1
BS02	56.64	5.09	1.70	5.50	7.23	21.13	0.14	0.61	7.90	1.41	0.15	9.13	11	3.8	4.1	0.3	1.3
BS03	56.17	4.98	1.68	5.23	7.52	20.90	0.15	0.60	8.00	1.44	0.14	8.97	12	3.8	4.1	0.3	1.2
BS04	54.79	3.85	2.50	3.56	8.30	22.86	0.14	0.81	6.96	1.42	0.15	8.81	6	4.3	4.4	0.4	1.7
BS05	47.82	0.68	5.01	0.21	9.09	28.42	0.05	3.59	1.92	0.24	0.19	4.39	1	6.4	4.8	2.9	14.8
BS06	46.47	0.66	5.16	0.18	9.42	26.99	0.05	3.64	1.90	0.24	0.19	4.41	15	6.7	4.9	1.9	15.5

TABLE B.4: Cosmogenic  $^{36}\text{Cl}$  data and surface exposure ages of the rock samples from the Sanetti Plateau. Data from Groos et al. (in revision). \*Erosion rate =  $0 \text{ mm ka}^{-1}$ . \*\*Erosion rate =  $1 \text{ mm ka}^{-1}$ . \*\*\*Erosion rate =  $2 \text{ mm ka}^{-1}$ 

Rock sample	Rock dissolved (g)	$^{35}\text{Cl}$ Spike (mg)	Cl (ppm)	$^{36}\text{Cl}$ ( $10^5 \text{ At g}^{-1}$ )	Exposure age (ka)*	Exposure age (ka)**	Exposure age (ka)***
BS01	30.0307	2.5682	20.7 ± 0.08	30.44 ± 0.82	84.2 ± 3.7	86.7 ± 3.9	90.9 ± 4.3
BS02	30.0068	2.5584	31.5 ± 0.07	85.93 ± 1.63	280.8 ± 11.8	332.0 ± 16.5	781.3 ± 40.0
BS03	29.9887	2.5584	29.1 ± 0.04	85.66 ± 2.45	280.8 ± 13.0	334.5 ± 17.6	859.4 ± 46.2
BS04	29.9982	2.5652	40.9 ± 0.22	153.56 ± 2.58	620.1 ± 28.0	-	-
BS05	30.0349	2.5719	1027.6 ± 11.19	1268.53 ± 25.03	-	-	-
BS06	30.0705	2.5682	1228.0 ± 13.43	1394.82 ± 46.40	-	-	-

## Appendix C

# Supplements to Chapter 4

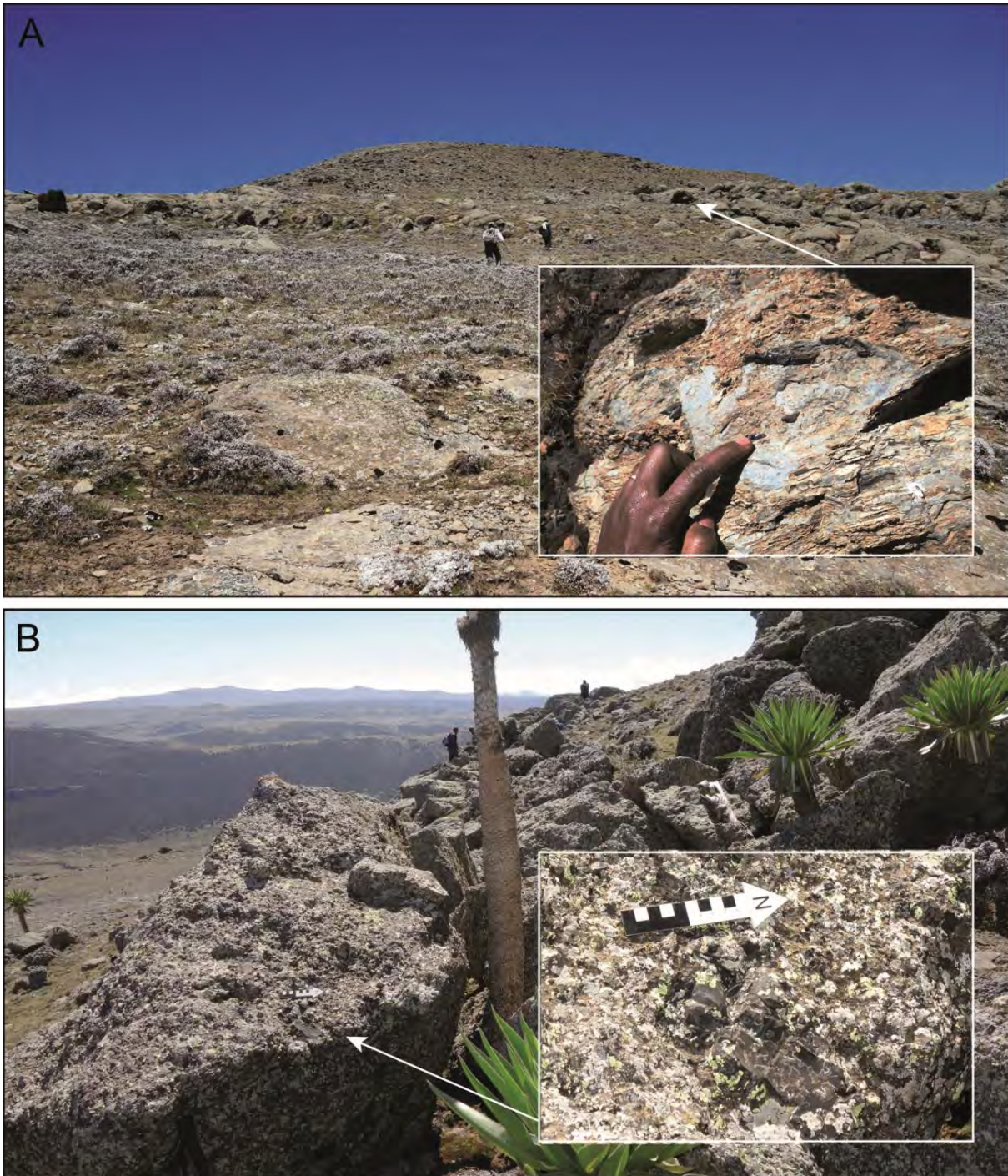


FIGURE C.1: Photographs of obsidian outcrops at Wasama Ridge. (A) Site B04 looking north and (B) site B06 looking west.

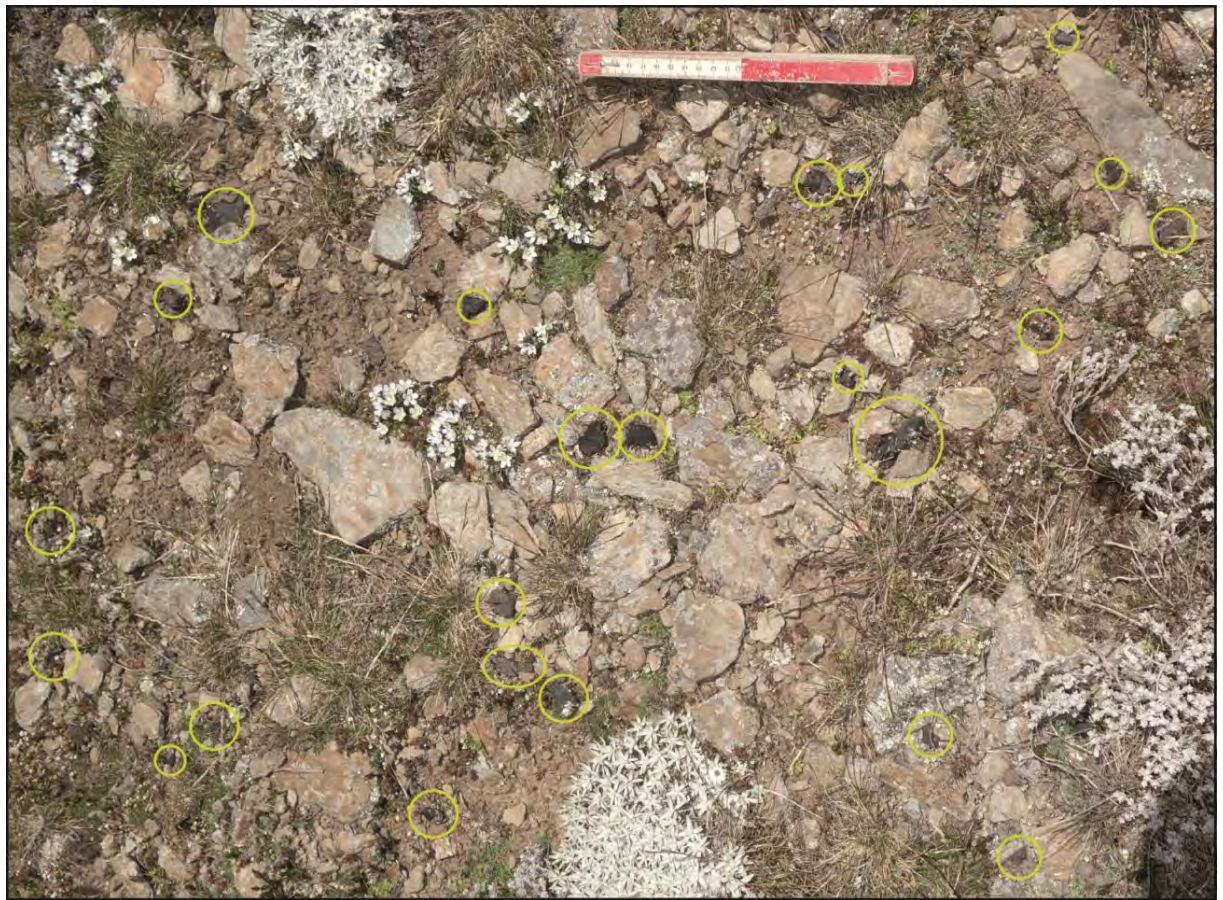


FIGURE C.2: Photograph of lithic surface scatters at Wasama Ridge. Flaked obsidian artifacts (circled in yellow) show different degrees of patination. The photograph was taken 150 m from the obsidian outcrop B04 (identical position as in Fig. C.1). Scale bar is 20 cm.

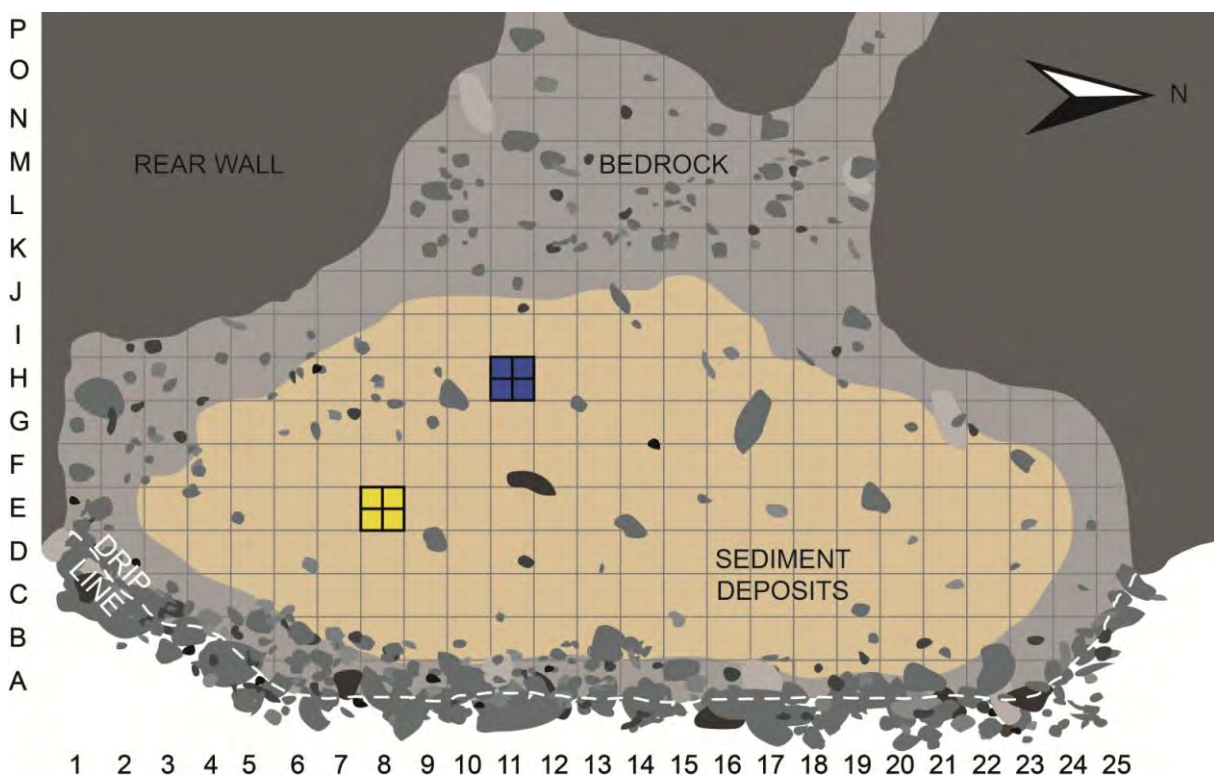


FIGURE C.3: Schematic plan view of Fincha Habera rock shelter. Grid square system with the locations of test units E8 (yellow square meter) and H11 (blue square meter).

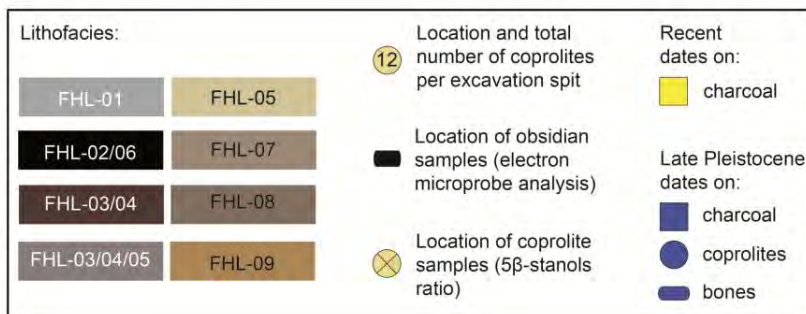
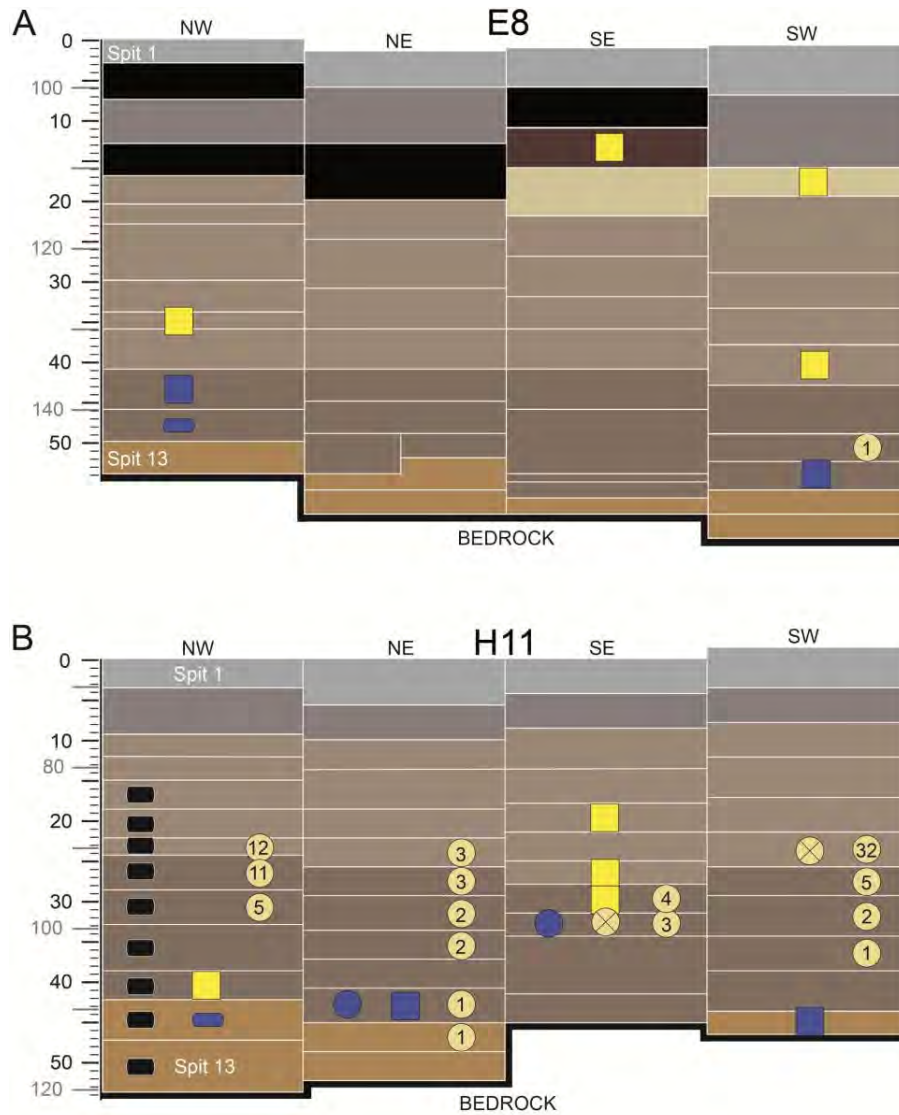


FIGURE C.4: Schematic representation of excavation spits at Fincha Habera rock shelter. The location, lithofacies association and excavation spits of coprolites, dating samples, electron microprobe samples, and 5 $\beta$ -Stanols samples is shown in excavation units E8 (A) and H11 (B).

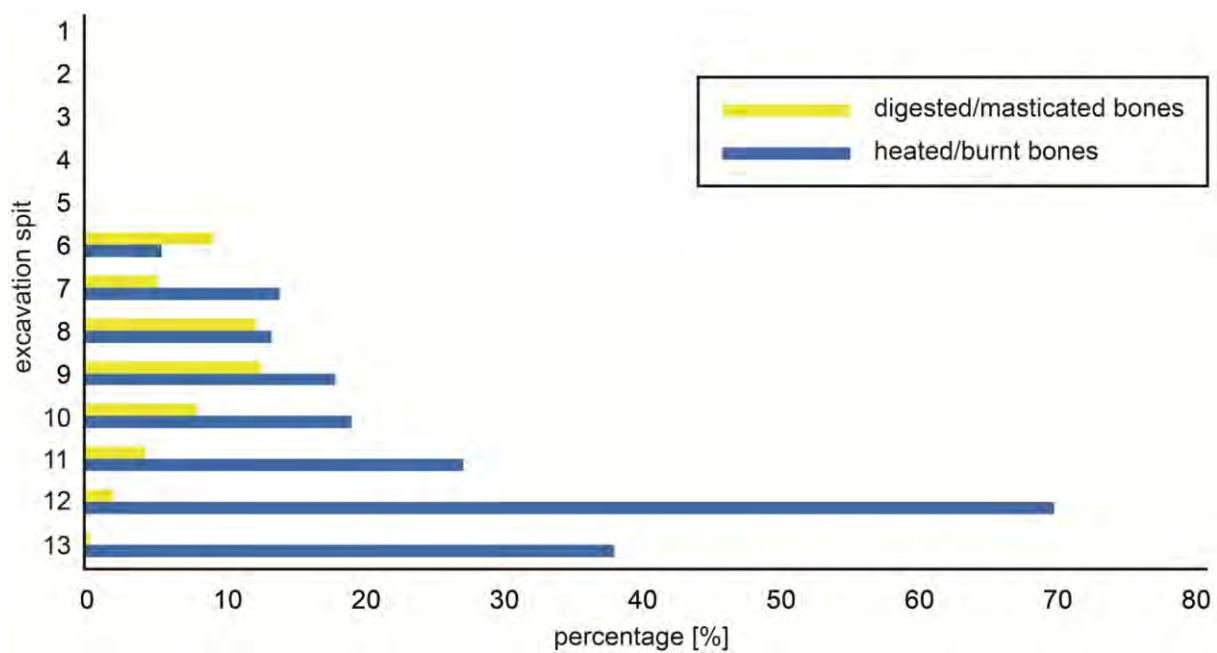


FIGURE C.5: Relative frequency of faunal remains at Fincha Habera. Digested/masticated faunal remains (yellow) compared to heated/burnt faunal remains (blue) according to the vertical excavation spits (square H11, see Fig. C.4).

FIGURE C.6: Images of sampled boulders from the Harcha and Wasama valleys are integrated in Fig. A.1

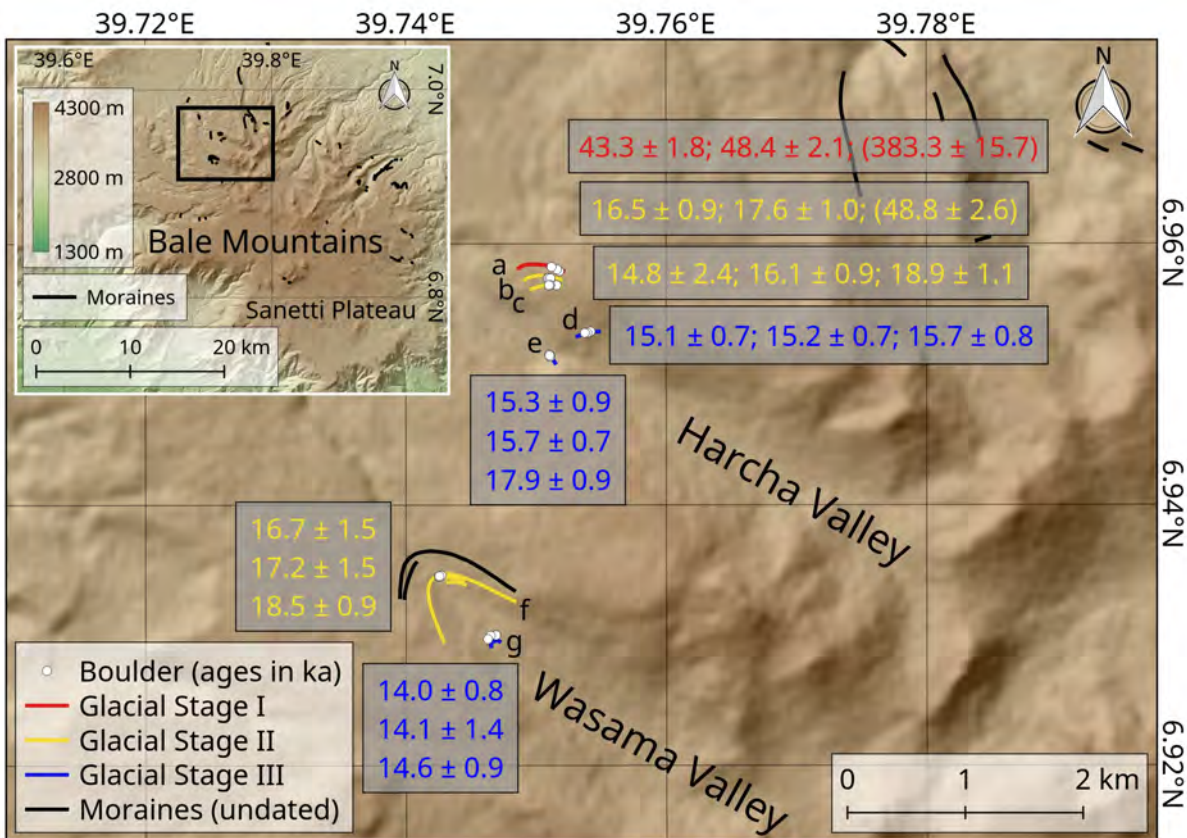


FIGURE C.7: Overview map of the  $^{36}\text{Cl}$  surface exposure ages obtained from 21 boulders sampled in the Harcha and Wasama Valleys of the Bale Mountains. Boulders HA02 and HA06 (represented by the ages in brackets) were not considered for the calculation of the three different Glacial Stages because of their complex exposure history (e.g. inherited cosmogenic  $^{36}\text{Cl}$  signal from pre-depositional exposure).

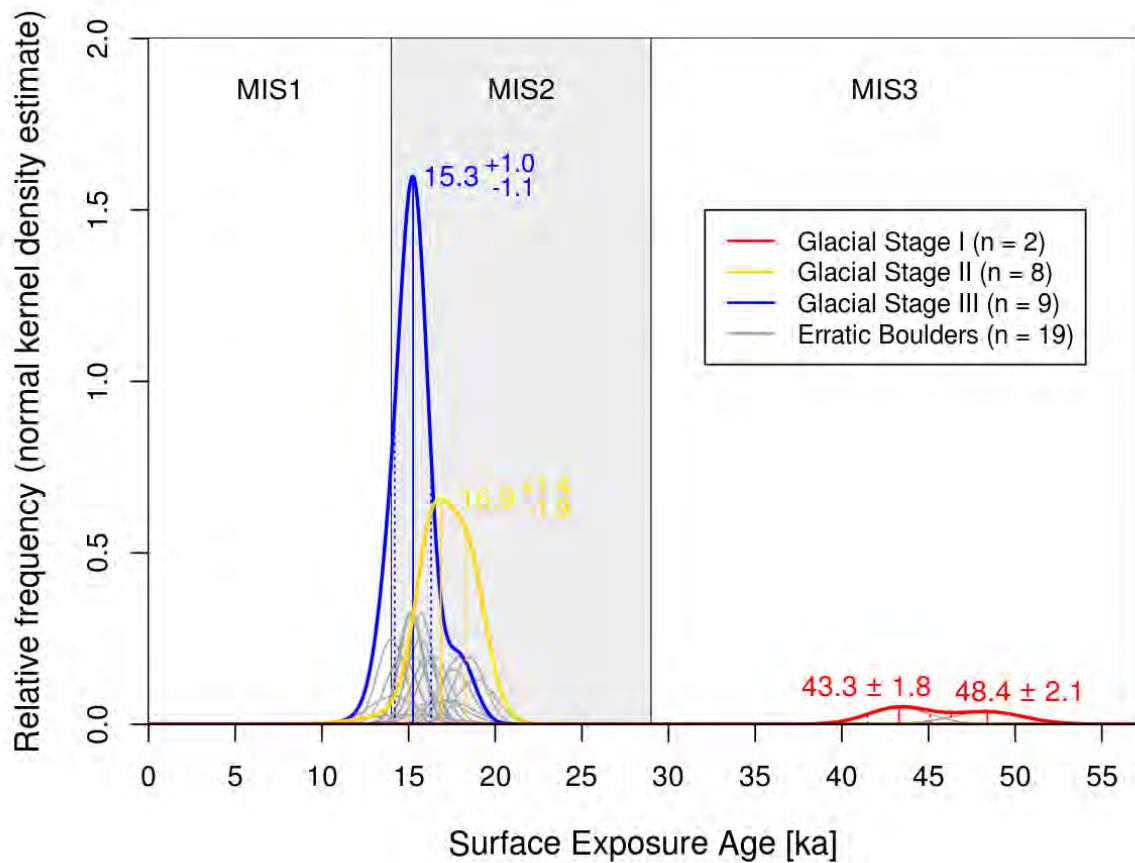


FIGURE C.8: Frequency distribution (normal kernel density estimate) of 19 <sup>36</sup>Cl surface exposure ages used for the determination of the glacial stages in the Harcha and Wasama Valleys of the Bale Mountains. Grey, thin lines are the Gaussian distributions of all <sup>36</sup>Cl surface exposure ages (excluding samples HA02 and HA06) with an analytical error of  $1\sigma$ . The flatter the respective curve the larger the analytical error related to the uncertainties of the accelerator mass spectrometry measurements. The red bimodal curve is the sum of the two considered boulder ages from moraine a (Glacial Stage I), the yellow unimodal curve the sum of the boulder ages from moraine b, c, f (Glacial Stage II) and the blue unimodal curve the sum of the boulder ages from moraine d, e, g (Glacial Stage III). Each weighted mean represented by a solid vertical line is reported with a  $1\sigma$  error (dashed vertical lines indicate the  $1\sigma$  limits). Grey and white bars in the background state the Marine Isotope Stages 1, 2 and 3 and serve as a time reference.

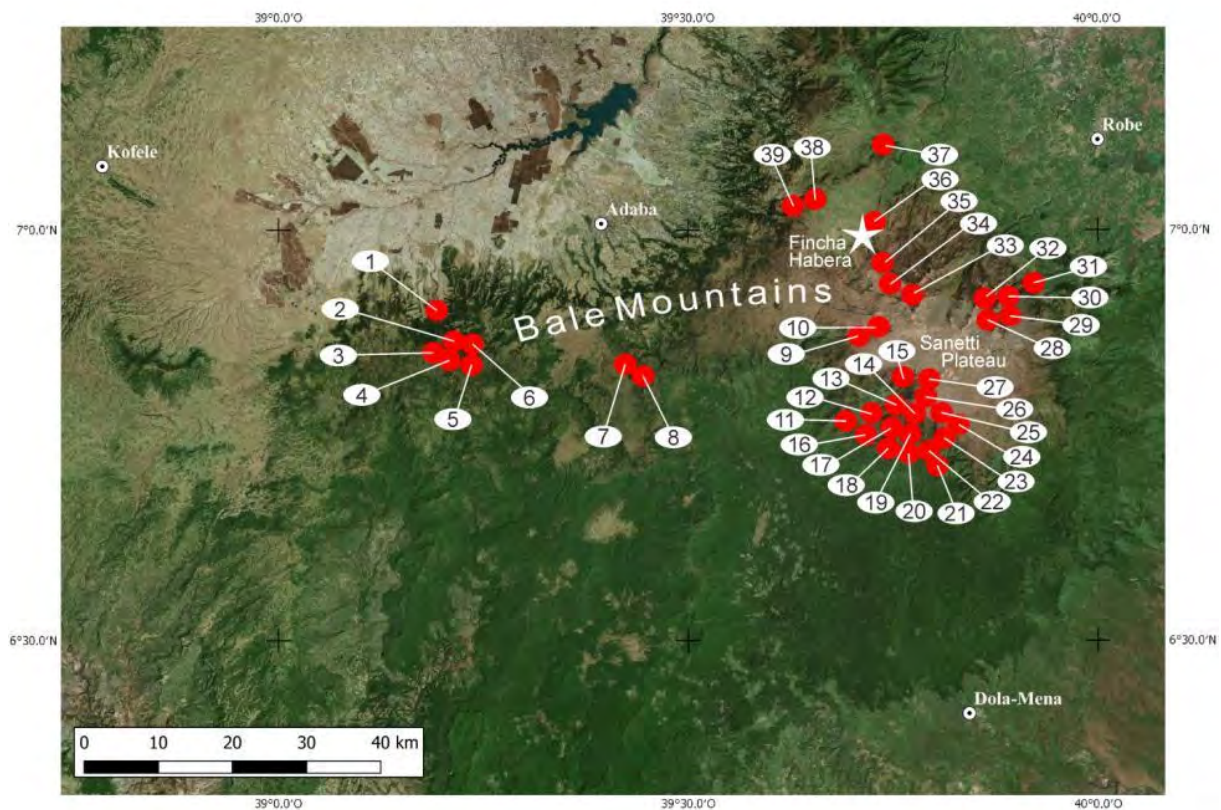


FIGURE C.9: Occurrences of micro-areal endemic species of the genus *Trechus* Clairville in the Bale Mountains. Each red dot refers to the distributional range of one species endemic to a certain valley along mountain slopes. Species occurring in more than one of the valley systems are not considered. Species' numbering refers to table S8. The white star refers to the location of Fincha Habera rock shelter.

TABLE C.1: Total organic carbon, black carbon, total N, total P, total Ca and total K contents, as well as content of 5 $\beta$ -stanols of the sampled Fincha Habera rock shelter sediments and coprolite samples (C1/C2). Samples marked with an asterisk (\*) were combined for fecal biomarker analysis due to the small amount of sample material.

Sampling Depth (cm)	Total Organic Carbon (g kg <sup>-1</sup> )	Black Carbon (g C <sub>BC</sub> kg <sup>-1</sup> )	Black Carbon rel. TOC (g C <sub>BC</sub> kg <sup>-1</sup> TOC)	N (g kg <sup>-1</sup> )	P (g kg <sup>-1</sup> )	Ca (g kg <sup>-1</sup> )	K (g kg <sup>-1</sup> )	Coprostanol (μg kg <sup>-1</sup> )	Epicoprostanol (μg kg <sup>-1</sup> )	5 $\beta$ -stanol (μg kg <sup>-1</sup> )	Epi-5 $\beta$ -stigmastanol (μg kg <sup>-1</sup> )
0-2	100.4	17.7	175.8	13.5	9.4	14.3	7.5	239.0	515.0	392.7	710.5
2-4	210.4	79.4	377.3	7.4	7.3	16.2	4.2	204.5	188.1	1111.0	1624.7
4-6	207.3	82.6	398.4	6.5	9.6	17.6	5.0	298.4	265.2	981.9	1463.3
6-7	122.5	46.1	376.2	6.1	13.0	22.2	6.2	161.6	113.8	267.8	282.7
7-9	26.1	7.8	300.1	1.9	41.5	63.5	7.3	68.2	83.4	29.8	57.0
9-17	270.0	81.8	302.8	10.5	3.4	12.6	3.1	205.6	165.0	433.1	519.8
17-19	21.5	6.8	315.6	1.3	23.7	31.0	7.7	58.6	39.2	61.4	44.2
19-21	12.6	3.5	281.6	1.1	33.6	34.1	6.8	80.6	51.9	46.0	29.4
21-23	13.5	3.2	236.1	1.2	29.3	45.9	6.0	98.5	68.5	41.6	20.0
23-25	10.7	2.0	190.8	1.1	31.6	63.5	4.7	230.9	47.8	60.9	54.7
25-27	11.1	1.3	115.9	1.1	33.7	80.2	11.1	304.2	70.8	161.2	81.4
27-29	11.1	2.1	184.8	1.2	36.4	100.7	4.6	101.7	54.1	15.5	6.9
29-34	12.7	2.4	192.1	1.4	35.8	85.0	4.8	209.9	50.4	81.2	37.6
34-36	18.0	3.4	187.6	2.2	43.9	102.3	4.1	465.9	55.9	74.6	39.2
36-39	21.4	2.0	94.8	1.8	84.4	192.4	2.7	713.4	189.1	5.9	13.9
39-41	25.6	5.5	213.9	2.0	53.0	135.9	3.7	192.4	64.4	36.0	43.9
41-43	20.9	5.7	274.8	1.8	19.3	42.8	5.5	79.8	64.0	18.1	20.8
43-45	13.1	2.7	206.1	1.4	27.5	52.0	4.4	392.6	87.6	69.4	48.6
45-47	12.8	2.5	196.7	1.4	27.5	52.1	4.1	320.0*	44.6*	150.4*	55.1*
47-49	10.7	2.0	190.0	1.2	21.0	40.0	3.9	320.0*	44.6*	150.4*	55.1*
49-51	1.6	0.0	0.0	0.2	3.6	13.0	3.1	39.7	32.5	5.4	8.6
51-53	1.2	0.0	0.0	0.2	2.9	8.9	2.6	40.0	48.5	3.1	9.2
C1	22.2	0.0	0.0	2.6	146.5	272.0	0.6	912.0	331.4	625.1	390.0
C2	23.7	0.0	0.0	2.0	n/a	n/a	n/a	361.5	134.3	421.9	981.6

TABLE C.2:  $^{14}\text{C}$  AMS ages from Fincha Habera rock shelter.

Lab No.	Context	Lithofacies	Depth (cm)	Material	$^{14}\text{C}$ BP	$\sigma$ $^{13}\text{C}$	95.4 % cal BP
COL5197.1.1	E8NW spit 6	FHL-07	-35	Charcoal	143 ± 37	-25.1	282 - 1
Beta - 486378	E8SW spit 7	FHL-07	-39	Charcoal	330 ± 30	-20.7	473 - 308
COL5196.1.1	E8SE spit 3	FHL-04	-13	Charcoal	533 ± 38	-22.9	639 - 506
COL5195.1.1	E8SW spit 4	FHL-05	-17	Charcoal	547 ± 36	-28.3	642 - 512
COL5199.1.1	H11SE spit 8	FHL-08	-30	Charcoal	558 ± 37	-24.0	646 - 517
Beta - 486376	H11SE spit 7	FHL-07	-27	Charcoal	660 ± 30	-23.5	603 - 557 (47.8%) / 674 - 628 (47.6%)
Beta - 507233	E8NW profile	FHL-06	-9 / -17	Black carbon	680 ± 30	-25.4	680 - 634 (60.4%) / 596 - 560 (35.0%)
Beta - 486375	H11NW spit 11	FHL-08	-40	Charcoal	780 ± 30	-21.6	740 - 669
COL5198.1.1	H11SE spit 5	FHL-07	-21	Charcoal	770 ± 38	-23.0	760 - 662
Beta - 507234	E8NW profile	FHL-07	-23 / -25	Black carbon	9,710 ± 30	-30.5	11,218 - 11,096
Beta - 503927	E8NW profile	FHL-08	-47 / -49	Black carbon	14,930 ± 60	-23.0	18,336 - 17,950
Beta - 506526	H11SE spit 9	FHL-08	-32	Coprolite	18,320 ± 60	-21.4	22,390 - 21,950
Beta - 507235	E8NW profile	FHL-08	-34 / -36	Black carbon	21,520 ± 80	-27.6	25,990 - 25,651
Beta - 486377	E8NW spit 11	FHL-08	-43	Charcoal	27,240 ± 120	-22.1	31,364 - 30,980
Beta - 506527	H11NE spit 11	FHL-08	-43	Charcoal	28,000 ± 140	-23.7	32,320 - 31,354
Beta - 507236	E8NW profile	FHL-08	-41 / -43	Black carbon	28,220 ± 130	-28.3	32,608 - 31,560
Beta - 506527	H11NE spit 11	FHL-08	-43	Coprolite	30,940 ± 170	-22.4	35,230 - 34,500
Beta - 506527	E8SW spit 10	FHL-08	-52	Charcoal	31,640 ± 200	-24.0	36,034 - 35,040
Beta - 522263	H11NW spit 13	FHL-09	-47	Bone collagen	33,600 ± 230	-19.7	38,598 - 37,111
Beta - 522264	E8NW spit 12	FHL-08	-45	Bone collagen	34,380 ± 250	-19.1	39,506 - 38,389
COL5451.1.1	H11SW spit 12	FHL-09	-46	Charcoal	42,086 ± 711	-23.5	46,957 - 44,236

TABLE C.3: Lithic assemblage composition of Fincha Habera rock shelter. Number of artifacts per technological category by excavation spit and lithofacies association (combined data of units E8 and H11).

Spit	Lithofacies	Tested nodules	Cores	Debris		Debitage			Bladelets	Hammerstone	Total
				Chips	Angular waste	Flakes	Flakes fragments	Blades			
1	FHL-01	-	-	-	-	-	-	-	-	-	-
2	FHL-02	-	-	-	-	-	-	-	-	-	-
3	FHL-03/04	-	-	1	-	-	-	-	-	-1	-
4	FHL-05/06	-	-	-	7	-	-	-	-	-	7
5	FHL-07	3	2	7	27	-	-	1	1	-	50
6	FHL-07	-	1	21	38	17	-	3	-	-	105
7	FHL-07	2	1	26	48	0	-	2	-	1	108
8	FHL-08	2	-	28	60	26	-	3	-	-	135
9	FHL-08	7	-	43	88	1	-	1	4	-	168
10	FHL-08	8	3	52	74	18	-	6	6	-	182
11	FHL-08	6	3	33	85	22	-	1	-	-	170
12	FHL-09	3	1	13	27	19	-	4	2	-	80
13	FHL-09	-	1	7	4	-	-	1	-	-	13
	Total	31	12	231	458	103	-	22	15	2	1019

TABLE C.4: Fauna from unit H11 at Fincha Habera according to the NISP (Number of Identified Specimens).

Taxa	FHL-07	FHL-08	FHL-09	Total
Baboon ( <i>Papio anubis</i> )	-	3	-	3
African buffalo ( <i>Syncerus caffer</i> )	-	-	1	1
Bovidae size 4	15	8	-	23
Mountain nyala ( <i>Tragelaphus buxtoni</i> )	-	1	1	2
Bovidae size 3	23	22	-	45
Reedbuck ( <i>Redunca</i> sp.)	1	3	-	4
Bovidae size 2	2	1	-	3
Bovidae	3	-	-	3
Fox ( <i>Vulpes</i> sp.)	4	6	1	11
Muridae	2	3	-	5
Giant mole-rat ( <i>Tachyoryctes</i> cf. <i>macrocephalus</i> )	266	758	418	1442
Ostrich ( <i>Struthio camelus</i> ): eggshell	-	-	1	1
Total Identified	316	805	422	1543
Unidentified	404	335	23	762
Total	720	1140	445	2305

TABLE C.5: Geographic location and description of the sampled boulders from the Harcha and Wasama Valleys in the Bale Mountains. This Table is integrated in Table A.2.

TABLE C.6: Major and trace element data of the rock samples from the Harcha and Wasama Valleys in the Bale Mountains. This Table is integrated in Table A.3.

TABLE C.7: Cosmogenic  $^{36}\text{Cl}$  data and surface exposure ages of the samples from the Harcha and Wasama Valleys in the Bale Mountains for three different erosion scenarios ( $\epsilon_{min} = 0 \text{ mm ka}^{-1}$ ,  $\epsilon_{med} = 1 \text{ mm ka}^{-1}$ ,  $\epsilon_{max} = 2 \text{ mm ka}^{-1}$ ). This Table is integrated in Table A.4.

TABLE C.8: Micro-areal endemic species of the genus *Trechus Clairville* strictly adapted to humid and humus-rich soil known to occur on different slopes of the Bale Mountains. Species occurring in more than one of the valley systems are not considered. Species' numbering refers to Fig. C.9.

No.	Species of the western Bale Mountains	Valley system to which the species is endemic	Vertical distribution (m)
1	<i>T. dodola</i> Schmidt & Faille 2018	Dodola-Angavo Valley	2700-2850
2	<i>T. oppositus</i> Schmidt & Faille 2018	Dodola-Angavo Valley	3400-3700
3	<i>T. angavoensis</i> Schmidt & Faille 2018	Dodola-Angavo Valley	3400-3700
4	<i>T. fragelaphus</i> Schmidt & Faille 2018	Dodola-Angavo Valley	3400-3500
5	<i>T. sp.n.</i> near <i>wiersbowski</i>	Dodola-Angavo Valley	3700
6	<i>T. nigrifemoralis</i> Schmidt & Faille 2018	Dodola-Angavo Valley	3400-3500
7	<i>T. adaba</i> Schmidt & Faille 2018	Adaba Valley	3170-3250
8	<i>T. balesylvestris</i> Schmidt & Faille 2018	Adaba Valley	3170
No.	Species of the southern escarpment	Valley system to which the species is endemic	Vertical distribution (m)
9	<i>T. sp.n.</i> 1 near <i>relictus</i>	Rafu Valley	3900-4100
10	<i>T. sp.n.</i> 1 near <i>ericalis</i>	Rafu Valley	3900-4100
11	<i>T. nanulus</i> Schmidt & Faille 2018	Rira Valley	2380-2690
12	<i>T. rira</i> Schmidt & Faille 2018	Rira Valley	3200
13	<i>T. wiersbowski</i> Schmidt & Faille 2018	Rira Valley	3150-3230
14	<i>T. sp.n.</i> 1 near <i>rira</i>	Rira Valley	3830
15	<i>T. sp.n.</i> 2 near <i>rira</i>	Rira Valley	3830
16	<i>T. mattisi</i> Schmidt & Faille 2018	Rira Valley	2900-3100
17	<i>T. harena</i> Schmidt & Faille 2018	Rira Valley	2900-3150
18	<i>T. hagenia</i> Schmidt & Faille 2018	Rira Valley	2900-3300
19	<i>T. bombi</i> Schmidt & Faille 2018	Rira Valley	3150
20	<i>T. grandipennis</i> Schmidt & Faille 2018	Rira Valley	2900
21	<i>T. iridescens</i> Schmidt & Faille 2018	Abalkhasim Valley	3250
22	<i>T. abalkhasimi</i> Schmidt & Faille 2018	Abalkhasim Valley	3250
23	<i>T. sanettii</i> Schmidt & Faille 2018	Abalkhasim Valley	3600-3800

24	<i>T. sp.n. 3</i> near <i>rira</i>	Abalkhasim Valley	3600-3800
25	<i>T. sanettii</i> ssp.n.	Abalkhasim Valley	3850
26	<i>T. sp.n.</i> near <i>clarkeianus</i>	Rira Valley	3830
27	<i>T. sp.n.</i> near <i>sanettii</i>	Rira Valley	3830-4200
No.	Species of the northern escarpment	Valley system to which the species is endemic	Vertical distribution (m)
28	<i>T. ericalis</i> Magrini et al. 2012	Goba-Tegona Valley	3750-4100
29	<i>T. relictus</i> Magrini et al. 2012	Goba-Tegona Valley	3700-4100
30	<i>T. fisehai</i> Schmidt & Faille 2018	Goba-Tegona Valley	3550-3800
31	<i>T. bastianini</i> Magrini & Sciaky 2006	Goba-Tegona Valley	2990-3200
32	<i>T. clarkeianus</i> Basilewsky 1974	Goba-Tegona Valley	3750-4150
33	<i>T. depressipennis</i> Schmidt & Faille 2018	Wasama Valley	3900-4150
34	<i>T. sp.n. 2</i> near <i>ericalis</i>	Wasama Valley	3700-3800
35	<i>T. sp.n. 2</i> near <i>relictus</i>	Wasama Valley	3700-3800
36	<i>T. haggei</i> Schmidt & Faille 2018	Fincha Habera (upper Web Valley)	3400-3500
37	<i>T. sp.n. 3</i> near <i>relictus</i>	Dinsho (lower Web Valley)	3100
38	<i>T. sp.n. 4</i> near <i>relictus</i>	Sebsebe Washia Valley	3900-4100
39	<i>T. sp.n. 3</i> near <i>ericalis</i>	Sebsebe Washia Valley	3900-4100



## *Declaration of Consent*

on the basis of Article 18 of the PromR Phil.-nat. 2019

Last, first name: Groos, Alexander Raphael

Registration number: 16-124-067

Study programme: Geography

Bachelor       Master       Dissertation

Title of the thesis: Glacial and periglacial history of the Bale Mountains,  
southern Ethiopian Highlands

Supervisors: Prof. Dr. Heinz Veit & PD Dr. Naki Akçar

I declare herewith that this thesis is my own work and that I have not used any sources other than those stated. I have indicated the adoption of quotations as well as thoughts taken from other authors as such in the thesis. I am aware that the Senate pursuant to Article 36 paragraph 1 litera r of the University Act of September 5<sup>th</sup>, 1996 and Article 69 of the University Statute of June 7<sup>th</sup>, 2011 is authorized to revoke the doctoral degree awarded on the basis of this thesis.

For the purposes of evaluation and verification of compliance with the declaration of originality and the regulations governing plagiarism, I hereby grant the University of Bern the right to process my personal data and to perform the acts of use this requires, in particular, to reproduce the written thesis and to store it permanently in a database, and to use said database, or to make said database available, to enable comparison with theses submitted by others.

Bern, 21<sup>st</sup> July 2020

Alexander Raphael Groos



# Curriculum Vitae

## Alexander Raphael Groos

### Personal Information

Date of birth: March 24<sup>th</sup> 1990  
 Place of birth: Netphen, Germany  
 Nationality: German  
 Email: alexander.groos@mailbox.org

### Education and Research Experience

02/2020	Attendance of the 6 <sup>th</sup> Snow Science Winter School, French Alps
06/2016 – present	PhD in Geography, University of Bern, Institute of Geography <i>PhD thesis: Glacial and periglacial history of the Bale Mountains, southern Ethiopian Highlands</i>
01/2015 – 09/2015	Research assistant, Karlsruhe Institute of Technology, Campus Alpin
12/2014 – 03/2016	Research assistant, University of Augsburg, Institute of Geography
10/2014 – 03/2016	Research semester and master thesis, Bavarian Academy of Sciences and Humanities, Geodesy and Glaciology Group
02/2014 – 04/2014	Internship, German Aerospace Centre (DLR), Remote Sensing Data Centre
10/2013 – 03/2016	Studies in Climate and Environmental Sciences (M.Sc.), University of Augsburg, Institute of Geography <i>Master thesis: "Analysis of the glacier surface mass balance in the Karakoram using an enhanced degree-day modelling approach"</i>
08/2012 – 10/2012	Internship, Estación Científica Rio San Francisco, Ecuador
04/2012 – 09/2013	Minor in Meteorology, Goethe University Frankfurt a. M., Department of Geosciences
11/2011 – 07/2013	Research assistant, Philipps University of Marburg, Department of Geography
10/2010 – 09/2013	Studies in Geography (B.Sc.), Philipps University of Marburg, Department of Geography <i>Bachelor thesis: "An analysis of the relationship between the occurrence of Taiwan's Tropical Montane Cloud Forest and low cloud frequencies derived from Terra/Aqua-MODIS"</i>